Trace Metal Speciation in Complex Aquatic Environments

The Cu^{2+}, Cd^{2+}, Ferrihydrite, Phthalic Acid and Bacteria System

Yantao Song

A thesis submitted in fulfillment of the requirements for the degree of Doctor of Philosophy, The University of Auckland, 2009.

Abstract

Trace metal speciation in aquatic environments is inherently complex due to the large number of possible interactions with dissolved and particulate components. Adsorption onto iron oxyhydroxide and bacterial surfaces, as well as the formation of metal-ligand complexes can play important roles in controlling the fate and transport of trace metals in natural environments. The objective of this study is to describe and understand metal speciation and distribution in a complex biogeochemical system by incrementally increasing the complexity from simple binary systems to a dynamic quaternary system containing a trace metal, iron oxide and bacteria that are active and metabolizing an organic ligand.

Copper, cadmium, and phthalic acid (H_2L_p) adsorption onto ferrihydrite in binary systems was well reproduced using the diffuse layer model (DLM). The adsorption of H_2L_p adsorption was analogous to that of inorganic diprotic acids in terms of the relationship between the adsorption constants and acidity constants. In ternary systems H_2L_p caused Cu^{2+} or Cd^{2+} adsorption to be either enhanced (due to surface ternary complex formation) or inhibited (due to solution complex formation) depending on the conditions. The DLM could only describe the effect of H_2L_p on metal ion sorption by including ternary complexes of the form $\equiv FeOHML_p^{(0)}$, where $\equiv FeOH$ is a surface site and M is Cu or Cd. The relationship between binary metal adsorption constants and the ternary complex adsorption constants from this and previous studies suggest several properties of ternary complexes. First, ternary complex structures on both ferrihydrite and goethite are either the same or similar. Second, those cations having large adsorption constants also have large equilibrium constants for ternary complex formation. Third, ligands forming stronger solution complexes with cations will also form stronger surface ternary complexes but because of the strong solution complexes these ligands will not necessarily enhance cation adsorption.

The bacterial strain *Comamonas spp.* was isolated from the activated sludge of a wastewater treatment plant. *Comamonas spp.* could effectively degrade H_2L_p in the presence of Cd^{2+} and ferrihydrite and was therefore chosen to study the effect of H_2L_p degradation on Cd^{2+} speciation. Proton, cadmium and H_2L_p adsorption onto *Comamonas spp.* were measured. The *Comamonas spp.* titration curve is flatter than that of ferrihydrite, indicating a higher degree of site heterogeneity at the bacterial surface. Adsorption edges of Cd^{2+} adsorption onto *Comamonas spp.* occurred over about 4~5 pH units compared to those of ferrihydrite which

occurred over ≈ 2 pH units on a dry weight basis. *Comamonas spp.* can accumulate a larger amount of Cd^{2+} than ferrihydrite especially under lower pH conditions. Proton and Cd^{2+} adsorption onto *Comamonas spp.* cells over a wide sorbent/sorbate and pH range was reasonably well described by a four site non-electrostatic model. The acid-base and Cd^{2+} adsorption behaviour of *Comamonas spp.* in this work were within the range of studies of bacteria adsorption. Phthalic acid adsorption onto inactive *Comamonas spp.* was negligible over a pH range of 3 to 8 and became significant only at pH < 3 where H_2L_p was fully protonated. This is consistent with the proposed mechanism for ligand adsorption onto bacterial surfaces which involved a balance between hydrophobic interaction and electrostatic repulsion. The presence of H_2L_p decreased Cd^{2+} adsorption onto *Comamonas spp.* due to competition for Cd^{2+} between the bacterial cell surface and the formation of solution complexes of Cd^{2+}. This was accurately modelled with the Cd-L_p solution species indicating that no significant surface ternary interaction occurred between Cd^{2+}, phthalic acid and *Comamonas spp.*.

Cadmium adsorption onto ferrihydrite-*Comamonas spp.* mixtures was slightly less than the simple additive predicted adsorption of ferrihydrite plus *Comamonas spp.*. This suggests there is a weak interaction between ferrihydrite and *Comamonas spp.* and this interaction could be modelled by including a generic reaction between the ferrihydrite and *Comamonas spp.* surface sites. Cadmium distribution in a system of inactive *Comamonas spp.*-ferrihydrite in the absence and presence of H_2L_p could be predicted by combining the ferrihydrite and bacteria models with the inclusion of the ferrihydrite-bacteria interaction. The effects of H_2L_p degradation on Cd^{2+} distribution were investigated in dynamic systems with live bacteria. Results showed that Cd^{2+} adsorption in these dynamic systems was reasonably estimated with the model parameters developed in the proceeding experiments though uncertainty exists in the dynamic process with regards to H_2L_p biodegradation products and changes in the bacteria population.

This thesis was therefore able to provide a better understanding of metal speciation in complex and heterogeneous realistic environments by experimentally examining and modelling metal speciation and distribution in various systems with increasing complexity. This helps to bridge the gap of quantitative description of metal speciation from simple laboratory experiment systems to real world systems, both natural and engineered.

Acknowledgements

Before saying heaps of thanks to a number of people, I would like first to express my appreciation for the New Zealand International Doctoral Research Scholarship, and the University of Auckland Scholarship for International Students. These scholarships made it possible to start and complete this work.

There are so many people that deserve special thanks for contributing to this thesis. First of all, my supervisors, Dr Naresh Singhal, Dr Peter James Swedlund and Dr Simon Swift whose research area is different from each other but have been always very supportive. Without their advice in engineering, geochemistry and bacteriology, it would have been impossible to achieve this work. I have been very impressed by their bravery at taking on a Chinese engineering student to undertake this project. Dr P. J. Swedlund has my unceasing gratitude for his boundless patience, loud laughs and endless answers to my unending chemistry questions. To me, he is a great mentor, just like Theodore Stephanides to little Gerald Durrel (Gerald Durrel, My Family and Other Animals). His insatiable interest, pure curiosity and enthusiasm for geochemistry, his ability and great patience to illuminate any question asked, coupled with an impish sense of humour made him an excellent supervisor. Without his guidance, I would have learnt nothing about geochemistry in New Zealand.

I am likewise grateful for the friendly and invaluable technical support of Mr Glenn Boyes, Mrs Maria Rowe, Mr Abel Francis, Ms Catherine Hobbis, Dr Alec Asadov, Dr Ron Etzion and Dr Sandra Uy, which meant a lot to me. I would also like to thank Dr Gordon Miskelly, Professor Jim Metson and Dr Slyvia Sander for not only being very generous letting me use laboratory instruments, but also providing inspiration ideas to solve some problems. Thank you.

The university library is one of the best libraries I have ever come across. The general library staff are always trying their best to get useful research material via various resources; while the engineering library staff have never let me down when I had problems using the library resource.

There are so many friends that I must say thank you. Latu Harper who has been very considerate and supportive, is one of the kindest, smartest and happiest friends that I have ever met. Denise Pilbrow, a patient and intelligent woman and an amazing expert in tricky

report templates and MS word. I learned a lot from her. Anthea, for her conversation and wit during tea breaks. Anthea along with the two Andrews (Andrew Rumsby and Andrew Baddeley), offered the first iron oxide field trip in New Zealand, which has, obviously built up my great enthusiasm in this project. Yuying Han, with whom working late and during weekend was a joy, not only was the work effectively done, but also the wonderful food we had cooked was shared together during lots of laughs. Maria Rowe, a great cook and elegant friend who taught me the meaning of bonhomie, has not only given me a lot of help since I started working in the molecular and pathology lab, but also provided her homemade tasty food and cheerful conversations during tea breaks. Chunxia Yang, one of my best friends, has taken the trouble to get and send documents overseas whenever required by my visa application. The long conversation on the phone with her has been always very enjoyable. Liangxin Wu's, a very friendly family, helped me move from place to place several times. Wanhua Feng, Eun Hea Jho, Anuradha Premathilaka, Claudia Kayser, Sasha Jattansingh, Avery Gottfried, Roy Elliot, Victoria Melville, Katherine Heays, Farhan Shams, Naeeem Ejaz, Janine Louie, Benedic Uy, Emily Voyde, Jie Han and Buddhika Gunawardana are all great friends to work and talk with. Without them, I would not have learned different interesting research topics during the weekly group meeting, nor would I have enjoyed working in the postgraduate student office in the last few years. I have been very lucky to meet and get along with them.

My family, the most important support team in my life, have been given me endless support and care. While dad is always good at reminding me of study whenever he found that I have been talking too much about cooking or gardening, mum and all my sisters will never forget to remind me of getting sufficient rest during research. Andrew and his nice family, who have made studying overseas a little less hard, have given me very warm supportive care. Andrew, in the last few years during my study, has been busy driving between places during weekends, looking for my favourite food, showing me interesting natural iron oxide fields, beautiful beaches, amazing waterfalls, curious forests, marvellous plants, insects, birds and animals.

Table of Contents

List of Figures

List of Tables

Chapter 1. Introduction

The speciation and distribution of trace metals in aquatic environments is highly complex due to the large number of possible interactions with dissolved and particulate components (Salomons and Förstner 1984). This chapter presents an overview of three important components that can affect the speciation and distribution of cationic trace metals in aquatic systems; mineral oxides (particularly iron oxides), organic ligands and bacteria. This chapter also summarizes the interactions between trace metals and these components and describes approaches used to investigate these systems, including batch experiments, modelling, and spectroscopic studies. Finally the objectives and approaches of this work are presented.

1.1. Aqueous metal-ligand interactions

Dissolved metal ions in aquatic systems are usually indicated as M^{n+} as if they were bare ions in solution, whereas they are present as complexes with water or other ligands present (Martell and Hancock 1996; Salomons and Förstner 1984). A complex is said to form "whenever a molecular unit, such as an ion, acts as a central group to attract and form a close association with other atoms or molecules" and a ligand (L) is the associated atoms or molecules (Sposito 1989). Metals exist in solution as complexes formed with water molecules (sometimes termed "free metal ions") and as metal-ligand complexes, where the ligand may be inorganic or organic. If the stability constants of the solution complexes were known, they could be used to calculate and predict the equilibrium concentration of aqueous metal speciation using geochemical modelling.

Various factors can govern the stability of metal-ligand complexes. For example it was found that the ligand protonation constant (pK_A) can be related to the metal-ligand complex stability constant ($logK_{ML}$). A typical observation of linear free energy relationship (LFER) was the correlation between the pK_{A1} values of unidentate ligands and $logK_{FeL}$, which indicated that ligands with a higher pK_{A1} may form more stable solution complex with metal ions (Sposito 1989). If a complex is formed by at least two functional groups of a ligand associated with a cationic metal ion, it is termed a chelate (Sposito 1989). Chelating ligands (n-dentate) can form more stable complexes with metal ions compared to unidentate analogous, and an increase of the size of the chelating ligand ring can either increase or decrease the stability of the complexes (Martell and Hancock 1996).

The complex formed by metal ions and ligands are usually considered to contain both inner-sphere and outer-sphere structures, i.e. ligand coordinated to metal ion through direct bonding or more loosely held by the metal ion without direct bonds formed, respectively. Inner-sphere complexes are generally more stable than outer-sphere complexes as the former involve bond formation between the metal ion and the ligand. Spectroscopic studies have shown that phthalic acid can form solution complexes with Cu(II), Cd(II) Zn(II), Co(II), Ni(II), Fe(III) and U(IV) with a variety of structures depending on the pH and phthalic acid/metal ratios. The coordination modes of metal-phthalic acid complexes ranged from monodentate to hexadentate (Baca et al. 2005; Baca et al. 2004; Hanzel et al. 1990; Lucas Vaz et al. 1996; Vazquez et al. 2008). Both inorganic and organic ligands can influence aqueous metal speciation by forming complexes, moreover they can affect metal mobility in natural water systems as described in the following section.

1.2. Trace metal and ligand adsorption onto iron oxides

1.2.1 Metal adsorption onto iron oxides

Metal adsorption onto mineral particles is often considered to be an important process regulating metal partitioning between soluble and particle phases. Adsorption is "the accumulation of a chemical species at the interface between a solid phase and a fluid phase" (Violante et al. 2008). Iron oxides can be significant sorbents of metals in the aquatic environment due to their prevalence, large surface area and reactive surface properties (Michel et al. 2007; Stumm and James 1996). Iron oxides, particularly ferrihydrite, have been widely used in surface water and wastewater treatment processes (Benjamin and Sletten 1993; Dyer et al. 2004a; Jang et al. 2006), and have shown to be capable of removing inorganic contaminants such as Cd^{2+}, Cu^{2+}, Pb^{2+}, Zn^{2+}, As(III) and As(V) from polluted water.

Ferrihydrite is the iron oxide phase formed by the rapid hydrolysis of ferric ions. There is no consensus on the structure of ferrihydrite due to the small particle size and low degree of crystal order. The particle size of freshly synthesized ferrihydrite was reported to range from 1 to 10 nm, and highly porous aggregates at micrometer size can form within several hours (Michel et al. 2007; Murphy et al. 1976; Tipping 1981). Ferrihydrite shows different XRD patterns due to a variable degree of ordering. The two most common ferrihydrites are referred to as 2-line and 6-line ferrihydrite based on the numbers of poorly defined and broad peaks

shown in their XRD patterns. Due to the lack of a consensus crystal structure, as well as the uncertainty in the content of water, ferrihydrite formula has not been defined though studies have suggested quite a few possible models (Carta et al. 2009; Mavrocordatos and Fortin 2002; Michel et al. 2007; Rancourt and Meunier 2008; Towe and Bradley 1967). The stoichiometry $Fe_2O_3 \cdot H_2O$ with a molecular weight of 89 $gmol^{-1}$ was assumed in surface complexation modelling, in the case of converting the concentration of ferrihydrite and site densities (Dzombak and Morel 1990).

Cationic metal adsorption onto iron oxides is generally considered to occur exclusively by inner-sphere coordination (Spadini et al. 2003; Trivedi et al. 2003). For example, lead (II) sorbed onto ferrihydrite via inner-sphere complexation based on macroscopic and spectroscopic studies (Trivedi et al. 2003). Extended X-ray absorption fine structure (EXAFS) spectroscopy has also shown that lead formed bidentate corner- and edge-sharing inner-sphere complexes at goethite surface (Ostergren et al. 1999). Infrared (IR) spectroscopy and EXAFS spectroscopy results showed cadmium coordinated to goethite surface by forming inner-sphere complex (Boily et al. 2005; Spadini et al. 2003). A study based on EXAFS spectra result also suggested that copper formed inner-sphere complexes at the surface of goethite, hematite and lepidocrocite (Peacock and Sherman 2004).

Many solution and solid phase parameters influence the amount of adsorption on ferrihydrite surface. The solution pH has been found to be an important factor that influences metal adsorption onto ferrihydrite surface. In a binary system containing only a metal cation and ferrihydrite, adsorption of metals increases from near zero to approximately 100 % as the pH increases over 1~2 units (Benjamin et al, 1983, Dzombak and Morell, 1990). Solution protons can compete with metal ion for ferrihydrite surface sites.

Besides pH, other factors that influence metal sorption in the natural environment include the presence of ligands and bacteria. They are ubiquitous in the environment and may play a myriad of important functions in the distribution of metals between various environmental phases. The reasons are given in the following sections in this chapter.

1.2.2 Ligand adsorption and its effects on metal speciation and distribution

Various ligands can absorb onto mineral oxides in natural aquatic systems. Common aqueous ligands such as phosphate, sulfate and carbonate are all found to adsorb onto goethite, hematite and ferrihydrite (Arai and Sparks 2001; Elzinga and Sparks 2007; Geen et al. 1994;

Peak et al. 1999). Their adsorption generally behaves like typical anion adsorption onto iron oxide, decreasing with an increase in pH. Attenuated total reflectance Fourier transform infrared (ATR–FTIR) spectroscopy has demonstrated that phosphate adsorption onto hematite and ferrihydrite surface occur via inner-sphere complex formation (Arai and Sparks 2001).

However, there is uncertainty about the surface structure of other ligands sorption onto iron oxides. For example, using ATR-FTIR to investigate sulfate adsorption onto goethite, two outer-sphere complexes were proposed by Persson and Lövgren (1996), but an outer-sphere complex and an inner-sphere complex were proposed by Peak et al. (1999). The debate regarding the structures of sulfate adsorption onto iron oxide has been well discussed by Swedlund et al (2009).

Environmental organic matter such as humic substances can be effective ligands for metal ions with carboxylic and phenolic groups being the predominant ionisable functional groups (Buerge-Weirich et al. 2003; Buerge-Weirich et al. 2002; Rybicka et al. 1995; 2006). The interactions between trace metal ions, humic substances and mineral surfaces (such as iron oxides) can significantly influence the toxicity, transport and fate of trace metals (Weng et al. 2002; Weng et al. 2005; Young and Harvey 1992).

However, due to the complex nature and behaviour of humic substances (Xue and Sigg 1999), it is difficult to fully understand the interactions that occur in these systems (Klavins et al. 1999). The effect of simple organic acids on cation adsorption by iron oxides can be qualitatively similar to that of humic acids (Ali and Dzombak 1996b). For this reason research has focused on simple organic ligands with the same functional groups as humic substances such as phthalic acid (H_2L_p) and other simple aromatic carboxylic acids (Ali and Dzombak 1996c; Boily et al. 2005; Evanko and Dzombak 1999; Filius et al. 1997; Hanna 2007; Hwang et al. 2007; Tejedor-Tejedor et al. 1992). Typically simple aromatic acids sorption onto iron oxide shows anion sorption behaviour: decreasing with an increase in pH, and the increase of sorbate/sorbent ratio. However, some aromatic organic acids such as benzoic acid, 6-phenylhexanoic acid and 1-naphthoic acid exhibited unusual sorption behaviour. Their adsorption onto goethite did not decrease with the increase of the sorbate/sorbent ratio. It has been suggested that hydrophobic interactions between the acid and goethite enhance sorption at higher sorbate/sorbent ratios (Evanko and Dzombak, 1999).

The sorption of several different organic ligands onto iron oxides has been examined by spectroscopic techniques (Boily et al. 2000; Boily et al. 2005; Evanko and Dzombak 1999; Filius et al. 1997; Hanna 2007; Hwang et al. 2007; Tejedor-Tejedor et al. 1992). For example, phthalic acid sorption onto goethite has been found to involve an inner sphere complex at pH < 6 and an outer sphere complex which becomes increasingly significant at higher pH (Boily et al. 2000). This is similar to the observed behavior of some adsorbed inorganic anions such as sulfate (Elzinga et al. 2001; Ostergren et al. 2000a; Peak et al. 1999). For hematite one outer sphere complex and two inner-sphere complexes were observed for H_2L_p sorption (Hwang et al. 2007). All complexes were fully deprotonated and the inner sphere complexes were chelating (with both carboxylate groups coordinated to the surface) to either one Fe or two Fe ions.

There are several ways that these ligands could affect metal sorption onto iron oxide (Salomons and Förstner 1984; Zhang and Peak 2007):

1) Ligands, especially strong ones, can form stable aqueous species with metal ion thus reduced metal adsorption onto iron oxide surface;

2) Ligands themselves may absorb onto iron oxides and compete for sites with metal ions and thereby suppress metal adsorption;

3) Ligand adsorption onto iron oxide may reduce the surface potential and promote metal sorption;

4) Ligands can also form ternary complex with metal ion at iron oxide surface and enhance metal adsorption.

These effects might occur simultaneously in a ternary system containing metal ion, ligand, and iron oxide. The observed metal adsorption in such systems therefore is a result of these competing effects under different environmental conditions.

The majority of the studies on interactions between organic acids, iron oxides and cations have used well ordered iron oxides such as goethite. For example Cu^{2+} and Cd^{2+} sorption onto goethite was found to be enhanced in the presence of H_2L_p particularly at lower pH (Ali and Dzombak 1996b; Angove et al. 1999; Boily et al. 2005). Other aromatic acids such as trimesic acid, trimellitic acid, hemimellitic acid, pyromellitic acid and mellitic acid were all found to enhance Cd^{2+} sorption onto goethite (Angove et al, 1999). The Cd^{2+} adsorption

enhancement however depends strongly on the concentration of organic acid. For example, cadmium adsorption was increased with mellitic acid concentration increasing from 0.05 mM to 0.1 mM, but started to be suppressed when the mellitic acid concentration was greater than 1 mM. Buerge-Weirich et al. (2003) found that oxalate mostly decreased Cu^{2+} sorption, pyromellitate increased Cu^{2+} sorption by goethite with pH < 6 but decreased Cu^{2+} adsorption with pH > 6. Studies have shown that the effects of organic ligands on metal speciation and distribution depend primarily on pH and sorbate/sorbent ratio. In general, the increased metal adsorption onto iron oxides was due to the ternary complex formed between organic ligand, metal and iron oxide; while the suppressed metal adsorption was normally observed under higher pH and higher concentration of the ligand, where aqueous metal-ligand complex might dominate metal species and distribution and therefore limit sorption.

Studies of ternary cation-ligand-iron oxide systems have identified several different possible mechanisms of co-adsorption. At one extreme there is the purely outer–sphere co-adsorbed species as proposed for the Cd^{2+}-citrate-goethite system based on ATR-FTIR and the Constant Capacitance model (Lackovic et al. 2004). On the other hand ternary complexes with inner-sphere Cd^{2+} coordinated to either an inner-sphere or outer-sphere L_p^{2-} (depending on the conditions) were proposed for the Cd^{2+}-L_p^{2-}-goethite system (Boily et al. 2005). A similar combination of co-adsorbed species was proposed for the SO_4^{2-}-Pb^{2+}-goethite ternary system (Elzinga et al. 2001; Ostergren et al. 2000b). Ternary complexes were proposed to form at the goethite surface through Pb^{2+}, which was bound as a bridging bidenate complex to two adjacent surface oxygens.

1.3. Modelling metal and organic ligand adsorption onto iron oxides

A model is a "simplified representation or description of a system or complex entity, especially one designed to facilitate calculations and predictions" (Hanks 2000). Various models have been used to interpret metal ion adsorption onto iron oxides. Models such as distribution coefficients, Langmuir adsorption isotherms, Freundlich adsorption isotherms, and multisite Langmuir adsorption isotherms can describe experimental data for the conditions under which the experimental data were obtained. These models have limited ability to predict metal distribution once the conditions (such as pH or ionic strength) are changed. Moreover, because only simple parameters are used in these models, metal speciation cannot be described in complex systems. In addition, metal ions, ligands and iron oxides encountered in aqueous systems have a surface charge which may be strongly affected

by pH. The surface charge at iron oxide surface may also change during metal and ligand adsorption. The effect of surface charge that need to be considered during sorption process cannot however be included by these models.

Several surface complexation models that include surface charge effects have been developed and used to describe potentiometric titration and sorption onto iron oxides. One of the major advantages of these models is that they can include all surface and solution species, so that metal speciation and distribution can be calculated. Therefore the parameters optimized under certain experimental conditions in surface complexation models can be applied to other conditions with changing pH, ionic strength, or sorbate/sorbent ratios. Four commonly used surface complexation models are the constant capacitance model, the diffuse layer model (DLM), the triple layer model (TLM) and the charge distribution multisite complexation model (CD-MUSIC). The constant capacitance model, DLM and TLM differ in their level of detail used to describe the charge distribution. These three models use a similar approach to describe reactions at an oxide surface without specific reference to the oxide surface structure. In contract, the CD-MUSIC model uses the oxide's crystal structure to distinguish between different types of surface sites and is applicable to metal adsorption onto iron oxides with well-defined crystal structure such as goethite (Boily et al. 2005; Venema et al. 1996), but not applicable to ferrihydrite for which the surface is not well defined.

The DLM was chosen for this work to describe adsorption onto ferrihydrite for several reasons. There is a large database of self consistent adsorption constants for the sorption of many species onto ferrihydrite (Dzombak and Morel 1990). The DLM can be readily incorporated into several geochemistry speciation models such as Visual MINTEQ, and mass transportation models therefore the adsorption parameters can be used for modelling metal geochemistry. Another reason is that the DLM has the ability to describe adsorption without the need for parameters such as capacitances or charge distribution. But it can describe the main features of adsorption reactions such as the effects of pH, ionic strength, or sorbent concentration. In addition the use of the DLM allows for comparison with adsorption constants for ternary complex formation with several previous studies, including ternanry systems such as goethite-metal-phthalic acid, goethite-metal-sulfate, and ferrihydrite-metal-sulfate.

1.3.1 Diffuse layer model (DLM)

The DLM depends on several main assumptions (Dzombak and Morel 1990; Sposito 1984): The oxide surface-water interface is assumed to comprise of a charged surface layer and a charged diffuse layer in solution. At this interface, sorption takes place at specific surface hydroxyl groups, while the distribution of the counterions in solution is assumed to occur in the diffuse layer. The sorption of cations (including protons) and anions by the surface hydroxyl groups results in a surface charge, which is assumed to reside in one surface layer. The surface charge is related to the surface potential by the Gouy-Chapman theory. All the surface sorption reactions are considered to be surface complexation and can be described by mass law equations. The equilibrium constant involves an intrinsic adsorption constant which is independent of surface charge, and a coulombic correction factor which is essentially an activity coefficient that takes account of the effect of surface charge on sorption reactions of charged species.

In aquatic systems, iron oxides contain specific surface hydroxyl groups on which cation or anion sorption occurs (Stumm and James 1996). Cation and anion sorption onto hydrous oxides surface depends strongly on pH. Generally, cation sorption increases with an increase in pH. Conversely, anion sorption decreases with an increase in pH. The sorption of cations and anions is commonly presented on plots of percent sorbed sorbate versus pH, termed “pH edges”. The position of a pH edge depends on the sorbate/sorbent ratio. An isotherm is a plot of log solution sorbate concentration versus log (sorption density) at constant pH. On an isotherm plot, data with a slope of 1 indicates that the sorption in this region is proportional to free ion concentration and there is just one type of surface site termed Langmuir adsorption. Anion sorption isotherms generally have a slope of one with a plateau to zero as site saturation is approached at higher sorbate/sorbent ratios, indicating that there is only one type of sites present. When there is more than one type of sites, sorption initially occurs at the high-affinity sites and then at the more abundant low-affinity sites. Sorption occurs at more than one site type it is not proportional to the free ion concentration and the slope of the isotherm is less than 1. This type of sorption isotherm is typically observed for cation sorption.

In the case of ferrihydrite, ≡FeOH is used to express a neutral surface hydroxyl group and two types of sorption sites are considered to be present at the surface to describe cation adsorption (Dzombak and Morel 1990). There is a small number of high affinity sites (termed

type one sites and denoted ≡Fe^{s}OH) and a larger number of low affinity sites (termed type two sites and denoted ≡Fe^{w}OH). This is supported by a Cd_K EXAFS study (Spadini et al. 2003), where Cd-Fe linkages were observed with one linkage becoming more evident at higher $Cd_{(T)}$/ferrihydrite ratio. The values of type one and type two site densities for ferrihydrite used in this work are 0.005 mol (mol Fe)$^{-1}$ and 0.2 mol (mol Fe)$^{-1}$, respectively (Dzombak and Morel 1990). The affinity of all surface sites for anion sorption is assumed to be the same, although more than one surface species with varying degrees of protonation might be considered (Dzombak and Morel 1990). The surface complexation reactions for proton, divalent cation (for example, Cu^{2+} and Cd^{2+}) and anion (such as phthalate) sorption onto ferrihydrite surface are given in Table 2.4.

In the DLM all the surface sorption reactions can be described by mass law equations and the equilibrium constants involve an intrinsic adsorption constant and a coulombic correction factor. For example, a divalent cation (M^{2+}) sorption onto ferrihydrite can be described by Equation 1.1, where K_M^{app} represents an apparent equilibrium constant and can be expressed by equation 1.2 ([ ] represents molar concentrations of surface species and {} represent the activities of solution species).

$$\equiv FeOH^0 + M^{2+} \Leftrightarrow \equiv FeOM^+ + H^+ \qquad K_M^{app} \qquad \text{Eq. 1.1}$$

$$K_M^{app} = \frac{[\equiv FeOM^+]\{H^+\}}{[\equiv FeOH^0]\{M^{2+}\}} \qquad \text{Eq. 1.2}$$

$$K_M{}^{app} = K_M{}^{INT} \exp\left(\frac{\Delta Z F \psi}{RT}\right) \qquad \text{Eq. 1.3}$$

An expression for the coulombic contribution to the position of the equilibrium can be obtained from Gouy-Chapman theory. The intrinsic constant (K_M^{INT}), which corresponds to sorption on an uncharged surface is related to K_M^{app} by Equation 1.3, where Ψ is the surface potential (V), R the molar gas constant (8.314 VC mol^{-1} K^{-1}), T the absolute temperature (K), $exp\ (-F\Psi/RT)$ the coulombic factor, ΔZ the net change in the charge of the surface species.

1.4. Metal adsorption onto bacterial cells

Bacteria can present a significant reactive surface area in both aquatic and soil systems. This is due to their large surface area-to-volume ratio as well as the presence of various surface functional groups which can have a high affinity for absorbing metal ions (Borrok et al. 2004;

Boyanov et al. 2003; Fowle and Fein 2000; Mullen et al. 1989). Since 1970s bacterial adsorption of metal ions has received increasing attention. The biosorption of metal ions onto bacterial cells mainly includes ionic interactions and complex formation between metal ions and organic acid functional groups at the cell surface (Boyanov et al. 2003; Gabr et al. 2008). Spectroscopic techniques such as IR and XAFS have demonstrated that there are numerous functional groups including carboxyl, phosphoryl, amino and phenolic groups (Boyanov et al. 2003; Kelly et al. 2001). For metal biosorption, numerous EXAFS spectroscopy studies have indicated that carboxyl and phosphoryl functional groups account for metal adsorption onto bacterial surface, no matter if the bacteria are Gram-positive (Boyanov et al. 2003; Kelly et al. 2001) or Gram-negative (Hennig et al. 2001; Toner et al. 2005). More recently EXAFS spectroscopy examined Cd^{2+} adsorption onto bacterial consortia containing both Gram-positive and Gram-negative bacteria growing from natural environment (river water) and engineered systems (manufacturing gas plant). It has been proposed that only a limited number of bacterial surface functional groups are responsible for Cd^{2+} biosorption despite of the complex mixture of the bacteria. Three types of bacterial surface functional groups (carboxyl, phosphoryl and sulfhydryl), or even only two types of bacterial surface functional groups (carboxyl and phosphoryl) were sufficient to model Cd^{2+} adsorption onto bacterial consortia from river water or a gas plant (Mishra et al. 2009).

Adsorption of a wide variety of metal ions onto both Gram-positive and Gram-negative bacteria has been qualitatively and quantitatively evaluated (Beveridge 1978; Beveridge and Koval 1981; Borrok and Fein 2005; Burnett et al. 2007; Daughney et al. 2000; Mullen et al. 1989). One important factor for metal adsorption onto bacterial surface is pH. The pH at which the total number of positive charges equals the number of negative charges is referred to as the point of zero charge (PZC). The PZC of bacterial cells was reported to be in the range of pH 1.75 ~ 4.15 (Harden and Harris 1953), and therefore bacterial cells were almost always negatively charged. In general metal adsorption onto bacterial cells increases with pH increasing from around 2 to 8 (Burnett et al. 2007; Ginn and Fein 2008; Johnson et al. 2007). However it has been observed that metal adsorption onto bacterial cells can also decrease as the pH increases above pH ≈ 8 (Burnett et al. 2007). Compared to metal adsorption onto ferrihydrite which increases from zero to 100 % over approximately 2 pH units (Dzombak and Morel 1990), metal sorption onto bacteria generally showed a more gradually sigmoid curve over about 3 ~ 5 pH units. This implies a higher degree of site heterogeneity at the surface of the bacteria than that on the ferrihydrite surface. The average pK_A values for

proton adsorption onto bacterial surface ranged from ~3 to ~13. Other factors such as ionic strength, bacterial growth phase and growth conditions have been shown to influence the bacterial metal adsorption process. Generally more metal adsorption onto bacterial cells was observed at lower ionic strength (Borrok and Fein 2005; Daughney and Fein 1998a; Ledin et al. 1997). However the opposite behaviour has also been observed (Daughney and Fein 1998a). Cadmium adsorption was lower for *Bacillus subtilis* cells from the exponential phase than those from the stationary or sporulated phases. Adsorption of Cd^{2+} remained constant from the stationary to the sporulated phase (Daughney et al. 2000).

The adsorption of organic ligands onto bacterial cells was proposed to be the result of a balance between hydrophobic interaction and electrostatic repulsion (Fein and Delea, 1999). The sorption of EDTA and 2,4,6-trichlorophenol by *Bacillus subtilis* cells increases below pH 2.5 and 8.5, respectively (Daughney and Fein 1998b; Fein and Delea 1999). The pK_{A1} values for EDTA and 2, 4, 6-trichlorophenol are 1.9 and 6.0, respectively and the bacterial surface is negatively charged at pH $\geq$ 2. For both organic ligands when the pH < pK_{A1}, they are fully protonated and hydrophobic interactions between bacterial surface and organic ligands dominate over electrostatic repulsion. When the pH increases above the pK_{A1}, the negative charge on the bacterial surface increases and electrostatic repulsion between the organic ligands and bacterial surface dominates hydrophobic interaction, and adsorption decreases. It has been suggested that there might be a correlation between the pK_{A1} and logK values for organic acid adsorption onto bacterial surface (Fein and Delea 1999).

Humic acid adsorption onto *Bacillus subtilis* decreased from ~ 100 % at pH ~ 2 to nearly zero at pH ~9 (Fein et al. 1999; Wightman and Fein 2001). It was proposed that hydrophobic interaction between humic acid molecule and bacterial surface caused the biosorption at lower pH, and an increase in repulsive force decreased humic acid biosorption at higher pH. Compared to EDTA and 2, 4, 6-trichlorophenol, the adsorption of humic acid onto *Bacillus subtilis* is over a wider pH range possibly due to its larger size and multi-functional group structure.

Even though organic ligands can form complexes with metal ions or absorb onto the bacteria, there has been few studies on the effect of organic ligands on metal adsorption by bacteria. One modelling study indicated that either Cd^{2+}-humic substances or Cd^{2+}-bacterial surface species could dominate cadmium speciation in aquatic systems depending on the conditions (Borrok and Fein 2004) (Figure 1.1). Cadmium adsorption onto *Bacillus subtilis* cells was

inhibited by humic acid under mid to high pH conditions due to the formation of aqueous humate-Cd^{2+} species (Wightman and Fein 2001). Aqueous EDTA significantly inhibited Cd^{2+} adsorption onto *Bacillus subtilis* because of the formation of solution complex between Cd^{2+} and EDTA (Fein and Delea 1999). Phthalic acid adsorption onto bacterial surface and its effect on metal adsorption onto bacterial cells has not been reported.

Figure 1.1 was removed. It can be found in Fig. 3 and Fig. 4, page 3050 in reference: Borrok D, Fein JB. 2004. Distribution of protons and Cd between bacterial surfaces and dissolved humic substances determined through chemical equilibrium modeling. *Geochimica et Cosmochimica Acta* 68(14):3043-3052.

Figure 1.1 Model results for 0.44 µM Cd^{2+} adsorption onto bacteria in the presence of humic acid. a) 0.05 mgC L^{-1}, Humic acid (HA)/Fulvic acid(FA), 10^8 cells mL^{-1}; b) 20 mgC L^{-1} HA/FA, 10^4 cells mL^{-1}. Solid curve represents Cd-HA/FA complexes and dashed curve represents Cd bacteria complexes (Borrok and Fein 2004).

1.5. Modelling metal adsorption onto bacterial surface

A range of geochemical and thermodynamic models have been developed to quantitatively evaluate metal adsorption onto bacterial cells, among which the Langmuir and Freundlich models were frequently used (Mullen et al. 1989; Seki et al. 1998; Small et al. 1999). More recently electrical double layer models, as well as Donnan electrostatic models have been used to describe metal sorption by taking electrostatic effects into account (Daughney and Fein 1998a; Martinez et al. 2002; Yee and Fein 2001; Yee and Fein 2003). Metal ion adsorption onto a variety of bacteria has been recently quantitatively evaluated using non-electrostatic surface complexation modelling (Borrok et al. 2004; Borrok and Fein 2005; Ginn and Fein 2008).

A non-electrostatic model was used to describe Pb^{2+} and Cd^{2+} adsorption onto several bacterial strains, and gave better fit for Sr^{2+} adsorption compared to the DLM or TLM (Borrok and Fein 2005). The four site non-electrostatic surface complexation model was used in this work to describe proton and Cd^{2+} sorption onto the surface of *Comamonas spp.*. In this

modelling approach, four types of site are used to describe proton or metal sorption onto the cells representing bacterial surface functional groups. The sites are termed RAH, RBH, RCH and RDH. A surface site deprotonation can be expressed as Equation 1.4 and the acidity constant K_{RAH} can be described with Equation 1.5, where RA^- and RAH^0 represent deprotonated and protonated sites, respectively with activity coefficients of 1.

$$RA^- + H^+ \Leftrightarrow RAH^0 \qquad K_{RAH} \qquad \text{Eq. 1.4}$$

$$K_{RHA} = \frac{[RA^-]\{H^+\}}{[RAH^0]} \qquad \text{Eq. 1.5}$$

Metal ion sorption onto the bacterial surface has been described by surface complex reactions. Borrok et al (2004) tested various reactions to model Cd^{2+} sorption onto bacterial surfaces using both protonated and deprotonated surface sites. The sorption model that best described the data involved a deprotonated monodentate species on each type of site. In other words, cadmium sorption onto bacterial cells due to the formation of complex with type A sites can be expressed by Equation 1.6, and the sorption equilibrium constant K_{RACd} is given in Equation 1.7.

$$RA^- + Cd^{2+} \Leftrightarrow RACd^+ \qquad K_{RACd} \qquad \text{Eq. 1.6}$$

$$K_{RACd} = \frac{[RACd^+]}{[RA^-]\{Cd^{2+}\}} \qquad \text{Eq. 1.7}$$

Cadmium adsorption onto *Comanonas spp.* cells has not been reported, though it has been proposed that metal-bacteria adsorption does not strongly depend on the bacteria species and can be described by a generalized model. This conclusion was drawn from the examination of Cd^{2+} adsorption onto seven bacterial strains (two Gram-negative and five Gram-positive species) and a range of natural bacterial consortia (Borrok et al. 2004). In contrast, some studies found that the concentrations of bacterial surface adsorption sites were remarkably different between different bacterial strains. For example, metal binding site concentrations on *Alcaligenes eutrophus* were reported to be 2.4 fold larger than those of *Rhodobacter sphaeroide* (Seki et al. 1998). Therefore while there may be a general trend that describes cation adsorption on many bacterial species, there are also exceptions to this trend.

1.6. Metal adsorption in bacteria-iron oxide systems

Little attention has been paid to metal speciation and distribution in systems containing both organic and inorganic surfaces, though bacterial-iron oxides composites have been found in various environmental systems and have important implications for metal fate and transportation in geochemical environments (Ferris et al. 2000; Ferris et al. 1999; Ferris et al. 1989; Kennedy et al. 2003; Martinez and Ferris 2005; Small et al. 1999). It has been shown that metal sorption of bacteria-mineral composites depended strongly on the relative proportion of bacterial matters in the composites (Ferris et al. 2000; Ferris et al. 1999; Martinez et al. 2003). In surface complexation modelling, "the equilibrium constants determined in systems that isolate specific adsorption reactions can be used to model more complex systems by these results into a computational model" (Yee and Fein 2003). Using surface complexation modelling, Yee and Fein (2003) predicted Cd^{2+} speciation in complex systems which contained both bacteria and ferrihydrite by combining adsorption reactions and thermodynamic stability constants for Cd^{2+} adsorption onto bacteria, as well as Cd^{2+} adsorption onto ferrihydrite. However the interaction between bacteria and ferrihydrite was not taken into account because cadmium adsorption onto ferrihydrite-bacteria composites was not experimentally examined.

Scan electron microscopy (SEM) and transmission electron microscopy (TEM) results have shown that there was a ferrihydrite masking of bacterial surface (Glasauer et al. 2001; Kulczycki et al. 2005; Small et al. 1999). Recently *in situ* ATR-FTIR spectroscopy has revealed significant bonding between surface functional groups of bacteria and hematite (Parikh and Chorover 2006). The interaction between iron oxides and bacterial surface is one reason that makes the sorption in such mixed adsorbents systems non-additive, which makes it difficult to quantify trace metal distribution in biotic multi-components systems (Kulczycki et al. 2005; Martinez and Ferris 2005; Martinez et al. 2003). Moreover, bacterial surfaces possess a variety of reactive sites resulting in a high degree of complexity when modelling metal distribution in mixed bacteria-iron oxide systems.

One site Langmuir sorption model was used to compare cationic metal ion adsorption onto bacteria, ferrihydrite and bacteria-ferrihydrite composites, and the sorbents showed different affinities for metal: bacteria > bacteria-ferrihydrite composite > ferrihydrite (Kulczycki et al. 2005; Small et al. 1999). Site densities of bacteria-iron oxide composites found in natural environment were derived by a multisite Langmuir model, and the result also supported the

conclusion that bacteria has higher Cd^{2+} affinity than the composite mixture (Martinez et al. 2004). However, the Langmuir adsorption model does not require detailed description of surface and solution reaction principles and therefore the model does not account for metal species distribution in the solution or on the surface.

Surface complexation modelling could be applied to metal-bacteria-iron oxide multi-component systems if reactions that describe the effects of the bacteria-iron oxide interaction on metal sorption could be included. This work experimentally examined Cd^{2+} adsorption onto ferrihydrite-bacteria composites, and quantified Cd^{2+} species distribution in these complex systems over a wide range of pH. Surface complexation modelling for ferrihydrite and *Comamonas spp.* were combined and attempts were made to model the effect of the interaction between bacteria and ferrihydrite on Cd^{2+} adsorption.

1.7. Biodegradation of phthalic acid

Aquatic systems that include a biological component will to some degree be in a state of flux. Therefore to understand trace metal speciation in natural systems it is necessary to consider the effect of biological activity. Organic ligands may be metabolised, new organic ligands may be produced and the partial pressure of oxygen and carbon dioxide might change. One of the objectives of this work is to explore the effect of bacterial activity on Cd^{2+} speciation, in particular, the biodegradation of H_2L_p. This section reviews H_2L_p biodegradation. Organic ligands can play an important role in controlling the toxicity, transport, and fate of trace metals in aquatic environment. Phthalic acid is the organic ligand used in this work for the reasons given in Section 1.1.2. In addition, phthalic acid can be an intermediate during phthalic acid ester metabolism (Staples et al. 1997; Wang et al. 2003). Phthalate biodegradation has been studied due to the interest in synthetic phthalic acid esters, which are used as plastizing agents and are now ubiquitous in the environment and have been listed as priority pollutants (Fan et al. 2004; Jianlong et al. 2004; Kleerebezem et al. 1999; Quan et al. 2005; Staples et al. 1997; Wang et al. 1996; Wang et al. 1997a; Wang et al. 1997b).

Various Gram-positive and Gram-negative bacterial strains, such as *Bacillus subtilis*, *Comamonas sp.*, *Pseudomonas sp.*, as well as bacteria mixtures were found to be able to degrade H_2L_p under both aerobic and anaerobic conditions (Aftring et al. 1981; Aftring and Taylor 1981; Engelhardt et al. 1976; Fan et al. 2004; Kleerebezem et al. 1999; Taylor and Ribbons 1983; Wang et al. 2003). The initial pH was found be the most important factor that

can influence phthalic acid metabolism. The preferred pH range for H_2L_p and phthalic acid esters metabolism is between 6.0 and 7.0 (Fan et al. 2004; Taylor and Ribbons 1983; Wang et al. 2003), and degradation was not detected with an initial pH of 4.0 (Fan et al, 2004). Other factors such as temperature and bacterial growth nutrients can affect the biodegradation process. However whether iron oxides or trace metals influence H_2L_p metabolism has not been reported. These two factors need to be considered in this work.

Staples et al (1997) summarized H_2L_p degradation pathways and the intermediates produced vary in aerobic or anaerobic environments, and with bacterial strains. Under aerobic conditions, phthalic acid was normally degraded through either 3,4 or 4,5-dihydroxyl phthalate to protocatechuate, with either acetate or pyruvate occurring in late degradation stage. Gram-negative bacteria such as *Pseudomonas sp.* metabolizes phthalate through *cis*-4,5-dihydroxy-4,5-dihydrophthalate and 4,5-dihydroxyphthalate to 3,4-dihydroxybenzoate (Nakazawa and Hayashi 1977; Ribbons and Evans 1960). However Gram-positive bacterium *Arthrobacter keyseri* 12B converts phthalate from *cis*-3,4-dihydroxy-3,4-dihydrophthalate and 3,4-dihydroxyphthalate to 3,4-dihydroxybenzoate (Eaton and Ribbon, 1982), which was further transformed to pyruvate (Eaton, 2001). This work focused on how Cd^{2+} distribution in complex aquatic environments might be affected due to H_2L_p metabolism in an aerobic system.

1.8. Objective and approach

1.8.1 Objectives

Since the 1950's metal sorption onto mineral surfaces has been recognized as an important process influencing metal speciation and distribution in aquatic environments and there have been a large number of studies on metal sorption onto iron oxides. Geochemical models have been developed to interpret this process and spectroscopic studies have been used to probe the surface structures formed during sorption. Over time more complex systems have been investigated to gain a better understanding of metal fate and transport in real environments. For example the interactions between metals, ligands and iron oxides in ternary systems have been and are currently being studied. Research has also focused on the role that biosorption has on the distribution of metal ions in the aquatic environment because microorganisms are ubiquitous in the environment and can also provide reactive surface for binding metal ions. Models to describe metal adsorption onto bacterial surface have been developed. Both

bacteria and mineral particles can be present in natural environment and engineered environments. Only recently have the interactions between bacteria and mineral oxides been investigated. To date no research has been done on metal speciation in systems containing bacteria, mineral oxides and organic ligands though these components are ubiquitous in most real aquatic environments and are important factors in determining the fate and distribution of metal ions.

Therefore the main objective of this thesis was to describe and understand metal speciation and distribution in a model complex biogeochemical systems by incrementally increasing the complexity of our experimental systems from binary to ternary, and then to quaternary systems. Cadmium, copper and phthalic acid adsorption onto either ferrihydrite or bacterial surfaces in binary systems were investigated to examine metal and organic ligand adsorption behaviour in simple systems. Several types of ternary systems were studied based on the results from binary systems: organic ligand-metal-iron oxide, organic ligand-metal-bacteria, and metal-bacteria-iron oxide. The aim of investigating ternary systems is to examine the effects of organic ligand on metal distribution in systems containing either iron oxide or bacteria, as well as to understand and describe metal adsorption onto iron oxide-bacteria composites. Metal distribution in iron oxide-bacteria-organic ligand-metal ion quaternary systems was initially investigated by using inactive bacteria to avoid organic ligand degradation. Finally a dynamic quaternary system is studied in which bacterial metabolism of the organic ligand occurs. Metal speciation in these systems is described by surface complexation modelling based on experimental data.

1.8.2 Approach

Chapter 1 gives an overview of studies on how mineral oxides, organic ligands and bacteria affect metal behaviour in complex systems. The principles of the models used to describe metal adsorption in abiotic and biotic systems are also described.

Chapter 2 describes the materials and methods used. The synthesis and characterization of ferrihydrite is presented, as well as the incubation, isolation, storage, identification, and quantification of the bacteria used in this work. Experimental approaches for metal and organic ligand adsorption onto ferrihydrite and bacteria in binary, ternary and quaternary systems are described. The experimental design to test and optimize phthalic acid biodegradation conditions is provided. The methods of optimizing model sorption parameters in abiotic and biotic systems are described.

Chapter 3 describes Cu^{2+}, Cd^{2+} and H_2L_p adsorption onto ferrihydrite in binary systems. Constants for Cu^{2+} and Cd^{2+} adsorption onto ferrihydrite derived from the experimental data in this work are compared with reported values. The optimized sorption parameters to describe phthalic acid adsorption onto ferrihydrite are presented.

Chapter 4 describes the effect of H_2L_p on Cu^{2+} and Cd^{2+} adsorption onto ferrihydrite. The data are compared to similar ternary systems with H_2L_p or sulphate and goethite or ferrihydrite. Several properties of ternary complexes are suggested by examining the relationship between binary metal adsorption constants and the ternary complex adsorption constants from these systems.

Chapter 5 tests the ability of two bacterial strains to degrade H_2L_p under the conditions of this study. The optimized conditions for H_2L_p biodegradation are presented. The results for determining bacteria cell concentrations by using dry weight/wet weight ratio and bacteria colony population are given. In this chapter the reasons for using *Comamonas spp.* and Cd^{2+} for subsequent are provided.

Chapter 6 describes Cd^{2+} and H_2L_p adsorption onto bacteria in binary and ternary systems, and includes acid-base titrations of *Comamonas spp.*. The titration and adsorption results for *Comamonas spp.* (the bacterium used in this work) are compared with those for other bacteria species from previous studies. The effect of H_2L_p on Cd^{2+} adsorption onto *Comamonas spp.* is described.

Chapter 7 describes Cd^{2+} adsorption onto *Comamonas spp.*-ferrihydrite composites in the absence and presence of H_2L_p in ternary and quaternary systems. Two quaternary systems were studied. Initially a "static" system using dead *Comamonas spp.* was studied where there was no change in H_2L_p concentration. Then a "dynamic" system with active *Comamonas spp.* metabolising H_2L_p was studied.

Chapter 8 summarizes the findings and presents the environmental significance of this work in natural environments and in engineered systems.

Chapter 2. Materials and Methods

2.1. Abiotic systems

2.1.1 Materials

Analytical grade reagents were used in this work. MilliQ 18.2 MΩ.cm grade water was acidified with HNO_3 to pH 3 and bubbled with $N_{2(g)}$ for 3~5 h to remove CO_2. At all times solutions were either in sealed vessels or kept under a stream of $N_{2(g)}$ to minimise CO_2 inclusion. The NaOH solutions used were prepared by diluting the clear supernatant from a 50 % w/w solution of NaOH in CO_2-free water. Phthalic acid (as sodium phthalate, 1 M, pH ≥ 12), copper nitrate (1000 ppm, pH ≤ 3) and cadmium nitrate (1000 ppm, pH ≤ 3) stock solutions were used for the adsorbents. High performance liquid chromatography (HPLC) grade methanol was used in analyzing dissolved phthalic acid (H_2L_p). Unless stated, all the solutions in this work were on a weight basis, using mols or millimoles per kilogram of solution. In dilute solutions, 1 mgL^{-1} is approximately equal to 1 $mgkg^{-1}$. For the sake of brevity, all the solution concentrations used in this work were expressed in terms of molarity, M (mol L^{-1}).

Ferrihydrite was synthesized based on the method described in Schwertman and Cornell (1991), by adding NaOH to a $Fe(NO_3)_3 \cdot 9H_2O$ solution (pH ≈ 2) in a polypropylene bottle while stirring vigorously until the pH was raised to 7.0~8.0. The ferrihydrite was observed to form as a fluffy dark reddish brown precipitate. The concentration of Fe in ferrihydrite suspension ranged from 1 to 13 mM. The synthesized ferrihydrite suspension was aged overnight (18~24 h) in the capped polypropylene bottle. To characterize the product the suspension was then washed by MilliQ water three times by centrifugation and decanting before being freeze-dried. The ferrihydrite structure was examined with X-ray diffraction (XRD, Bruker D8 Advanced) at the Department of Chemical and Materials Engineering, University of Auckland (UoA). The power was 40 kV and 40 mA with a Cu Kα (λ =1.5406Å) irradiation. Two poorly defined and broad peaks in the XRD verified the precipitate to be 2-line ferrihydrite. As discussed in Chapter 1, there has been no defined stoichiometry for ferrihydrite. In this thesis, the concentration or dry weight of ferrihydrite is

all on a basis of stoichiometry $Fe_2O_3 \cdot H_2O$ with a molecular weight of 89 $gmol^{-1}$ (Dzombak and Morel 1990).

The specific surface area of freeze-dried ferrihydrite was determined with the Brunauer–Emmett–Teller (BET) method from $N_{2(g)}$ adsorption isotherms obtained at 77K. An analysis of the isotherm indicated that the surface area was 206 m^2g^{-1}, which is consistent with the previously reported range for BET values of 200~300 m^2g^{-1} (Dzombak and Morel 1990). However the reported surface areas for ferrihydrite vary from 100 to 700 m^2g^{-1} depending on the measurement method (Cornell and Schwertmann 2003). For example, for the same ferrihydrite sample, the surface area was determined to be around 200 m^2 g^{-1} using BET method from $N_{2(g)}$ sorption isotherm but an ethylene glycol surface area value over 600 m^2 g^{-1} was obtained (Pyman and Posner 1978). An estimated value of 600m^2 g^{-1} was used in this work for the surface complexation modelling as recommended (Davis and Leckie 1978; Dzombak and Morel 1990; Pichler and Veizera 1999).

2.1.2 Methods to measure adsorption onto ferrihydrite

Ferrihydrite suspensions were prepared as described above and aged overnight and then the ionic strength was adjusted to the desired value. Samples were prepared by adding 30 mL of the ferrihydrite suspension to a number of 50 mL polyethylene centrifuge tubes. Phthalic acid, Cu^{2+}or Cd^{2+} was added to the ferrihydrite suspension at the required concentrations. In ternary experiments the Cu^{2+} or Cd^{2+} was added directly after the addition of H_2L_p. Nitric acid (0.001 to 0.1 M) or sodium hydroxide (0.001 to 0.1 M) solution was then added to each sample to yield data over a range of pH values between 3.5 and 8.5. The capped tubes were then equilibrated at room temperature for 24~48 h on an end-over-end mixer.

The pH was then re-measured before the sample was centrifuged and the supernatant was filtered through a 0.2 μm Satorius Minisart single use cellulose acetate membrane filter. The first 1-2 mL filtrate was discarded for all samples to minimize the loss of sorbate (Ali and Dzombak 1996a). To analyze the concentration of aqueous-phase H_2L_p, about 1.5 mL of the filtrate was collected in 2 mL autosampler chromatography vial. For the analysis of Cu^{2+} or Cd^{2+}, about 10 mL of the filtered supernatant was collected in 15 mL polyethylene tubes and acidified with HNO_3 to pH≤2. Dilution was performed if needed for the analytical requirements. Adsorbed concentrations of Cu^{2+}, Cd^{2+} and H_2L_p were calculated as the difference between the total and solution concentrations.

2.1.3 Analytical methods

The pH was measured using a WTW pH electrode Sen Tix 20 with an inoLab 740 pH meter. The pH electrode was calibrated using pH 4, 7 and 10 buffer solutions 16~24 h before use. The pH value of each sample was measured with $N_{2(g)}$ purging of the headspace while stirring. Dissolved Cu^{2+} and Cd^{2+} concentrations were determined by flame atomic absorption spectrometry (FAAS) (PerkinElmer). Dissolved Cd^{2+} was analyzed by FAAS or graphite furnace atomic absorption spectrometry (GFAAS, Varian) with atomizer pyrolytic coated partitioned graphite tube. Samples with Cd^{2+} concentrations lower than 50 ppb were analyzed by GFAAS. The analysis difference between FAAS and GFAAS ranged from 1.4 % to 7.1 % according to the results from eight samples analyzed using both instruments. The concentrations of ferrihydrite were determined by measuring Fe with FAAS after acidification of the unfiltered parent suspension. The instrumental parameters for FAAS and GFAAS are given in Tables 2.1 and 2.2, respectively. The H_2L_p concentration was analyzed by HPLC (Dionex DX-120). The analysis conditions are: a mobile phase of methanol : H_2O : H_3PO_4 = 30 : 70 : 0.01 (V : V : V) with pH of 3.5 and a flow rate of 1.5 mL min^{-1}, a Phenomenex® Gemini 5u C18 110a 150 mm × 4.6 mm × 5 μm Reversed Phase HPLC Column, and a UV-VIS detector with a wavelength of 280 nm.

Table 2.1 Instrumental parameters for the measurement by FAAS

Element	*Wavelength (nm)*	*Lamp current (mA)*	*Flame stoichiometry*	*Bandwidth (nm)*	*Fuel*	*Support*
Cu	324.7	4	oxidizing	0.5	acetylene	air
Cd	228.8	4	oxidizing	0.5	acetylene	air
Fe	248.3	5	oxidizing	0.2	acetylene	air

Table 2.2 Operating conditions of heating programs for Cd^{2+} analysis by GFAAS [a]

Step No.	*Temperature (°C)*	*Time (sec)*	*$N_{2(g)}$ purging flow (L min^{-1})*
1	85	5	3.0
2	95	40	3.0
3	120	10	3.0
4	250	5	3.0
5	250	1	3.0
6	250	2	0.0
7	1800	0.8	0.0
8	1800	2	0.0
9	1800	2	3.0

[a] lamp current, wavelength and bandwidth are the same as that given in Table 2.1 for Cd.

2.1.4 Model parameter optimization

The DLM was used in this work to describe Cu^{2+}, Cd^{2+} and H_2L_p sorption onto ferrihydrite. Solution reactions are given in Table 2.3 and the equilibrium constants for the aqueous reactions were taken from the Visual MINTEQ version 2.51 database (Gustafsson 2006). Visual MINTEQ is a Windows version of MINTEQA2 ver 4.0, which was released by the USEPA in 1999. In Visual MINTEQ, surface complexation models are included that can calculate metal speciation and simulate the distribution of ions between adsorbed and dissolved phases in a colloidal suspension. The database "HFO with DLM" for cation and ions sorption onto ferrihydrite based on DLM from Visual MINTEQ was used for the modelling. Adsorption reactions for H_2L_p were added to the database.

Table 2.3 Aqueous reactions used in the model [a]

aqueous reaction expressions	*logK (I=0)*
$[OH] = [H^+]^{-1}(\gamma)^{-2}K$	-13.998
$[H_2L_p]_{aq} = [H^+]^2[L_p^{2-}](\gamma_1)^2\gamma_2K$	8.361
$[HL_p^-] = [H^+][L_p^{2-}]\gamma_2K$	5.411
$[NaL_p^-] = [Na^+][L_p^{2-}]\gamma_2K$	0.8
$[Cu(OH)_2^0]_{aq} = [Cu^{2+}][H^+]^{-2}(\gamma_1)^{-2}\gamma_2K$	-16.23
$[Cu(OH)_3^-] = [Cu^{2+}][H^+]^{-3}(\gamma_1)^{-4}\gamma_2K$	-26.64
$[Cu(OH)_4^{2-}] = [Cu^{2+}][H^+]^{-4}(\gamma_1)^{-4}K$	-39.73
$[Cu_2(OH)_2^{2+}] = [Cu^{2+}]^2[H^+]^{-2}(\gamma_1)^{-2}\gamma_2K$	-10.494
$[Cu_2OH^{3+}] = [Cu^{2+}]^2[H^+]^-(\gamma_1)^{-1}(\gamma_2)^{2+}(\gamma_3)^{-1}K$	-6.710
$[Cu_3(OH)_4^{2+}] = [Cu^{2+}]^3[H^+]^{-4}(\gamma_1)^{-4}(\gamma_2)^2K$	-20.788
$[CuOH^+] = [Cu^{2+}][H^+]^{-1}(\gamma_1)^{-2}\gamma_2K$	-7.497
$[CuL_p^0]_{aq} = [Cu^{2+}][L_p^{2-}](\gamma_2)^2K$	4.02
$[CuHL_p^+] = [H^+][Cu^{2+}][L_p^{2-}](\gamma_2)^2K$	7.14
$[CuL_{p2}^{2-}] = [Cu^{2+}][L_p^{2-}]^2(\gamma_2)^2K$	5.3
$[Cd(OH)_2^0]_{aq} = [Cd^{2+}][H^+]^{-2}(\gamma_1)^{-2}\gamma_2K$	-20.294
$[Cd(OH)_3^-] = [Cd^{2+}][H^+]^{-3}(\gamma_1)^{-4}\gamma_2K$	-33.3
$[Cd(OH)_4^{2-}] = [Cd^{2+}][H^+]^{-4}(\gamma_1)^{-4}K$	-47.288
$[Cd_2OH^{3+}] = [Cd^{2+}]^2[H^+]^-(\gamma_1)^{-1}(\gamma_2)^{2+}(\gamma_3)^{-1}K$	-9.397
$[CdOH^+] = [Cd^{2+}][H^+]^{-1}(\gamma_1)^{-2}\gamma_2K$	-10.097
$[CdL_p^0]_{aq} = [Cd^{2+}][L_p^{2-}](\gamma_2)^2K$	3.42
$[CdHL_p^+] = [H^+][Cd^{2+}][L_p^{2-}](\gamma_2)^2K$	6.3
$[CdL_{p2}^{2-}] = [Cd^{2+}][L_p^{2-}]^2(\gamma_2)^2K$	3.69

[a] γ_n is the activity coefficient of a species with charge n.

At the ferrihydrite surface, there are two site types, and the site densities for the type one and type two sites were taken from Dzombak and Morel (1990) to be 0.005 mol (mol Fe)$^{-1}$ and 0.2 mol (mol Fe)$^{-1}$, respectively. Copper and Cd^{2+} sorption on to ferrihydrite surface involve both type one and type two sites, while only type two sites are needed to describe H_2L_p sorption. The surface reactions for Cu^{2+}, Cd^{2+} and H_2L_p are given in Table 2.4. The equilibrium constants for Cu^{2+} and Cd^{2+} sorption onto ferrihydrite determined in this work will be compared with the values given by Dzombak and Morel (1990).

Table 2.4 Equilibrium equations for surface reactions used in the model [a]

surface complexation equilibrium expression	logK^{INT} (with I=0)
Acid-base equilibria	
$[\equiv Fe^sOH_2^+] = [\equiv Fe^sOH^0][H^+]\ exp(-F\Psi/RT)\ \gamma_1(K_{A1}^{INT})^{-1}$	-7.29
$[\equiv Fe^sO^-] = [\equiv Fe^sOH^0][H^+]^{-1}\ exp(F\Psi/RT)\ (\gamma_1)^{-1}K_{A2}^{INT}$	-8.93
$[\equiv Fe^wOH_2^+] = [\equiv Fe^wOH^0][H^+]\ exp(-F\Psi/RT)\ \gamma_1(K_{A1}^{INT})^{-1}$	-7.29
$[\equiv Fe^wO^-] = [\equiv Fe^wOH^0][H^+]^{-1}\ exp(F\Psi/RT)\ (\gamma_1)^{-1}K_{A2}^{INT}$	-8.93
Copper sorption reactions	
$[\equiv Fe^sOCu^+] = [\equiv Fe^sOH^0][H^+]^{-1}[Cu^{2+}]\ exp(-F\Psi/RT)(\gamma_1)^{-1}\gamma_2\ K_1^{INT}$	2.89
$[\equiv Fe^wOCu^+] = [\equiv Fe^wOH^0][H^+]^{-1}[Cu^{2+}]\ exp(-F\Psi/RT)(\gamma_1)^{-1}\gamma_2\ K_2^{INT}$	0.60
Cadmium sorption reactions	
$[\equiv Fe^sOCd^+] = [\equiv Fe^sOH^0][H^+]^{-1}[Cd^{2+}]\ exp(-F\Psi/RT)(\gamma_1)^{-1}\gamma_2\ K_1^{INT}$	0.47
$[\equiv Fe^wOCd^+] = [\equiv Fe^wOH^0][H^+]^{-1}[Cd^{2+}]\ exp(-F\Psi/RT)(\gamma_1)^{-1}\gamma_2\ K_2^{INT}$	-2.90
Phthalic acid sorption (H_2L_p)	
$[\equiv Fe^wHL_P^0] = [\equiv Fe^wOH^0][H^+]^2[L_p^{2-}](\gamma_1)^2\gamma_2 K_1^{INT}$	[b]
$[\equiv Fe^wL_P^-] = [\equiv Fe^wOH^0][H^+][L_P^{2-}]\gamma_1\gamma_2\ exp(F\Psi/RT)K_2^{INT}$	[b]
$[\equiv Fe^wOHL_P^{2-}] = [\equiv Fe^wOH^0][L_P^{2-}]\gamma_2\ exp(2F\Psi/RT)K_3^{INT}$	[b]

[ ] = molar concentration; γ_n = aqueous phase activity coefficient for species with charge n;
[a] (Dzombak and Morel 1990) , [b] to be determined.

FITEQL 4.0

The equilibrium constants were optimized with FITEQL 4.0 (Herbelin and Westall 1999) in this work using the following components H^+, Cu^{2+}, Cd^{2+}, L_p^{2-}, Na^+, $\equiv Fe^wOH$, $\equiv Fe^sOH$, the surface potential and a "dummy" component described below. Three main steps are involved in FITEQL. First, set up the equilibrium model; second the equilibrium model must be solved at each of the data points. Finally, selected parameters in the model are adjusted to minimize the difference between values calculated from the model and the values observed

experimentally. The chemical equilibrium problem is set up as a matrix of mass action equations for the species involved and mass balance equations for components.

In FITEQL, three groups of components are defined: Group I-components for which only the total molar concentration (T) is known; Group II-components for which both the free molar concentration (X) and T are known; and Group III-components for which only X is known. The X and T data for the Group II component is used for the optimization of sorption constants in FITEQL. The "total sorbed sorbate" is sometimes considered as the "dummy" Group II component (Dzombak and Morel 1990; Herbelin and Westall 1999). It is obtained from the difference between the solution and total sorbate concentration. Alternatively, since the "total soluble sorbate" concentration is directly measured, it can also be considered as the "dummy" Group II component. It has been demonstrated that the difference between using these two components as Group II components in FITEQL is small (Swedlund 2004). In this work the "total soluble sorbate" was chosen as the "dummy" Group II component for modelling because this concentration is measured directly and a more direct and realistic measure of experimental error is obtained (as described below) compared to "total sorbed sorbate" where the experimental error need to be further calculated from estimated errors for both total and solution sorbate concentrations.

The basic scheme of the sorption equilibrium constants optimization is given in Figure 2.1. The residues are the difference between the calculated and the input value of the total component concentrations. WSOS/DF is the weighted sum of the squares of these residuals divided by the number of degrees of the freedom. Initial estimates for the values of the adjustable parameters are needed. They were normally obtained from similar previous studies. To compute the WSOS/DF, values of estimated error for experimental total concentration (s_T) and estimated error for experimental free concentration (s_X) are needed. They can be calculated using Equations 2.1 and 2.2, where s(abs) and s(rel) are estimates for the absolute and relative error in the experimental measurement.

$$s_T = s_T(abs) + s_T(rel) \times T \qquad \text{Eq. 2.1}$$

$$s_X = s_X(abs) + s_X(rel) \times X \qquad \text{Eq. 2.2}$$

In this work, the input errors were determined using the method of Dzombak and Morel (1990). For total Cu^{2+}, total Cd^{2+}, total H_2L_p and total H^+, the $s_T(rel)$ was taken as 0.01, and the $s_T(abs)$ was 0.01 × the minimum value. For the H^+ concentration, the $s_T(rel)$ was taken as

0.05, representing an uncertainty of ± 0.02 pH units. For free Cu^{2+} and Cd^{2+} concentrations, the s_X(rel) was taken as 0.01 for FAAS analyzed values but 0.05 for GFAAS analysis. The s_X(abs) was set at zero (Dzombak and Morel 1990). The WSOS/DF is an indicator of the goodness of fit. Values between 0.1 and 20 are generally accepted as reasonably good fits. Data with greater than ≈ 90 % adsorption can have a disproportionate weighting in FITEQL 4.0 and were not included in the parameter optimization (Ali and Dzombak 1996b).

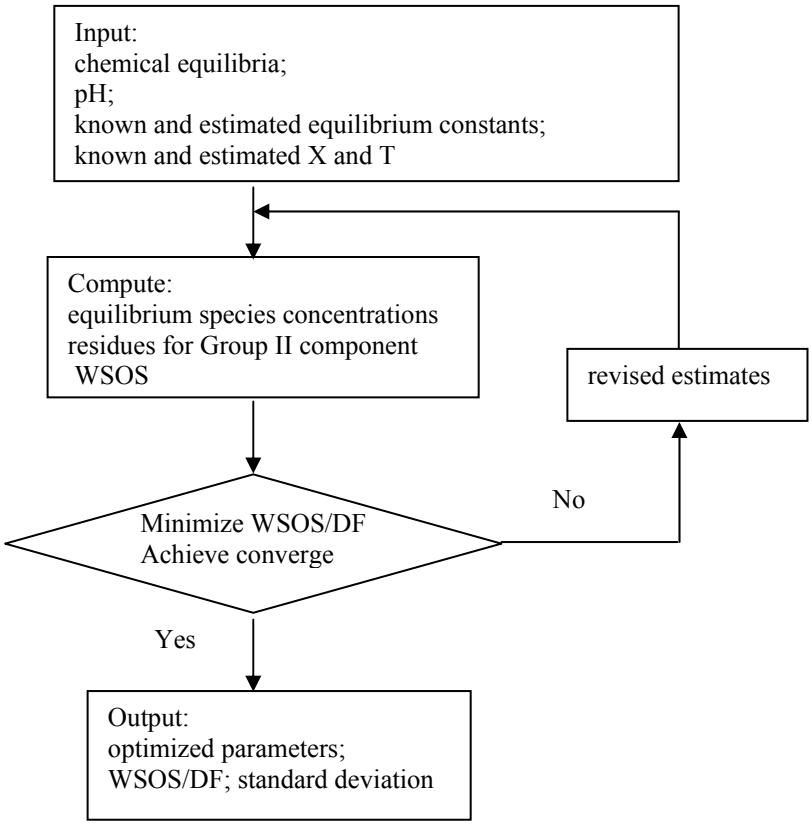

Figure 2.1 FITEQL procedure of optimizing equilibrium constant

As the experiments were performed at a fixed ionic strength, the log*K* values used in the model for all aqueous species were corrected to the corresponding ionic strength using the single ion activity coefficients given in Dzombak and Morel (1990). All optimized equilibrium constants reported are given after correction to an ionic strength of zero. All site densities, adsorption densities or sorbate to sorbent ratios are given on a mol (mol Fe)$^{-1}$ basis, unless stated otherwise.

2.2. Biotic systems

2.2.1 Material

Saline (0.85 % NaCl) was prepared from analytical grade sodium chloride. Analytical grade $MgSO_4 \cdot 7H_2O$, $CaCl_2 \cdot 2H_2O$, KNO_3, and $NaH_2PO_4 \cdot H_2O$ were used to prepare the bacteria growth media to examine H_2L_p degradation. Other reagents were described in Section 2.1.1. All solutions used in the biotic experiments were either autoclaved or filtered through 0.2 μm Sartorius Minisart single use cellulose acetate membrane filter. Laboratory glassware was autoclaved and plastic ware was purchased sterile.

Bacteria were cultured in Brain Heart Infusion Broth (BHI, Difco™), Trypticase Soy Broth (TSB, Difco™) supplemented with 0.5 % (V/V) yeast extract (Difco™) (TSBYE). Bushnell-Hass Broth (Difco™) (BHB) was initially used to evaluate microbial utilization of phthalic acid where H_2L_p is the sole carbon source (Bushnell and Hass 1940). The approximate formula for the BHB is (per liter): magnesium sulfate 0.2 g, calcium chloride 0.02 g, monopotassium phosphate 1.0 g, diammonium hydrogen phosphate 1.0 g, potassium nitrate 1.0 g and ferric chloride 0.05 g. Bacteria were grown at 28 °C with aerobic agitation at 200 rpm, or on nutrient agar plates in a 28 °C incubator.

A pure *Bacillus subtilis* strain was obtained from the Department of Molecular Medicine and Pathology, Faculty of Medical and Health Sciences, University of Auckland, New Zealand. *Bacillus subtilis* was chosen not only because it is a common bacterial strain found in natural environments or engineered systems, but also because it has been reported to have the ability to metabolize H_2L_p (Quan et al. 2005). Three pure bacterial strains were isolated from an activated sludge collected from the aerobic activated sludge reactors at the sewage wastewater treatment plant, Rosedale, Auckland, New Zealand. One of the bacterial strains was identified to be *Comamonas spp*. which can metabolize H_2L_p under the experimental conditions of this work.

Dead and live bacterial cells were examined by observing differentially stained cells under fluorescence microscope. The LIVE/DEAD® BacLight™ Bacterial Viability Kit (Molecular Probes) was used to provide a two-colour fluorescence assay of bacterial viability. SYTO®9, a green-fluorescent nucleic acid stain identifies bacteria with intact cell membranes (live cells), and propidium iodide, a red-fluorescent nucleic acid stain identifies bacteria with damaged membranes (dead cells) (Lloyd and Hayes 1995).

2.2.2 Phthalic acid metabolism

The metabolism of phthalic acid (as the only carbon source) was examined under various conditions using *Bacillus subtilis*, and three bacterial strains isolated from activated sludge. These include pH, metal ions, the presence of ferrihydrite, and growth nutrients such as $MgSO_4$, $CaCl_2$, KNO_3, and NaH_2PO_4. After the broth was removed by centrifugation and five washes with 0.01 M $NaNO_3$, the washed bacteria were added to prepared solutions or ferrihydrite suspensions containing various components at the desired concentrations. For systems that did not contain ferrihydrite, bacterial ability to degrade H_2L_p as the sole carbon source was estimated by examining bacterial growth with the measurement of optical density at 600 nm (OD_{600}) over a certain time range. When there was ferrihydrite present, phthalic acid degradation was determined by analyzing dissolved H_2L_p and total H_2L_p. The pH was measured (Section 2.2.7) during H_2L_p metabolism.

2.2.3 Isolation, storage and identification of *Comamonas spp.*

Aerobic activated sludge was plated on nutrient agar plates and incubated overnight at 28 °C. Three visually different independently growing colonies were identified and subcultured to individual nutrient agar plates. The colony types were named C1, small and opaque; C2, opaque; and C3, translucent. Individual colony was grown overnight on nutrient agar plates. Single cultures were used in a BHI broth for incubation overnight. The bacterial culture (0.5 mL) and 50 % glycerol (0.5 mL) were mixed in a 1 mL sterile Cryo tube and stored at -80 °C. The bacteria were recovered to nutrient agar plates for further experiments: phthalic acid biodegradation, Cd^{2+} and phthalic acid biosorption.

Only one of the three isolated bacteria (termed C1) was found to utilize H_2Lp as a sole carbon source and C1 was identified as a Gram-negative rod following Gram staining and the observation of cells by light microscopy with a ×100 oil immersion objective lens and a ×10 eyepiece lens (Beveridge 2001). Genomic DNA was extracted from the C1 bacterial cells using the Qiagen Generation Capture column kit according to the manufacturer's instructions for Gram-negative bacteria. Following genomic DNA extraction from biofilm samples 16S rDNA was amplified using primers P0 (5-GAGAGTTTGATCCTGGCTCAG) and P6 (5-CTACGGCTACCTTGTTACGA) according to the method of Di Cello et al. (1997). Briefly, amplification with these primers produced DNA nearly the entire 16S rDNA gene and gave a 1500 base pair fragment. PCR mixtures contained P6 primer 112.3 $ng\mu L^{-1}$, P0

primer 105.9 ngμL^{-1}, dNTPs 100 mM, 1 unit Taq polymerase in 1× Taq polymerase buffer (Roche Applied Science, Penzburg, Germany). PCR reaction conditions were an initial denaturation at 95 °C for 1 min, 30 cycles of: denaturation at 95 °C for 1 min, annealing at 52 °C for 30 s, elongation at 72 °C for 1min, and a final extension of 72 °C for 1min.

The PCR product was cloned using the TOPO TA Cloning® kit (Invitrogen) according to the manufacturer's instructions. Plasmid DNA for sequencing was prepared using a Zyppy plasmid miniprep kit (Zymo Research, CA, USA) according to the manufacturer's instructions. DNA sequencing with M13 universal forward and reverse primers was performed at the DNA Sequencing and Genotyping Facility, School of Biological Sciences, University of Auckland, New Zealand. Partial 16S rDNA (664 nucleotides at the front of the gene and 642 nucleotides at the end of the gene) sequences obtained were used to search other bacterial DNA sequences using the BLASTn program (Altschul et al. 1997) identifying (Altschul et al., 1997) C1 as a member of the *Comamonas spp.*, with 662/664 and 642/642 (99.8%) identity to *Comamonas* strain DJ12 (Accession number AY600616.1).

2.2.4 Bacteria incubation and quantification

1. Bacterial growth curve, cell dry weight and colony-forming unit

Bacteria were grown on nutrient agar plates at 28 °C over night, and a pre-culture of the cells was inoculated from the agar plate into 25 mL bacterial growth broth and incubated overnight. To observe bacterial growth over time, 2 mL of this culture was then used to inoculate 200 mL bacterial growth broth. The cells were grown at 28 °C and an agitation of 200 rpm with OD_{600} measured every hour. The growth curve of bacteria was obtained by plotting the OD_{600} versus time. At the same time a tenfold dilution series of broth culture in saline was spread on nutrient agar plates, cultivated overnight and the colony-forming units (CFU) were counted the next day.

To quantify bacterial cells the bacterial dry weight was determined. Each 2 mL of an overnight broth culture in growth broth was used to inoculate in 400 mL bacterial growth broth at 28 °C and an agitation of 200 rpm. Four samples of the growth media with volumes of 20, 50, 100, 200 mL were collected at OD_{600} = 0.5. The growth media was removed from the cells by centrifugation for 10 min (approximate 7,000 × g), followed by the disposal of supernatant and washing with 20 mL 0.01 M $NaNO_3$. The same centrifuge and washing procedure was repeated three times before two washes with MilliQ water. Cells were then

quantitatively transferred onto four pre-weighted aluminium plates with 5~10 mL MilliQ water, dried at 60 °C for 60 h and cooled down to room temperature in a desiccator to determine the dry weight (Yee and Fein 2001).

2. Bacterial wet weight/dry weight ratio

The ratio of wet/dry weight of the bacterial cells was determined by doing five parallel experiments. The bacterial culture was incubated in five flasks containing the same volume of bacterial growth broth under the same conditions as described above for about 8 h until the OD_{600} reached 1.0. After each 5 min centrifugation, the supernatant was discarded and replaced with 0.01 M $NaNO_3$ solution. This centrifuge-wash process was repeated five times. For the sixth wash, the bacteria cells were resuspended and transferred to pre-weighed tubes and centrifuge for 15 min, stopping the centrifugation at 5 min intervals to decant the supernatant. The wet weight of the bacteria cells was then determined. Samples were dried as described above. Unless stated, the bacterial cell concentration was expressed as g (wet weight) L^{-1}.

2.2.5 Titration for proton adsorption onto *Comamonas spp.*

Acid-base titrations were performed using a bacterial cell suspension to determine the site densities and proton binding constants for modelling Cd^{2+} sorption onto bacterial cells. The cells were prepared for titrations based on the method of Borrok et al (2004). Bacterial culture was grown for 10~12 h in TSBYE up to a stationary phase with OD_{600} reaching 1.0. The cells were removed from the growth media by centrifugation, washed as described in Section 2.2.4, and resuspended in the electrolyte (0.01 M $NaNO_3$) using a vortex mixer. The sodium nitrate used for potentiometric titration was prepared from autoclaved MilliQ water and then purged with $N_{2(g)}$ for 2~3 h to remove $CO_{2(g)}$. Sodium nitrate was used as the electrolyte to be consistent with the other experimental systems.

Aliquots of 0.114 M NaOH titrant used for acid/base titration were calibrated against potassium hydrogen phthalate. Acid/base titrations were conducted under $N_{2(g)}$ atmosphere using an autotitrator (Metrohm model 716 DMS Titrino) with the NaOH titrant added to the bacteria suspension after a stability of 2 mV min^{-1} was attained. To calibrate the electrode the background electrolyte solution was titrated. For the bacteria titration the *Comamonas spp.* cells were resuspended in 10 mL 0.01 M $NaNO_3$ solution to make a concentration of 56.3 gL^{-1} (wet weight) bacteria. Acid titrations using 0.212 M HNO_3 were also performed for

both blank and bacterial cells solutions to test the reversibility of the surface protonation reactions.

2.2.6 Cadmium sorption onto *Comamonas spp.*

1. Cadmium and H_2L_p adsorption onto *Comamonas spp.*

A stock bacteria suspension was prepared in 0.01 M sodium nitrate electrolyte solution with $CO_{2(g)}$ removed and pH adjusted to approximately 7 (Borrok et al. 2004; Borrok and Fein 2005). A suspension was then obtained by adding washed (Section 2.2.3) *Comamonas spp.* cells to the required concentration. Dead *Comamonas spp.* cells were obtained by leaving the cells in a 70 °C water bath for 15 min and cell death was confirmed using florescence microscopy.

The bacteria stock suspension in 0.01 M $NaNO_3$ was prepared by vortex mixing for ~1 min until a homogenous suspension was observed. The bacteria stock suspension was distributed to 50 mL centrifuge tubes and H_2L_p and Cd^{2+} were added as necessary. The pH of each sample was adjusted before they were capped and equilibrated at room temperature on an end-over-end mixer for 72 h. For Cd^{2+} adsorption in the presence of H_2L_p, to be consistent with abiotic systems, cadmium was always added directly after H_2L_p. A two hour equilibration time has been used for Cd^{2+}, Cu^{2+} and Pb^{2+} adsorption onto various bacterial cells (Borrok and Fein 2005; Daughney et al. 2000; Fowle and Fein 2000; Vasconcelos et al. 1997). For organic ligands, i.e. EDTA, 2,4,6-triclorophynol and humic acid, a 24 h equilibration time was suggested (Daughney and Fein 1998b; Fein et al. 1999; Fein and Delea 1999). Because this work examined H_2L_p metabolism (which can take 48~72 h), a 72 h equilibrium time was used to be consistent with the systems with H_2L_p biodegradation.

2. Cadmium sorption in dead *Comamonas spp.*-ferrihydrite-H_2L_p systems

A *Comamonas spp.* stock suspension was added to a ferrihydrite suspension at neutral pH with thorough stirring. The ferrihydrite-*Comamonas spp.* mixed suspension was then distributed in 50 mL centrifuge tubes. The desired volumes of H_2L_p and/or Cd^{2+} stock solution were added and the pH of each sample was adjusted before they were capped and equilibrated at room temperature on an end-over-end mixer. After equilibration time, the pH was re-measured, and the dissolved Cd^{2+} and H_2L_p were analyzed.

3. Cadmium sorption in live *Comamonas spp.*-ferrihydrite- H_2L_p systems

For the system with H_2L_p biodegradation by live *Comamonas spp*., the experiments were carried out in 500 mL polycarbonate vessels on magnetic stirrers with head spaces purged with a 4:1 (V:V) $N_{2(g)}$:$O_{2(g)}$ mix. Samples were collected from the reaction vessel several times over the reaction period to measure pH, the concentrations of dissolved Cd^{2+}, dissolved H_2L_p, total H_2L_p and *Comamonas spp.* growth.

2.2.7 Analytical methods

The pH was measured as described before, the pH electrode was rinsed with 99 % ethanol followed by autoclaved MilliQ water before use. Dissolved Cd^{2+}, Fe^{3+} and H_2L_p concentrations were determined as described in Section 2.1.3. Total unmetabolized H_2L_p ($H_2L_{p(TL)}$ = sorbed and soluble H_2L_p) was measured by heating unfiltered and sealed samples in a 70 °C water bath for 15 min, followed by adding 20 µL 1 M NaOH to adjust the pH to ~9 and equilibrating for 2 h to allow for H_2L_p desorption before filtration. In this way the amount of metabolized H_2L_p was calculated: degraded $H_2L_p = H_2L_{p(T)} - H_2L_{p(TL)}$. The degradation products from phthalic acid metabolism by *Comamonas spp.* were examined by HPLC and gas chromatography-mass spectrometry (GC-MS). Filtered samples were injected to HPLC directly with a UV-VIS detector with four wavelengths of 224, 235, 280 and 290 nm. The GC-MS analysis was based on the method from Eaton and Nitterauer (1994). The pH of the filtered samples that were collected during phthalic acid degradation was adjusted to ~2.0 before extraction three times with ethyl acetate. Sodium sulfate was used to dry the ethyl acetate extracted samples. Sodium sulfate was removed by filtration then the ethyl acetate was removed under a gentle N_2 flow. The ethyl acetate extracted sample was then derivatized using Trimethysilyl (TMS) derivatives before being analyzed by GC-MS (QP 2010S, Shimadzu). Samples were injected at 290 °C onto a SLB 5MS capillary column (30 m × 0.25 mm × 0.25 µm), using helium as the carrier gas at a linear velocity of 37 cm s^{-1}. The oven temperature retained at 50 °C for 1 min and then increased to 90 °C at a rate of 10 °C min^{-1} and held for 2 min, then increased to 290 °C at a rate of 8 °C min^{-1} and held for 8 min. The total analysis time was 40 min.

2.2.8 Modelling adsorption onto *Comamonas spp.*

The non-electrostatic four site model (NFSM) of Borrok et al (2004) was used to model biosorption in this work. The components H^+, RA^-, RB^-, RC^-, RD^- were included in FITEQL 4.0 during the optimization of proton adsorption constants, where RA^-, RB^-, RC^- and RD^-

represent four types of sites at *Comamonas spp.* surface. The related reactions are given in Equations 2.1~2.4. FITEQL optimizes values for $\log K_{RXH}$ and the total concentration of each site type in $molg^{-1}$ wet weight bacteria. The initial estimated values of these parameters were taken from Borrok et al (2004).

$$RA^- + H^+ \Leftrightarrow RAH^0 \quad \text{Eq. 2.1}$$

$$RB^- + H^+ \Leftrightarrow RBH^0 \quad \text{Eq. 2.2}$$

$$RC^- + H^+ \Leftrightarrow RCH^0 \quad \text{Eq. 2.3}$$

$$RD^- + H^+ \Leftrightarrow RDH^0 \quad \text{Eq. 2.4}$$

The titration data were obtained and expressed as total proton molar concentration (TOTH) versus pH where TOTH is given by Equation 2.5.

$$TOTH=[H^+]-[OH^-]+[RAH]+ [RBH]+ [RCH]+ [RDH] \quad \text{Eq. 2.5}$$

To model Cd^{2+} adsorption onto *Comamonas spp.* in binary systems used reactions between Cd^{2+} and four types of sites at *Comamonas spp.* surface given in Equations 2.6~2.9. Cadmium sorption equilibrium constants were then optimized in FITEQL 4.0 with the inclusion of proton sorption constants and site concentration derived from the titration data.

$$RA^- + Cd^{2+} \Leftrightarrow RACd^+ \quad \text{Eq. 2.6}$$

$$RB^- + Cd^{2+} \Leftrightarrow RBCd^+ \quad \text{Eq. 2.7}$$

$$RC^- + Cd^{2+} \Leftrightarrow RCCd^+ \quad \text{Eq. 2.8}$$

$$RD^- + Cd^{2+} \Leftrightarrow RDCd^+ \quad \text{Eq. 2.9}$$

Chapter 3. Copper, Cadmium, and Phthalic Acid Sorption onto Ferrihydrite in Binary Systems

Contents published in Environmental Science &Technology (Song et al. 2008).

3.1. Introduction

The interactions between metal ions, organic ligands and mineral surfaces can influence the fate and transport of both trace metals and organic ligands in aquatic systems. Examination of sorption onto iron oxides in simple binary systems is a precursor for understanding the interactions in more complex systems. Surface complexation modelling has been widely used to describe metal ion sorption by iron oxides in binary systems (Hwang et al. 2007), and simple organic ligands sorption by iron oxides can also be described by surface complexation modelling (Ali and Dzombak 1996a; Evanko and Dzombak 1999). While organic ligand sorption by goethite and hematite has been reported (Ali and Dzombak 1996b; Boily et al. 2000; Evanko and Dzombak 1999; Hanna 2007; Hwang et al. 2007), there are no reported studies of H_2L_p sorption onto ferrihydrite.

The objective of this chapter is to investigate Cu^{2+}, Cd^{2+} and H_2L_p sorption onto ferrihydrite in binary systems for a range of conditions, to provide a basis for studying ternary systems. Sorption onto ferrihydrite was experimentally determined and sorption constants were optimized using FITEQL. The constants for Cu^{2+} and Cd^{2+} sorption onto ferrihydrite were compared with previously reported values. For H_2L_p sorption onto ferrihydrite, three surface sorption reactions were taken into account for modelling (Table 2.4).

3.2. Results and discussion

3.2.1 Copper sorption onto ferrihydrite

Copper sorption onto ferrihydrite in the absence of H_2L_p was determined over a pH range of 3.5~8.5 for $Cu_{(T)}$/Fe (mol/mol) values of 0.0017 and 0.025 and the experimental data are shown in Figure 3.1. The data show that Cu^{2+} sorption edge has a typical sigmoidal shape with adsorption increasing from zero to around 100 % over approximately two pH units. A pH edge shift is also evident with the $Cu_{(T)}$/Fe ratio increases from 0.0017 to 0.025. The pH_{50} (the pH of 50 % sorption) with $Cu_{(T)}$/Fe of 0.0017 and 0.025 occurs at pH ≈ 4.7 and 5.6,

respectively. The pH edges shift to the right (higher pH values) by approximately 1 pH unit at pH_{50} indicates the increasing importance of the low affinity surface sites as would be expected with a high affinity site density of 0.005 mol (mol Fe)$^{-1}$. Moreover, a decrease in the midpoint slopes can be observed in Figure 3.1 when $Cu_{(T)}$/Fe increases from 0.0017 to 0.025.

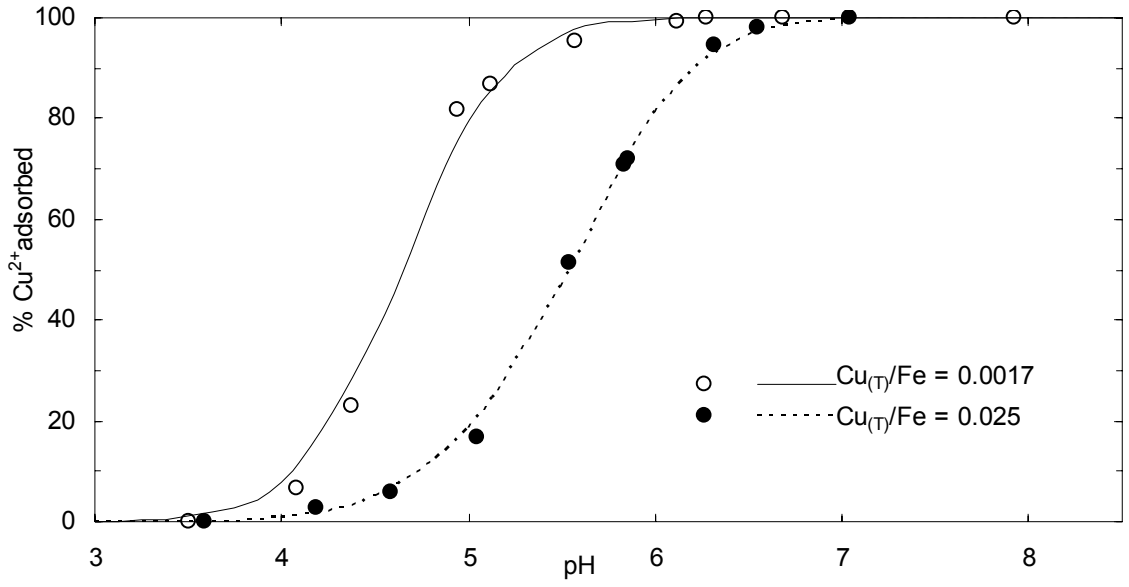

Figure 3.1 Experimental (symbols) and modelled (lines) results for Cu^{2+} sorption onto ferrihydrite. Model results use the values from Dzombak and Morel (1990). Actual concentrations values of ferrihydrite and $Cu_{(T)}$ are given in Table 3.1.

Adsorption of Cu^{2+} with $Cu_{(T)}$/Fe of 0.0017 will only be significant on the type one sites (with a site density of 0.005) while for $Cu_{(T)}$/Fe of 0.025 the type two sites will be most significant. This is reflected in the surface sorption constants optimization results (Table 3.1) where $logK_1^{INT}$ can only be derived from the data set with $Cu_{(T)}$/Fe of 0.0017, and $logK_2^{INT}$ is optimized from the experimental results with $Cu_{(T)}$/Fe of 0.025. The constants for $logK_1^{INT}$ and $logK_2^{IN}$ derived from the experimental data in this work (2.91 and 0.58 respectively) are consistent with the values given by Dzombak and Morel (1990) of 2.89 for $logK_1^{INT}$ and 0.60 for $logK_2^{INT}$. Therefore the Dzombak and Morel (1990) values were used in modelling copper sorption by ferrihydrite in the presence of H_2L_p so that the adsorption constants for ternary complex formation from this thesis are consistent with the database of Dzombak and Morel (1990). The modelling results obtained using the $logK^{INT}$ values from Dzombak and Morel (1990) show that the modelling results are in good agreement with experimental data in this work (Figure 3.1).

Table 3.1 Optimization of $logK_1^{INT}$ and $logK_2^{INT}$ for Cu^{2+} sorption on ferrihydrite. Data sets are given in Figure 3.1. The $logK^{INT}$ values are given for I = 0 (with standard deviations in parentheses).

$Cu_{(T)}/Fe$ (mol mol^{-1})	$Cu_{(T)}$ (μM)	Ferrihydrite (mM)	$logK_1^{INT}$ $\equiv Fe^sOCu^+$	$logK_2^{INT}$ $\equiv Fe^wOCu^+$	WSOS/DF
0.0017	16.0	9.4	2.91 (0.032)	0.58[a]	5.27
0.025	23.6	0.94	2.91[a]	0.58 (0.034)	1.01
Weighted average from Dzombak and Morel (1990) (95 % confidence interval)			2.89 (2.82, 2.96)	0.60[b]	

[a] No convergence of this value so the value was fixed at the weighted average for consistency
[b] Estimated from the Linear Free Energy Relationships (LFERs) data for other metals

3.2.2 Cadmium sorption onto ferrihydrite

Cadmium sorption onto ferrihydrite in the absence of H_2L_p was determined over pH 4.0~8.5 for $Cd_{(T)}/Fe$ of 7.8×10^{-5} and 7.9×10^{-3} and the experimental results are given in Figure 3.2. Similarly to the case of Cu^{2+} sorption onto ferrihydrite, cadmium sorption onto ferrihydrite depends strongly on pH and $Cd_{(T)}/Fe$ ratios. The pH edges show a similar S-curve pattern with increasing pH. About one pH unit shift can also be observed with $Cd_{(T)}/Fe$ increasing from 7.8×10^{-5} to 7.9×10^{-3}, i.e. the pH_{50} for Cd^{2+} sorption occurs at pH ≈ 6.1 for $Cd_{(T)}/Fe$ of 7.8×10^{-5} and pH ≈ 7.0 for $Cd_{(T)}/Fe$ of 7.9×10^{-3}.

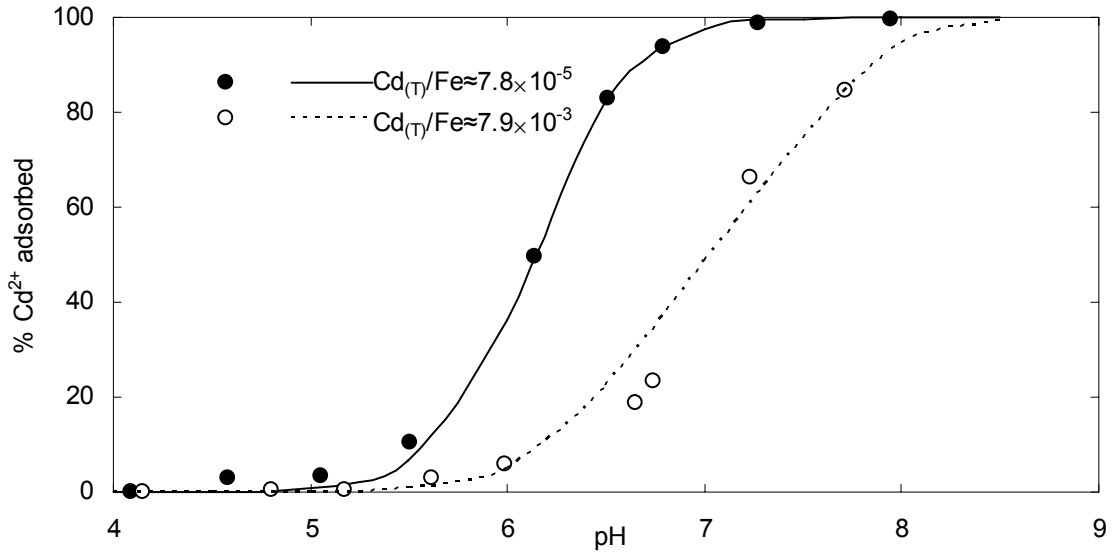

Figure 3.2 Experimental (symbols) and modelled (lines) results for Cd^{2+} sorption by ferrihydrite. Model results use the values from this work. Actual concentrations values of ferrihydrite and $Cd_{(T)}$ are given in Table 3.2.

Compared to Cu^{2+} sorption onto ferrihydrite, Cd^{2+} adsorption pH edges occur at higher pH values, which corresponds to the fact that $logK_1^{INT}$ for Cd^{2+} (discussed below) is smaller than $logK_1^{INT}$ for Cu^{2+}. This is consistent with the correlation of $logK^{INT}$ values with the first hydrolysis constants ($logK_{MOH}$) for divalent (Dzombak and Morel 1990), such that cations with a lower $logK_{MOH}$ (for example $logK_{CdOH} = 3.9$ is smaller than $logK_{CuOH} = 6.5$) was found to have lower $logK_1^{INT}$ values.

Values for $logK_1^{INT}(\equiv Fe^sOCd^+)$ and $logK_2^{INT}(\equiv Fe^wOCd^+)$ were optimized by FITEQL 4.0 from the experimental data and the results are shown in Table 3.2. Similarly to Cu^{2+} sorption onto ferrihydrite $logK_1^{INT}$ could only be optimized from the data set with $Cd_{(T)}/Fe$ of 7.8×10^{-5} (which is smaller than type 1 site density 0.005mol mol Fe^{-1}) where the high affinity surface sites are most important for the sorption. The $logK_2^{INT}$ could be derived from the data set with higher $Cd_{(T)}/Fe$ ratio of 7.9×10^{-3} (which is larger than type 1 site density 0.005) where the importance of low affinity surface sites to the sorption is significant.

Table 3.2 Optimization of $logK_1^{INT}$ and $logK_2^{INT}$ for Cd^{2+} sorption on ferrihydrite. Data sets are given in Figure 3.3. The $logK^{INT}$ values are given for I = 0 (with standard deviations in parentheses).

$Cd_{(T)}/Fe$ (mol mol^{-1})	$Cd_{(T)}$ (μM)	Ferrihydrite (mM)	$logK_1^{INT}$ $\equiv Fe^sOCd^+$	$logK_2^{INT}$ $\equiv Fe^wOCd^+$	WSOS/DF
7.8×10^{-5}	0.89	10.24	0.22 (0.031)	-2.94[a]	0.96
7.9×10^{-3}	9.14	1.02	0.22[a]	-2.94 (0.049)	8.79
Weighted average from Dzombak and Morel (1990) (95 % confidence interval)			0.47 (0.44, 0.50)	-2.90[b]	

[a] No convergence of this value so the value was fixed at the weighted average value for consistency
[b] Only one value so no confidence interval was given

The optimized value for $logK_2^{INT}$ was -2.94, which is in agreement with the reported values of -2.90 (Dzombak and Morel 1990) and -2.69 (Swedlund et al. 2003). All modeling for Cd^{2+} sorption in this thesis used a $logK_2^{INT}$ of -2.90. The $logK_1^{INT}$ value for the formation of the species $\equiv Fe^sOCd^+$ was 0.22 which is in the range of values -0.14~1.03 (Dzombak and Morel 1990; Swedlund 2004). The weighted average $logK_1^{INT}$ value of Dzombak and Morel (1990) was 0.47. There is, however, a general trend whereby the optimized values for $logK_1^{INT}$ for a given data set decreased as the $Cd_{(T)}/Fe$ increased (Figure 3.3) (Dzombak and Morel 1990) which could be an indication of more complex site heterogeneity for Cd^{2+} (Swedlund et al. 2003).

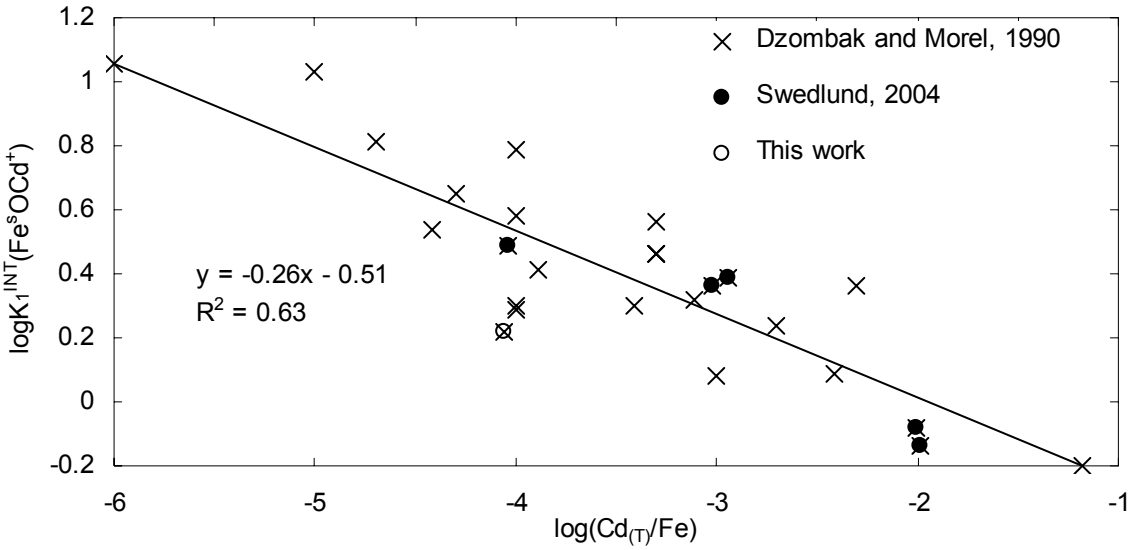

Figure 3.3 Comparison of $\log K_1^{INT}(\equiv Fe^sOCd^+)$ from this work with the values reported.

The experimental and modelled data using the $\log K_1^{INT}$ value of 0.22 and 0.47 for Cd^{2+} sorption as a function of pH are shown in Figure 3.2 and Figure 3.4, respectively. Modelling using both of the constants can fit the experimental reasonably well. However using the $\log K_1^{INT}$ of 0.47 slightly overestimated Cd^{2+} sorption onto ferrihydrite by approximate 5 % for data with $Cd_{(T)}/Fe$ of 7.8×10^{-5} at the pH range of 5.5 ~ 6.8.

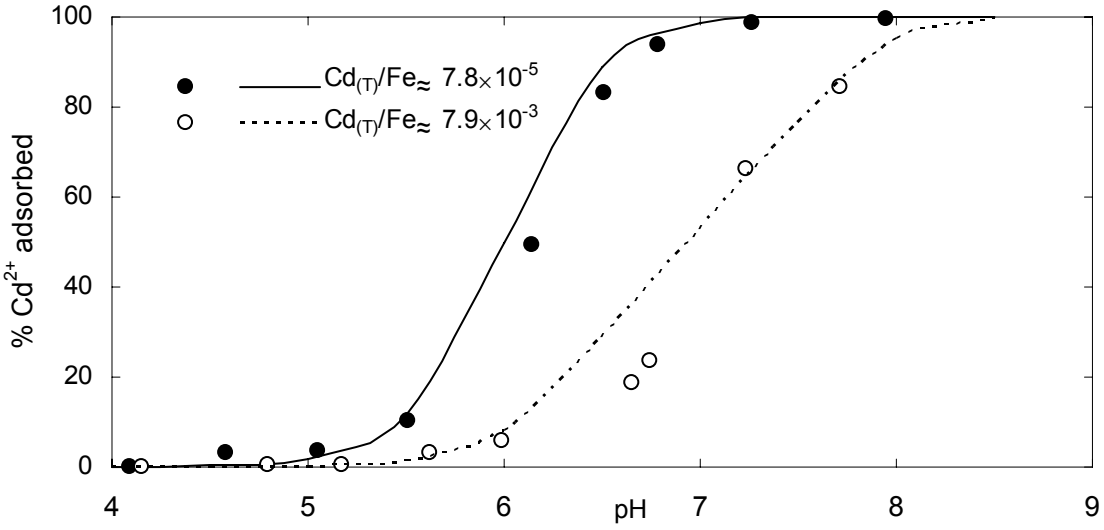

Figure 3.4 Cadmium sorption by ferrihydrite: Experimental (symbols) and modelled (lines) results. Model results use the values from Dzombak and Morel (1990). Ferrihydrite and $Cd_{(T)}$ concentrations are given in Table 3.2.

Therefore modelling Cd^{2+} sorption by ferrihydrite in the presence of H_2L_p was done both with the $\log K_1^{INT}$ value of 0.22 from this work and with the cited value of 0.47. The difference between ternary surface complex constants caused by using these two values in ternary systems is discussed in Chapter 4.

3.2.3 Phthalic acid sorption onto ferrihydrite

Phthalic acid sorption by ferrihydrite was determined for a total H_2L_p to ferrihydrite ratio ($H_2L_{p(T)}$/Fe) ranging from 0.06 to 30.2 mol mol^{-1} (Figure 3.5 a and b), and the results are typical of anion sorption. In contrast to cation sorption where the sorption plot shows a sigmoidal curve and reaches the greatest sorption at higher pH values, the greatest phthalic acid sorption onto ferrihydrite occurs at lower pH and then decreases gradually as pH increases. As the case of cation sorption, the pH edges for H_2L_p sorption also depend on sorbate/sorbent ratios. As the $H_2L_{p(T)}$/Fe ratio increases the pH edges shift to lower pH values and plateau at a lower % adsorption. For example, all the data with $H_2L_{p(T)}$/Fe ratio higher than 0.06 plateau at low pH at less than 100 % adsorption indicating surface sites saturation.

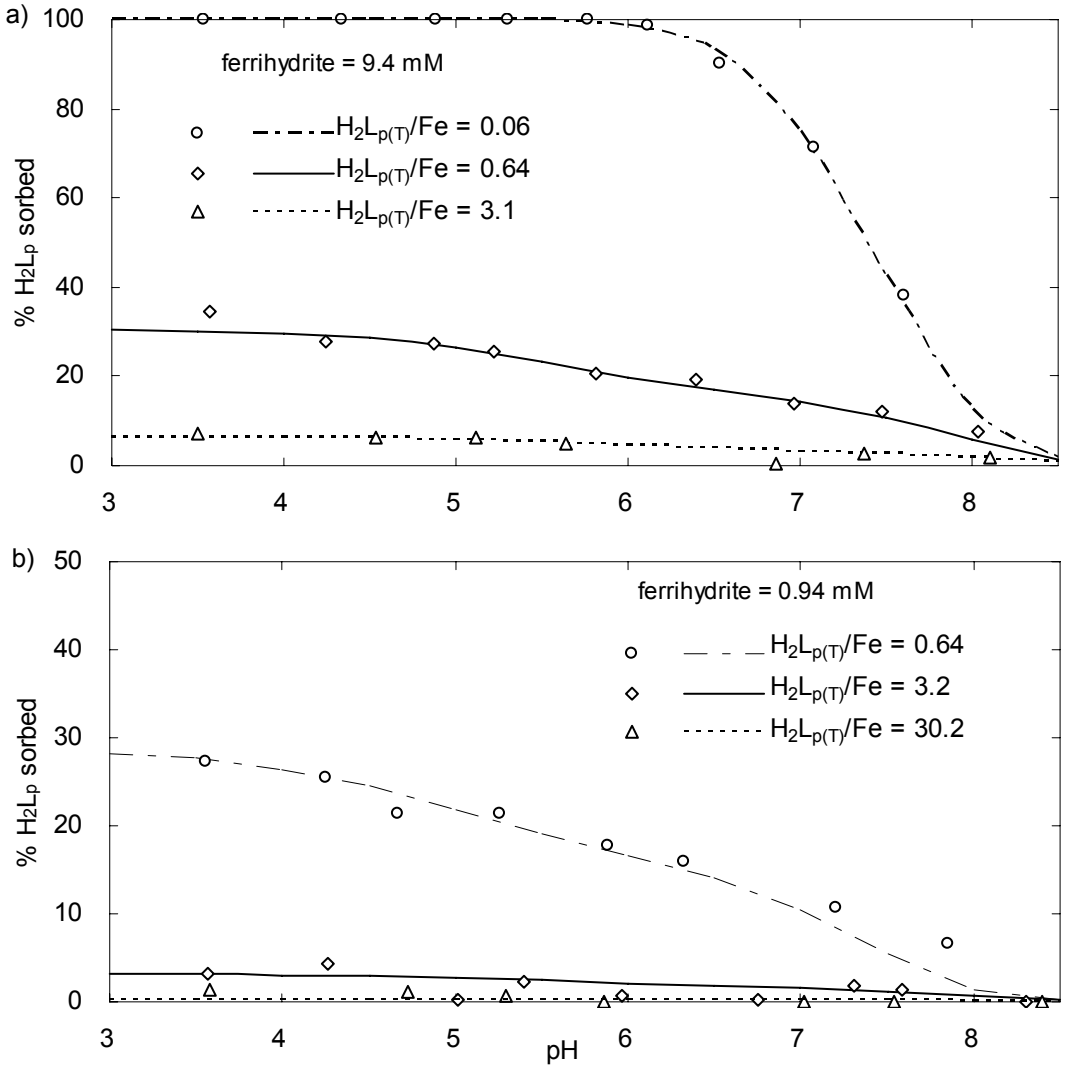

Figure 3.5 Phthalic acid sorption onto ferrihydrite: Experimental (symbols) and modelled (lines) results. Model results use the weighted average values from Table 3.3.

Site heterogeneity is not observed for anion adsorption by ferrihydrite and the type two sites, is sufficient to describe anion sorption onto ferrihydrite using surface species with varying degrees of protonation (Dzombak and Morel 1990). As a diprotic weak acid there are three surface species were considered to describe H_2L_p sorption by ferrihydrite (Table 2.4). Sorption constants of $\log K_1^{INT}(\equiv Fe^wHL_p^0)$, $\log K_2^{INT}(\equiv Fe^wL_p^-)$ and $\log K_3^{INT}(\equiv Fe^wOHL_p^{2-})$ were optimized by FITEQL 4.0 from the experimental data. The value of $\log K_3^{INT}$ was not constrained using the experimental data with $H_2L_{p(T)}$/Fe (mol mol^{-1}) of 0.064 in this work. However all the H_2L_p sorption by ferrihydrite data could be modelled with only two sorption constants; $\log K_1^{INT}(\equiv Fe^wHL_p^0)$ and $\log K_2^{INT}(\equiv Fe^wL_p^-)$. Values for these constants were derived from experimental data and are shown in Table 3.3.

Table 3.3 Optimization of $\log K_1^{INT}$ and $\log K_2^{INT}$ for H_2L_p sorption on ferrihydrite. Data sets are given in Figure 3.5. The $\log K^{INT}$ values are given for I = 0 (with standard deviations in parentheses).

$H_2L_{p(T)}$/Fe [a] (mol mol^{-1})	$H_2L_{p(T)}$ (mM)	Ferrihydrite (mM)	I (M)	$\log K_1^{INT}$ $\equiv Fe^wHL_p^0$	$\log K_2^{INT}$ $\equiv Fe^wL_p^-$	WSOS/DF
0.064	0.6	9.4	0.01	15.85[b]	10.23 (0.043)	1.82
0.64	6.0	9.4	0.01	15.90 (0.12)	10.23[b]	1.23
0.64	0.6	0.94	0.01	15.80 (0.13)	10.23[b]	0.93
Weighted average (95 % confidence interval)				15.85 (15.40, 16.30)	n.a.[c] 10.23 used	

[a] Values could not be determined from data sets with higher $H_2L_{p(T)}$ as described in the text.
[b] No convergence of this value so the value was fixed at the weighted average for consistency
[c] For $\log K_2^{INT}$ only one value could be determined so no average or confidence interval can be given.

As is generally found the more negative surface species are most important at lower anion/ferrihydrite ratios. This is evident from the constant optimization shown in Table 3.3, where $\log K_2^{INT}$ for the negative surface species $\equiv Fe^wL_p^-$ could only be optimized from the data set with lower $H_2L_{p(T)}$/Fe ratio of 0.064. The importance of the neutral surface species increases with higher $H_2L_{p(T)}$/Fe ratio therefore the $\log K_1^{INT}$ could be optimized from data with $H_2L_{p(T)}$/Fe ratio of 0.64. Parameters could not be optimised from the data with higher $H_2L_{p(T)}$/Fe where the maximum % of adsorption was < 10 % because of the high inherent uncertainties in calculating the small amount of adsorbed phthalate from the difference between the total phthalate and the large amount remaining in solution. Modelled adsorption shown in Figure 3.5 can reasonably predict the experimental data for the wide range of pH and $H_2L_{p(T)}$/Fe.

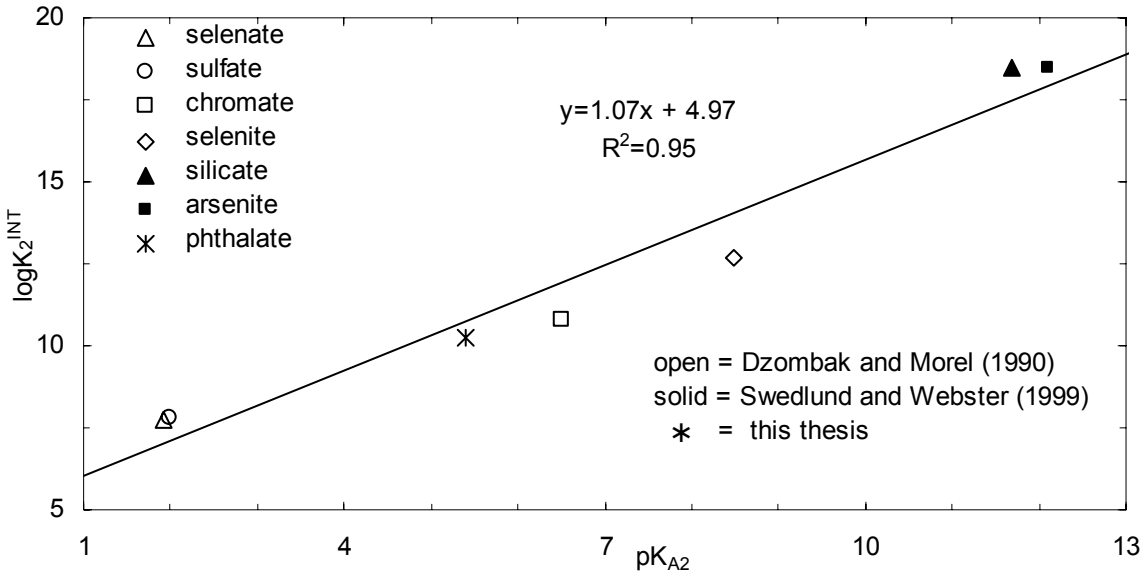

Figure 3.6 Linear Free Energy Relationship between the values of $logK_2^{INT}$ for the adsorption of a divalent anion and the pK_{A2} for the corresponding conjugate acid. The data point for L_p^{2-} from this thesis is shown with data from Dzombak and Morel (1990) and Swedlund and Webster (2001).

The value for $logK_1^{INT}(\equiv Fe^wHL_p^0)$ of 15.85 from this work is in close agreement with Ali and Dzombak (1996a) who reported a value for an analogous reaction of H_2L_p adsorption on goethite to be 15.74. Ali and Dzombak (1996a) could not optimise a value for $logK_2^{INT}(\equiv Fe^wL_p^-)$ but rather modelled all their H_2L_p adsorption on goethite using the two species $\equiv Fe^wHL_p^0$ and $\equiv Fe^wOHL_p^{2-}$. This was in contrast to sulfate and chelidamic acid adsorption by goethite in the same paper where the species $\equiv Fe^wL^-$ (where L is the ligand) was included in the model though no chemical reason was given for the difference. Both the $logK^{INT}$ values optimised in this work for H_2L_p adsorption by ferrihydrite are consistent with the values for inorganic anion adsorption by ferrihydrite as compiled by Dzombak and Morel (1990). For example the values of $logK_2^{INT}$ determined for a range of divalent inorganic anions form a linear relationship when plotted as a function of the pK_{A2} for the conjugate of the anions (Figure 3.6). This illustrates that the tendency of a divalent anion to become protonated in solution is related to its tendency to form a surface complex. The $logK_2^{INT}$ value for H_2L_p adsorption on ferrihydrite fits this relationship very closely as is shown in Figure 3.7. It also suggests that ligands with higher pK_{A2} that form strong complexes in solution form strong surface complexes with higher $logK^{INT}$. For example, there is a linear relationship between solution constants for Fe^{3+}-ligand complexes and their analogous surface complexation constants as is shown in Figure 3.7. Though the value for Fe^{3+}-

phthalate solution complex stability constant has not been reported, it might be estimated to be ≈10.

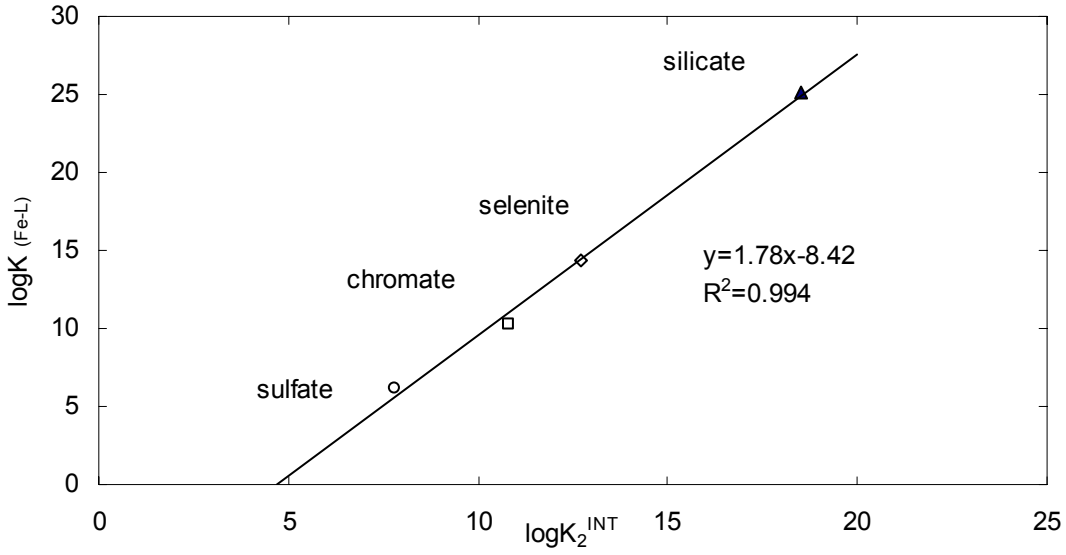

Figure 3.7 Relationship between solution Fe-ligand constants logK(Fe-L) and surface complex constants $logK_2^{INT}$. Data for chromate and selenate are from Dzombak and Morel (1990), sulfate from Swedlund and Webster (2001) and silicate from Swedlund and Webster (1999).

There have been recent infrared spectroscopy studies on the structure of H_2L_p surface complexes on the iron oxides goethite and hematite. Boily et al. (2000) proposed that there were an inner-sphere and an outer-sphere complex of phthalate on the goethite surface with the outer sphere complex becomes more dominant as the pH increased from 3 to 7. For hematite one outer-sphere complex and two inner-sphere complexes were proposed for H_2L_p sorption (Hwang et al. 2007). All complexes were fully deprotonated and the inner-sphere complexes were chelating, with both carbonate groups coordinated to either one Fe or two Fe ions. This result is similar to that observed for the iron oxyhydroxide adsorption of inorganic ions such as sulfate and selenate. Various studies indicated that the mechanism for anions such as selenate, sulfate and arsenate sorption onto goethite and ferrihydrite is similar (Elzinga et al. 2001; Manceau and Charlet 1994; Peak et al. 1999; Sposito 1984; Zhang and Peak 2007). The DLM does not include outer-sphere complexes, however anion adsorption can be described by the addition of adsorbed species with varying states of protonation as discussed in Dzombak and Morel (1990). For instance, the monovalent surface species $\equiv Fe^wSO_4^-$ for DLM modelled sulfate sorption is more significant than the divalent $\equiv Fe^wOHSO_4^{2-}$ at lower pH (Figure 3.8 a). This compares to ATR-FTIR studies of sulphate (Elzinga et al. 2001; Peak et al. 1999; Zhang and Peak 2007) on goethite surface, where the inner-sphere complexes were more prevalent under lower pH conditions. Similarly, species in

the DLM for H_2L_p adsorbed on ferrihydrite shows that high pH and low ionic strength increase the significance of the more negative charged surface species $\equiv Fe^wL_p^-$ (Figure 3.8 b), and these conditions were shown to favour outer-sphere complexes of goethite adsorbed H_2L_p (Boily et al. 2000). In general spectroscopic studies have shown that oxyanions adsorbed onto iron oxyhydroxide typically involve some outer-sphere surface complexes. However the DLM can predict the main features of anion adsorption including the effects of ionic strength, pH and adsorption density with a simple and consistent set of reactions that do not include outer-sphere complexes. It is possible that the more negatively charged sorbed ligand species are behaving in a similar way to an outer-sphere complex. However, a full consideration of the reasons for this, given the discrepancy with the spectroscopic data, is beyond the scope of this work.

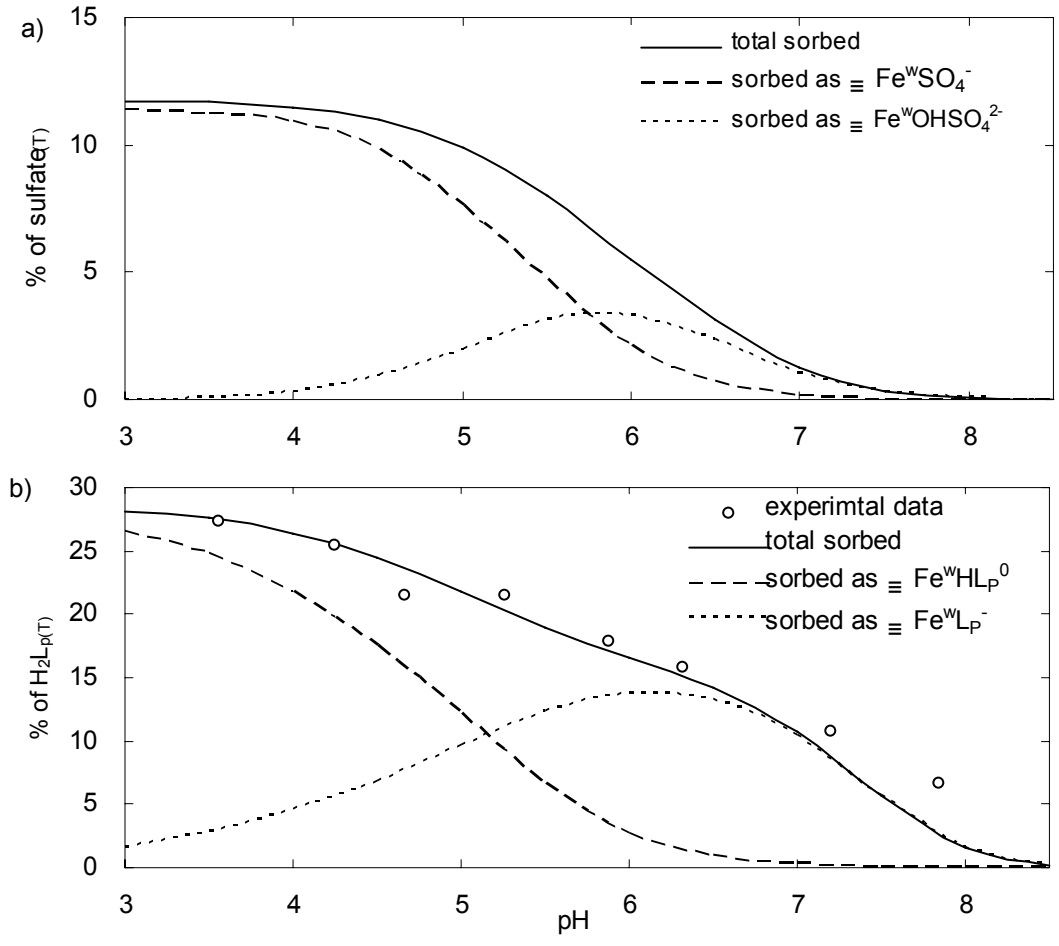

Figure 3.8 Modelled surface species for a) sulfate and b) H_2L_p sorption onto ferrihydrite. Data use with 0.6 mM sorbate and 0.94 mM ferrihydrite at I = 0.01 M $NaNO_3$. Model results use complex formation constants from Swedlund and Webster (2001) for sulfate, and Table 3.3 (this thesis) for H_2L_p, respectively.

While much work has been conducted with crystalline oxides, little has been done on organic ligands sorption onto a poorly ordered iron oxide such as ferrihydrite and spectroscopic studies of H_2L_p sorption onto ferrihydrite have not been reported. This process can be well described by the DLM using the sorption constants derived from experimental data in this study, even though the DLM cannot include outer sphere complexes. To explain this mechanism further work such as infrared spectroscopy, will be needed.

3.3. Conclusions

Cu^{2+}, Cd^{2+} and H_2L_p adsorption onto ferrihydrite in binary systems was examined. Cu^{2+} and Cd^{2+} showed typical cation sorption onto ferrihydrite, their sorption increases with the increase of pH. While results of H_2L_p sorption onto ferrihydrite are typical of anion sorption, adsorbed H_2L_p deceases gradually with the increase of pH. Using the DLM, Cu^{2+}, Cd^{2+} and H_2L_p adsorption was well reproduced. The constants for $\equiv Fe^sOCu^+$ and $\equiv Fe^wOCu^+$ derived from the experimental data in this work were consistent with the reported values. For Cd^{2+}, the optimized value for $\log K_2^{INT}(\equiv Fe^wOCd^+)$ was in agreement with the reported value, and the $\log K_1^{INT}(\equiv Fe^sOCd^+)$ value is in the reported range but slightly below the cited weighted average value. H_2L_p sorption onto ferrihydrite could be modelled with only two sorption constants; $\log K_1^{INT}(\equiv Fe^wHL_p^0)$ and $\log K_2^{INT}(\equiv Fe^wL_p^-)$. The value for $\log K_1^{INT}(\equiv Fe^wHL_p^0)$ from this work is in close agreement with Ali and Dzombak (1990) who reported a value for an analogous reaction of H_2L_p adsorption on goethite. Phthalic acid adsorption onto ferrihydrite was analogous to that of inorganic diprotic acids in terms of the relationship between the adsorption constants and acidity constants.

Chapter 4. Copper, Cadmium, and Phthalic Acid Sorption onto Ferrihydrite in Ternary Systems

Contents published in Environmental Science &Technology (Song et al. 2008).

4.1. Introduction

There is only limited modelling data available for ternary systems with metal ions, ligands and an iron oxide, though surface complexation modelling has been widely used to describe sorption in complex systems. This chapter uses the model parameters derived from binary sorption systems described in Chapter 3, to investigate the effect of H_2L_p on Cu^{2+} and Cd^{2+} adsorption onto ferrihydrite in ternary systems. The significance of ternary complexes on ferrihydrite (about which little is known) compared to goethite by comparing the values from this study to other previously reported ternary systems. Unless specified, all modelling in this chapter uses the binary adsorption constants discussed in Chapter 3.

4.2. Copper sorption onto ferrihydrite in the presence of phthalic acid

Copper sorption by ferrihydrite in the presence of H_2L_p was measured with $Cu_{(T)}$/Fe of either ≈ 0.0017 or 0.025 mol mol^{-1} and H_2L_p concentration ranging from 0.6 to 28 mM. The experimental results are shown in Figure 4.1. Modelled adsorption is shown in Figure 4.1 using just the adsorption constants derived from the binary systems and given in Tables 3.1 and 3.3. Copper sorption by ferrihydrite in the presence of H_2L_p was either enhanced or decreased depending on the H_2L_p concentration, pH and the $Cu_{(T)}$/Fe ratio. The presence of 0.6 mM $H_2L_{p(T)}$ slightly enhanced Cu^{2+} sorption in all cases. As the H_2L_p concentration increased to 6 mM the sorption of Cu^{2+} was enhanced for pH values < 5 but was inhibited at higher pH values. As H_2L_p concentration further increased to 28 mM the sorption of Cu^{2+} was quite significantly inhibited, particularly at higher pH values and for the data with $Cu_{(T)}$/Fe ≈ 0.025 mol mol^{-1}. The adsorption of H_2L_p was not noticeably affected by the presence of Cu^{2+} because the H_2L_p concentration was so much greater than that of Cu^{2+}, as is shown in Figure 4.2.

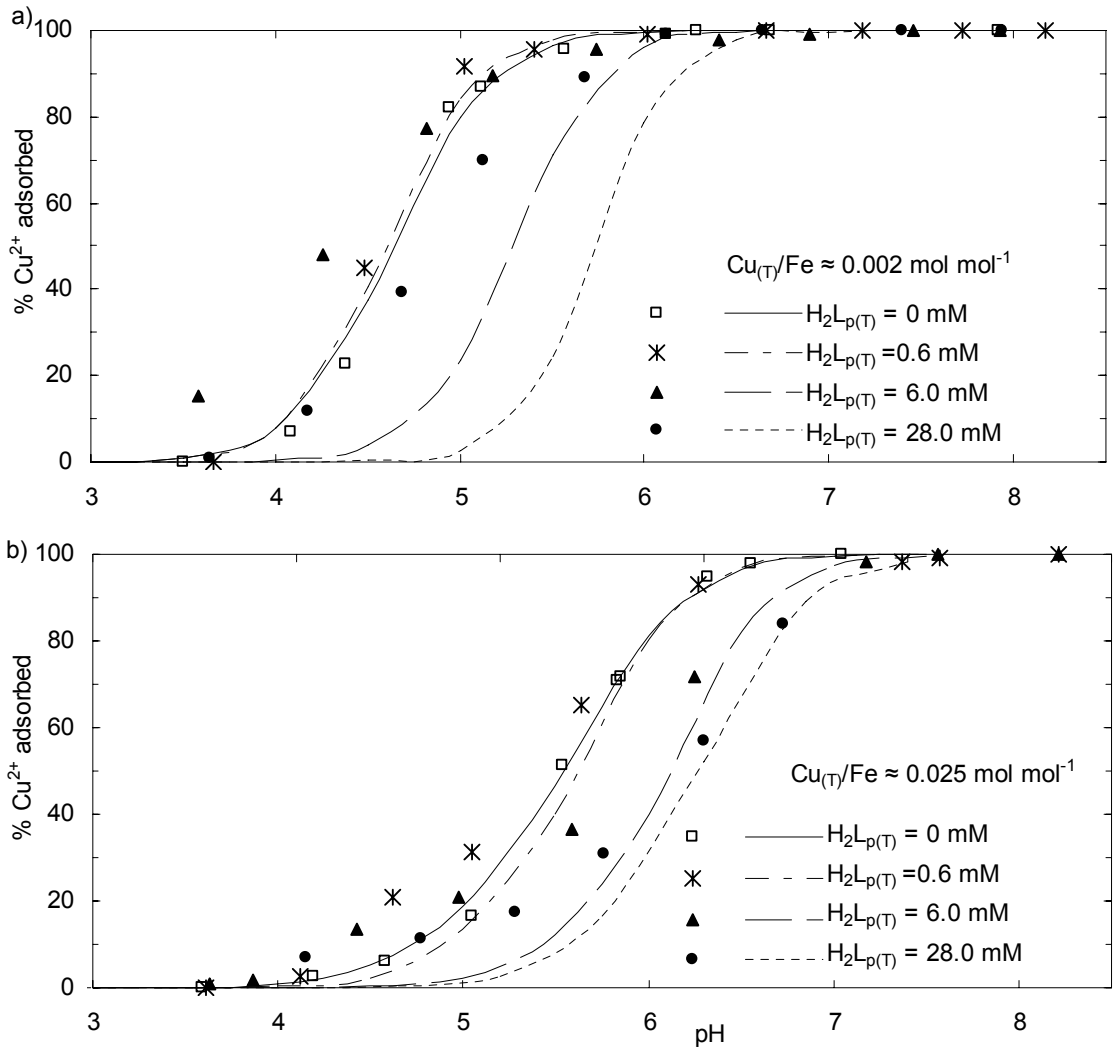

Figure 4.1 Copper sorption by ferrihydrite in the presence of H_2L_p: Experimental (symbols) and modelled (lines) results. Actual concentration values of I, ferrihydrite and $Cu_{(T)}$ are given in Table 4.1.

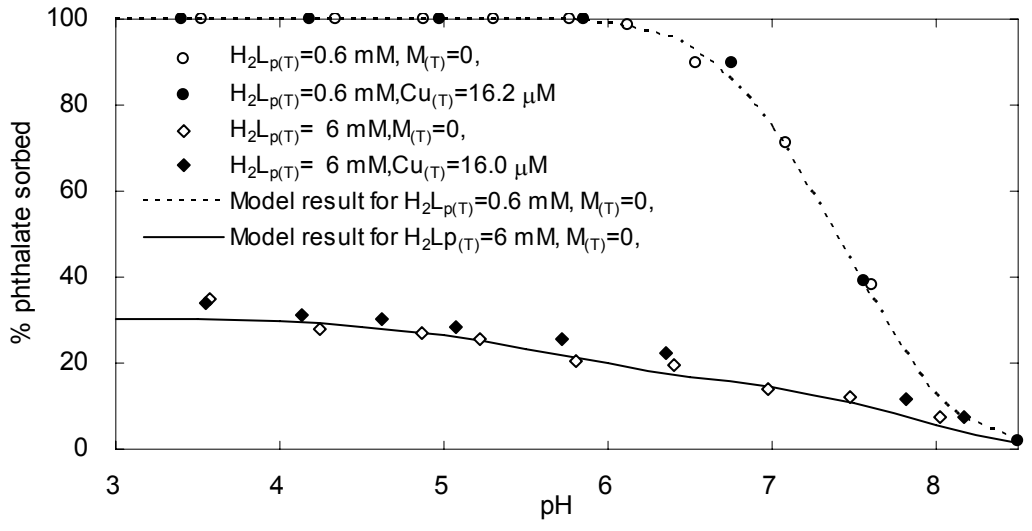

Figure 4.2 Phthalic acid sorption onto ferrihydrite with/without the presence of Cu^{2+}: Experimental (symbols) and modelled results (lines). [Fe]= 9.4 mM

Ali and Dzombak (1996a) observed H_2L_p only enhancing Cu^{2+} sorption by goethite, however the highest concentration of H_2L_p in their study was 1 mM compared to 28 mM in the current study. All data with 0.6 mM H_2L_p in the current study showed enhanced Cu^{2+} sorption to ferrihydrite, with inhibition only evident at 6 mM H_2L_p. The inhibition of Cu^{2+} sorption generally observed at higher pH could be the result of two forms of competition. Firstly H_2L_p and Cu^{2+} compete for surface sites and secondly there is competition between Cu^{2+} adsorption and the formation of Cu-phthalate complexes in solution. Of these two forms of competition it is the formation of solution Cu-phthalate complexes that accounts for almost all of the observed inhibition of Cu^{2+} adsorption. This is shown by modelling the data for a variety of scenarios. For example, for the $Cu_{(T)}/Fe \approx 0.025$ and 28 mM phthalate data, the model fairly accurately predicts the observed inhibition of Cu^{2+} adsorption due to the presence of H_2L_p for pH > 6.5. If the adsorption reactions for phthalate are omitted from the model there is only a small effect on modelled Cu^{2+} adsorption, with the adsorbed phthalate actually slightly promoting Cu^{2+} adsorption at pH > 6.5 due to electrostatic effects. However, if all of the Cu-phthalate solution complexes are omitted from the model (and the phthalate adsorption reactions are retained) then the modelled Cu^{2+} adsorption approaches that predicted in the absence of phthalate. This demonstrates that it is the solution Cu-phthalate complexes that inhibit Cu^{2+} adsorption.

The observed effect of H_2L_p inhibiting Cu^{2+} adsorption contrasts to the effect of SO_4^{2-}on the ferrihydrite adsorption of Cu^{2+} where adsorption always increased as the SO_4^{2-} concentration increased up to 20.8 mM (Swedlund and Webster 2001). The difference between the sulfate and phthalate ligands is the relative strength of the interaction with Cu^{2+} in solution. For example the logK for the formation of the aqueous complexes $CuA^0_{(aq)}$ are 4.02 and 2.36 where A is respectively phthalate or sulfate. In general the anion of a weaker acid, which has a higher affinity for a proton, will also have a higher affinity for other cations. The pK_{A2} values for sulfate and phthalate are 1.99 and 5.41, respectively. Figure 3.7 also showed that the affinity of an anion for Fe^{3+} on the ferrihydrite surface depends on the anion pK_A. Figure 4.3 shows the solution Cu-ligand complex species distribution for Cu^{2+} in the presence of sulphate and H_2L_P (Figure 4.3), which illustrates that H_2L_p forms stronger solution complexes with Cu^{2+} than sulfate at pH > 4. The concentration of solution Cu^{2+} due to the formation of complex with H_2L_p is about 40 times higher than that of Cu^{2+}-SO_4^{2-} solution complex. It is for this reason that the inhibition of Cu^{2+} adsorption was observed with phthalate concentration but not for similar conditions with sulfate.

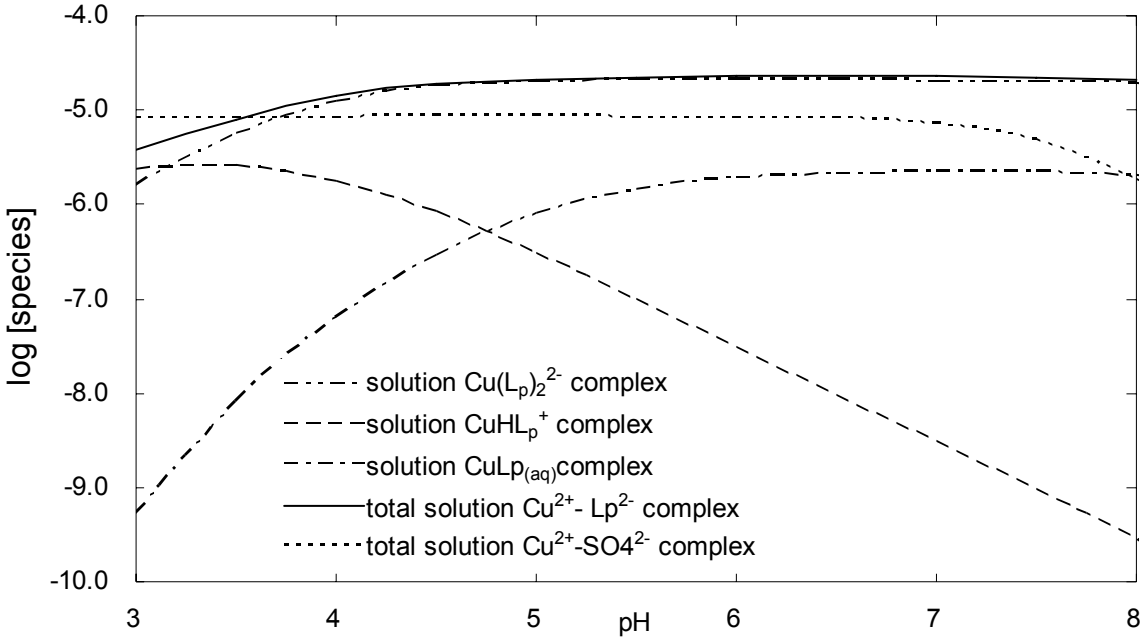

Figure 4.3 Modelled Cu^{2+}-ligand solution complexes. Modelling parameters were taken from Visual MINTEQ database (Gustafsson 2006). I = 0.01 M $NaNO_3$, $Cu_{(T)}$ = 23.6 μM, $H_2L_{p(T)}$ (or $H_2SO_{4(T)}$) = 6 mM.

Figure 4.1 shows that using the binary sorption constants the model does predict Cu^{2+} adsorption inhibition with increasing H_2L_p concentration. However, in general, the modelled inhibition is greater than the observed inhibition and almost none of the observed enhancement of Cu^{2+} adsorption due to H_2L_p is predicted. This suggests that there is some interaction between the Cu^{2+} and H_2L_p on the ferrihydrite surface (which would not be evident in the binary experiments) and this interaction is enhancing Cu^{2+} adsorption. The enhanced Cu^{2+} sorption could be the result of the reduced positive surface charge due to phthalate sorption onto ferrihydrite (especially under more acidic conditions) or from the formation of a ternary surface complex with some interaction between Cu^{2+} and phthalate. Using the sorption constants derived from the binary system the model does predict some enhanced Cu^{2+} sorption for the $Cu_{(T)}$/Fe of 0.0017 with 0.6 mM phthalic acid. This small modelled enhancement of Cu^{2+} adsorption is due to the effect of phthalate sorption on the surface potential.

The enhanced Cu^{2+} sorption by goethite in the presence of H_2L_p has been successfully modelled by including a ternary surface complex with stoichiometry $\equiv FeOHCuL_p^0$ (Ali and Dzombak 1996b) however all their data had a sufficiently high $Cu_{(T)}$/α-FeOOH that only one site type was needed to describe cation adsorption. In this work the effect of H_2L_p on Cu^{2+} adsorption was studied at two $Cu_{(T)}$/Fe ratios; the low $Cu_{(T)}$/Fe ratio of 0.0017-0.0020 is less

than the type one site density (so that only the type one sites will be important) and the high $Cu_{(T)}$/Fe ratio of 0.025-0.030 which is sufficiently above the type one site density that the type two site will be most important. In this way the significance of ternary complexes on both the high and low affinity sites could be assessed.

The initial approach to modelling in this work was to add one ternary complex ($\equiv Fe^{w}OHCuL_p^{0}$) on the type 2 sites as given in Equation 4.1. The detailed results for this modelling approach are shown in Table 4.1. While each data set could be fitted by including this species the optimised values of $\log K_2^{TC}$ ranged from 9.3 to 9.7 for the data sets with $Cu_{(T)}$/Fe ≈ 0.025 but ranged from 10.6 to 10.9 for the data sets with $Cu_{(T)}$/Fe ≈ 0.002.

Table 4.1 Optimization of $\log K^{TC}$ for ternary complex formation between Cu^{2+}, H_2L_p and ferrihydrite. Data sets given in Figure 4.1. The $\log K^{TC}$ values are given for I = 0 (with standard deviations in parentheses).

$Cu_{(T)}$/Fe (mol mol^{-1})	$Cu_{(T)}$ μM	$H_2L_{p(T)}$ (mM)	Ferrihydrite (mM)	I (M)	$logK^{TC}$ $\equiv Fe^{w}OHCuL_p^{0}$	WSOS/DF
0.0017	16.0	0.6	9.4	0.01	no converge	
0.0017	16.0	6.0	9.4	0.01	10.56 (0.031)	5.26
0.0020	13.7	28	7.0	0.1	10.93 (0.11)	42.87
0.025	23.6	0.6	0.94	0.01	9.58 (0.060)	1.90
0.025	23.6	6.0	0.94	0.01	9.68 (0.051)	6.17
0.030	20.6	28	0.7	0.1	9.34 (0.076)	15.22

An acceptable model needs to be able to describe all the experimental data in a consistent way and the above results indicate that another surface complex might be involved on the high affinity sites. For this reason, an additional ternary complex $\equiv Fe^{s}OHCuL_p^{0}$ on the type 1 sites was added to the model as given in Equation 4.2. Values for $\log K_1^{TC}$ and $\log K_2^{TC}$ were optimized from experimental data and the results are shown in Table 4.2.

$$[\equiv Fe^{w}OHCuL_P^{0}] = [\equiv Fe^{w}OH^{0}][Cu^{2+}][L_p^{2-}](\gamma_2)^2 K_2^{TC} \quad \text{Eq. 4.1}$$

$$[\equiv Fe^{s}OHCuL_P^{0}] = [\equiv Fe^{s}OH^{0}][Cu^{2+}][L_p^{2-}](\gamma_2)^2 K_1^{TC} \quad \text{Eq. 4.2}$$

Only a value for $\log K_1^{TC}$ could be optimised from the data with a $Cu_{(T)}$/Fe of ≈ 0.0017, as would be expected because the type 2 sites are not significant until the type 1 sites are appreciably occupied. The values ranged from 12.29 to 12.48 and all the WSOS/DF were

between 1.9 and 6.0. A value for $\log K_2^{TC}$ could be optimised from each data set with $Cu_{(T)}$/Fe of ≈ 0.025 and these values ranged from 9.02 to 9.52. Values for $\log K_1^{TC}$ could be optimised from two data sets with a $Cu_{(T)}$/Fe of ≈ 0.025 although the standard deviations for $\log K_1^{TC}$ were comparatively large reflecting the minor role the type one sites play under these conditions. The values for $\log K_1^{TC}$ with $Cu_{(T)}$/Fe of ≈ 0.025 were reasonably consistent with those from $Cu_{(T)}$/Fe of ≈ 0.0017 given the high standard deviation. Furthermore the modelling of the data with $Cu_{(T)}$/Fe of ≈ 0.0017 was not significantly affected by fixing the value of $\log K_2^{TC}$ to the weighted average value that was determined from the data with $Cu_{(T)}$/Fe of ≈ 0.025. This demonstrates that the model is consistent across all the conditions studied.

Table 4.2 Optimization of $\log K_1^{TC}$ and $\log K_2^{TC}$ for ternary complex formation between Cu^{2+}, H_2L_p and ferrihydrite. Data sets given in Figure 4.1. The $\log K^{TC}$ values are given for I = 0 (with standard deviations in parentheses).

$Cu_{(T)}$/Fe (mol mol^{-1})	$Cu_{(T)}$ (μM)	$H_2L_{p(T)}$ (mM)	Ferrihydrite (mM)	I (M)	$\log K_1^{TC}$ $\equiv Fe^sOHCuL_p^0$	$\log K_2^{TC}$ $\equiv Fe^wOHCuL_p^0$	WSOS/DF
0.0017	16.0	0.6	9.4	0.01	12.48 (0.20) [a]	9.43[b]	1.63
0.0017	16.0	6.0	9.4	0.01	12.29 (0.023)	9.43[b]	5.44
0.0020	13.7	28	7.0	0.1	12.33 (0.024)	9.43[b]	3.88
0.025	23.6	0.6	0.94	0.01	12.31 (0.18)[a]	9.52 (0.067)	1.58
0.025	23.6	6.0	0.94	0.01	12.34[b]	9.52 (0.058)	2.62
0.030	20.6	28	0.7	0.1	12.61 (0.26) [a]	9.02 (0.14)	2.36
Weighted average (95 % confidence interval)					12.34 (12.29, 12.39)	9.43 (9.10, 9.76)	

[a]: Fixed at 0.15 to calculate weighted average when actual value is larger than 0.15 (Ali and Dzombak 1996b).
[b]: No convergence of this value so the value was fixed at the weighted average for consistency

Figure 4.4 shows the sorption of Cu^{2+} by ferrihydrite in the presence of H_2L_p with modelling results that include ternary complex formation (using the weighted average values from Table 4.2) with the binary adsorption constants from Tables 3.1 and 3.3. By including the ternary complexes the ability of the model to predict the effect of H_2L_p on Cu^{2+} sorption is significantly improved, predicting both the inhibition of Cu^{2+} sorption at higher pH and the enhancement of Cu^{2+} sorption at lower pH. The discrepancies between the experimental and the predicted values of Cu^{2+} adsorption in the presence of H_2L_p are of comparable magnitude to those in the absence of H_2L_p. For Cu^{2+} sorption onto ferrihydrite in the presence of SO_4^{2-}, it was found that only ternary complexes on type 2 sites are needed after trying different modelling options, including only assuming ternary complexes on type 1 sites, or taking

ternary complexes on both type 1 and type 2 sites into account (Swedlund and Webster 2001; Swedlund et al. 2003).

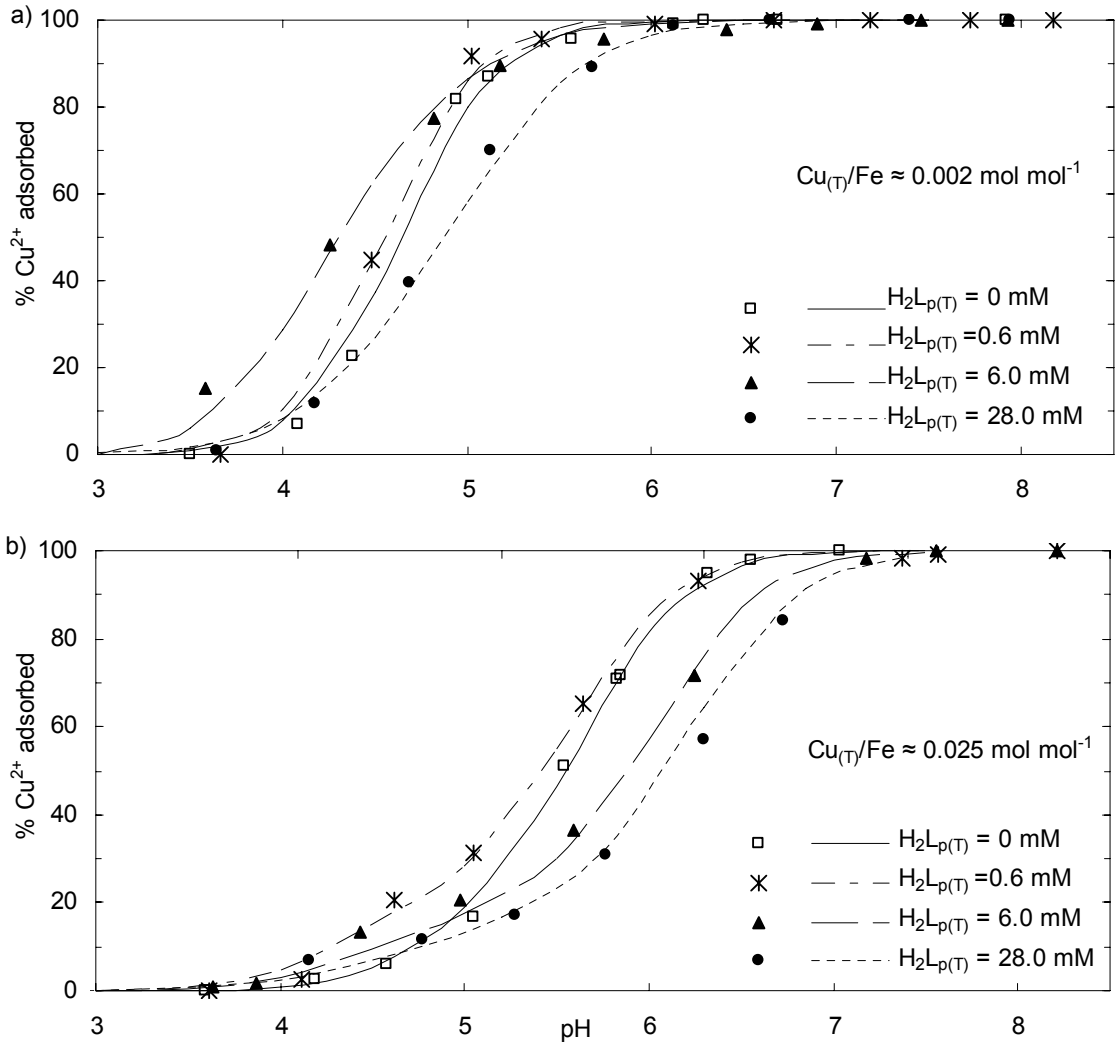

Figure 4.4 Copper sorption by ferrihydrite in the presence of H_2L_p: Experimental (symbols) and modelled (lines) results. Model results use the weighted average ternary complex formation constants from Table 4.3 in conjunction with the adsorption constants from binary systems. Actual concentration values of I, ferrihydrite and $Cu_{(T)}$ are given in Table 4.2.

To illustrate the significance of ternary complexes in Cu^{2+} sorption by ferrihydrite in the presence of H_2L_p Figure 4.5 shows the calculated speciation for Cu^{2+} in the ternary system with $Cu_{(T)}/Fe \approx 0.025$. Species are arranged in three groups; firstly solution Cu^{2+}-phthalate complexes, secondly sorbed ternary complexes ($\equiv Fe^sOHCuL_p^0$ or $\equiv Fe^wOHCuL_p^0$) and thirdly sorbed Cu^{2+} binary complexes ($\equiv Fe^sOCu^+$ or $\equiv Fe^wOCu^+$). For all H_2L_p concentrations ternary complexes account for between 30 and 40 % of the $Cu_{(T)}$, peaking from pH 5.5 to 6.5. At lower pH Cu solution complexes dominate while at higher pH adsorbed binary Cu^{2+} dominates the speciation. By comparing Figure 4.5 with Figure 4.1b, which shows the binary

model the Cu-phthalate data it can be seen how the presence of ternary complexes account for the enhancement of Cu^{2+} adsorption in the presence of H_2L_p.

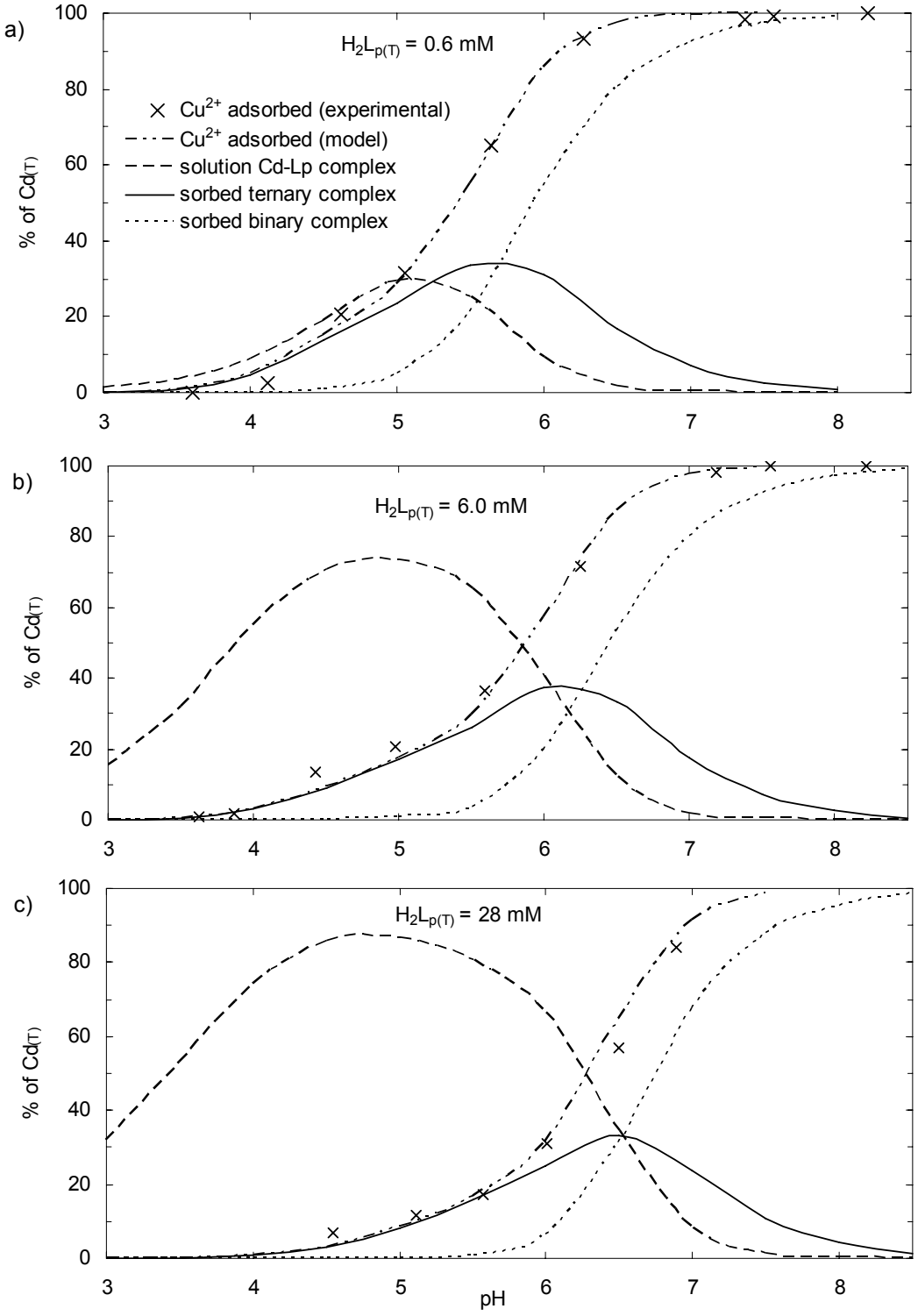

Figure 4.5 Modelled speciation of Cu^{2+} in the H_2L_p-Cu^{2+}-ferrihydrite system. $Cu_{(T)}$/Fe of ≈ 0.025. Legends used in b) and c) represent the same Cd speciation as those in a). Actual concentration values of I, ferrihydrite and $Cu_{(T)}$ are given in Table 4.2.

These results represent similar conditions to some of the data from Ali and Dzombak (1996b), where Cu^{2+} sorption by goethite was found to be enhanced in the presence of H_2L_p especially at pH < 5. No inhibition of Cu^{2+} sorption due to H_2L_p was seen, however the highest phthalate concentration in their work was 1 mM. Figure 4.6 shows the modelled effect of higher concentrations of H_2L_p on Cu^{2+} sorption by goethite using the parameters from Ali and Dzombak (1996b). This shows a very similar behaviour to that of ferrihydrite with Cu^{2+} sorption enhanced at lower pH by 6.0 mM $H_2L_{p(T)}$ but inhibited at higher pH by 6.0 mM $H_2L_{p(T)}$ and over the whole pH range by 28 mM $H_2L_{p(T)}$. Even though the concentration (1.6 gL^{-1}) of goethite used by Ali and Dzombak (1996b) was much higher than that of ferrihydrite (≈ 0.084 gL^{-1}) in this work, because of the lower site density of goethite (0.016 mol (mol Fe^{-1})), the actual concentrations of total surface sites in the two works are comparable (29 mM for Ali and Dzombak (1996b) and 19 mM in this work), as is the $Cu_{(T)}$ of 23.0 μM in Ali and Dzombak (1996b) and 23.6 μM in this work.

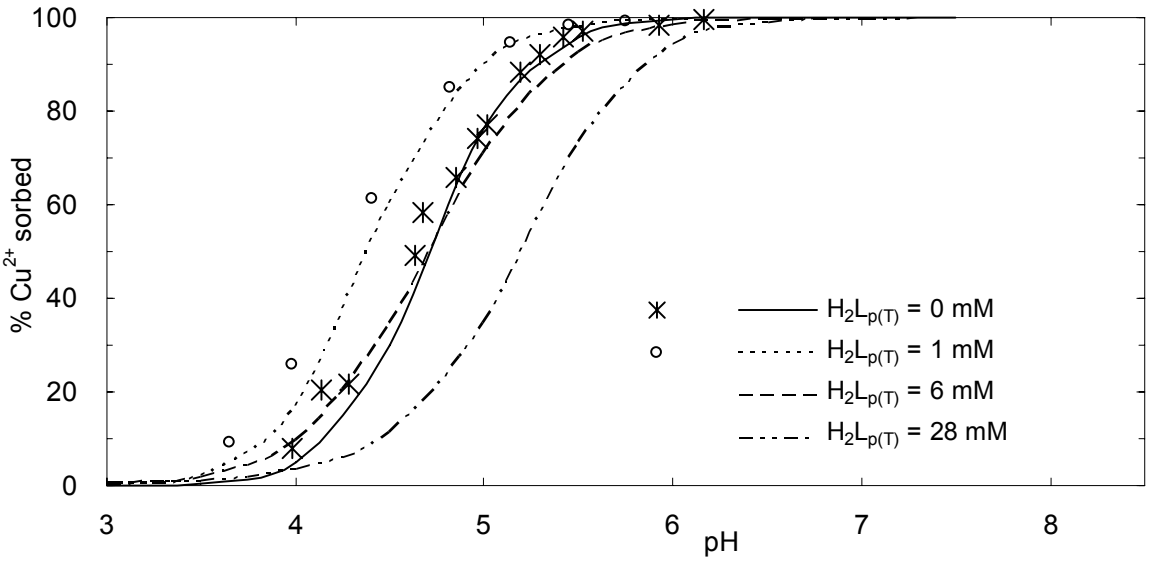

Figure 4.6 Experimental (symbols) and modelled (lines) results for Cu^{2+} sorption by goethite as reported in Ali and Dzombak (1996b). Model results use the values from Ali and Dzombak (1996b) including surface area, site density, surface acidity and adsorption constants. Modelling is shown for 6.0 and 28 mM $H_2L_{p(T)}$ for which no experimental data was reported.

4.3. Cadmium sorption onto ferrihydrite in the presence of phthalic acid

The experimental results for Cd^{2+} sorption by ferrihydrite in the presence of H_2L_p are shown in Figure 4.7. The adsorption of H_2L_p was not noticeably affected by the presence of Cd^{2+}

because the H_2L_p concentration was much greater than that of Cd^{2+} (data not shown). Phthalic acid either enhanced or decreased Cd^{2+} adsorption depending on the H_2L_p concentration, pH and $Cd_{(T)}$/Fe ratio. The presence of 0.6 and 6 mM $H_2L_{p(T)}$ enhanced Cd^{2+} sorption in all cases. But for 30 mM $H_2L_{p(T)}$ the adsorption of Cd^{2+} was enhanced in most conditions but inhibited at higher pH. As observed for Cu^{2+} sorption onto ferrihydrite in the presence of H_2L_p, the observed inhibition of Cd^{2+} sorption is due to the formation of solution Cd-L_p complexes.

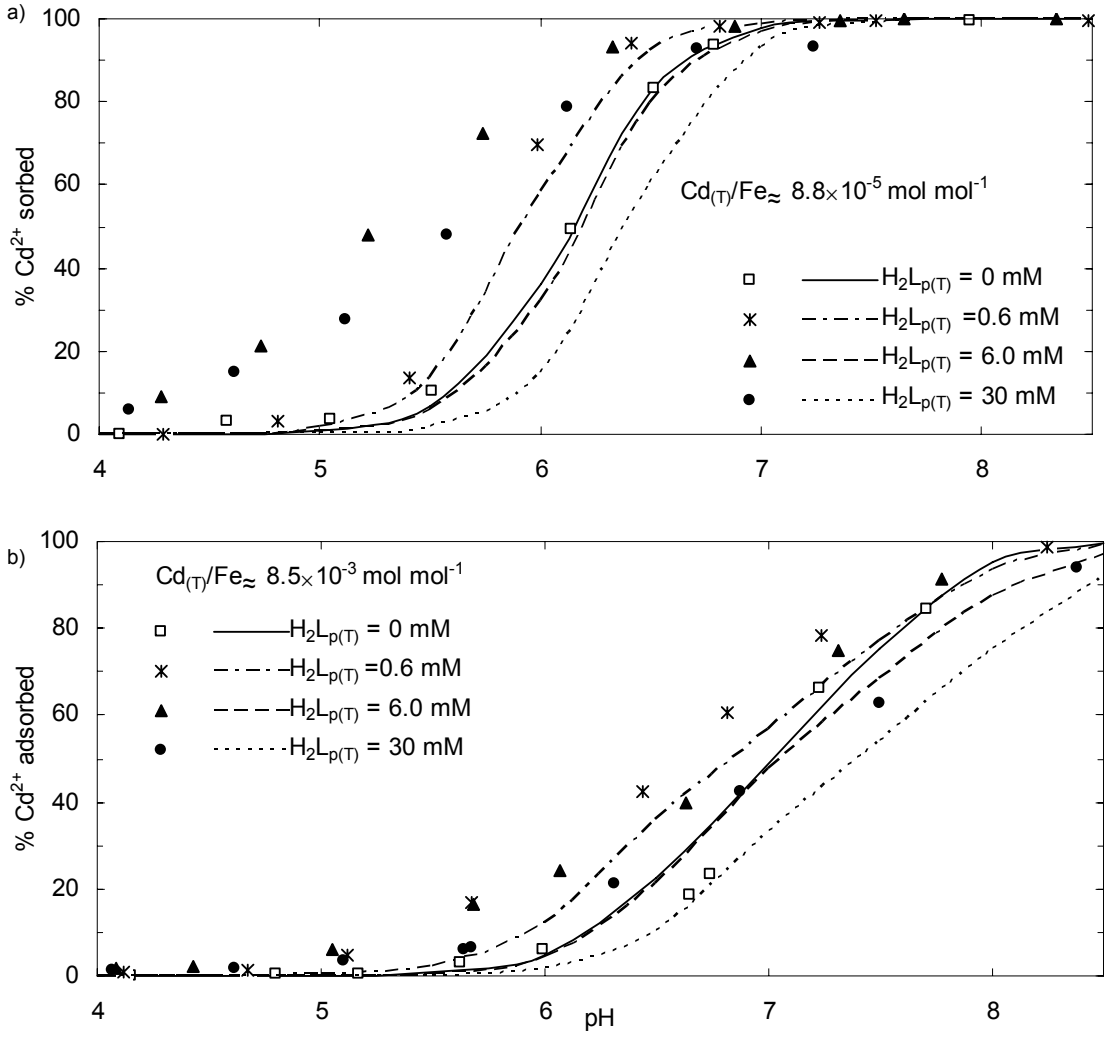

Figure 4.7 Experimental (symbols) and modelled (lines) results for Cd^{2+} sorption onto ferrihydrite in the presence of H_2L_p. Model results use only binary adsorption constants binary. Actual concentration values of I, ferrihydrite and $Cd_{(T)}$ are given in Table 4.3.

Boily et al. (2005) investigated the effect of H_2L_p on Cd^{2+} sorption onto goethite and only observed H_2L_p enhancing Cd^{2+} sorption by goethite. However the concentrations of $H_2L_{p(T)}$ in their study were 0.5 and 1 mM compared to 30 mM in the current study. All data with 0.6 and 6.0 mM $H_2L_{p(T)}$ in the current study showed enhanced Cd^{2+} sorption to ferrihydrite, with

inhibition only evident at 30 mM $H_2L_{p(T)}$ and pH > 7. Figure 4.8 shows the modelled result for distribution of solution species formed between Cd^{2+} and H_2L_p in a system with 9.14 μM $Cd_{(T)}$, and 0.6 or 30 mM $H_2L_{p(T)}$. The concentrations of solution Cd^{2+}-Lp^{2-} complex with $H_2L_{p(T)}$ = 30 mM is about as 10 times higher than that for $H_2L_{p(T)}$ = 0.6 mM when pH ranges from 4 to 8.5.

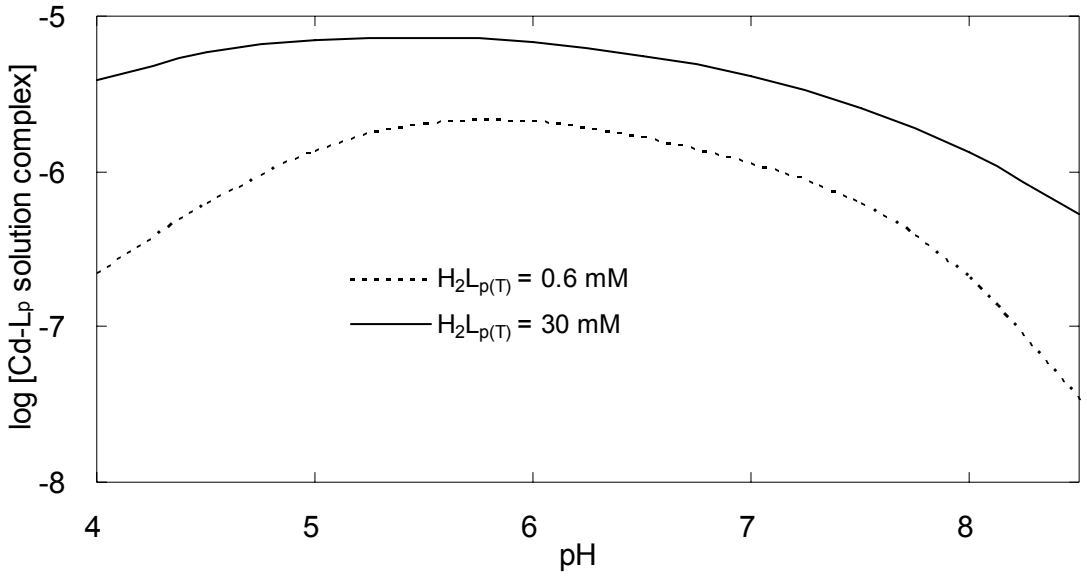

Figure 4.8 Modelled solution Cd^{2+}-H_2L_p speciation. I = 0.1 M $NaNO_3$, $Cd_{(T)}$ = 9.14 μM, and $H_2L_{p(T)}$ = 0.6 or 30 mM.

With only the binary sorption constants the model predicts the increased Cd^{2+} adsorption with 0.6 mM $H_2L_{p(T)}$ and decreased Cd^{2+} adsorption with 6 mM $H_2L_{p(T)}$ or greater (Figure 4.7). There are at least three factors that can affect Cd^{2+} sorption under such conditions; the electrostatic effects, the competition between H_2L_p and Cd^{2+} for surface site, and the competition for Cd^{2+} between the surface sites and the Cd-phthalate aqueous complexes. The increase in modelled Cd^{2+} sorption with 0.6 mM H_2L_p is caused by the electrostatic effects due to the presence of the species $\equiv FeL_p^-$, which makes the ferrihydrite surface more negatively charged and promotes Cd^{2+} sorption. Cadmium adsorption occurs at higher pH than Cu^{2+} sorption (Figures 4.1 and 4.7). For example, with $M_{(T)}/Fe < 0.005$, the pH_{50} is between 4.3 and 4.8 for Cu^{2+} but is between 5.3 and 5.8 for Cd^{2+}. In the region of the Cu^{2+} and Cd^{2+} adsorption edges, approximately 100 % H_2L_p occurs for the data with 0.6 mM $H_2L_{p(T)}$ (Figure 3.5a). However, there is more of the negatively charged $\equiv FeL_p^-$ species at the higher pH of the Cd^{2+} adsorption edge so the modelled electrostatic effect of 0.6 mM $H_2L_{p(T)}$ on Cd^{2+} adsorption at low $M_{(T)}/Fe$ is greater than that for Cu^{2+} (Figure 4.1a). Using just

binary sorption constants the modelled enhancement of Cd^{2+} adsorption by $H_2L_{p(T)}$ was much less than the measured enhancement. At higher concentration of $H_2L_{p(T)}$, the formation of Cd^{2+} and H_2L_p becomes, and Cd^{2+} sorption is modelled to be inhibited when using the binary constants. But as with Cu^{2+} such inhibition is overestimated by only using binary sorption constants, suggesting the existence of other surface ternary interactions.

Similarly to Cu^{2+} sorption onto ferrihydrite in the presence of H_2L_p, the effects of H_2L_p on Cd^{2+} sorption onto ferrihydrite could not be modelled by only using the binary constants. Therefore two ternary surface complexes were added in the model to describe the H_2L_p-Cd-ferrihydrite interaction on both type 1 and type 2 sites (Equations 4.3 and 4.4). Values for $\log K_1^{TC}$ and $\log K_2^{TC}$ were optimized from the experimental data and the results are shown in Table 4.3.

$$[\equiv Fe^wOHCdL_P^0] = [\equiv Fe^wOH^0][Cd^{2+}][L_p^{2-}](\gamma_2)^2K_2^{TC} \quad \text{Eq. 4.3}$$

$$[\equiv Fe^sOHCdL_P^0] = [\equiv Fe^sOH^0][Cd^{2+}][L_p^{2-}](\gamma_2)^2K_1^{TC} \quad \text{Eq. 4.4}$$

Table 4.3 Optimization of $\log K_1^{TC}$ and $\log K_2^{TC}$ for ternary complex formation between Cd^{2+}, H_2L_p on ferrihydrite. Data sets given in Figures 4.7. The $\log K^{TC}$ values are given for I = 0 (with standard deviations in parentheses).

$Cd_{(T)}/Fe$ (mol/mol)	$Cd_{(T)}$ (μM)	$H_2L_{p(T)}$ (mM)	Ferrihydrite (mM)	I (M)	$\log K_1^{TC}$ $\equiv Fe^sOHCdL_p^0$	$\log K_2^{TC}$ $\equiv Fe^wOHCdL_p^0$	WSOS/DF
8.7×10^{-5}	0.89	0.6	10.24	0.01	10.37 (0.11)	7.56[a]	0.41
9.2×10^{-5}	0.89	6.0	9.69	0.01	9.92 (0.020)	7.56[a]	0.58
8.8×10^{-5}	0.89	30	10.13	0.1	9.80 (0.019)	7.56[a]	1.29
8.9×10^{-3}	9.14	0.6	1.02	0.01	9.72 (0.12)	7.72 (0.060)	1.45
8.2×10^{-3}	9.14	6.0	1.12	0.01	9.75 (0.070)	7.56 (0.077)	2.88
9.4×10^{-3}	9.14	30	0.97	0.1	9.71 (0.078)	7.28 (0.11)	0.25
Weighted average (95 % confidence interval)					9.86 (9.79, 9.93)	7.56 (7.26, 7.86)	

[a] No convergence of this value so the value was fixed at the weighted average for consistency

Only a value for $\log K_1^{TC}$ could be optimized from the data with a $Cd_{(T)}/Fe$ of $\approx 8.8\times10^{-5}$, as would be expected because the type 2 sites are not significant until the type 1 sites are appreciably occupied. The values ranged from 9.80 to 10.37, the WSOS/DF were between 0.41 and 1.29, and the standard deviations less than 0.12. The value for $\log K_2^{TC}$ could be optimized from the data with $Cd_{(T)}/Fe$ ranging from 8.2×10^{-3} to 9.4×10^{-3} and these values ranged from 7.28 to 7.72, the WSOS/DF between 0.25 and 2.88, and the standard deviations

less than 0.13. The values for $\log K_1^{TC}$ with $Cd_{(T)}/Fe$ of $\approx 8.8\times10^{-5}$ were reasonably consistent with those from $Cd_{(T)}/Fe$ of $\approx 8.5\times10^{-3}$. This demonstrates that the model is consistent across all the conditions studied. Modelling Cd^{2+} sorption onto ferrihydrite in binary systems used the value 0.22 for $\log K_1^{INT}$ (Section 3.2.2). If the $\log K_1^{INT}$ for Cd^{2+} is taken as 0.47 (Dzombak and Morel 1990) then the values of $\log K_1^{TC}$ and $\log K_2^{TC}$ change only slightly to 9.81 and 7.46 respectively. The details were shown in Table 4.4.

Table 4.4 Optimization of $\log K_1^{TC}$ and $\log K_2^{TC}$ for ternary complex formation between Cd^{2+}, H_2L_p on ferrihydrite. Data sets given in Figures 4.8 and 4.9. The $\log K^{TC}$ values are given for I = 0 (with standard deviations in parentheses). Binary constants used for Cd^{2+} were $\log K_1^{INT}$=0.47, $\log K_2^{INT}$=-2.90

$Cd_{(T)}/Fe$ (mol/mol)	$Cd_{(T)}$ (μM)	$H_2L_{p(T)}$ (mM)	Ferrihydrite (mM)	I (M)	$\log K_1^{TC}$ $\equiv Fe^sOHCdL_p^0$	$\log K_2^{TC}$ $\equiv Fe^wOHCdL_p^0$	WSOS DF
8.7×10^{-5}	0.89	0.6	10.24	0.01	No converge	7.46[a]	
9.2×10^{-5}	0.89	6.0	9.69	0.01	9.91 (0.021)	7.46[a]	0.56
8.8×10^{-5}	0.89	30	10.13	0.1	9.78 (0.020)	7.46[a]	0.87
8.9×10^{-3}	9.14	0.6	1.02	0.01	9.65 (0.15)	7.60 (0.070)	2.57
8.2×10^{-3}	9.14	6.0	1.12	0.01	9.73 (0.077)	7.46 (0.089)	3.84
9.4×10^{-3}	9.14	30	0.97	0.1	9.65 (0.090)	7.16 (0.14)	0.09
Weighted average (95 % confidence interval)					9.81 (9.75, 9.86)	7.46 (7.16, 7.75)	

[a] No convergence of this value so the value was fixed at the weighted average for consistency

Figure 4.9 shows the sorption of Cd^{2+} onto ferrihydrite in the presence of H_2L_p with the modelling results that include ternary complex formation (using the weighted average values from Table 4.3) with the associated binary adsorption constants (Tables 3.2 and Table 3.3). By including the ternary complexes the model can predict the effect of H_2L_p on Cd^{2+} sorption and the discrepancies between the experimental and the predicted values of Cd^{2+} adsorption in the presence of H_2L_p are of comparable magnitude to those in the absence of H_2L_p. The calculated speciation for the ternary system with $Cd_{(T)}/Fe \approx 8.5\times10^{-3}$ is shown in Figure 4.10 to illustrate the significance of ternary complexes. Species are arranged in three groups; firstly solution Cd^{2+}-L_p^{2-} complexes, secondly sorbed ternary complexes ($\equiv Fe^sOHCdL_p^0$ and $\equiv Fe^wOHCdL_p^0$) and thirdly sorbed Cd^{2+} binary complexes ($\equiv Fe^sOCd^+$ and $\equiv Fe^wOCd^+$).

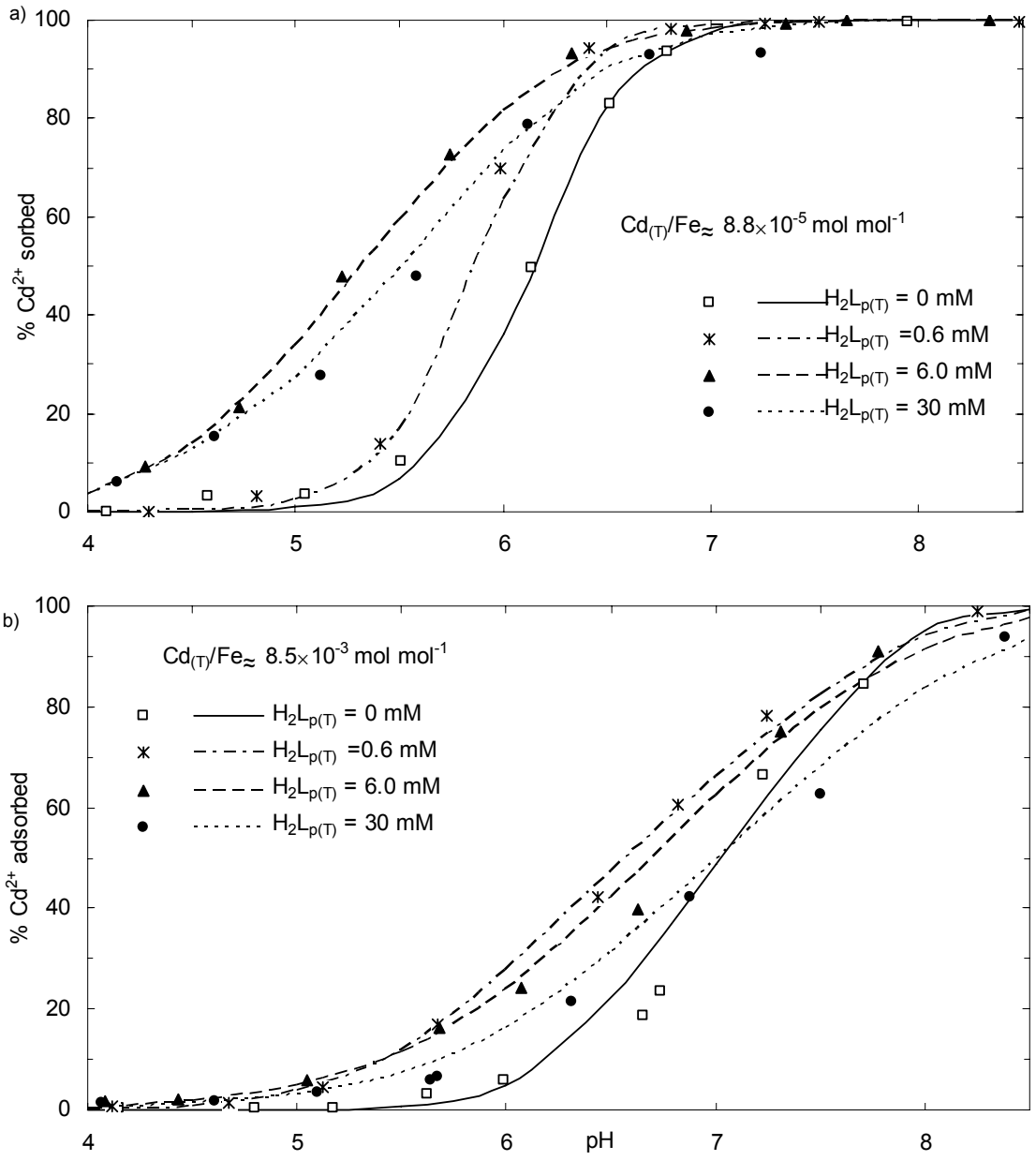

Figure 4.9 Experimental (symbols) and modelled (lines) results for Cd^{2+} sorption by ferrihydrite in the presence of H_2L_p. Model results use the weighted average ternary complex formation constants from Table 4.3 in conjunction with the adsorption constants from binary systems. Actual concentration values of I, ferrihydrite and $Cd_{(T)}$ are given in Table 4.3.

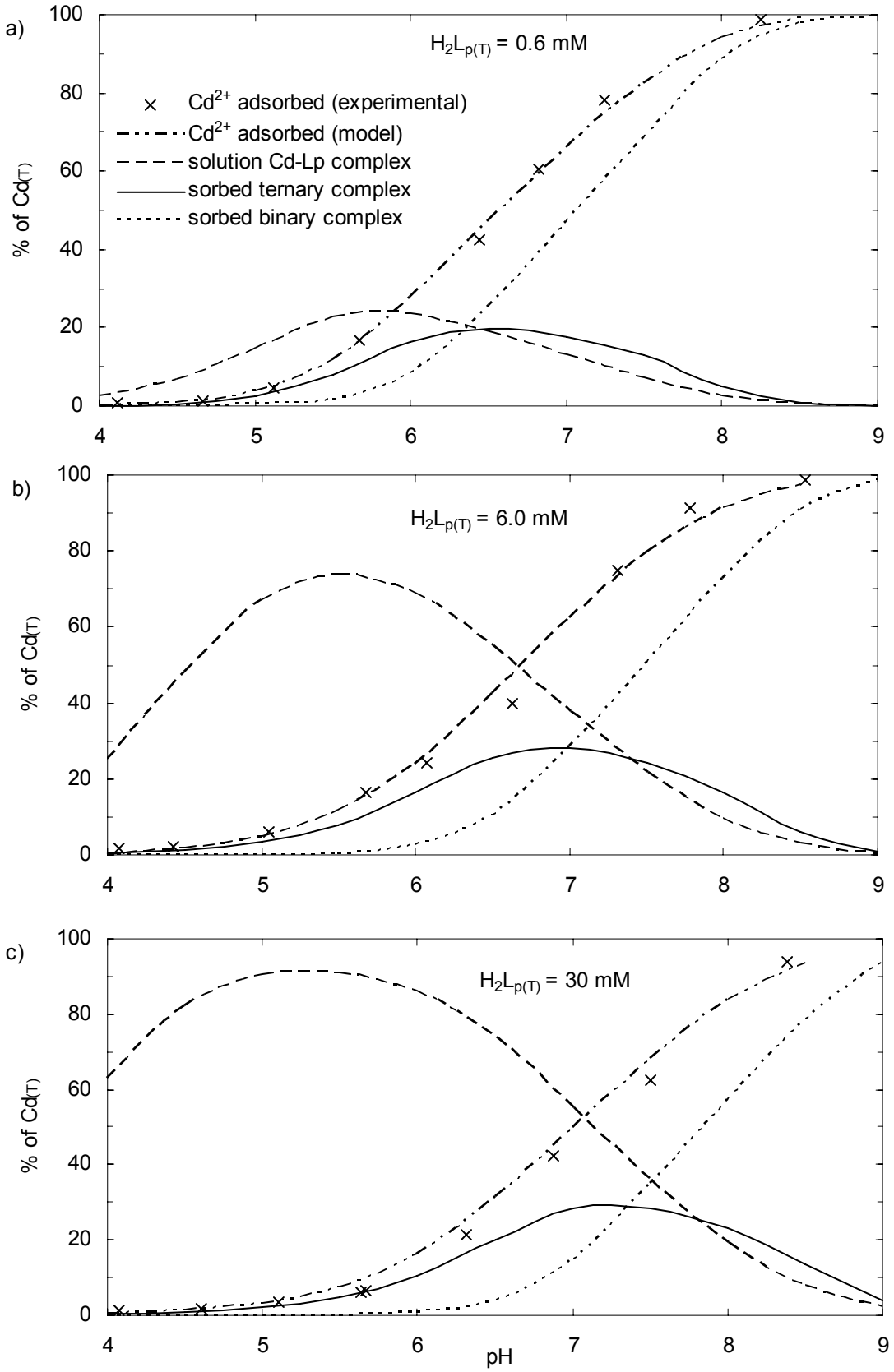

Figure 4.10 Modelled speciation of Cd^{2+} in the H_2L_p-Cu^{2+}-ferrihydrite system. $Cd_{(T)}/Fe \approx 8.5\times10^{-3}$. Legends used in b) and c) represent the same Cd speciation as those in a). Actual concentration values of I, ferrihydrite and $Cd_{(T)}$ are given in Table 4.3.

A similar species distribution pattern for the Cd^{2+}-L_P^{2-}-ferrihydrite ternary system was observed as in the L_P^{2-}-Cu^{2+}-ferrihydrite ternary system. For all $H_2L_{p(T)}$ concentrations ternary complexes account for approximately 20~30 % of the $Cd_{(T)}$, peaking from pH 6.5 to 7.5. At lower pH Cd^{2+}-L_p^{2-} solution complexes dominate while at higher pH adsorbed binary Cd^{2+} dominates the speciation. The modelled species distribution for ternary complex formation is similar to that calculated for Cd^{2+} sorption onto goethite in the presence of H_2L_p. Boily et al. (2005) calibrated the CD-MUSIC model such that the calculated species distribution was consistent with EXAFS and ATR-FTIR data. For a system with 0.5 mM $Cd_{(T)}$, 0.5 mM $H_2L_{p(T)}$ and 8.1 gL^{-1} goethite, about 40 % $Cd_{(T)}$ occurred as ternary complexes in the pH region just below where binary adsorption complexes becomes dominant (Figure 4.11). The ternary complexes identified by Boily et al. (2005) involved an inner sphere Cd^{2+} and either an inner-sphere phthalate or an outer-sphere phthalate (Figure 4.12) compared to the DLM where there are no outer sphere species. The CD-MUSIC modelled surface species distribution was consistent with the ATR-IR results in their work (Boily et al. 2005), and the surface complex formed by the inner-sphere phthalate with Cd^{2+} was found to be relatively more significant than the outer-sphere phthalate with Cd^{2+} at pH<7.6 as is shown in Figure 4.11.

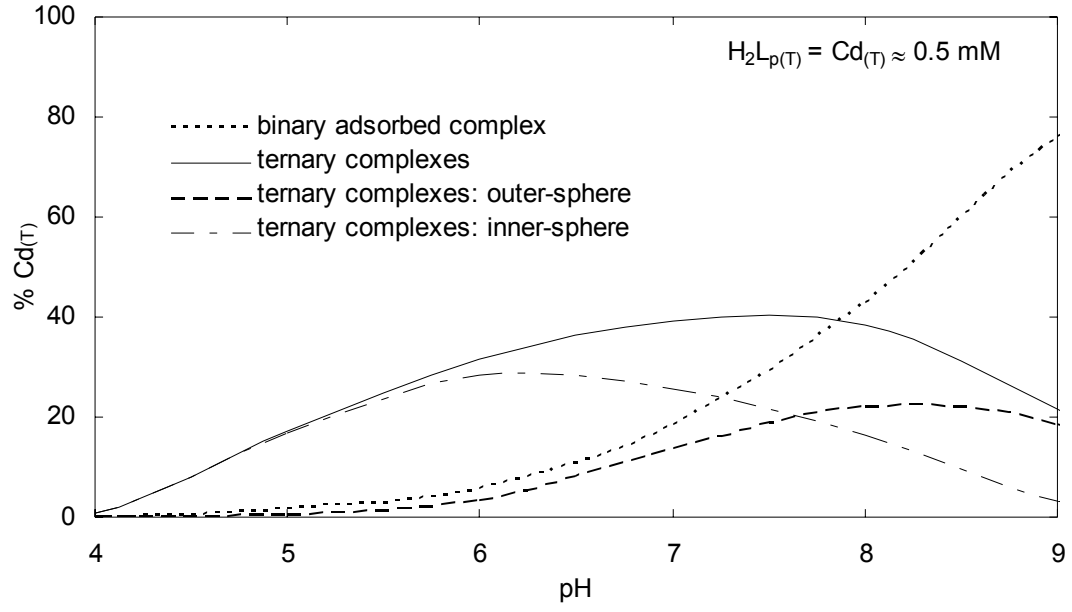

Figure 4.11 Modelled Cd^{2+} surface species distribution in a H_2L_p-Cd^{2+}-goethite system. Data are from Boily et al. (2005). Goethite ≈ 8.1 gL^{-1}, with surface area 37m^2 g^{-1}.

4.4. Ternary surface complex properties

Surface structures of complex formed between ligand, cation ion and iron oxide have been investigated for goethite ternary systems with EXAFS and ATR-IR. Two types of ternary complex structures were proposed: one is that metal ion is bound directly to the iron oxide surface, the other is that metal ion is bound through a ligand on the surface. Although there has been no spectroscopic investigation of the cation-L_p^{2-}-ferrihydrite system it has been proposed that the mechanism for the SO_4^{2-} induced enhancement of metal sorption on ferrihydrite and goethite might be the same or similar (Swedlund et al. 2003; Swedlund et al. 2009). This was based on investigations of the effect of SO_4^{2-} on Cu^{2+}, Cd^{2+}, Pb^{2+} and Zn^{2+} sorption by ferrihydrite and goethite. A linear relationship was found between sorption constants for ternary complex formation ($logK^{TC}$) and metal sorption ($logK^{INT}$) in binary systems and data for the Cu^{2+}-SO_4^{2-}-goethite system also fitted the same relationship (Swedlund et al. 2003). It is possible to compare the sorption constants for ternary complex formation in the Cu^{2+}-L_p^{2-}-ferrihydrite system with previously reported value for Cu^{2+}-L_p^{2-}-goethite (Ali and Dzombak 1996c). Ali and Dzombak (1996c) used the species $\equiv FeOHL_p^{2-}$ as opposed to $\equiv FeL_p^{-}$ used in this work. However in the region of the Cu^{2+} adsorption edge the neutral phthalate surface species ($\equiv FeHL_p$ that was used in both studies with similar formation constants) accounts for > 97 % of the binary adsorbed phthalate. These data are shown in Figure 4.12 along with data for cations adsorbing in the presence of SO_4^{2-}. For both ligands Figure 4.12 shows that ternary complex stability increases with the increase in the stability of the adsorbed cation. This is consistent with the spectroscopically determined ternary complex structures for these ligands with Cd^{2+} (Boily et al. 2005) or Pb^{2+} (Elzinga et al. 2001) on goethite which showed the cation binding on the surface.

No spectroscopic studies have been done on the structure of the ternary surface complexes on ferrihydrite, but the fact that both data points for goethite closely fit the relationships for ferrihydrite in Figure 4.12 suggests that the ternary complex structures on ferrihydrite could be expected to be the same or at least similar to those formed on goethite. In addition the fact that the $logK^{TC}$ values for ternary complexes with L_p^{2-} are higher than the corresponding values for SO_4^{2-} would suggest that the stability of the ternary complex also depends on the strength of the ligand metal interaction, as would be intuitive. The logK values for forming the solution complex CuA^0, where A is either L_p^{2-} or SO_4^{2-}, are 4.02 and 2.36 respectively. The difference between these two values is similar to the difference between $logK_2^{TC}$ for Cu-

L_p and Cu-SO_4 ternary complexes on both ferrihydrite (9.43 (this thesis) and 7.83 (Swedlund and Webster 2001), respectively) and on goethite (10.91 and 9.68, respectively) (Ali and Dzombak 1996c) and more generally, to the difference between the intercepts of the two lines in Figure 4.12. It should be noted that having a ligand with a higher value of $\log K_x^{TC}$ does not necessarily mean that the ligand will increase cation adsorption more significantly. Because the corresponding solution complexes are also formed more strongly the converse can be true, depending on the ligand concentration. For example sulfate enhanced Cu^{2+} adsorption by ferrihydrite up to 20 mM sulfate (Swedlund and Webster 2001) whereas H_2L_p inhibited Cu^{2+} adsorption at concentrations greater than about 6 mM in the current work.

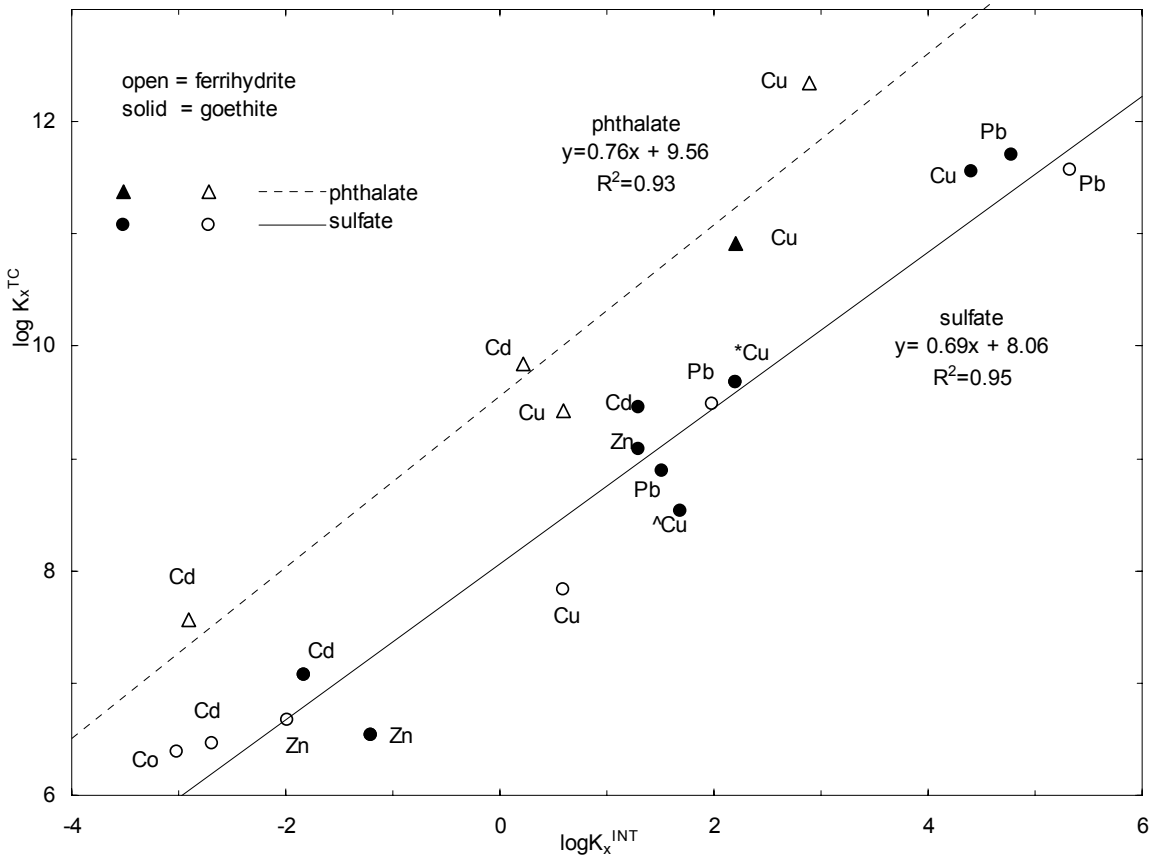

Figure 4.12 Linear Free Energy Relationship between the values of $\log K_x^{TC}$ for ternary complex formation and $\log K_x^{INT}$ for binary adsorption of the corresponding cation on the corresponding site. Data for $^{*}Cu^{2+}$ adsorption on goethite with L_p^{2-} or sulfate are from Ali and Dzombak (1996c) . Data for Cu^{2+}, Zn^{2+}, Cd^{2+}, Pb^{2+} and Co^{2+} adsorbing on ferrihydrite with SO_4^{2-} are from Swedlund and Webster (2001) and Swedlund et al. (2003). Data for $^{\wedge}Cu^{2+}$, Zn^{2+}, Cd^{2+} and Pb^{2+} adsorbing on goethite with SO_4^{2-} are from Swedlund et al (2009).

4.5. Conclusions

In ternary systems H_2L_p caused both the enhancement and inhibition of Cu^{2+} and Cd^{2+} sorption depending on the conditions such as the pH, $M_{(T)}$/Fe and $H_2L_{p(T)}$/Fe ratios. Generally, when Cu^{2+} and Cd^{2+} sorption onto ferrihydrite is increased in the presence of H_2L_p, this is predominantly due to the formation of surface ternary complexes. At higher pH and $H_2L_{p(T)}$/Fe ratios, copper and cadmium adsorption was inhibited by H_2L_p because of the formation of M-phthalate complexes in solution.

The sorption of Cu^{2+} and Cd^{2+} onto ferrihydrite in the presence of H_2L_p over a wide pH range and sorbate/sorbent ratio was accurately modelled by the DLM with the inclusion of two ternary surface complexes on both type one ($\equiv Fe^sOHML_p^0$) and type two ($\equiv Fe^wOHML_p^0$) sites on the ferrihydrite surface. Adsorption constants for ternary complex formation were determined which produced a consistent set of equations to describe the observed results. The relationship between binary metal adsorption constants and the ternary complex adsorption constants from this and previous studies suggest several properties of ternary complexes. By comparing results from different iron oxides, ternary complex structures on both ferrihydrite and goethite are presumably either the same or similar. Secondly, by comparing results from different metal cations, those cations forming strong binary surface complexes also form strong ternary complexes. This is consistent with EXAFS studies of ternary complex structures on goethite showing that they involve the cation being coordinated to the goethite surface. Thirdly, by comparing results from ternary systems with H_2L_p and sulfate, ligands forming stronger solution complexes with cations will also form stronger surface ternary complexes. One corollary of this is that ligands forming stronger surface ternary complexes will not necessarily strongly enhance cation adsorption.

Chapter 5. Phthalic Acid Biodegradation

5.1. Introduction

The objective of this study was to provide insight into trace metal speciation and distribution in aquatic systems. Bacterial activity occurs in almost all aquatic systems and one of this work's objectives was to study how metal speciation is influenced by the metabolism of organic ligands by bacteria. To achieve this target a suitable bacteria strain needed to be chosen that was able to utilize phthalic acid as an energy source. The preferable bacteria should be common in natural or engineered environments and be able to metabolize phthalic acid within a time frame of a few days. Several bacterial strains have been found capable of degrading phthalic acid in either anaerobic or aerobic conditions (Aftring et al. 1981; Aftring and Taylor 1981; Jianlong et al. 2004; Quan et al. 2005; Wang et al. 1996; Wang et al. 1997a; Wang et al. 1997b; Wang et al. 2003). Four bacteria strains were investigated in this work: *Bacillus subtilis*, which is commonly found in soil and aqueous environments, and another three bacteria strains that were isolated from a common wastewater treatment plant (Section 2.2.1). The ability of each strain to metabolize phthalic acid was tested under various conditions, including pH, concentrations of Cu^{2+}, Cd^{2+} and essential nutrients, the presence of ferrihydrite. These experiments were performed in capped tubes with H_2L_p as the only carbon source.

5.2. *Bacillus subtilis*

5.2.1 *Bacillus subtilis* growth and quantification

The growth curve of *Bacillus subtilis* in BHI was expressed by plotting the OD_{600} versus time and the relationship between *Bacillus subtilis* colonies and OD_{600} is given in Figure 5.1. Figure 5.1a shows the typical three phases of bacterial growth, lag phase, log phase and stationary phase. The lag phase (first 2 h) is the adjustment period for *Bacillus subtilis* cells to break down the energy source within the immediate environment. The log phase appeared after 2 h and during this period *Bacillus subtilis* grew rapidly for another 2 h, followed by the stationary phase which occurred after 4 h. Figure 5.1d shows the linear relationship between the dry weight of cells within a volume of BHI broth at $OD_{600} = 0.5$. Using Figure 5.1 the

amount of bacterial cells used in the H_2L_p degradation and sorption experiments can be quantified, and the dry weight of each *Bacillus subtilis* cell was estimated to be 2×10^{-13} g. This is within the reported values obtained from transmission electron microscopy and densitometric image analysis, ranging from 8.3×10^{-14} to 1.2×10^{-12} g (Lofferer-Krößbacher et al. 1998). Under these experimental conditions when OD_{600} reaches 0.5, the bacterial cell concentration in the growth media BHI is approximately 10^9 cells mL^{-1} or 0.25 mgL^{-1} (Figure 5.1).

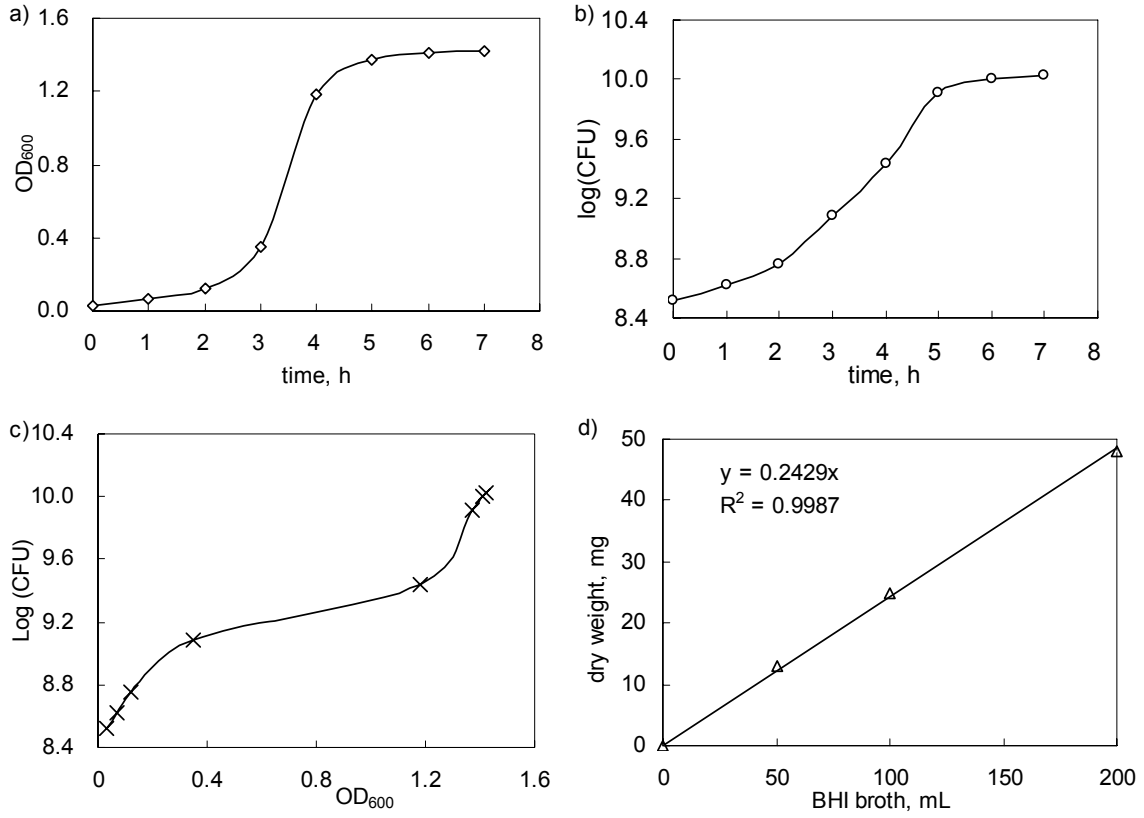

Figure 5.1 Quantification of *Bacillus subtilis* cells grown in BHI broth. a) shows increasing broth turbidity with time; b) shows the increase of bacterial colony-forming units (CFU) with time; c) the relationship between turbidity and CFU; d) a linear relationship between broth volume and bacterial cell dry weight

5.2.2 Phthalic acid metabolism by *Bacillus subtilis* in the absence of ferrihydrite

Phthalic acid degradation by *Bacillus subtilis* was initially examined in systems that did not contain ferrihydrite. The experimental suspensions were made by adding washed *Bacillus subtilis* cells (Section 2.2.4) from the bacterial growth log phase (0.1 gL^{-1}, dry weight) into 0.01 M $NaNO_3$ solution with 6 mM $H_2L_{p(T)}$, with or without 16 μM Cd^{2+}. The initial pH

values of the samples were adjusted to range from 3.5 to 9.6 and typical results are shown in Figures 5.2 and 5.3. In all samples with an initial pH ≥ 5.91 more than 80 % $H_2L_{p(T)}$ was degraded by *Bacillus subtilis* within 169 h in the absence of Cd^{2+} (Figure 5.2). This is consistent with reported results showing that *Bacillus subtilis* was capable of metabolizing phthalic acid (Quan et al. 2005). In the experiments without Cd^{2+} more than 40 % $H_2L_{p(T)}$ degradation was observed within 96 h for most samples with initial pH ≥ 5.91. In contrast less than 20 % $H_2L_{p(T)}$ degradation was found in the presence of 16 μM Cd^{2+} within 96 h for all samples, although about 40 % ~ 65 % $H_2L_{p(T)}$ degradation occurred among samples with pH ≥ 5 after 169 h (Figure 5.3). The presence of Cd^{2+} appeared to suppress bacterial metabolism. One possible reason is that cadmium might have inhibited *Bacillus subtilis* growth, as it has been found that the growth of *Burkholderia cepacia* PR_{1301} was prohibited at pH of 7 with 2.22 mM Cd^{2+} (Van Nostrand et al. 2005). In the first 96 h it is possible that *Bacillus subtilis* adjusted to the environmental conditions, and became tolerant to Cd^{2+} and therefore its ability to degrade H_2L_p increased. Viable bacteria were recovered from those samples with initial pH < 6 even though H_2L_p had not been degraded, indicating Cd^{2+} inhibited cell activity rather than toxicity.

Both Figure 5.2 and Figure 5.3 show that the initial pH affects H_2L_p metabolism. In the absence of Cd^{2+} more than 80 % degradation was only obtained for samples with initial pH > 5.9. Samples with an initial pH < 5.9 had less than 20 % H_2L_p metabolism (Figure 5.2). Similarly, in the presence of Cd^{2+} less than 20 % H_2L_p degradation was observed for the sample with an initial pH of 4. It was observed that during H_2L_p degradation the pH for all systems changed towards a neutral pH (Figure 5.4). The pH effects on H_2L_p degradation and changes during the degradation indicated that the optimal pH for H_2L_p degradation by *Bacillus subtilis* is close to neutral.

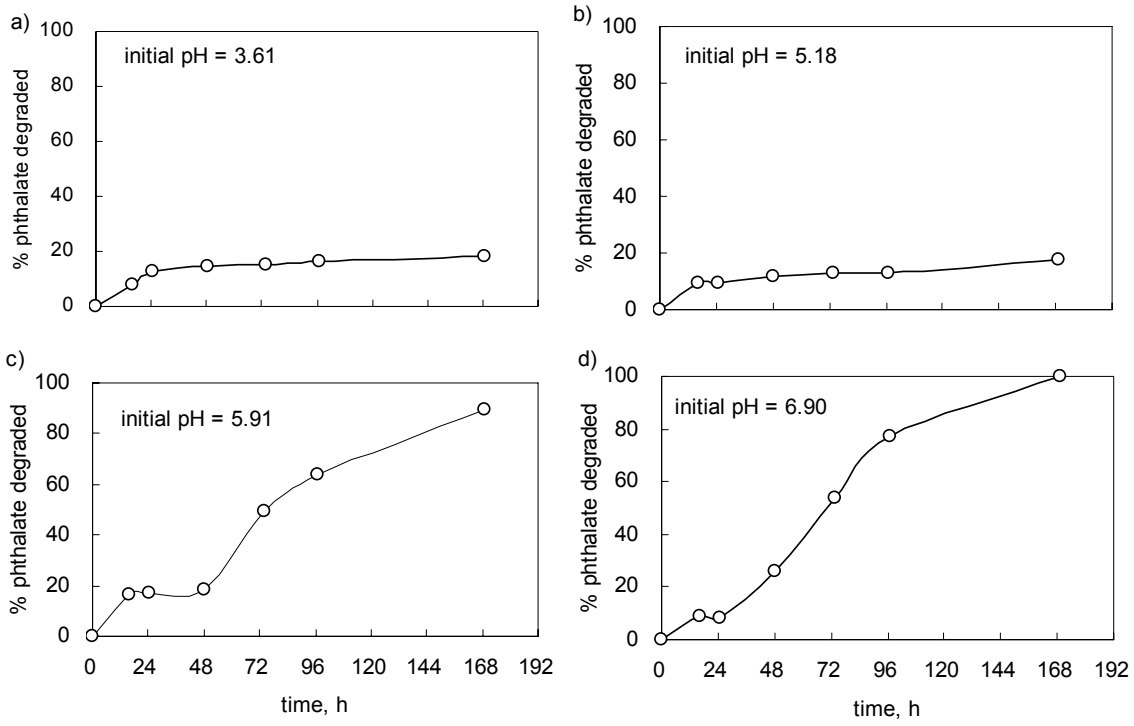

Figure 5.2 Phthalic acid metabolism by *Bacillus subtilis* in 0.01 M $NaNO_3$

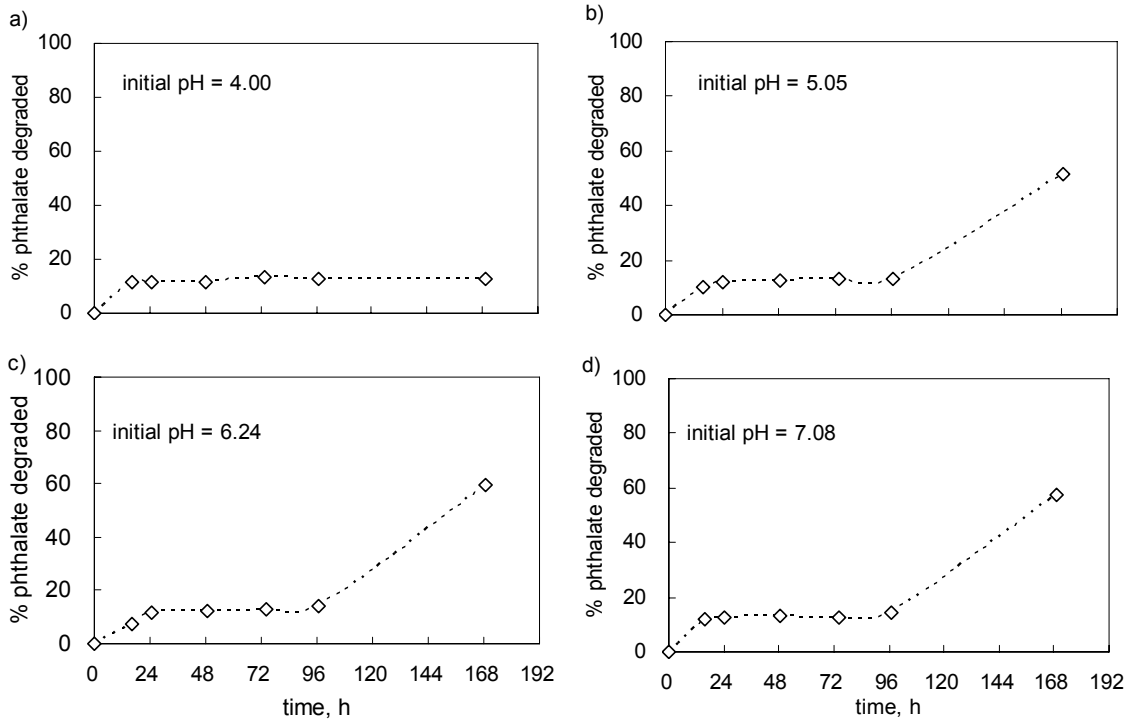

Figure 5.3 Phthalic acid metabolism by *Bacillus subtilis* in the presence of Cd^{2+}. a, b, c, and d represent batches with different starting pH values. $Cd_{(T)}$ = 16 µM, I = 0.01 M $NaNO_3$

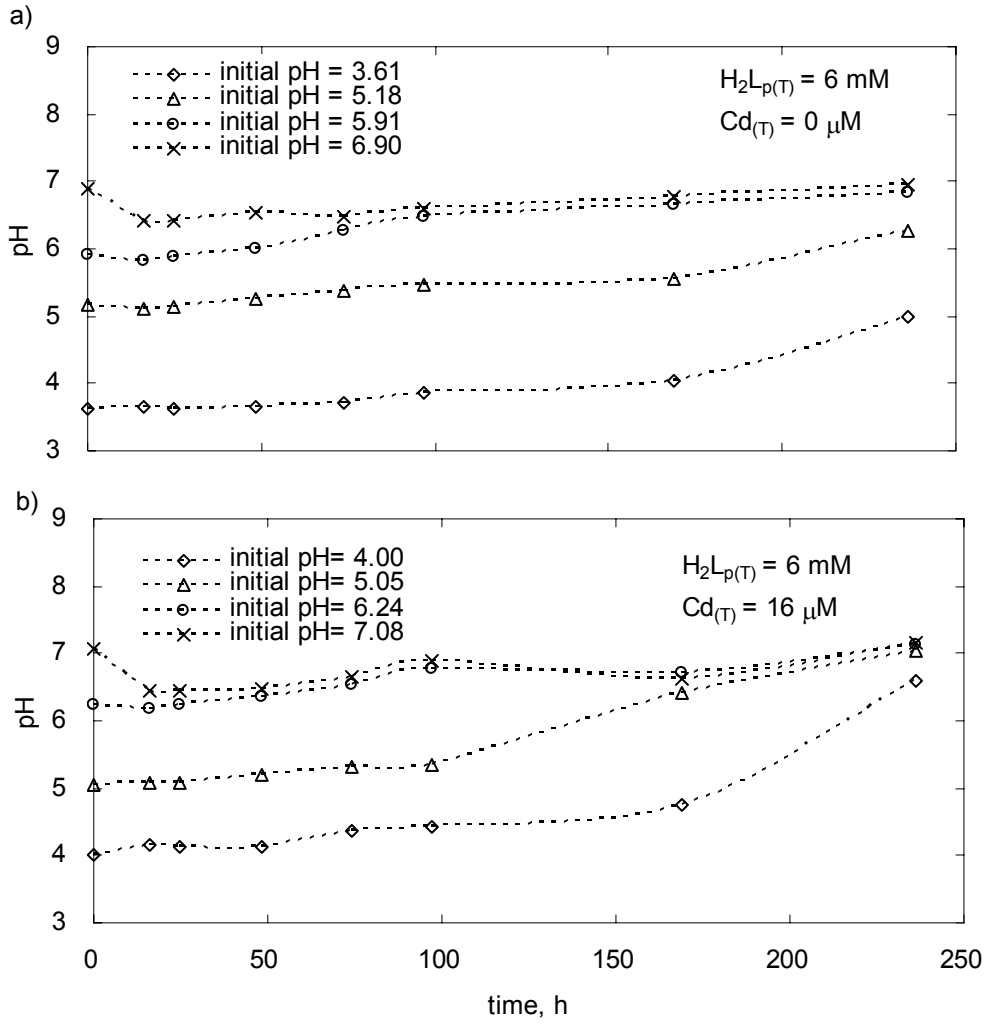

Figure 5.4 pH changes during *Bacillus subtilis* degradation of H_2L_p in the absence (a) and presence (b) of Cd^{2+}

5.2.3 Phthalic acid degradation by *Bacillus subtilis* in the presence of ferrihydrite

Previous experiments (Section 5.2.2) demonstrated that *Bacillus subtilis* was able to degrade phthalic acid in the absence of ferrihydrite. However, its ability to degrade H_2L_p in the presence of ferrihydrite must be examined to achieve the objectives of this thesis. Therefore H_2L_p metabolism by *Bacillus subtilis* was further carried out by adding washed *Bacillus subtilis* from the log phase to H_2L_p-Cd^{2+}-ferrihydrite suspensions with the pH pre-adjusted to range from 4 to 9. The amount of metabolized H_2L_p was determined as described in Section 2.2.7. The % sorbed H_2L_p as a function of pH, is shown in Figure 5.5 with the results from modelling ferrihydrite adsorption. Compared to abiotic systems, phthalic acid sorption was decreased in the ternary biotic systems, possibly due to the screening of the ferrihydrite

surface sites by *Bacillus subtilis*. Coatings of iron oxides on bacterial surfaces have been observed in many studies and are discussed in Chapter 7.

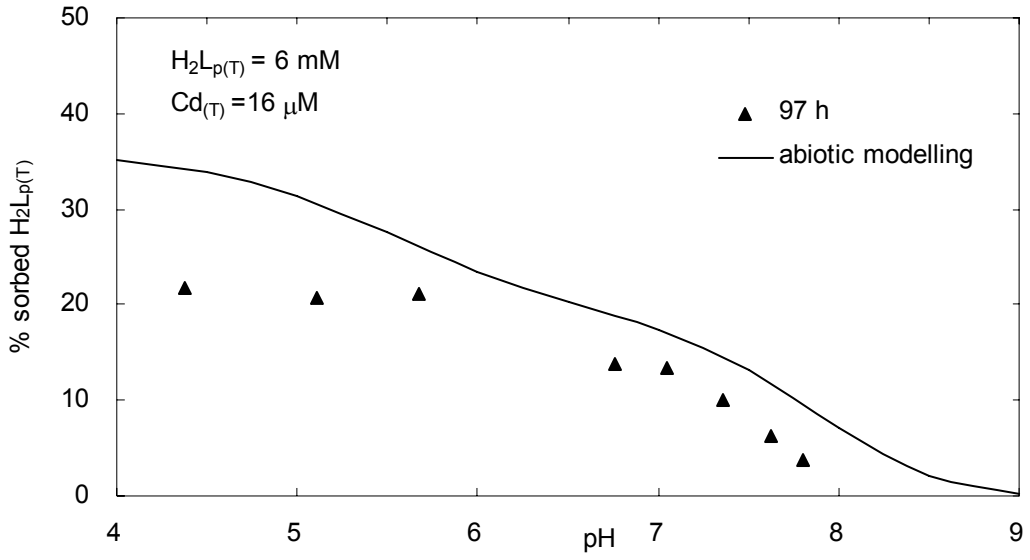

Figure 5.5 Sorption of H_2L_p in Cd^{2+}-ferrihydrite biotic and abiotic systems (I = 0.01 M $NaNO_3$). Abiotic result is from modelling using parameters described in Chapter 4.

Unlike the systems in the absence of ferrihydrite, phthalic acid degradation was found to be negligible in the presence of ferrihydrite (Figure 5.6). One possible reason is that ferrihydrite particles have formed a barrier to the soluble H_2L_p by coating the surface of *Bacillus subtilis* cells. Another possible reason for *Bacillus subtilis* being unable to decompose H_2L_p might be the unavailability of some essential nutrients for *Bacillus subtilis* activity in ferrihydrite suspensions. Bacteria require several nutrients for their growth to sustain their bioactivity (Beveridge and Koval 1981). The H_2L_p metabolism experiments were performed in 0.01 M $NaNO_3$ in 18 MΩ·cm water. In systems without ferrihydrite trace levels of nutrients present are evidently sufficient to sustain *Bacillus subtilis* bioactivity. In the presence of ferrihydrite the sorption of nutrients (such as SO_4^{2-}, PO_4^{3-}, Ca^{2+} or Mg^{2+}) may reduce their concentration to below necessary levels to sustain bioactivity. This theory was tested by adding a Bushnell-Hass Broth (BHB) containing SO_4^{2-}, PO_4^{3-}, Ca^{2+}, Mg^{2+}, Na^+, K^+, NO_3^- into the system with ferrihydrite and at neutral pH. The effect on the degradation of H_2L_p is shown in Figure 5.6. The addition of BHB did increase *Bacillus subtilis* degradation of H_2L_p presumably by providing trace nutrients, but only about 40 % of the $H_2L_{p(T)}$ was degraded within 300 h. Therefore, even though *Bacillus subtilis* is able to metabolize H_2L_p it is not able to do this effectively in the presence of ferrihydrite. For this reason an alternative bacteria strain was sought.

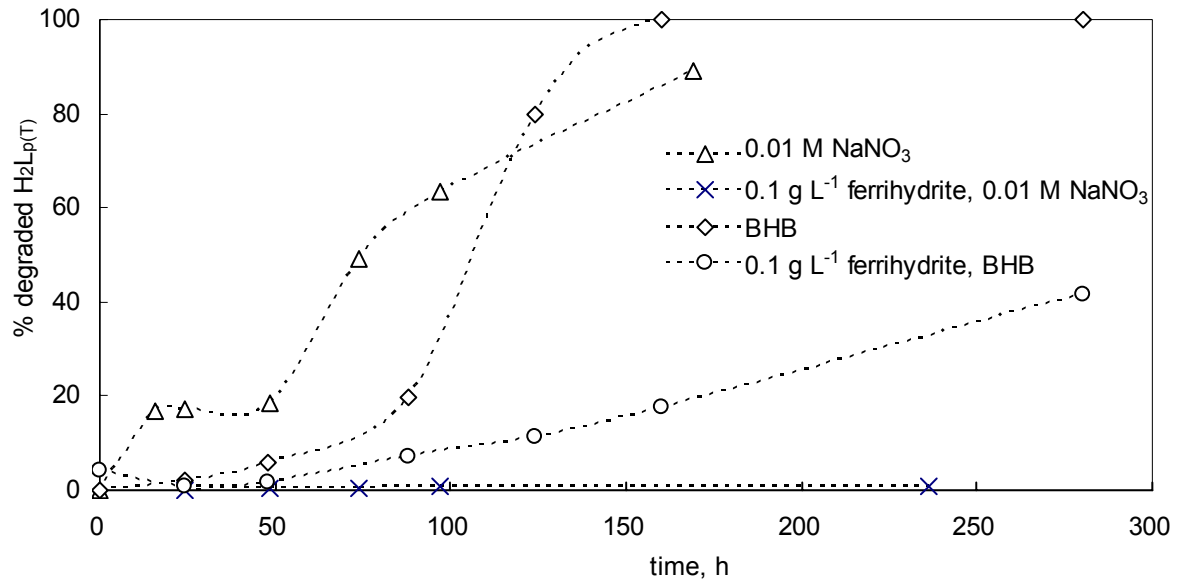

Figure 5.6 Phthalic acid degradation by *Bacillus subtilis* in the absence and presence of ferrihydrite. $H_2L_{p(T)}$ = 6 mM, initial pH ≈ 6

5.3. Selecting bacteria by growth in H_2L_p

Because *Bacillus subtilis* was not able to efficiently metabolize H_2L_p in the presence of ferrihydrite. The ability of other bacterial strains to metabolize H_2L_p was investigated as described in this section. Three bacteria strains (designated C1, C2 and C3) were isolated and purified from aerobic activated sludge of a sewage wastewater treatment plant as described in Section 2.2.2. Their ability to utilize phthalic acid as a sole carbon source was examined before further identification. The washed cells of C1, C2 and C3 were individually or in combinations added to the BHB solutions (pH from 6.0 to 7.5) containing H_2L_p and then they were continuously shaken at room temperature. The growth, as an indicator of the ability to degrade H_2L_p was observed by measuring the OD_{600} over time, and the results are given in Figure 5.7.

Of all the systems only those containing C1 showed obvious growth and reached a peak value of OD_{600} within 32 h. The OD_{600} did not increase for samples with only C2 or C3 or both C2 and C3 throughout the experimental time of 145 h. This indicated that the bacteria strain C1 was able to grow when H_2L_p was present as the carbon source but not C2 or C3. This bacterial strain was then identified by 16S rDNA sequencing to be *Comamonas spp.*. Several *Comamonas* strains isolated from either sewage activated sludge or soil have shown their

ability to metabolize numerous organic compounds including phthalic acid (Cui et al. 2004; Jadhav et al. 2008; Wang et al. 2003; Wu et al. 2005).

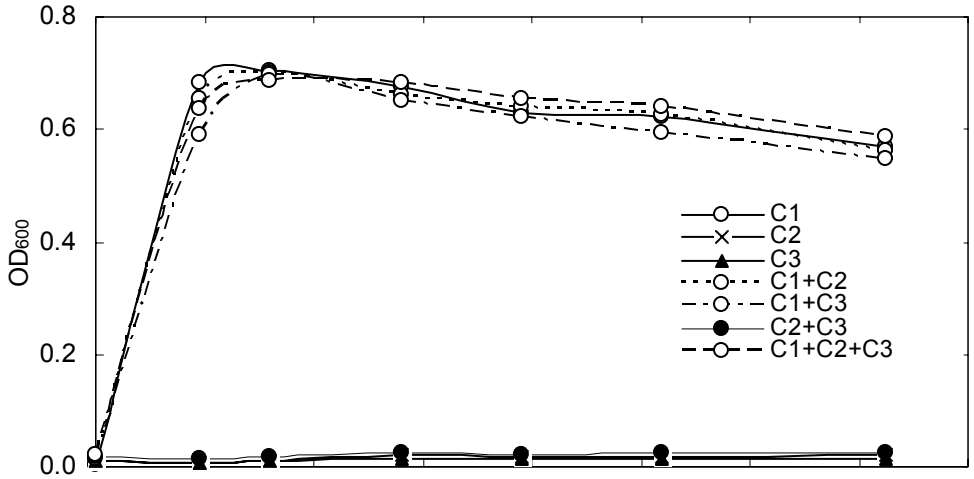

Figure 5.7 Growth of bacterial strains C1, C2 and C3 in the presence of $H_2L_{p(T)}$ in BHB. $H_2L_{p(T)}$ = 6 mM, neutral pH.

5.4. *Comamonas spp.*

5.4.1 *Comamonas spp.* incubation and quantification

Comamonas spp. growth in Trypticase Soy Broth supplemented with 0.5 % (V/V) yeast extract (TSBYE) showed the typical three phases, lag phase, log phase and stationary phase, as shown in Figure 5.8a. The stationary phase occurred after about 7 h. The measured CFU versus time and OD_{600}, and the cell dry weight versus growth broth volume are also given in Figure 5.8. The ratio of wet/dry weight of *Comamonas spp.* cells was determined (Section 2.2.4) to be 5.4 based on an average value from five parallel experiments (detailed experimental data are given in appendix). It has been reported that the cell wet to dry weight ratio is fairly reproducible but varies over a modest range depending on the bacterial species examined (Borrok et al. 2004; Burnett et al. 2006). The value of 5.4 obtained from this work for *Comamonas spp.* is in close agreement with reported values for several other bacterial species following a similar cell wash process. For example, values ranging from 5.7 to 7.7 for *Anoxybacillus flavithermus* cell wet to dry ratio were determined by Burnett et al (2006), and an average value 5.0 was suggested for general use based on values ranging 3.1 to 6.5 determined from individual experiments for *Pseudomonas fluorescens*, *Shewenella*

oneidensis, *Staphyloccocs aureus*, *Bacillus subtilis*, and *Bacillus cereus* (Borrok et al. 2004; Burnett et al. 2006).

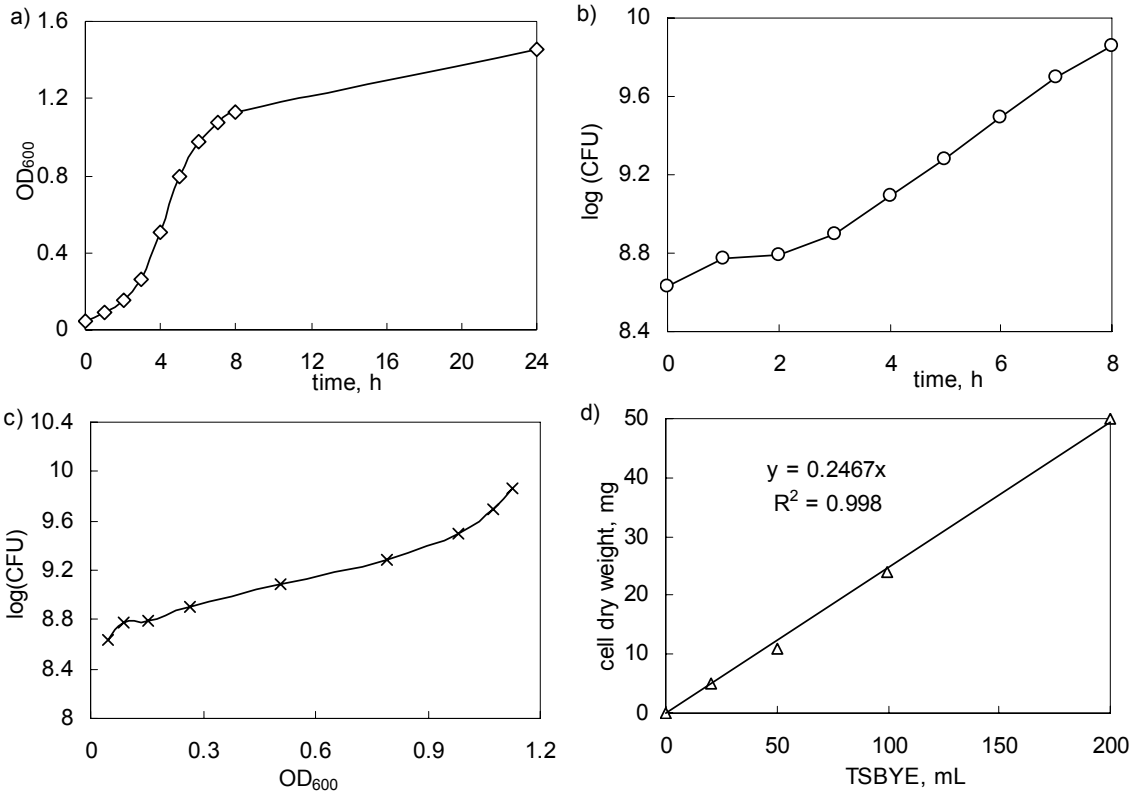

Figure 5.8 Quantification of *Comamonas spp.* cells under neutral pH in TSBYE broth. a) shows increasing broth turbidity with time; b) shows the increase of bacterial colony-forming units (CFU) with time; c) the relationship between turbidity and CFU; d) a linear relationship between broth volume and bacterial cell dry weight

5.4.2 Phthalic acid metabolism by *Comamonas spp.*

1. Phthalic acid degradation media and the presence of Cu^{2+} and Cd^{2+}

BHB is designed to provide bacteria with non-carbon nutrients (Bushnell and Hass 1940). Unfortunately it contains high concentrations of nutrients which can act as inorganic ligands such as sulfate (1.7 mM), phosphate (14.7 mM) and ammonium (15.2 mM), and therefore BHB could influence trace metal speciation and distribution in systems in this work (Elzinga et al. 2001; Kuo and McNeal 1984; Li et al. 2006; Lin et al. 2004; Nilsson et al. 1996; Ostergren et al. 1999; Venema et al. 1997; Wang and Xing 2004; Xu et al. 2007). The concentrations of these components in BHB are higher than those in general aquatic systems. For example, the $[PO_4^{3-}]$ in a river water was at ppb level (< 1 μM) compared to ~15 mM $[PO_4^{3-}]$ in BHB (Motomizu et al. 1983). To avoid the undesirable complication due to the high concentrations of sulfate, phosphate or ammonium in this work, experiments were

undertaken to prepare a solution based on the formula for the BHB from $MgSO_4 \cdot 7H_2O$, $CaCl_2 \cdot 2H_2O$, KNO_3 and $NaH_2PO_4 \cdot H_2O$ which will provide *Comamonas spp.* with sufficient nutrients to metabolize H_2L_p as the carbon source without metal adsorption being significantly affected. Because the experiments are performed in 0.01 M $NaNO_3$ the BHB ammonium salt was not used. The modified BHB (termed solution Y) contained 1 μM $MgSO_4$, 2 μM $CaCl_2$, and 20 μM KNO_3. Initial investigation on the effect of Cu^{2+} and Cd^{2+} on the *Comamonas spp.* growth used 0.2 ~ 1 mM NaH_2PO_4. Subsequent experiments examining H_2L_p metabolism used 1 μM NaH_2PO_4.

The effect of Cu^{2+} or Cd^{2+} on H_2L_p biodegradation by *Comamonas spp.* was tested by observing the bacterial growth in systems containing H_2L_p and Cu^{2+} or Cd^{2+}. The initial pH values were adjusted to be 6.0 and 7.5, and all the systems were prepared in 0.01 M $NaNO_3$ containing H_2L_p and solution Y with NaH_2PO_4 ranging from 0.2 to 1.0 mM. The bacterial growth was examined by measuring the OD_{600} over one week and typical results are given in Figure 5.10. In the absence of Cu^{2+} or Cd^{2+}, *Comamonas spp.* showed the same growth at all PO_4^{3-} concentrations with the peak value of $OD_{600} \approx 0.6$ occurring at about 80 h. This indicated that *Comamonas spp.* was able to grow under these conditions with PO_4^{3-} as low as 0.2 mM. The bacterial growth in samples containing 8.9 μM $Cd^{2+}_{(T)}$ was similar to that in samples in the absence Cd^{2+}, with a peak OD_{600} value of ~0.6 occurring within 80 h, indicating that *Comamonas spp.* bioactivity was not affected by Cd^{2+}. The presence of 23.6 μM $Cu_{(T)}$ appeared to suppress the growth of *Comamonas spp.* under all the investigated conditions. The OD_{600} never reached 0.4 for most samples containing Cu^{2+} within one week, indicating that the presence of Cu^{2+} inhibited the activity of *Comamonas spp.*.

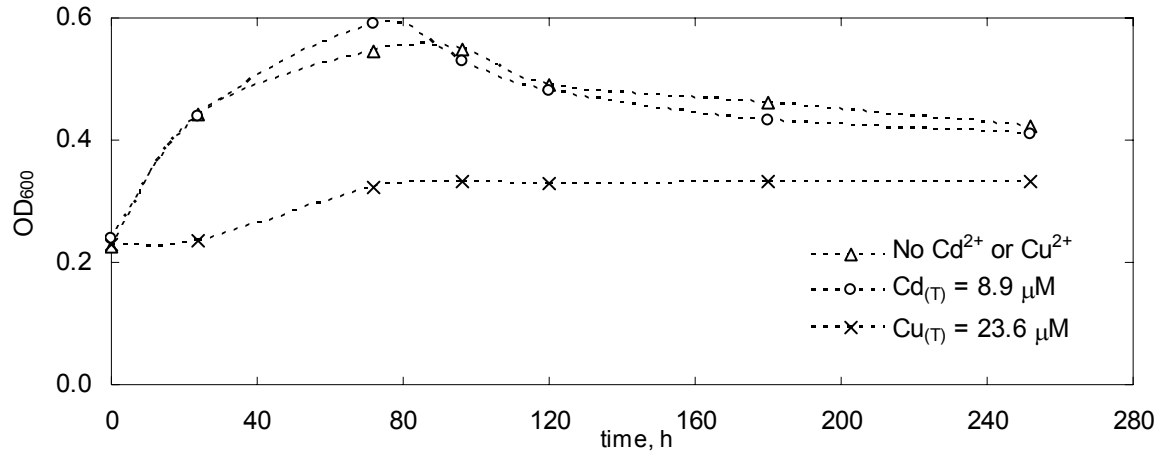

Figure 5.9 *Comamonas spp.* growth in the presence of $H_2L_{p(T)}$ and solution Y. I = 0.01 M $NaNO_3$, initial $H_2L_{p(T)}$ = 0.6 mM, initial $[PO_4^{3-}]_{(T)}$ = 0.2mM, neutral pH.

2. Determining suitable conditions for H_2L_p metabolism

Further experiments using less NaH_2PO_4 (1μM) were performed to examine H_2L_p degradation in the systems developed to investigate the effect of H_2L_p degradation on Cd^{2+} adsorption onto ferrihydrite. Three types of systems were examined. The first one (T1) did not contain ferrihydrite or Cd^{2+}, the second one (T2) contained Cd^{2+} but not ferrihydrite, and the third one (T3) contained both ferrihydrite and Cd^{2+}. In all systems, the initial *Comamonas spp.* concentration was 0.1 gL^{-1} (dry weight), the $H_2L_{p(T)}$ concentration was 0.6 mM, the ionic strength was 0.01 M $NaNO_3$. Solution Y was added to all samples with 1 μM NaH_2PO_4. The pH change and H_2L_p degradation were determined over 96 h.

The results from T1 (details are in Table A5.11, Appendix) showed that without Cd^{2+}, H_2L_p was completely degraded within 60 h for samples with initial pH ≥ 5.5. For samples with pH ≤ 5.5 there was less than 15 % $H_2L_{p(T)}$ degradation over 96 h. For samples with initial pH ranging from 5.5 to 7.5, the pH values changed to a range of 6.4 ~ 6.7 over 96 h. The results indicated that the best pH for H_2L_p degradation by *Comamonas spp.* was near neutral pH. This is consistent with the reported result that a neutral pH is preferable for *Comamonas* strains to utilize H_2L_p (Wang et al. 2003) and other organic pollutants such as the dye Direct Red 5B (Jadhav et al. 2008). In T2 the presence of 8.9 μM Cd^{2+} did not significantly suppress H_2L_p biodegradation, and complete H_2L_p degradation occurred within 60 h for all the samples with pH ≥ 5.6.

The effect of ferrihydrite on H_2L_p degradation by *Comamonas spp.* was examined (T3) with an initial pH of 6.3. The pH for all T3 samples did not change dramatically over time presumably due to the buffering effect of the ferrihydrite. This was also found for similar *Bacillus subtilis*-ferrihydrite systems. Complete H_2L_p degradation was obtained within 60 h, indicating that 1 μM $[H_2PO_4^-]_{(T)}$ was sufficient to ensure efficient H_2L_p degradation in the presence of 0.1 gL^{-1} ferrihydrite, and the presence of ferrihydrite did not significantly influence H_2L_p metabolism by *Comamonas spp.*, even though initially some H_2L_p would have been adsorbed onto ferrihydrite. Therefore, in the following sections and chapters, unless stated, solution Y refers to a solution containing 1μM $MgSO_4$, 2 μM $CaCl_2$, 20 μM KNO_3 and 1 μM NaH_2PO_4.

3. Phthalic acid degradation products

In the proposed pathway of phthalic acid metabolism, organic ligands with carboxylic acid group such as protocatechuate, oxaloacetate and pyruvate might be the intermediates (Eaton 2001). To examine if other ligands are produced during H_2L_p degradation by *Comamonas spp.* samples were collected over time in the dynamic systems described above and were analyzed using both HPLC and GC-MS (Section 2.2.7). HPLC was used to analyze H_2L_p in all samples. As the HPLC H_2L_p peak area decreased due to H_2L_p metabolism there were no new peaks observed to develop. Because these samples were in 0.01 M $NaNO_3$ it is possible that small polar organic compounds co-eluted with NO_3^-, and were therefore not detected. GC-MS detected H_2L_p but no other organic carboxylic acids were found during H_2L_p metabolism.

5.5. Conclusions

The metabolism of H_2L_p was investigated with four different pure bacteria strains: *Bacillus subtilis,* and another three species isolated from wastewater treatment plant (one of which was identified to be *Comamonas spp*.). Only *Bacillus subtilis* and *Comamonas spp*. were able to metabolize H_2L_p as the only carbon source with most metabolism at neutral pH. The presence of ferrihydrite inhibited H_2L_p degradation by *Bacillus subtilis* but not *Comamonas spp*.. Because ferrihydrite did not inhibit H_2L_p metabolism by *Comamonas spp.*, and this bacteria was chosen to investigate bacterial effects on metal ion speciation and distribution in systems with ferrihydrite and H_2L_p. Copper was found to suppress *Comamonas spp.* growth when its concentration was above 23.6 μM. In addition Cu^{2+} adsorption occurs at a lower pH than Cd^{2+} and as the preferred pH range for H_2L_p degradation was from 6.0 to 7.5, it would be difficult to observe the effect of H_2L_p degradation on Cu^{2+} sorption in this system. Cadmium adsorption edges occur about one pH unit greater than those of Cu^{2+} (Figure 4.9). Model results showed that the presence of 0.6 mM H_2L_p increased Cd^{2+} ($Cd_{(T)}$ = 1.78 μM) adsorption onto 0.1 gL^{-1} ferrihydrite by ~ 30 % at pH = 6 (Figure 7.6). Therefore experiments in Chapter 6 and Chapter 7 on metal speciation in systems containing bacteria used *Comamonas spp.* with Cd^{2+} as the metal.

Conditions for studying biotic systems in this work were therefore developed, under which H_2L_p can be efficiently degraded, and the effect of organic ligand degradation on Cd^{2+} adsorption onto ferrihydrite can be examined. The conditions for *Comamonas spp.* to metabolize H_2L_p in the presence of ferrihydrite are: initial pH ranging from 5.5 to 8.0, ≤ 8.9

μM Cd^{2+}, essential trace nutrients provided by solution Y which contains 1 μM $MgSO_4$, 2 μM $CaCl_2$, and 20 μM KNO_3 and 1 μM NaH_2PO_4. The degradation time depended on the amount of H_2L_p and *Comamonas spp.*. Results show that 0.6 mM H_2L_p could be entirely utilized by 0.055 gL^{-1} *Comamonas spp.* cells within three days under the conditions described above.

Chapter 6. Cadmium and Phthalic Acid Sorption onto *Comamonas spp.*

Contents accepted to publish in Environmental Science &Technology (Song et al. 2009)

6.1. Introduction

In most natural aquatic or soil environments, bacteria can not only degrade various organic compounds, but also present a significant surface that can absorb metal ions. To understand the effect of bacteria on metal ion distribution in a system involving bacteria, ferrihydrite, and organic ligands, the biosorption of metal ions and organic ligands onto bacteria should be taken into account. Similar to the approach used in abiotic ternary systems, cadmium and H_2L_p adsorption onto *Comamonas spp.* was initially examined in binary systems before ternary systems and more complex systems were investigated. Copper speciation and distribution in these systems was not studied for the reasons given in Chapter 5. The objective of this chapter is to examine Cd^{2+} and H_2L_p adsorption onto *Comamonas spp.* in both binary and ternary systems for a range of conditions. Acid-base titrations of *Comamonas spp.* suspensions were conducted followed by experimental examination of Cd^{2+} and H_2L_p adsorption onto *Comamonas spp.*. Cadmium speciation in the presence of both ferrihydrite and *Comamonas spp.* will be discussed in Chapter 7.

6.2. Acid/base titration of *Comamonas spp.* suspensions

One of the assumptions for quantitative evaluation of metal sorption onto bacteria is that there are different surface functional groups on the surface of bacterial cells and these are considered as different sorption types of sites. Each type of site will have a site concentration (usually expressed per gram of bacteria) and logK values for reactions with protons and metal ions. Four surface site types were required for modelling proton and Cd^{2+} adsorption onto various single bacteria strains such as *Deinococcus radiodurans, Thermus thermophilus, Flavobacterium aquatile,* and *Flavobacterium hibernum*, as well as natural consortia of bacteria (Borrok et al. 2004; Ginn and Fein 2008). Models with fewer site types could not adequately describe the experimental data while models with more site types had parameters that were not constrained by the data. To model metal ion adsorption onto bacterial cells the parameters including the concentration and deprotonation constant for each site must be

determined (Fein et al. 1997), and these values can be derived from acid/base titration data. The titration data for *Comanonas spp.* in 0.01 M $NaNO_3$ are given as $-\log[H^+]$ versus total concentration of proton added (Figure 6.1). Model parameters were optimized from the data with FITEQL 4.0 using the NFSM as described in Sections 1.6 and 2.2.5. The modelled result shown in Figure 6.1 uses the weighted average optimized proton adsorption constants and site density values (Table 6.1). The ferrihydrite titration used the parameters of Dzombak and Morel (1990). Bacteria 56.3 gL^{-1} and ferrihydrite 10.4 gL^{-1} were used in Figure 6.1. In this way, the dry weight of *Comamonas spp.* is equal to that of ferrihydrite on a basis of its stoichiometry $Fe_2O_3 \cdot H_2O$ with a molecular weight of 89 $gmol^{-1}$. Unless stated, the concentration or dry weight of ferrihydrite in this thesis is all on this basis.

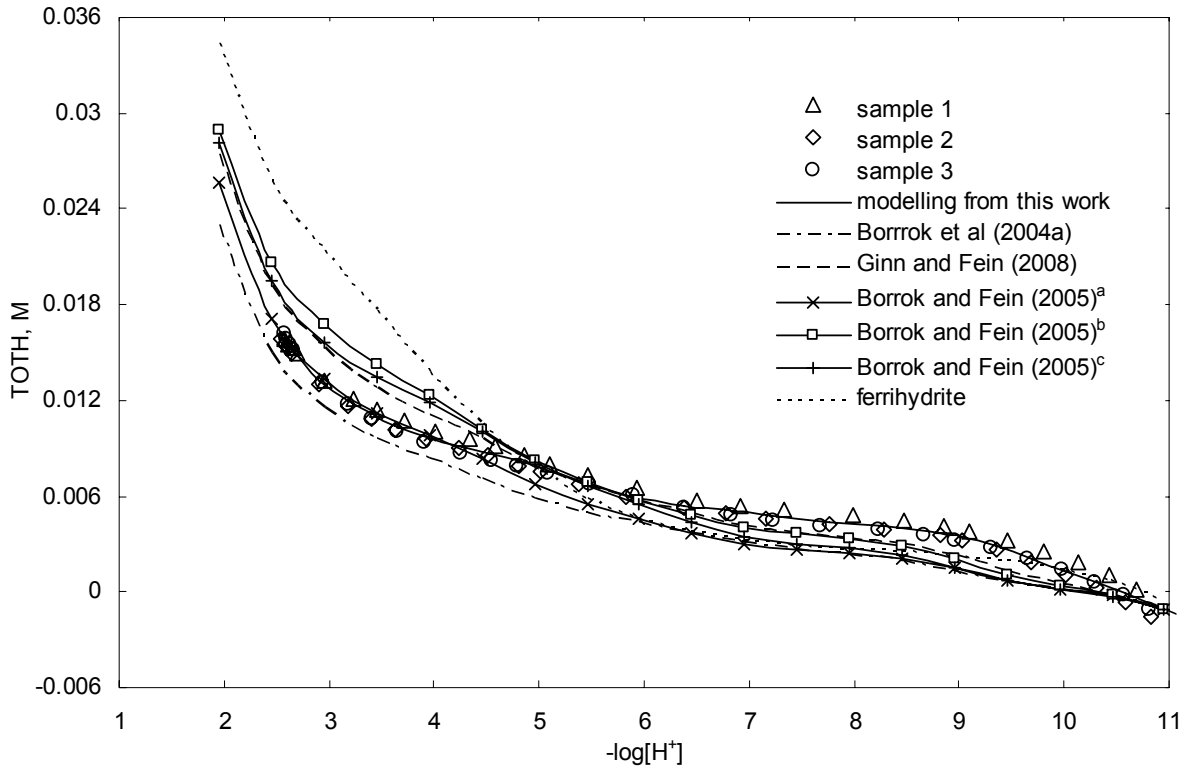

Figure 6.1 Proton sorption onto *Comamonas spp.* and ferrihydrite. I=0.01 M $NaNO_3$, three replicate experimental (symbols) and modelled (lines) results. Bacteria and ferrihydrite 10.4 gL^{-1} (dry weight). Bacteria and ferrihydrite titration was modelled with the weighted average parameters from Table 6.1, and Dzombak and Morel (1990), respectively. [a]Data from *Pseudomonas putida* in I = 0.01 M $NaClO_4$, [b]from *Pseudomonas putida* in I = 0.1 M $NaClO_4$, [c]data from *Pseudomonas mendocina* in I = 0.01 M $NaClO_4$ (Borrok and Fein 2005).

Figure 6.1 indicates that proton adsorption onto *Comanonas spp.* between pH 3 and 11 could be well reproduced with the inclusion of four types of sorption sites. Proton adsorption parameters in this work have been compared with results obtained at ionic strength of 0.01 and 0.1 M. The proton adsorption constants for the four sites determined from this work are

reasonably close to previous reported values (Table 6.1). All logK values in Table 6.1 were obtained using the NFSM. Borrok et al (2004) and Johnson et al (2007) studied proton adsorption onto a variety of natural bacterial consortia from wetland soil, forest soil, wastewater effluent, river, and wetland water. Ginn and Fein (2008) studied proton adsorption on five bacteria species that were diverse in a wide genetic and habitat range using the same model approach as that of Borrok et al (2004). The value of 3.16 for $\log K_{RHA}$ from this work is within the reported average values (Table 6.1). The values for $\log K_{RBH}$, $\log K_{RCH}$ and $\log K_{RDH}$ are however slightly higher (by approximately half a log unit) than the previous reported corresponding ranges shown in Table 6.1. Proton adsorption constants and the site densities obtained from the same bacterial might slightly differ under different pH ionic strength. It has been suggested that proton adsorption onto bacterial surface is not significantly influenced by the ionic strength between 0.01 and 0.5 M (Borrok and Fein 2005).

The range of average site density values on bacterial surface varies between 2.04×10^{-5} and 12.4×10^{-5} $molg^{-1}$ (Table 6.1). The wide range of site concentrations for different bacterial strains indicates the variety in the abundance of functional groups on various bacterial surfaces. The four site concentrations derived from the experimental data in this work are within the reported average ± standard deviation values (Table 6.1). Concentrations of type A, B and D sites are within the reported range of average values while the type C site concentrations is less than the average values reported. However site concentrations can vary over in a wide range and there have been no reported titration data for *Comamonas spp.*. The titration data from this work is within the modelled results from pH 2 to 9 (Figure 6.1). The titration curves predicted using various reported average values of proton adsorption constants and bacterial site densities gave close fit to the experimental data in this work (Figure 6.1). Using the values derived from *Pseudomonas mendocina* titration at I = 0.01 M ionic strength, modelling result is consistent with the experimental data in this work at pH < 4.5, but underestimated at pH > 4.5. The titration curve predicted from the average values of Borrok et al (2004) slightly underestimated the titration data from this work over the pH range of 2~11. Modelled titration curves using average values from other studies generally overestimated the experimental data from *Comamonas spp.* at lower pH but underestimated it at higher pH range (Borrok and Fein 2005; Fein et al. 2005; Ginn and Fein 2008; Johnson et al. 2007). To accurately describe proton adsorption onto *Comanonas spp.* and the site densities, the weighted average values optimized from the experimental data in this work were used for modelling Cd^{2+} speciation systems with bacteria.

Table 6.1 Optimized proton adsorption constants and site densities at *Comamonas spp.* surface compared to other bacteria. All logK values are given for an ionic strength of 0; site densities are expressed in $\times 10^{-5}$ mol per gram bacteria; the bacteria concentration of samples 1, 2, and 3 is 56.3 gL^{-1}; Standard deviation σ or 95 % confidence interval was given.

	$logK_{RAH}$	$logK_{RBH}$	$logK_{RCH}$	$logK_{RDH}$	TOTA	TOTB	TOTC	TOTD	$\frac{WSOS}{DF}$
Sample 1	3.21 (0.049)	5.30 (0.029)	7.30 (0.056)	9.75 (0.025)	7.78 (0.049)	6.89 (0.029)	1.95 (0.056)	6.84 (0.025)	4.32
Sample 2	3.10 (0.050)	5.24 (0.030)	7.19 (0.054)	9.77 (0.021)	8.88 (0.050)	6.77 (0.030)	2.02 (0.054)	8.12 (0.021)	3.44
Sample 3	3.16 (0.037)	5.47 (0.034)	7.22 (0.055)	9.76 (0.023)	10.94 (0.037)	5.83 (0.034)	2.18 (0.055)	7.12 (0.023)	4.17
Weighted average (95 % confidence interval)	3.16 (3.07, 3.25)	5.33 (5.16, 5.50)	7.24 (7.15, 7.32)	9.76 (9.75, 9.77)	9.17 (6.86, 11.47)	6.55 (5.77, 7.32)	2.04 (1.88, 2.20)	7.35 (6.39, 8.31)	
Average value(σ)[a]	3.12 ± 0.13	4.70 ± 0.11	6.57 ± 0.17	8.99 ± 0.21	6.65 ± 1.96	6.78 ± 2.65	3.68 ± 1.71	4.47 ± 2.19	
Average value (σ)[b]	3.1 ± 0.3	4.8 ± 0.2	6.7 ± 0.1	9.2 ± 0.3	10.0 ± 1.7	9.0 ± 3.0	4.6 ± 1.8	6.1 ± 2.3	
Average value (σ)[c]	2.84 ± 0.37	4.68 ± 0.13	6.33 ± 0.14	9.16 ± 0.11	8.71 ± 4.28	9.09 ± 0.92	4.83 ± 0.69	4.40 ± 0.39	
Average value (σ)[d]	3.04 ± 0.06	4.57 ± 0.02	6.34 ± 0.02	9.18 ± 0.02	9.30 ± 0.51	11.7 ± 0.35	5.28 ± 0.13	6.21 ± 0.20	
Average value (σ)[e]	2.86 ± 0.19	4.66 ± 0.07	6.33 ± 0.07	9.04 ± 0.04	9.07 ± 1.47	11.1 ± 0.24	6.03 ± 0.18	5.13 ± 0.12	
Average value (σ)[f]	3.42 ± 0.11	4.74 ± 0.11	6.51 ± 0.12	9.25 ± 0.11	9.58 ± 1.54	12.4 ± 0.96	5.08 ± 0.30	8.06 ± 1.30	
Average value (σ)[g]	3.3 ± 0.2	4.8 ± 0.1	6.8 ± 0.3	9.1 ± 0.2	8.1 ± 1.6	11.2 ± 3.6	4.4 ± 1.3	7.4 ± 2.1	

[a] bacteria from wetland soil and water, wastewater effluent, forest soil, river. I=0.1 M $NaClO_4$ (Borrok et al. 2004).
[b] value for *Thermus thermophilus, Flavobacterium aquatile,* and *Flavobacterium hibernum*. I=0.1 M $NaClO_4$ (Ginn and Fein 2008).
[c, d] value obtained for *Pseudomonas putida* from I=0.01 M and I = 0.1 M $NaClO_4$, respectively (Borrok and Fein 2005).
[e, f] value obtained for *Pseudomonas mendocina* from I=0.01 M and I = 0.1 M $NaClO_4$, respectively (Borrok and Fein 2005).
[g] value of *Bacillus subtilis.* I = 0.1 M $NaClO_4$ (Fein et al. 2005).

6.3. Cadmium sorption onto *Comamonas spp.*

Cadmium adsorption onto *Comamonas spp.* in binary systems was determined over a pH range from 2 to 8 for $Cd_{(T)}$/*Comamonas spp.* ratios of 0.65, 1.08, 3.24 and 32.4 $\mu molg^{-1}$. The experimental data for Cd^{2+} sorption as a function of pH are shown in Figure 6.2. The pH dependence of Cd^{2+} biosorption has been observed for other bacteria (Borrok and Fein 2005; Burnett et al. 2006; Daughney and Fein 1998a; Kelly et al. 2001; Yee and Fein 2001). In general Cd^{2+} adsorption increases with an increase in pH up to 8, however Cd^{2+} adsorption sorption was found to decrease at pH > 8 (Burnett et al. 2006). This phenomenon was not observed for *Comamonas spp.* in this work because the pH investigated was less than 8.

Similar to Cd^{2+} adsorption onto ferrihydrite, Cd^{2+} sorption onto *Comamonas spp.* depends on pH and the $Cd_{(T)}$/bacteria ratio. Cadmium sorption onto *Comamonas spp.* shows a more gradually sigmoid curve over about 5 pH units compared to Cd^{2+} adsorption onto ferrihydrite which increases from zero to 100 % over approximately 2 pH units (Figure 3.2). This implies a higher degree of site heterogeneity at the surface of the bacteria than that on the ferrihydrite surface. Bacteria's having flatter titration curves than that of ferrihydrite (Figure 6.1) is evidence showing the presence of surface sites with a greater range of pK_A values. The high degree of site heterogeneity on bacteria has been demonstrated by titration experiments and electrostatic force microscopy that showed pK_A values for proton adsorption onto *Shewanella putrefaciens* ranged from 3.72 to 9.99 (Sokolov et al. 2001).

The Cd^{2+} adsorption edges in Figure 6.2 clearly shift to higher pH as the $Cd_{(T)}$/*Comamonas spp.* ratio increases from 0.65 to 32.4 $\mu molg^{-1}$. The pH_{50} for Cd^{2+} sorption onto *Comamonas spp.* occurs at pH ≈ 4.5, 4.8, 5.5 and 7.0, for the data with $Cd_{(T)}$/*Comamonas spp.* ratio of 0.65, 1.08, 3.24, and 32.4 $\mu molg^{-1}$, respectively. A similar pH edge shift was observed for Cd^{2+} adsorption onto ferrihydrite as a function of $Cd_{(T)}$/Fe ratios. For example, about one pH unit shift to the higher pH when the $Cd_{(T)}$/Fe increased from 7.8×10^{-5} to 7.9×10^{-3} mol mol^{-1} (Figure 3.2). The pH edges of Cd^{2+} adsorption onto *Comamonas spp.* suggested that for the same dry weight of *Comamonas spp.* and ferrihydrite, the bacteria absorb more Cd^{2+} at a given pH, i.e. Cd^{2+} biosorption has a lower pH_{50} value. This conclusion is confirmed by comparing 1.78 μM $Cd_{(T)}$ adsorption onto 0.1 gL^{-1} ferrihydrite and *Comamonas spp.* (Figure 6.3). It shows that *Comamonas spp.* accumulates more Cd^{2+} than ferrihydrite over a pH range

of 2~7. At pH of 6, *Comamonas spp.* absorbed about 5 times more Cd^{2+} than ferrihydrite. *Bacillus subtilis* and *Escherichia coli* were also found to be more efficient accumulators of metal ions compared to smectite and kaolinite clay on a basis of the same dry weight (Walker et al. 1989). The higher affinity of *Comamonas spp.* for Cd^{2+} compared to ferrihydrite is similar to Cd^{2+} adsorption in activated sludge (Fristoe and Nelson, 1983). In their study, cadmium adsorption was greater on the sludge with larger amount of bacteria but less mineral particles.

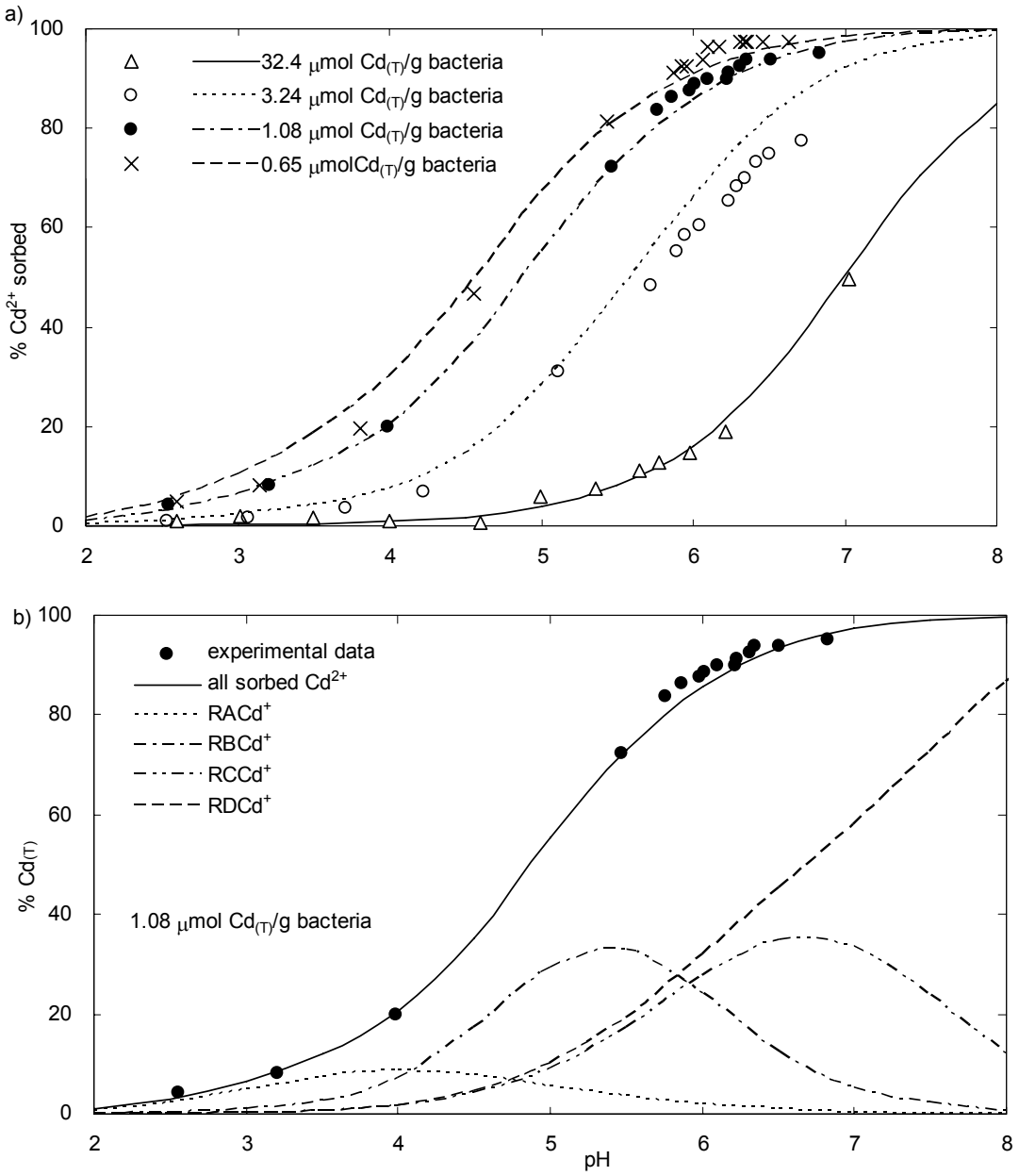

Figure 6.2 Cadmium adsorption and speciation at *Comamonas spp.* surface: Experimental (symbols) and modelled (lines) results. Model uses the weighted average values from this work. a) Cadmium sorption onto *Comamonas spp.* with $Cd_{(T)}$ and bacteria concentrations given in Table 6.2. b) Cadmium speciation on *Comamonas spp.* surface.

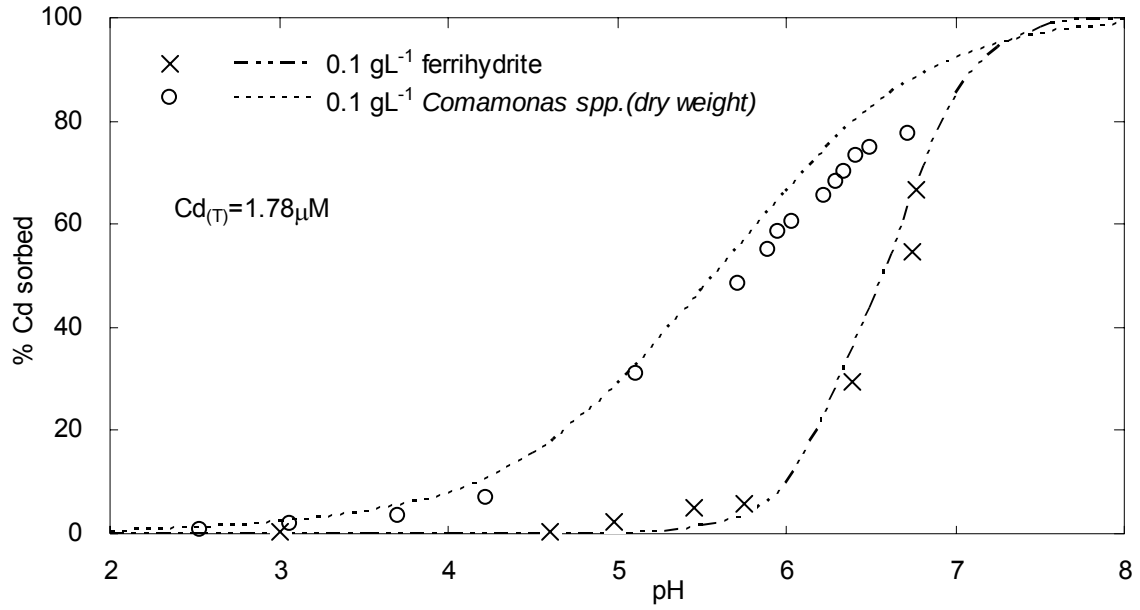

Figure 6.3 Comparison of cadmium adsorption onto bacteria and ferrihydrite in binary systems. I = 0.01 M $NaNO_3$

The non-electrostatic four site surface complexation model was used to describe Cd^{2+} adsorption onto *Comamonas spp.*, which included the proton and Cd^{2+} adsorption reactions given in Table 2.4, and the average proton adsorption constants and site concentrations derived from the titration data as given in Table 6.1. The optimized Cd^{2+} biosorption constants are given in Table 6.2. It shows that $logK_{RCCd+}$ could only be optimized from data with a $Cd_{(T)}$/bacteria ratio of 32.4 $\mu molg^{-1}$ but not lower ratios. Similarly in the modelling results from Borrok et al (2004) values for four types of sites were optimized for the majority but not all of the investigated bacteria. For example, the constant for Cd^{2+} adsorption onto type C site was not constrained by the data with bacteria from wastewater effluent with a $Cd_{(T)}$/bacteria ratio of 8.9 $\mu molg^{-1}$. All logK values optimized from the data with a $Cd_{(T)}$/bacteria of 32.4 $\mu molg^{-1}$ had a high standard deviation because all but one data point had less than 20 % adsorption so the difference between $Cd_{(T)}$ and dissolved Cd^{2+} was small (Figure 6.2a). The $logK_{RACd+}$ of 3.11 is in close agreement with published values, while values for $logK_{RBCd+}$, $logK_{RCCd+}$ and $logK_{RDCd+}$ are all higher than the reported values (Table 6.2). This indicates that Cd^{2+} biosorption behaviour can vary between different bacteria. For example, a comparison of 89 μM Cd^{2+} adsorption onto 10 gL^{-1} *Bacillus subtilis, Bacillus licheniformis* and *Comamonas spp.* at I = 0.01 M showed that the bacteria exhibit affinity for

Cd^{2+} in the following order *Comamonas spp.*> *Bacillus subtilis* > *Bacillus licheniformis* (Figure 6.4 a).

Table 6.2 Optimization of logKs for Cd^{2+} sorption on *Comamonas spp.*. Data sets are given in Figure 6.2. The logK values are given for I = 0. Standard deviations or confidence interval is in parentheses when available.

$Cd_{(T)}$/bacteria cells ($\mu molg^{-1}$)	Bacteria (gL^{-1})	$logK_{RACd+}$	$logK_{RBCd+}$	$logK_{RCCd+}$	$logK_{RDCd+}$	WSOS/DF
32.4	0.055	3.52 (0.79)[a]	4.54 (0.41)[a]	6.21 (0.56)[a]	7.78 (0.46)[a]	0.36
3.24	0.55	3.11[b]	4.49 (0.031)	6.21[b]	7.24 (0.16)[a]	1.39
1.08	1.65	3.02 (0.12)	4.50 (0.051)	6.21[b]	8.34 (0.034)	4.66
0.65	2.75	2.88 (0.11)	4.17 (0.14)	6.21[b]	8.55 (0.059)	0.20
Weighted average (95 % confidence interval)		3.11 (2.64, 3.57)	4.46 (4.35, 4.58)	6.21[c]	8.21 (7.76, 8.66)	
Average value (σ)[d]		2.83 ± 0.30	2.70 ± 0.47	3.95 ± 0.22	5.22 ± 0.40	
Average value (σ)[e]		2.4 ± 0.4	3.2 ± 0.1	4.4 ± 0.1	5.3 ± 0.1	
Average value[f]		NA	3.77	5.30	NA	
Average value[g]		NA	4.01	4.77	NA	

[a] Fixed at 0.15 to calculate weighted average when actual value is larger than 0.15 (Ali and Dzombak 1996b).
[b] No convergence of this value so the value was fixed at the weighted average for consistency.
[c] Only one value so no confidence interval was given.
[d] Bacteria from wetland soil and water, wastewater effluent, forest soil, river. I = 0.1 M $NaClO_4$. bacteria = 10 gL^{-1}, $Cd_{(T)}$ = 89 μM (Borrok et al. 2004).
[e] *Thermus thermophilus, Flavobacterium aquatile,* and *Flavobacterium hibernum*. I = 0.1 M $NaClO_4$, bacteria = 10 gL^{-1}, $Cd_{(T)}$ = 89 μM (Ginn and Fein 2008).
[f] *Pseudomonas putida* in I=0.01 M $NaClO_4$. Bacteria = 10 gL^{-1}, $Cd_{(T)}$ = 89 μM (Borrok and Fein 2005).
[g] *Pseudomonas mendocina in* I=0.01 M $NaClO_4$ Bacteria = 10 gL^{-1}, $Cd_{(T)}$ = 89 μM (Borrok and Fein 2005) ferrihydrite

However, a comparison of Cd^{2+} adsorption onto *Comamonas spp.*, *Pseudomonas pudita* and *Pseudomonas mendocina* indicates that the parameters derived for *Comamonas spp.* from this work can accurately model Cd^{2+} adsorption onto the other two bacterial strains (Borrok and Fein 2005) (Figure 6.4b). It has been observed that there is a wide range of bacteria that exhibit similar proton and metal adsorption behaviour and the metal adsorption onto these bacterial cells can be reasonably well modelled using only one set of averaged parameters for site densities and adsorption constants. But this doesn't deny the existence of some bacteria with significantly different adsorption behaviour (Ginn and Fein, 2008). For example, a universal adsorption edge was proposed to model Cd^{2+} adsorption onto different types bacterial strains and bacterial consortia (Borrok et al. 2004; Yee and Fein 2001). Examples of

bacteria with exceptional for Cd^{2+} adsorption were *Anoxybacillus flavithermus* and *Acidiphlium angustum* (Burnett et al. 2007; Ginn and Fein 2008), where Cd^{2+} adsorption was far less than that of other bacteria in the pH range of 4 to 8.

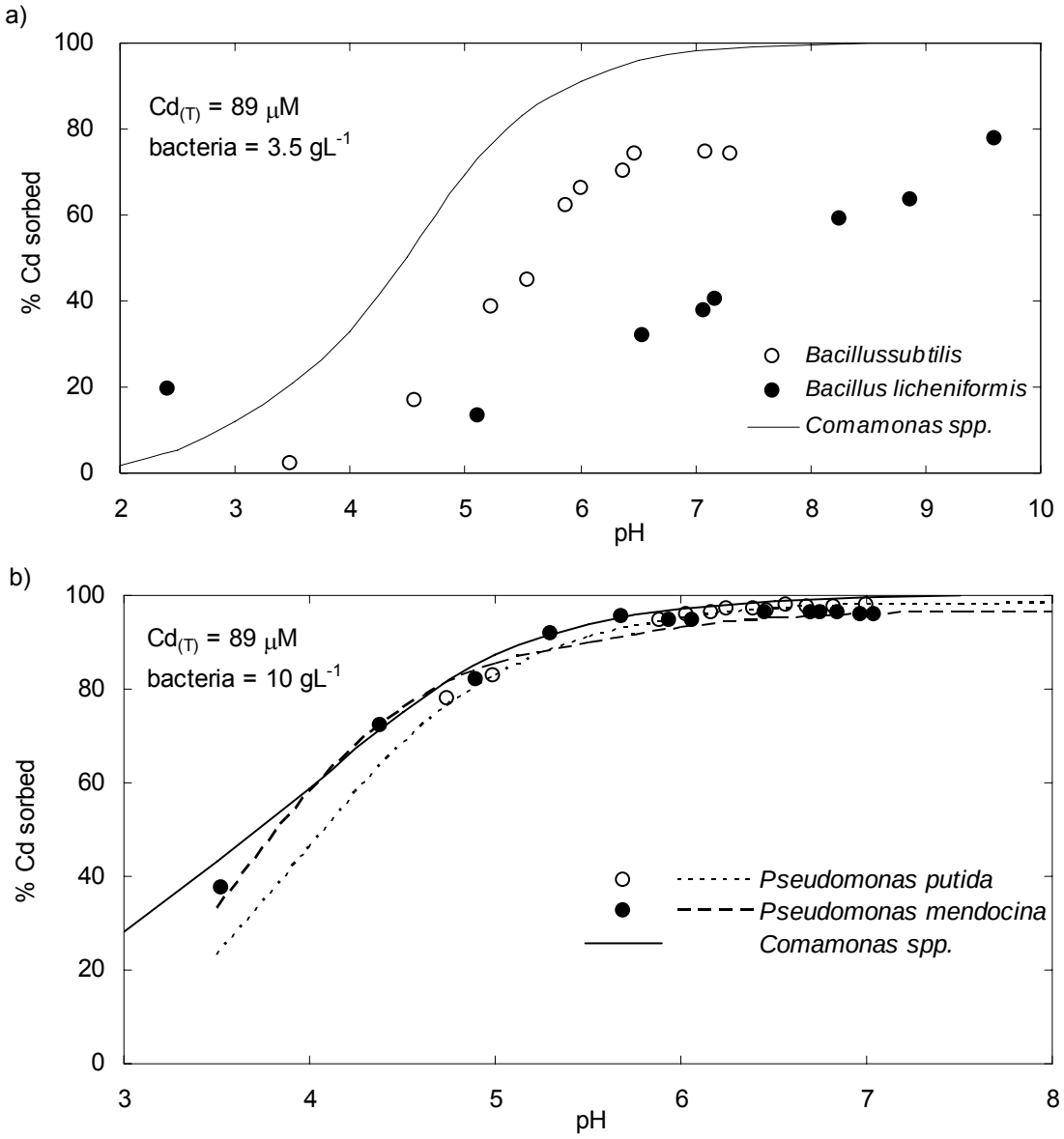

Figure 6.4 Comparison of Cd^{2+} adsorption onto *Comamonas spp.* and other bacteria. I = 0.01 M. *Comamonas spp.* data was modelling results using sorption constants derived from this work. a) Data for *Bacillus subtilis* and *Bacillus licheniformis* were from Daughney and Fein (1998a); b) Experimental (symbols) and modelling (lines) results for *Pseudomonas putida* and *Pseudomonas mendocina* were from Borrok and Fein (2005).

Most research work on Cd^{2+} adsorption onto bacteria has focused on a limited range of $metal_{(T)}$/bacteria ratio, ranging from 5 to 27 $\mu molg^{-1}$, with metal concentration ranging from 26 to 267 μM, and bacterial cells concentration ranging from 1.6 to 10 gL^{-1} at I = 0.1 M (Borrok et al. 2007; Borrok et al. 2004; Boyanov et al. 2003; Burnett et al. 2006; Daughney

and Fein 1998a; Daughney et al. 2000; Fein 2000; Fein et al. 1999; Fowle and Fein 2000; Johnson et al. 2007; Yee and Fein 2001; Yee and Fein 2003). Cadmium adsorption onto bacterial cells over a wide range of sorbate/sorbent ratio has not previously been reported. This work examined Cd^{2+} adsorption onto a pure bacterial strain of *Comamonas spp.* with $Cd_{(T)}$/bacteria ratios ranging from 0.65 to 32.4 $\mu molg^{-1}$. Using the H^+ and Cd^{2+} adsorption constant values obtained from the experimental data in this work, cadmium adsorption onto *Comamonas spp.* cells can be reasonably well reproduced over a wide range of $Cd_{(T)}$/bacteria ratios and pH values (Figure 6.2).

6.4. Phthalic acid sorption onto *Comamonas spp.*

Phthalic acid adsorption onto *Comamonas spp.* was examined in binary systems by following the same steps used for the H_2L_p and ferrihydrite systems. Dead bacterial cells were used to investigate this sorption process to avoid H_2L_p metabolism by live *Comamonas spp.* cells. The dead cells were examined under fluorescence microscope after staining the cells with two dyes provided by Live/Dead® BacLight™ Bacterial Viability Kits (Invitrogen). All cells fluoresced red indicating that no *Comamonas spp.* survived under the heat treatment described in Section 2.2.6.

The result of experiments for H_2L_p adsorption onto dead *Comamonas spp.* showed that aqueous H_2L_p adsorption onto bacteria is negligible under most pH conditions, with adsorption becoming significant only at pH less than 3. About 7 % H_2L_p was observed to be absorbed onto *Comamonas spp.* surface at pH 2. The adsorption behaviour of H_2L_p onto *Comamonas spp.* is compared to EDTA and 2,4,6-trichlorophenol (TCP) adsorption onto *Bacillus subtilis* in Figure 6.5 (Daughney and Fein 1998b; Fein and Delea 1999). Phthalic acid, EDTA and TCP adsorption onto bacteria deceases with increasing pH. For EDTA and TCP the bacteria/ligand ratio is substantially larger than that in our work. This explains the difference in the percentage of ligand absorbed. It has been proposed that organic acid adsorption behaviour onto bacterial cells appears to be controlled by their acid dissociation constants (pK_A). For example, the pK_{A1} of EDTA is 1.9 and EDTA adsorption onto *Bacillus subtilis* becomes significant as the pH approaches this value. Similarly TCP adsorption onto *Bacillus subtilis* becomes significant at pH lower than the pK_{A1} of TCP which is 6.0. Phthalic acid appears to behave in a similar way, its sorption onto *Comamonas spp*. is negligible when the pH is larger than 3 (pK_{A1} of H_2L_p is 2.95). The results from H_2L_p, EDTA and TCP adsorption onto different bacteria illustrate the proposed mechanism for organic acid

adsorption onto bacterial cells, i.e. the balance between electrostatic and hydrophobic interactions. An organic acid is fully protonated and therefore uncharged when the pH is lower than the pK_{A1}. The hydrophobic interaction between the organic acid and bacterial surface dominates the adsorption. With increasing pH both the organic acid and the bacterial surface become more negatively charged, and absorption is observed to decrease due to the significance of the coulombic repulsion, which is proposed to dominate the hydrophobic interaction at pH > pK_{A1} (Fein and Delea 1999). Because the Cd^{2+} adsorption edge by ferrihydrite and *Comamonas spp.* occurs between pH 3 and 8, and because $H_2L_{p(T)}$ adsorption onto *Comamonas spp.* was negligible at pH > 3, modelling H_2L_p adsorption onto *Comamonas spp.* was not included in this work.

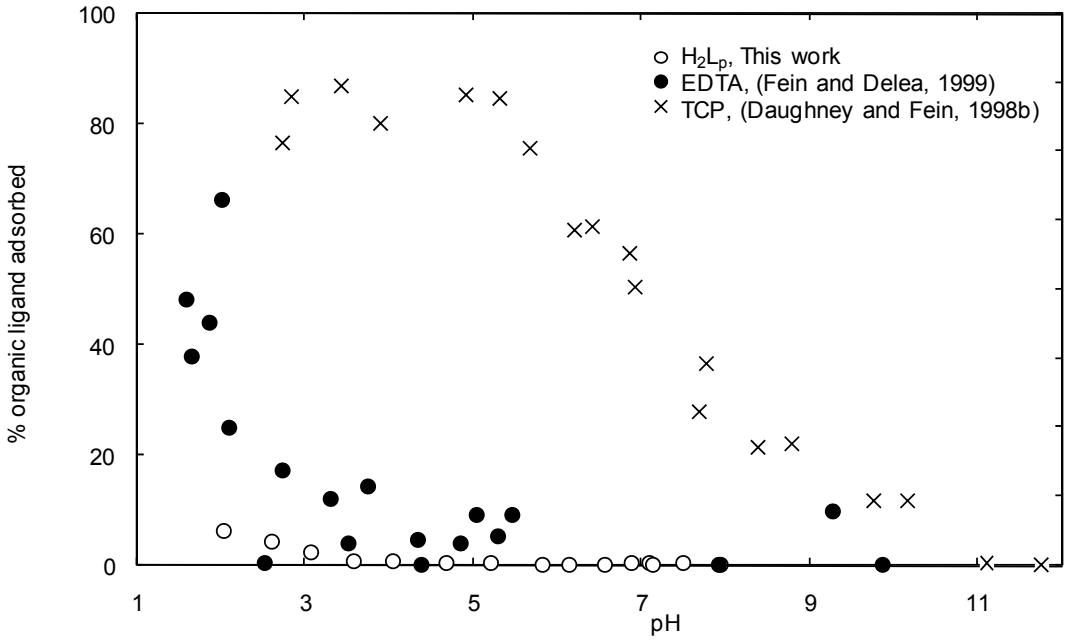

Figure 6.5 Experimental results for H_2L_p, EDTA and TCP adsorption onto bacteria. Data include 0.6 mM $H_2L_{p(T)}$ sorption onto 0.55 gL^{-1} dead *Comamonas spp.* (I = 0.01 M $NaNO_3$), 1 mM EDTA sorption onto 70 gL^{-1} *Bacillus subtilis* (I = 0.1 M $NaClO_4$), and 0.1 mM TCP sorption onto 6 gL^{-1} *Bacillus subtilis* (I = 0.1 M $NaClO_4$)

6.5. Cadmium adsorption onto dead *Comamonas spp.* in the presence of H_2L_p

Cadmium adsorption onto *Comamonas spp.* in the presence of H_2L_p was examined in ternary systems by following the same steps used for the Cd^{2+}, phthalic acid and ferrihydrite systems. To avoid H_2L_p metabolism dead bacteria were used for the initial investigation of the effects

of H_2L_p on Cd^{2+} adsorption by *Comamonas spp.*. The experimental results for 1.78 μM $Cd_{(T)}$ adsorption onto either 0.055 or 0.275 gL^{-1} dead *Comamonas spp.* in the presence of 0.6 mM $H_2L_{p(T)}$ are shown in Figure 6.6. More Cd^{2+} was absorbed for the system where *Comamonas spp.* concentration was five times higher than that of the other. Compared to Cd^{2+} adsorption onto *Comamonas spp.* in the absence of H_2L_p, the presence of 0.6 mM H_2L_p slightly decreased Cd^{2+} adsorption for both concentrations of *Comamonas spp.*.

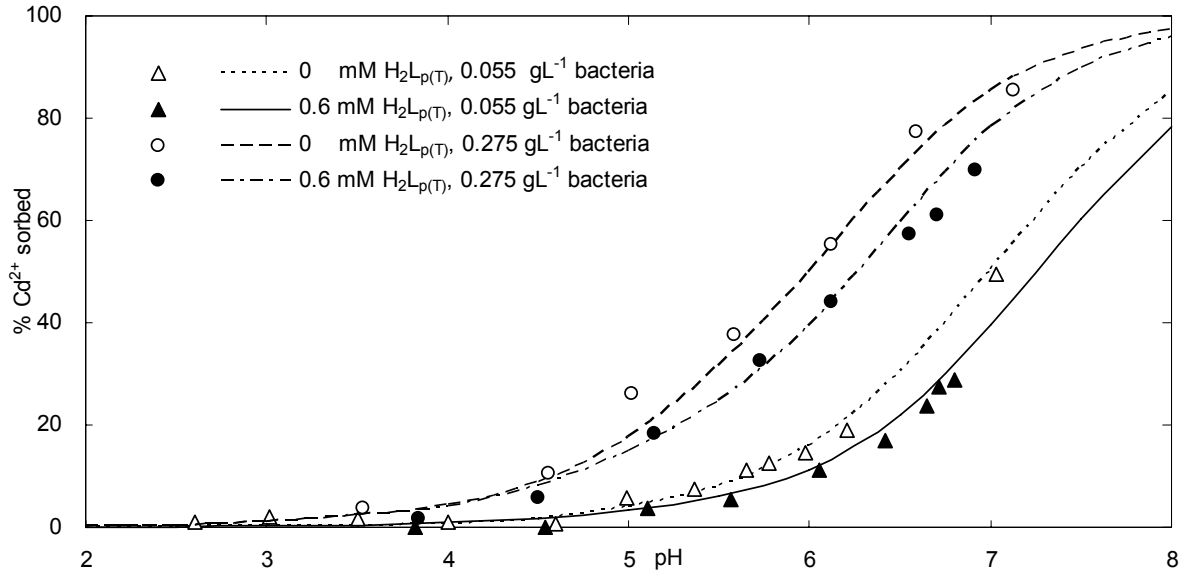

Figure 6.6 Experimental (symbols) and modelled (lines) results for Cd^{2+} sorption onto *Comamonas spp.* in the absence and presence of H_2L_p.

Cadmium adsorption onto *Comamonas spp.* cells in the presence of H_2L_p was accurately modelled using the weighted average proton and Cd^{2+} biosorption parameters (Tables 6.1 and 6.2), and the related Cd^{2+} and H_2L_p solution species as given in Table 2.3. A good fit between experimental data and modelled result was obtained and is shown in Figure 6.5. The modelled species distribution for Cd^{2+} (1.78 μM) in *Comamonas spp.* suspension in the absence and presence of 0.6 mM $H_2L_{p(T)}$ is shown in Figure 6.7. Figure 6.7 shows that the formation of solution species between Cd^{2+} and phthalate diminished Cd^{2+} adsorption onto *Comamonas spp.* in the presence of H_2L_p. The formation of Cd-phthalate solution species due to presence of $H_2L_{p(T)}$ in the Cd^{2+}-*Comamonas spp.*-H_2L_p system accounts for up to 30 % of the $Cd_{(T)}$ over the pH ranging from 3 to 8 with the maximum at pH ≈ 6. Other organic acids (such as EDTA) were found to decrease Cd^{2+} adsorption onto bacteria (Fein and Delea 1999). Because EDTA is a much stronger ligand than H_2L_p, 1 mM EDTA diminished Cd^{2+} (0.1 mM) adsorption onto 10 gL^{-1} *Bacillus subtilis* from 100 % to nearly zero in the pH range of 3 to 8.

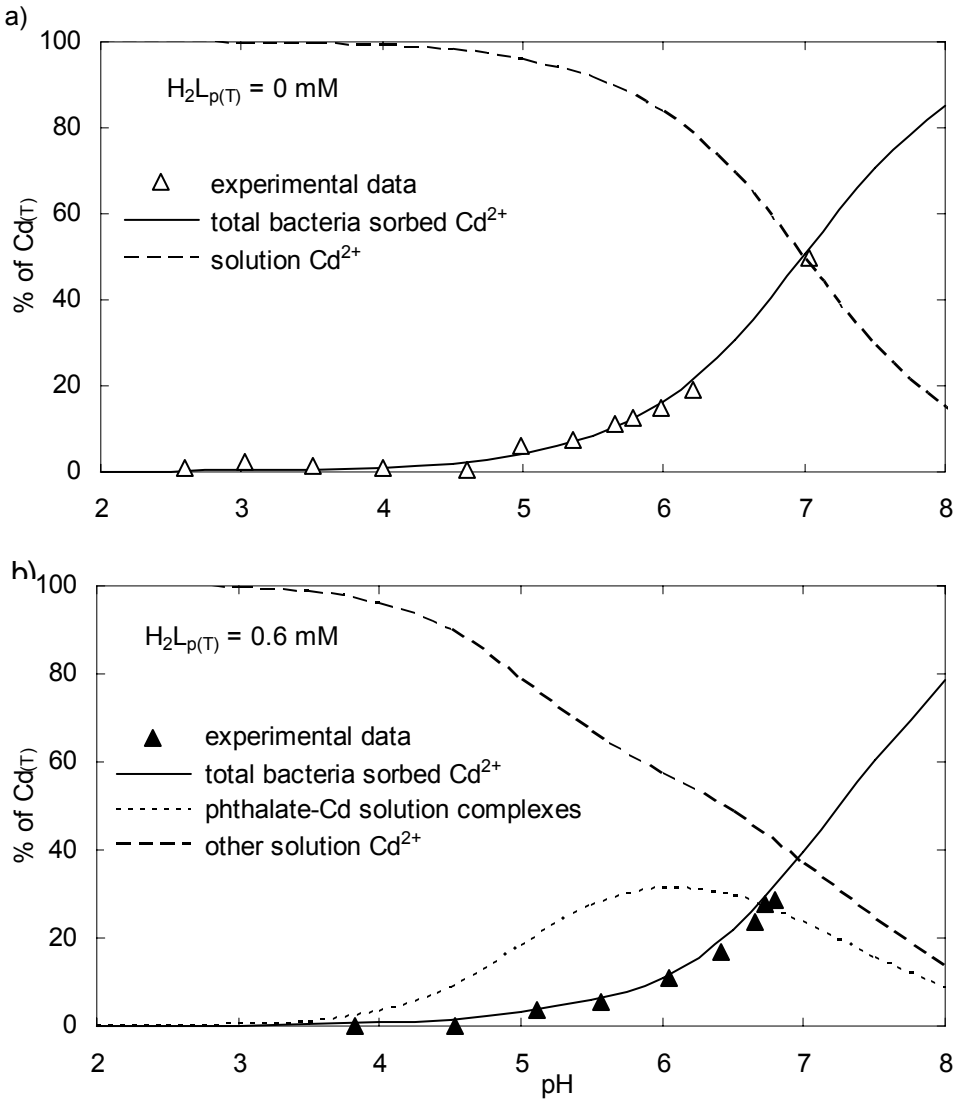

Figure 6.7 Modelled species distribution for Cd^{2+} sorption onto *Comamonas spp.*. I = 0.01 M $NaNO_3$; $Cd_{(T)}$= 1.78 μM; *Comamonas spp.*= 0.055 gL^{-1}.

6.6. Conclusions

Proton, cadmium and H_2L_p adsorption onto *Comamonas spp.* was examined. A non-electrostatic four site model was used to describe the titration data for *Comamonas spp.*, from which the proton adsorption constants along with the site concentrations at the bacterial surface were derived from the experimental data. The weighted average values for surface site pK_A range from 3.16 to 9.76, and the average site densities vary between 2.04×10^{-5} to 9.17×10^{-5} $molg^{-1}$ bacteria. This indicates a high degree heterogeneity on the bacterial surface. The modelling result provided a reasonably good fit to the titration data.

Cadmium adsorption onto *Comamonas spp.* increases with an increase in pH. Whereas on ferrihydrite Cd^{2+} adsorption increased from near zero to 100 % over a narrow pH range of about 2 units, on *Comamonas spp.* Cd^{2+} adsorption increased from near zero to 100 % over a wider pH range of ~ 6 pH units. This indicates that the bacterial surface sites occur over a wider pH range than ferrihydrite. It was also demonstrated that *Comamonas spp.* can accumulate a larger amount of Cd^{2+} than the same dry weight of ferrihydrite especially under lower pH conditions, indicating the potential usage of bacterial biosorption in toxic metal removal from contaminated environments. Cadmium adsorption onto *Comamonas spp.* over a wide sorbent/sorbate and pH range was reasonably well described by the NFSM using the adsorption constants and site densities from the titration data. The acid-base and Cd^{2+} adsorption behaviour of *Comamonas spp.* in this work were both in close agreement with previous studies.

Phthalic acid adsorption onto *Comamonas spp.* was negligible over a pH range of 3 to 8, and became significant only at pH < 3 where H_2L_p was fully protonated. This is consistent with the proposed mechanism for ligand adsorption onto bacterial surfaces which involved a balance between the hydrophobic interaction and electrostatic repulsion. The presence of H_2L_p inhibited Cd^{2+} adsorption onto *Comamonas spp.* due to the solution complex formed between H_2L_p and Cd^{2+}. Such effects can be well modelled with the inclusion of H_2L_p solution species, indicating that no significant surface ternary complex interaction occurred between Cd^{2+}, phthalic acid and *Comamonas spp.*.

Chapter 7. Sorption in Ferrihydrite-*Comamonas spp.* Systems

Contents accepted to publish in Environmental Science &Technology (Song et al. 2009)

7.1. Introduction

In previous chapters several systems have been investigated by incrementally increasing the complexity from binary to ternary systems. These include Cd^{2+} and H_2L_p adsorption onto ferrihydrite, and Cd^{2+} and H_2L_p adsorption onto *Comanonas spp.*. The complex interactions in these systems have been well described and accurately modelled. Moreover, the biodegradation of H_2L_p by *Comamonas spp.* under various conditions has been investigated. These are all prerequisites to understanding the quaternary systems discussed in this chapter. The experimental and modelling methods, as well as the parameters derived from the previous experimental data, are applied here. In this chapter Cd^{2+} adsorption onto mixtures of ferrihydrite and *Comanonas spp.* (live and dead) was examined followed by the quaternary system of Cd^{2+}, phthalic acid, ferrihydrite and dead *Comanonas spp.*. Finally Cd^{2+} adsorption in the more complex system of H_2L_p, ferrihydrite and live *Comanonas spp.* (with trace amounts of nutrients) was investigated in which the biodegradation of H_2L_p was occurring.

Surface complexation modelling has been applied to the description of metal species and distribution in increasing complex systems at either inorganic surfaces, such as mineral oxides, or organic surfaces such as bacterial cells. However there has been little research on modelling metal adsorption in a system with both bacteria and a metal oxide surface and modelling metal adsorption onto combination of ferrihydrite and bacterial cells in the presence of an organic ligand has not been reported. No studies have been published on metal speciation during the biodegradation of organic ligands due to the complexity and uncertainties of such systems. These processes are however important as they occur in both natural environments and in engineered systems, such as water treatment plants, and therefore should be considered. The objective of this chapter is to provide insight into cadmium chemistry in a complex system simulating the real environment by exploring Cd^{2+} adsorption in systems containing both *Comanonas spp.* and ferrihydrite, including the effect that H_2L_p, and the biodegradation of H_2L_p, has on Cd^{2+} distribution.

7.2. Cadmium sorption in dead *Comamonas spp.*-ferrihydrite systems

Both ferrihydrite and bacteria can absorb Cd^{2+} and play important roles in determining Cd^{2+} speciation. Because both ferrihydrite and bacteria are ubiquitous in natural environments it is necessary to understand Cd^{2+} distribution in ternary systems containing bacteria and ferrihydrite. The results for Cd^{2+} adsorption by a mix of ferrihydrite and dead bacterial cells after 72 h are given in Figure 7.1. *Comamonas spp*. suspensions were added to preformed ferrihydrite suspensions to obtain the desired concentrations of bacteria and ferrihydrite in the mixture. The ferrihydrite was not dried and its dry weight concentration is on the basis of stoichiometry $Fe_2O_3 \cdot H_2O$ with a molecular weight of 89 $gmol^{-1}$ (Dzombak and Morel 1990). The 72 h time frame was based on the H_2L_p metabolism study as well as H_2L_p adsorption onto ferrihydrite.

The shape of Cd^{2+} adsorption edges depended on the ratio of ferrihydrite/*Comamonas spp.* (g g^{-1}, dry weight). At the highest ferrihydrite/*Comamonas spp.* ratio of 10:1 adsorption was similar to Cd^{2+} adsorption onto ferrihydrite in a binary system in that Cd^{2+} adsorption ranged from nearly zero to almost 100 % over a narrow pH range of ≈ 2 pH units. This is because the concentration of ferrihydrite is much higher than that of *Comamonas spp.* and ferrihydrite is dominating Cd^{2+} adsorption under such conditions. As the ratio of ferrihydrite/*Comamonas spp.* (g g^{-1}, dry weight) decreased from 10 to 0.2 adsorption showed a pattern more similar to Cd^{2+} adsorption onto bacteria in a binary system in that Cd^{2+} adsorption ranged from nearly zero to almost 100 % over a wider range of ≈ 4 pH units which was almost as wide as that observed in the absence of ferrihydrite.

The first modelling approach (AP1, Figure 7.1) was a simple addition approach to fit the experimental data. Parameters for Cd^{2+} adsorption onto ferrihydrite (Table 3.2), and for Cd^{2+} adsorption onto *Comamonas spp.* (Table 6.2) were used to model Cd^{2+} adsorption in the mixtures. This modelling generally slightly overestimated the experimental data, indicating that Cd^{2+} adsorption onto bacterial cells and ferrihydrite was less than the additive result. There might be surface sites that are screened or occupied due to the interactions between the ferrihydrite and bacterial cell surfaces which caused the diminished Cd^{2+} adsorption. The interaction decreased Cd^{2+} adsorption under conditions when bacteria or ferrihydrite was the dominant adsorbent. The results of Cd^{2+} adsorption onto ferrihydrite-*Comamonas spp.* in this work are similar to that for Cd^{2+} adsorption onto ferrihydrite- *Escherichia coli* (Kulczycki et al. 2005) and Sr^{2+} adsorption onto ferrihydrite-*Shewanella alga* (Small et al. 1999) where less

Cd^{2+} and Sr^{2+} adsorption was observed than predicted using combined Langmuir sorption parameters of ferrihydrite and bacteria. It was proposed that specific surface sites might be masked due to the interaction between bacterial cells and ferrihydrite based on their Langmuir sorption modelling and scanning electron microscope images. Similar phenomena were observed between *Shewanella putrefaciens* and the iron oxides goethite, hematite, and ferrihydrite (Figure 7.2) (Glasauer et al. 2001), as well as between *Gallionella ferruginea* and ferrihydrite (Martinez and Ferris 2005). Parikh and Chorover (2006) examined adhesion of both Gram-positive and Gram-negative bacterial cells onto hematite surfaces with *in situ* ATR-FTIR spectroscopy and proposed interactions between the surface functional groups of bacterial cells and the hematite surface.

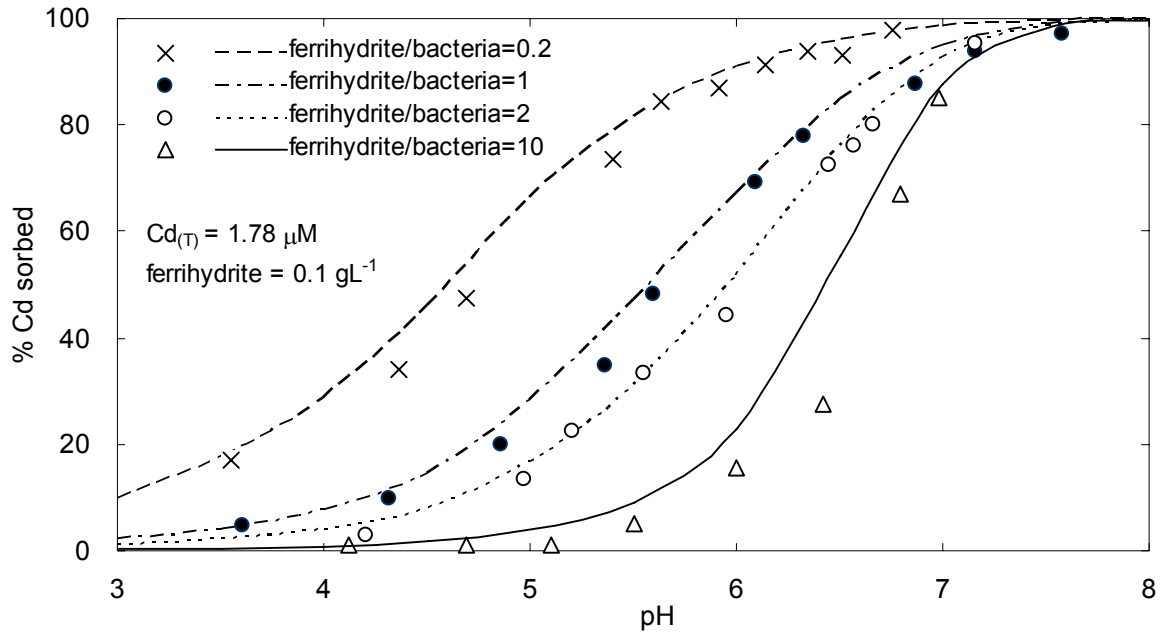

Figure 7.1 Cadmium sorption onto dead *Comamonas spp.* and ferrihydrite in ternary systems: Experimental (symbols) and AP1 modelled (lines). The ferrihydrite/*Comamonas spp.* is on a dry weight basis.

There have been two ways to make bacteria-ferrihydrite suspensions. One is by adding bacterial cells into ferric solution before the precipitation of ferrihydrite (Kulczycki et al. 2005; Small et al. 1999), and the other is by adding bacteria into an already precipitated ferrihydrite suspension (Glasauer et al. 2001; Parikh and Chorover 2006). There has been no study that compared the interactions between ferrihydrite and bacteria composites synthesized in these two ways. However, the interactions between bacteria and ferrihydrite might be greater in the first way, as it has been suggested that to get a significant ferrihydrite

precipitation on the bacterial surface, it was essential that ferric ion sorb onto the bacterial surface before ferrihydrite precipitation (Kulczycki et al. 2005; Small et al. 1999). In our work bacteria were added after ferrihydrite precipitation therefore the interaction between ferrihydrite and bacteria is probably less significant and has a weak influence on Cd^{2+} distribution under the conditions investigated in this work.

Figure 7.2 was removed. The original figure can be found in FIG.8. in page 5549 in reference: Glasauer S, Langley S, Beveridge TJ. 2001. Sorption of Fe (Hydr)Oxides to the Surface of *Shewanella putrefaciens*: Cell-Bound Fine-Grained Minerals Are Not Always Formed De Novo. *Applied and Environmental Microbiology* 67(12):5544-5550.

Figure 7.2 Transmission electron microscopy observation of *S. putrefaciens* CN32 cell after 30 min exposure to ferrihydrite. The solid arrows indicate sites on the cell wall where ferrihydrite appears to be attached to the bacterial surface (Glasauer et al. 2001).

The main modelling approaches that have attempted to quantitatively describe metal adsorption onto bacteria-iron oxide mixtures have used the Langmuir equation (Kulczycki et al. 2005; Martinez and Ferris 2005; Small et al. 1999; Violante et al. 2003). However modelling using the Langmuir equation cannot predict metal speciation for changing solution conditions such as pH. Fein (2000) suggested that surface complexation modelling could be used to quantify adsorption in bacteria-water-rock systems. Yee and Fein (2003) used surface complexation modelling to predict Cd^{2+} speciation in a bacteria-ferrihydrite complex system by combining adsorption reactions and thermodynamic stability constants for Cd^{2+} adsorption onto bacteria with Cd^{2+} adsorption onto ferrihydrite. However there was no experimental data

provided in their work, and the interaction between bacteria and ferrihydrite was not taken into account.

This work tried various modelling approaches to describe the interactions between ferrihydrite and *Comamonas spp.*. Because the interaction has a fairly minor influence on Cd^{2+} adsorption on ferrihydrite-*Comamonas spp.* composites, attempts to model this interaction must be a general approach where all bacterial surface sites were treated equivalently. By assuming different stoichiometries for the interaction between these two surfaces it was found that one approach (AP2) using the reactions given in Equations 7.1 and 7.2 could provide a reasonable description of the effects of ferrihydrite-*Comamonas spp.* interaction on Cd^{2+} adsorption as shown in Figure 7.3. Values for $\log K(\equiv Fe^{s}(ABCD)_{0.25}{}^{0})$ and $\log K(\equiv Fe^{w}(ABCD)_{0.25}{}^{0})$ were optimized from the experimental data and the results are shown in Table 7.1.

$$Fe^{s}OH + 0.25RA^{-} + 0.25RB^{-} + 0.25RC^{-} + 0.25RD^{-} + H^{+} \Leftrightarrow Fe^{s}(ABCD)_{0.25} + H_2O \quad \text{Eq. 7.1}$$

$$Fe^{w}OH + 0.25RA^{-} + 0.25RB^{-} + 0.25RC^{-} + 0.25RD^{-} + H^{+} \Leftrightarrow Fe^{w}(ABCD)_{0.25} + H_2O \quad \text{Eq. 7.2}$$

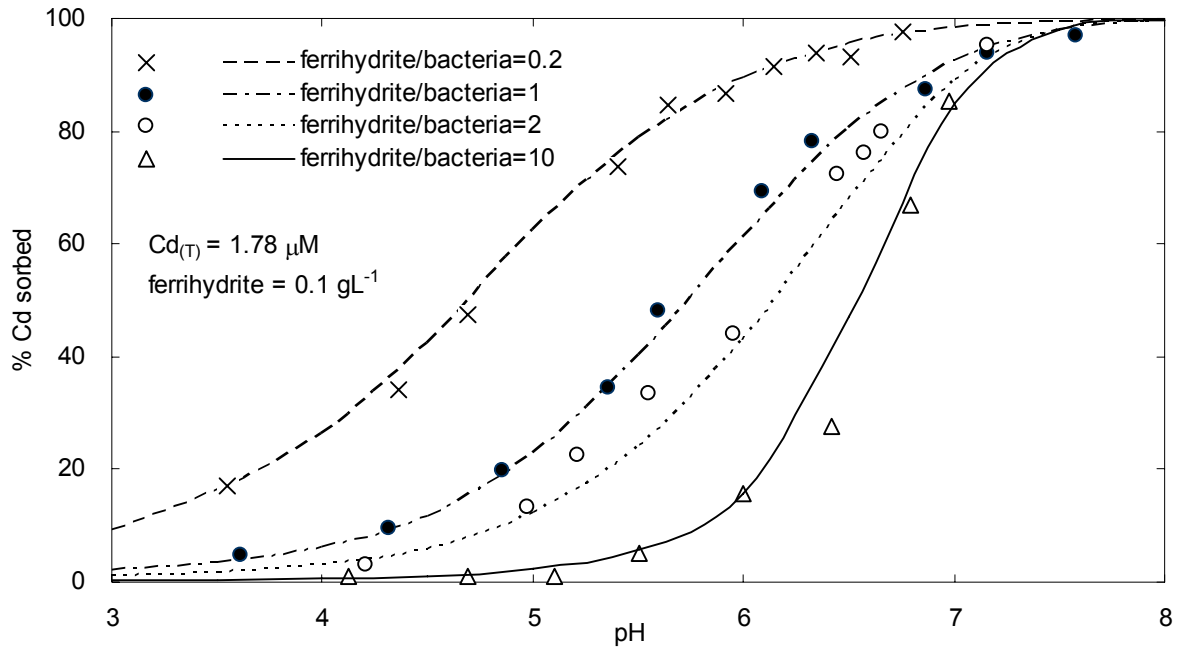

Figure 7.3 Experimental (symbols) and modelled (lines) results (AP2) for Cd^{2+} sorption onto *Comamonas spp.* and ferrihydrite composites. I = 0.01 M $NaNO_3$. The ferrihydrite/*Comamonas spp.* is on a basis of bacteria dry weight.

Table 7.1 Optimization of logK values for surface interaction between *Comamonas spp.* and ferrihydrite. Data sets are in Figure 7.1. Ferrihydrite = 0.1 gL^{-1}, $Cd_{(T)}$ = 1.78 μM, I = 0.01 M $NaNO_3$. The logK values are given for I = 0 (with standard deviations in parentheses).

Ferrihydrite/Bacteria (dry weight)	*Comamonas spp. (gL^{-1}, wet weight)*	*logK* $\equiv Fe^{s}(ABCD)_{0.25}{}^{0}$	*logK* $\equiv Fe^{w}(ABCD)_{0.25}{}^{0}$	*WSOS/DF*
10	0.055	13.35(0.082)	10.77 [b]	2.83
2	0.275	12.33(0.18) [a]	10.03(0.52) [a]	1.38
1	0.55	12.99 [b]	10.67(0.087)	7.13
0.2	2.75	12.99 [b]	11.27 (0.087)	7.02
Weighted average (95 % confidence interval)		12.99 (8.61, 17.37)	10.77 (9.92, 11.62)	

[a] Fixed at 0.15 to calculate weighted average when actual value is larger than 0.15 (Ali and Dzombak 1996b).
[b] No convergence of this value so the value was fixed at the weighted average for consistency

Only a value for $\log K(\equiv Fe^{s}(ABCD)_{0.25}{}^{0})$ could be optimised from the data with ferrihydrite/*Comamonas spp.* ratio of 10. Because the $Cd_{(T)}$/Fe ratio was 0.0016 and sorption onto ferrihydrite dominated Cd^{2+} speciation (Figure 7.4a). The ferrihydrite type 1 sites are more important than type 2 sites. Therefore it is the masking of the ferrihydrite type 1 sites by *Comamonas spp.* that is accounting for changes in Cd^{2+} distribution due to the interaction between ferrihydrite and *Comamonas spp.* (Figure 7.5a). Both $\log K(\equiv Fe^{s}(ABCD)_{0.25}{}^{0})$ and $\log K(\equiv Fe^{w}(ABCD)_{0.25}{}^{0})$ can be optimized from data for ferrihydrite/*Comamonas spp.* ratio of 2, and only $\log K(\equiv Fe^{w}(ABCD)_{0.25}{}^{0})$ can be optimized from data for ferrihydrite/*Comamonas spp.* ratios of 1 or 0.2. With the decrease in ferrihydrite/*Comamonas spp.* ratios the bacteria dominate Cd^{2+} adsorption (Figure 7.4). Under these conditions it is the type 2 ferrihydrite sites masking the bacterial sites that causes the changed in Cd^{2+} distribution (Figure 7.5b). Therefore $\log K(\equiv Fe^{w}(ABCD)_{0.25}{}^{0})$ can be optimized from data with lower ferrihydrite/*Comamonas spp*. ratio. Figure 7.3 shows the sorption of Cd^{2+} by ferrihydrite-*Comamonas spp.* mixtures with modelling results that include this approach to quantify the interaction between the iron oxide and bacteria (Table 7.1) with the adsorption constants from Tables 3.2, 6.1 and 6.2. By including the interactions between ferrihydrite and bacteria, the model predictions of Cd^{2+} distribution in the mixed systems are reasonably accurate (Figure 7.3). Modelled Cd^{2+} speciation and distribution in the iron oxide-bacteria system are shown in Figure 7.4.

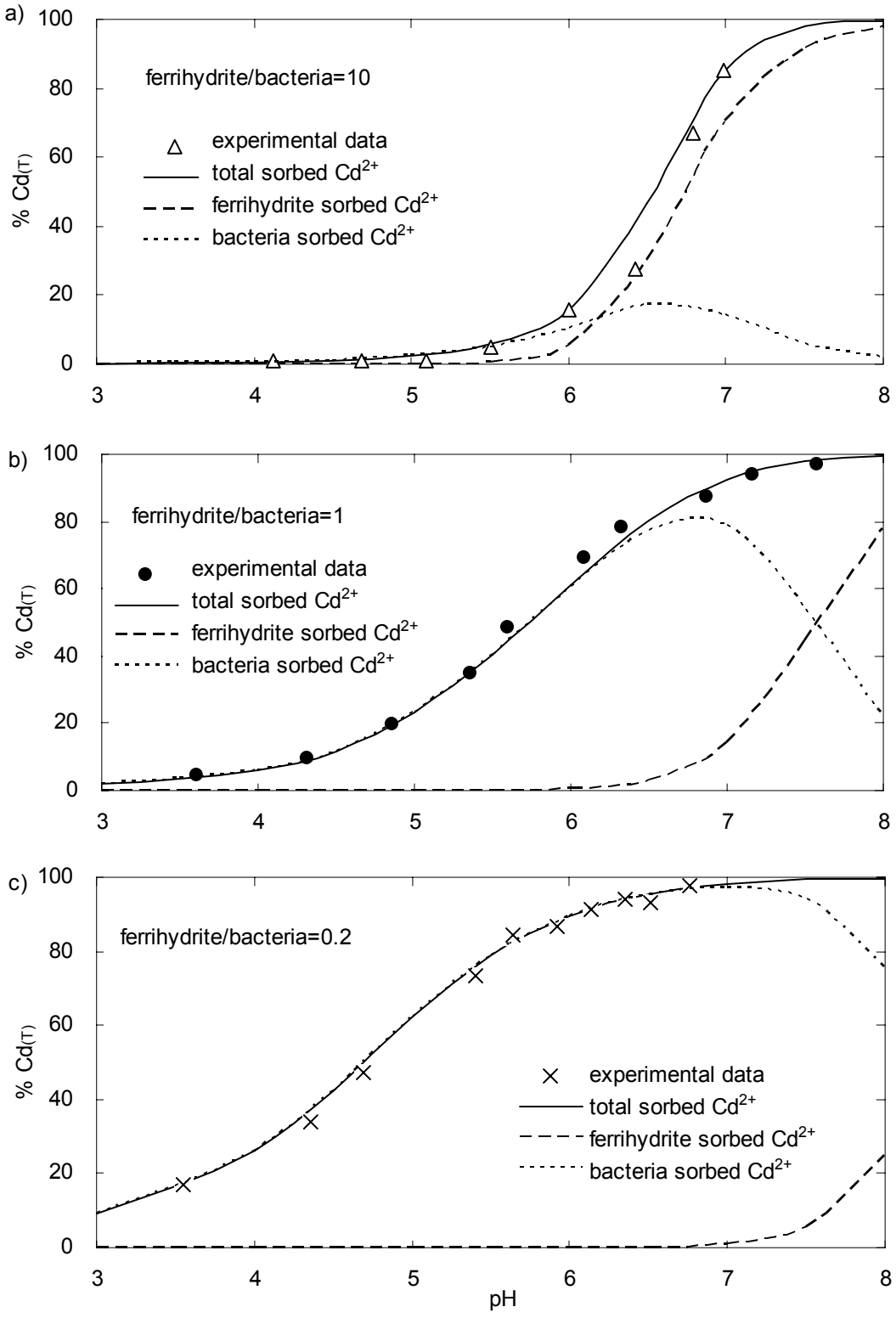

Figure 7.4 Surface Cd^{2+} speciation in the *Comamonas spp.*-ferrihydrite systems: experimental data (symbols) and modelled results (lines). I = 0.01 M $NaNO_3$, $Cd_{(T)}$ = 1.78 μM, ferrihydrite = 0.1 gL^{-1}. The ferrihydrite/*Comamonas spp.* is on a basis of dry weight of bacteria.

To our knowledge, this is the first surface complexation modelling approach to describe the interactions between bacteria and iron oxides and their effects on metal distribution in a bacteria-mineral oxide system. The effect of this interaction in our work was small and the model approach is by necessity general. The model in this work can reasonably fit the experimental data but given the wide 95 % confidence interval for $\log K(\equiv Fe^{s}(ABCD)_{0.25}{}^{0})$. Further research work will be needed to gain more insight into modelling the interaction between bacteria and mineral oxides.

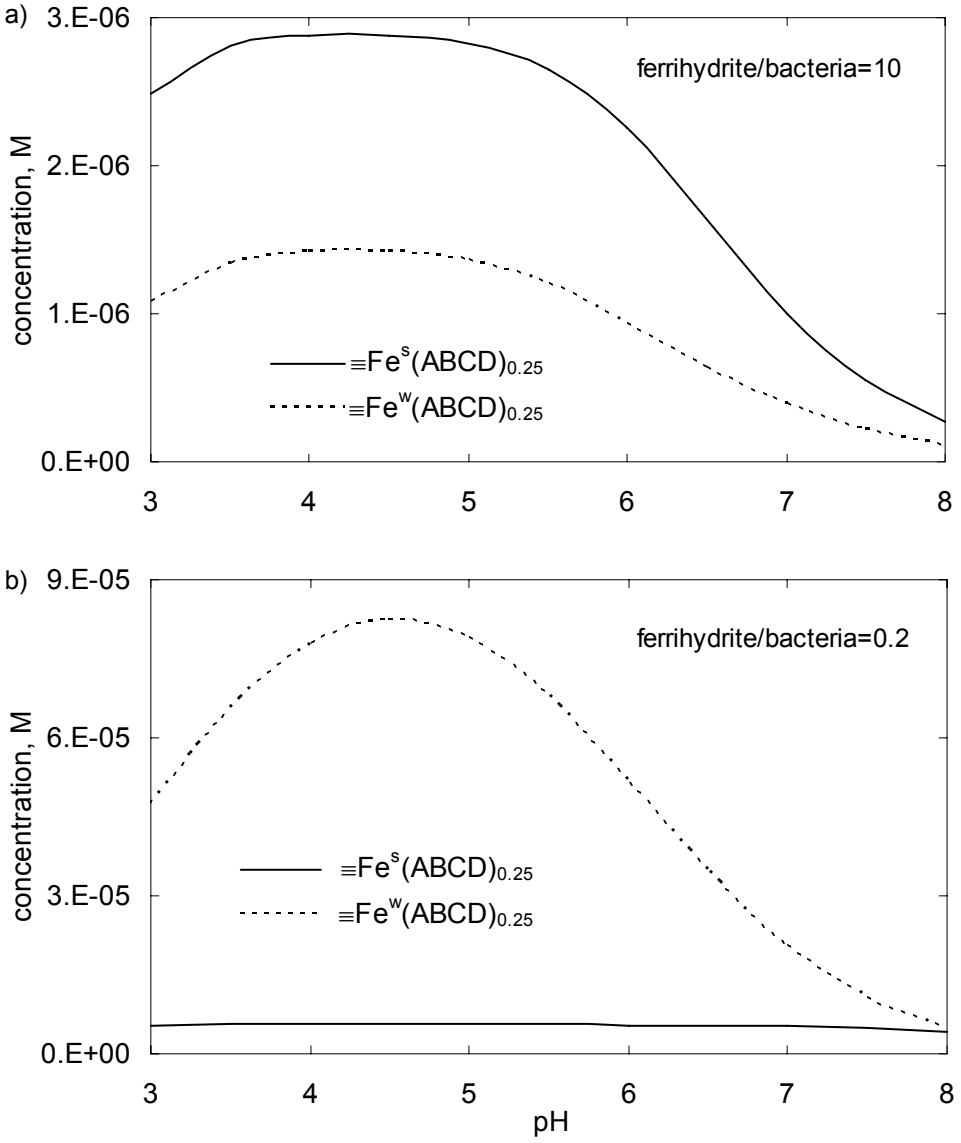

Figure 7.5 Modelled speciation of ≡ Fe(ABCD)$_{0.25}$ in the *Comamonas spp.*-ferrihydrite systems. I = 0.01 M $NaNO_3$, $Cd_{(T)}$ =1.78 μM, ferrihydrite = 0.1 gL^{-1}. The ferrihydrite/*Comamonas spp.* is on a basis of dry weight of bacteria.

7.3. Sorption in dead *Comamonas spp.*-ferrihydrite–H_2L_p systems

This section describes Cd^{2+} adsorption in a quaternary system involving ferrihydrite, H_2L_p and dead *Comamonas spp.*. Dead bacteria were obtained using the method described in Section 2.2.6 and were used to prevent the metabolism of H_2L_p. Two systems were studied that differred in the amount of bacteria present. In one system (QS1), ferrihydrite was the dominant adsorbing phase, in the other system (QS2) *Comamonas spp.* dominated Cd^{2+} adsorption. The results for these two systems are given in this section, along with Cd^{2+} adsorption in related but simpler systems. Cadmium adsorption in quaternary systems with ferrihydrite, H_2L_p and *Comamonas spp.* was modelled by taking the following adsorption into account: Cd-ferrihydrite binary surface complexes, H_2L_p-ferrihydrite binary complexes, H_2L_p-Cd-ferrihydrite ternary complexes, Cd-*Comamonas spp.* binary complexes, and the reactions to describe the interactions between ferrihydrite and *Comamonas spp.*. The weighted average values used in modelling Cd^{2+} adsorption in the quaternary system are given in Tables 3.2, 3.3, 4.4, 6.1, 6.2 and 7.1.

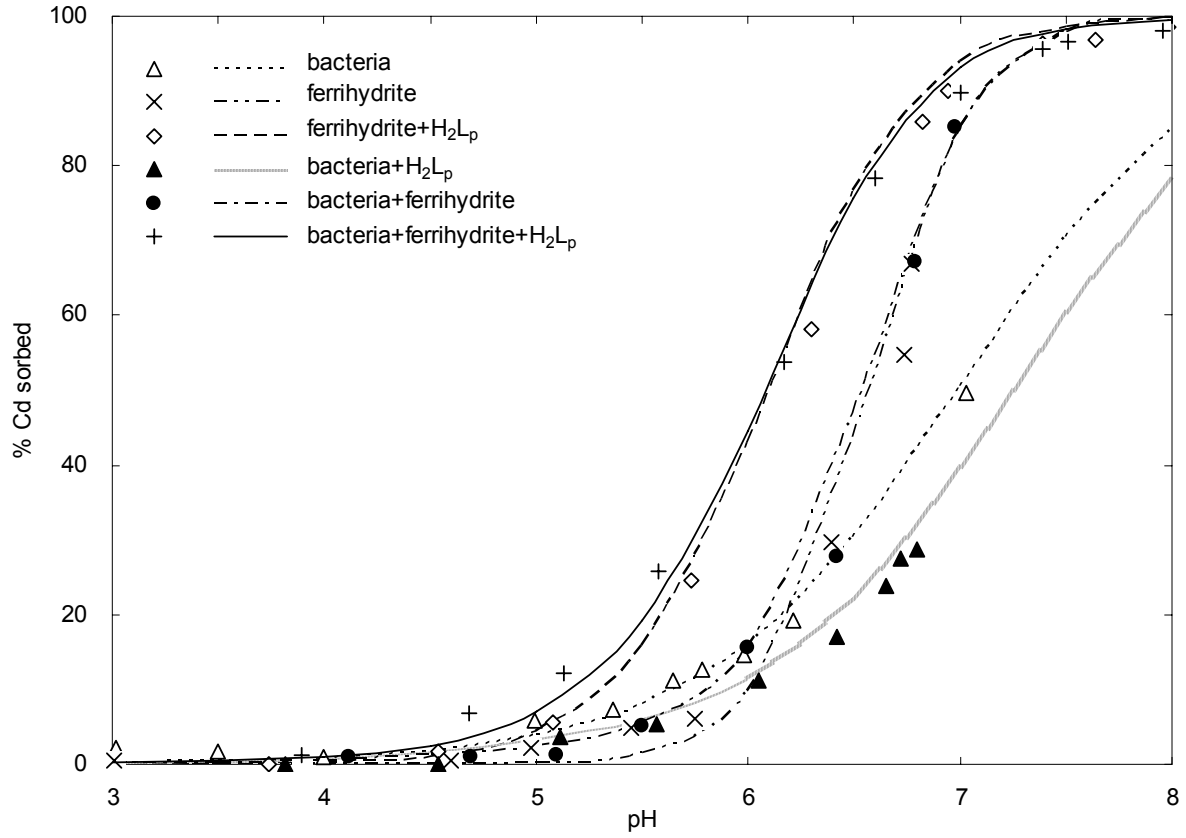

Figure 7.6 Experimental (symbols) and modelled (lines) results for Cd^{2+} sorption at various systems. I = 0.01 M $NaNO_3$, *Comamonas spp.*= 0.01 gL^{-1} (dry weight), ferrihydrite =0.1 gL^{-1}, $H_2L_{p(T)}$=0.6 mM, $Cd_{(T)}$ = 1.78 μM.

Figure 7.6 shows the results in QS1 (where ferrihydrite was the dominant adsorbing phase) with the related binary and ternary systems. The two binary systems shown in Figure 7.6 are Cd^{2+} adsorption onto ferrihydrite and Cd^{2+} adsorption onto *Comamonas spp.*. Bacteria appear to accumulate more Cd^{2+} than ferrihydrite at pH < 6.2 (though the ferrihydrite/*Comamonas spp.* (dry weight) ratio is 10), and more Cd^{2+} adsorption is observed on ferrihydrite compared to *Comamonas spp.* at pH > 6.2.

In ternary systems (Figure 7.6), the presence of H_2L_p has opposite effects on Cd^{2+} adsorption onto ferrihydrite and Cd^{2+} adsorption onto *Comamonas spp.*. While Cd^{2+} adsorption onto ferrihydrite was significantly enhanced in the presence of H_2L_p due to the surface ternary complex formation (Chapter 4), phthalic acid inhibited Cd^{2+} adsorption onto *Comamonas spp.* due to the formation of solution complexes between Cd^{2+} and H_2L_p as discussed in Chapter 6.

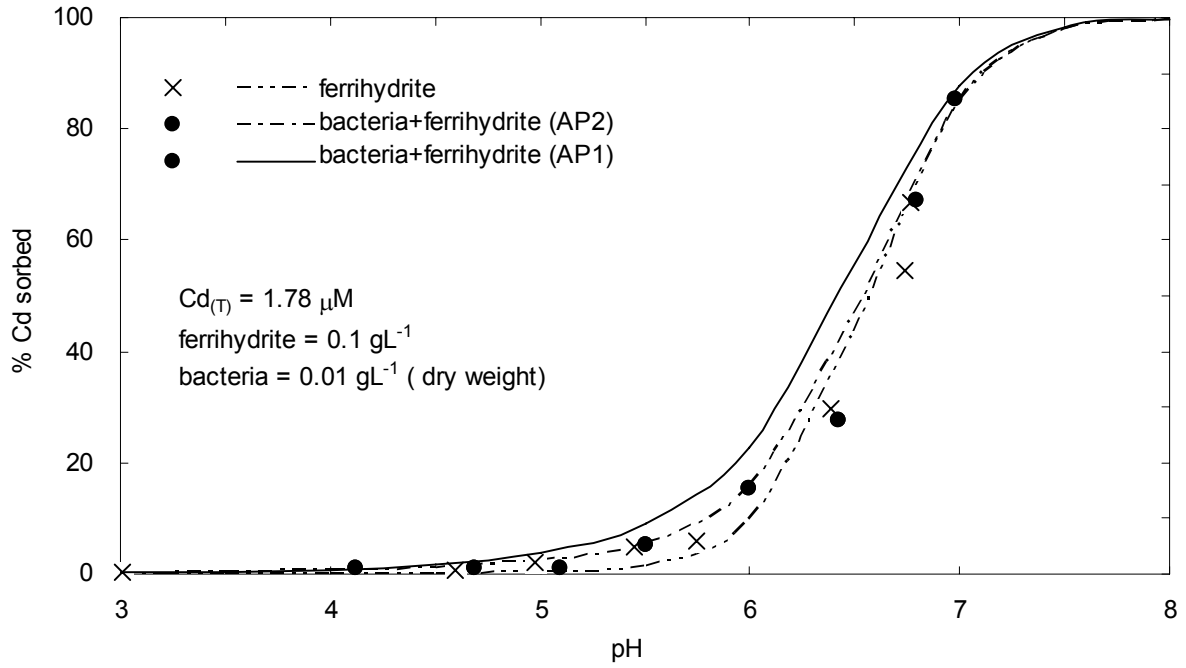

Figure 7.7 Comparison of modelled Cd^{2+} adsorption onto ferrihydrite-*Comamonas spp.* in ternary systems using AP1 and AP2: Experimental (symbols) and modelled (lines) results. I = 0.01 M NaNO3.

Compared to binary Cd-ferrihydrite systems, the presence of *Comamonas spp.* in ternary Cd-ferrihydrite-*Comamonas spp.* systems did not notably contribute to increased Cd^{2+} adsorption due to the high ferrihydrite/*Comamonas spp.* (dry weight) ratio of 10. Slightly more Cd^{2+} adsorption was observed at pH < 6 for the ferrihydrite with *Comamonas spp.* systems because at low pH *Comamonas spp.* dominates Cd^{2+} surface speciation as shown in the two binary systems. The presence of ferrihydrite actually inhibited adsorption by *Comamonas spp.* at pH

< 6 due to the interaction between bacteria and ferrihydrite. Figure 7.7 compares modelling results using two different modelling approaches, one of which did not take the interaction between bacteria and ferrihydrite into account (AP1) while the other did (AP2). The result from AP1 shows Cd^{2+} adsorption onto ferrihydrite-bacteria composites if there were no interaction between the two sorbents. However it overestimated the experimental data. With the inclusion of reactions to describe the interaction between ferrihydrite and bacteria, AP2 more accurately reproduced the experimental data. Therefore in ferrihydrite-bacteria systems, the observed enhanced Cd^{2+} adsorption is a total result of bacterial biosorption and the effects of the interaction between bacteria and ferrihydrite.

Compared to all related binary and ternary systems (Figure 7.6), cadmium adsorption in QS1 was enhanced under most conditions, except for a slight decrease at higher pH compared to that in H_2L_p-Cd-ferrihydrite ternary systems. As discussed above, there are both negative and positive effects that can either inhibit or enhance Cd^{2+} adsorption and the observed Cd^{2+} adsorption is a result of the sum of these effects. Cadmium adsorption in QS1 is closest to that in ferrihydrite-Cd^{2+}-H_2L_p ternary system with a slight increase at pH < 6, but QS1 is quite different from that in other binary or ternary systems. This indicates that among all the effects in the quaternary system it is the surface ferrihydrite-Cd^{2+}-H_2L_p ternary complex that dominates Cd^{2+} surface species (Figure 7.8). Compared to ferrihydrite-Cd^{2+}-H_2L_p ternary systems, the slight increase of Cd^{2+} at pH < 6 in quaternary systems was due to the bacterial sorption.

The significance of bacterial surface absorbing Cd^{2+} can be more clearly observed by decreasing the ferrihydrite/*Comamonas spp.* (dry weight) ratio from 10 (Figure 7.6) to 2 (Figure 7.9). In this case adsorption in the binary system with *Comamonas spp.* was substantially greater than with ferrihydrite at pH < 7. This indicates that 0.05 gL^{-1} (dry weight) *Comamonas spp.* can significantly accumulate more Cd^{2+} than 0.1 gL^{-1} ferrihydrite, particularly at lower pH range. Adding H_2L_p inhibited Cd^{2+} adsorption by *Comamonas spp.* but enhanced Cd^{2+} adsorption onto ferrihydrite so that Cd^{2+} adsorption in the presence of H_2L_p was greater on ferrihydrite than *Comamonas spp.* at pH > 6.

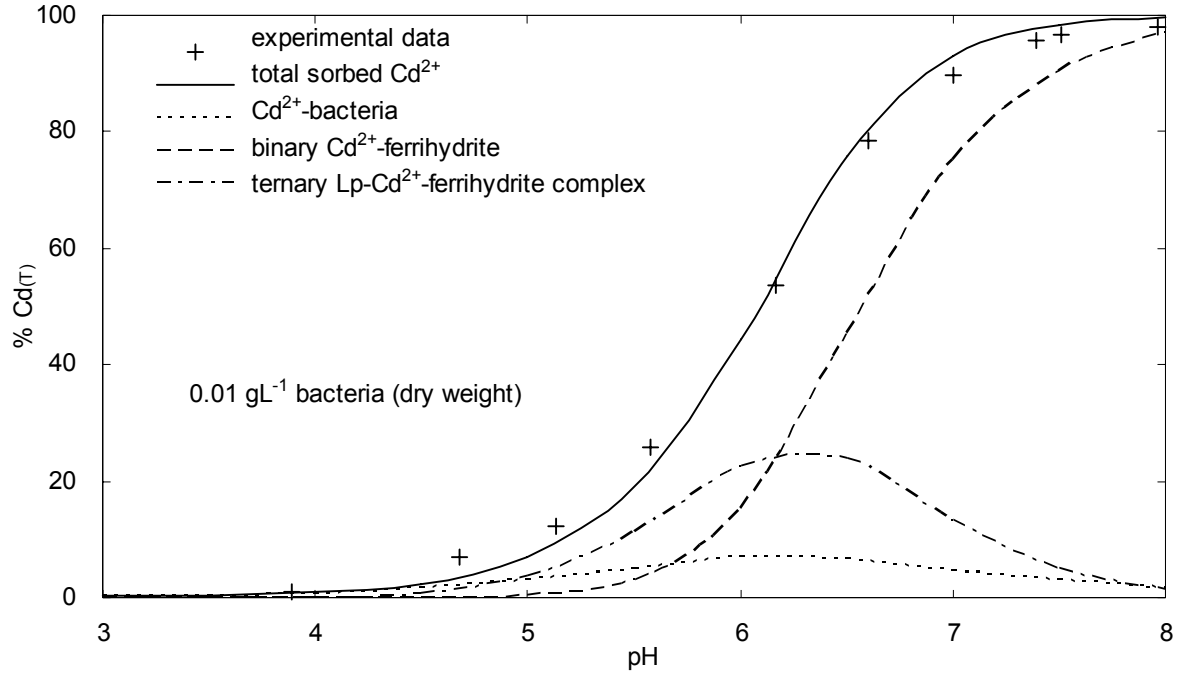

Figure 7.8 Cadmium speciation in Cd-ferrihydrite-*Comamonas spp.*-H_2L_p quaternary systems (QS1): experimental data (symbols) and modelled results (lines). I = 0.01 M $NaNO_3$, 1.78 μM $Cd_{(T)}$, 0.1gL^{-1} ferrihydrite, 0.6 mM $H_2L_{p(T)}$.

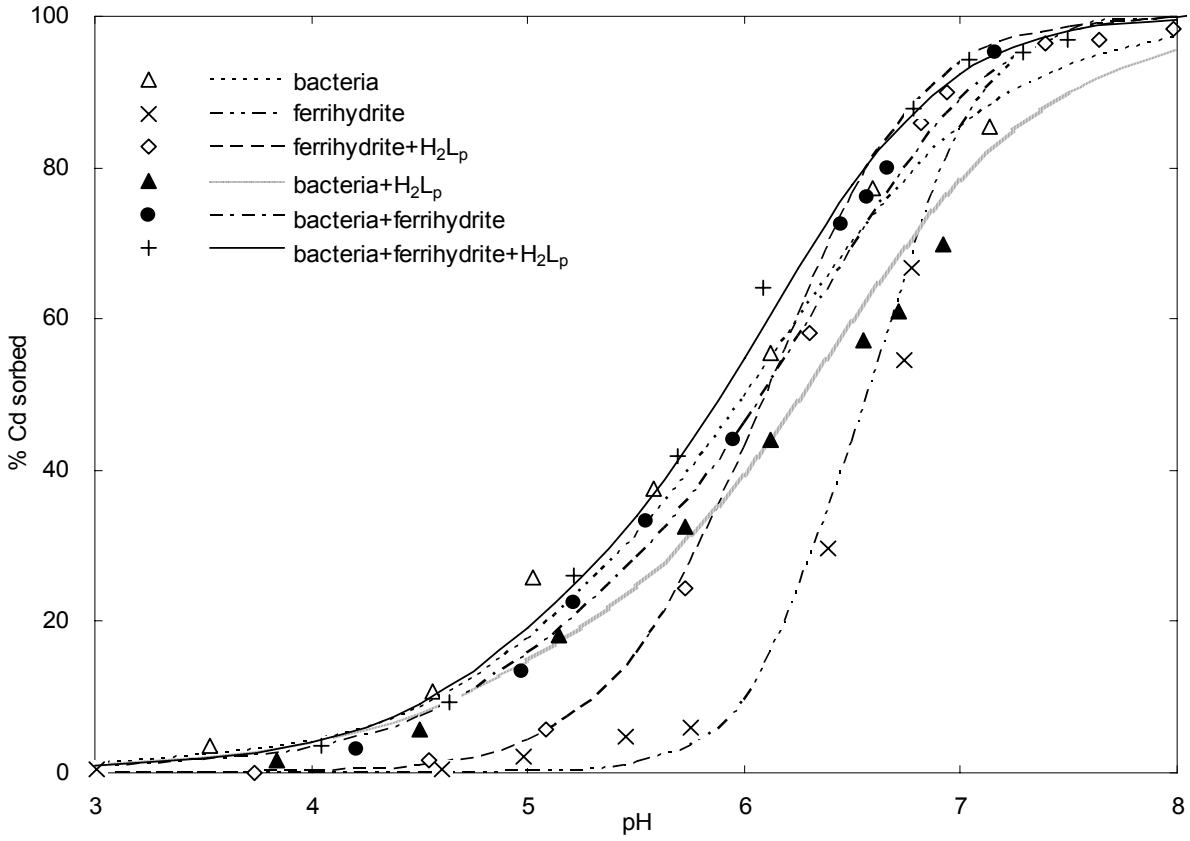

Figure 7.9 Experimental (symbols) and modelled (lines) results for Cd^{2+} sorption in various systems. I = 0.01 M $NaNO_3$, *Comamonas spp.*= 0.05 gL^{-1} (dry weight), ferrihydrite =0.1 gL^{-1}, $H_2L_{p(T)}$=0.6 mM, $Cd_{(T)}$ = 1.78 μM.

The presence of 0.275 gL^{-1} *Comamonas spp.* significantly enhanced Cd^{2+} sorption over the investigated pH range (Figure 7.9), indicating that the increased bacterial cells are important absorbent of Cd^{2+} in ferrihydrite-*Comamonas spp.* systems, particular at lower pH range. In contrast the presence of 0.055 gL^{-1} *Comamonas spp.* slightly enhanced Cd^{2+} adsorption at pH < 6 in ferrihydrite-*Comamonas spp.* ternary systems compared to ferrihydrite binary systems (Figure 7.6).

Similarly Cd^{2+} adsorption was significantly increased by the addition of 0.275 gL^{-1} *Comamonas spp.* to the ferrihydrite-Cd^{2+}-H_2L_p system in Figure 7.9. The difference in enhanced Cd^{2+} adsorption between these two systems is much larger than that in the same types of systems with 0.055 gL^{-1} *Comamonas spp.* due to increased amount of bacterial cells. This conclusion is confirmed by comparing Cd^{2+} surface speciation in QS1 and QS2. The bacterial sorbed Cd^{2+} in QS2 (Figure 7.11) is more significant than that in QS1 (Figure 7.8).

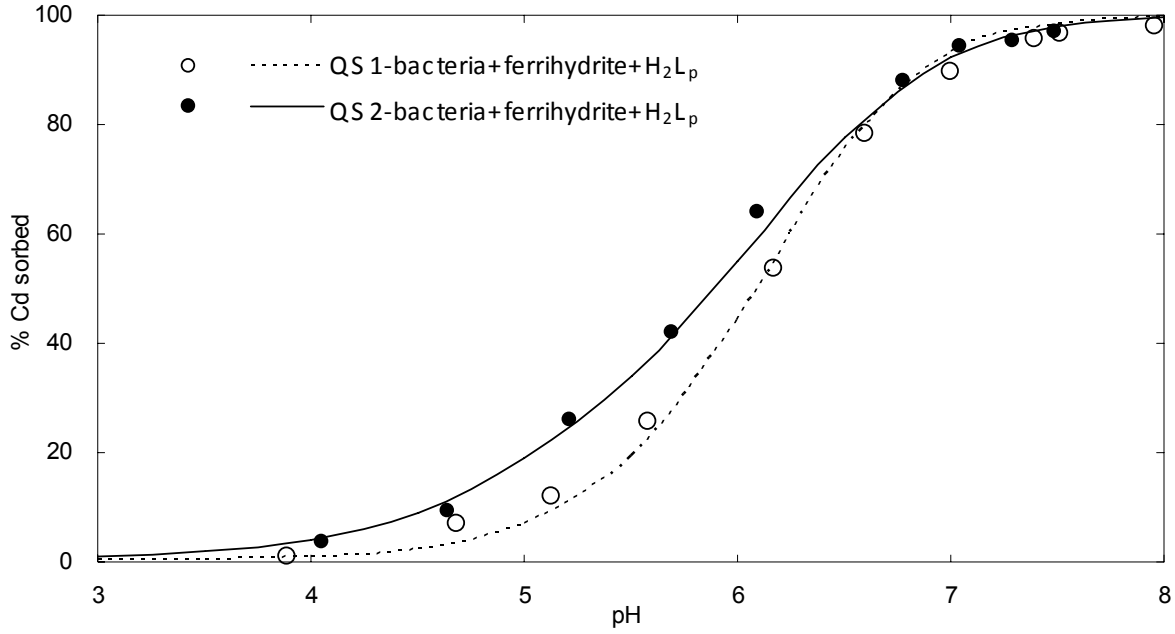

Figure 7.10 Cadmium sorption in Cd-bacteria-ferrihydrite-H_2L_p quaternary systems (QS1 and QS2): Experimental (symbols) and modelled (lines) results. Bacteria in QS1 and QS2 is 0.055 and 0.275 gL^{-1}, respectively. I = 0.01 M, ferrihydrite = 0.1 gL^{-1}, $H_2L_{p(T)}$ = 0.6 mM, $Cd_{(T)}$ = 1.78 μM.

In contrast the effect of adding H_2L_p to the *Comamonas spp.*-ferrihydrite mixtures was much lower with 0.275 gL^{-1} than 0.055 gL^{-1} *Comamonas spp.*. This is because the ferrihydrite surface, on which the ternary ferrihydrite-Cd-L_p complexes form, is less important with 0.275 gL^{-1} *Comamonas spp.*. The net effect of these complex interactions is that Cd^{2+} adsorption in the quaternary systems with 0.275 gL^{-1} *Comamonas spp.* is only slightly greater

than that with 0.055 gL^{-1} *Comamonas spp.* (Figure 7.10). For example in the absence of H_2L_p and ferrihydrite Cd^{2+} adsorption was substantially greater with 0.275 gL^{-1} rather than 0.055 gL^{-1} *Comamonas spp.* (Figure 6.6). Similarly in ternary systems with *Comamonas spp.* and either ferrihydrite or H_2L_p Cd^{2+} was much greater with 0.275 gL^{-1} compared to 0.055 gL^{-1} *Comamonas spp.* (Figures 7.3 and 6.6).

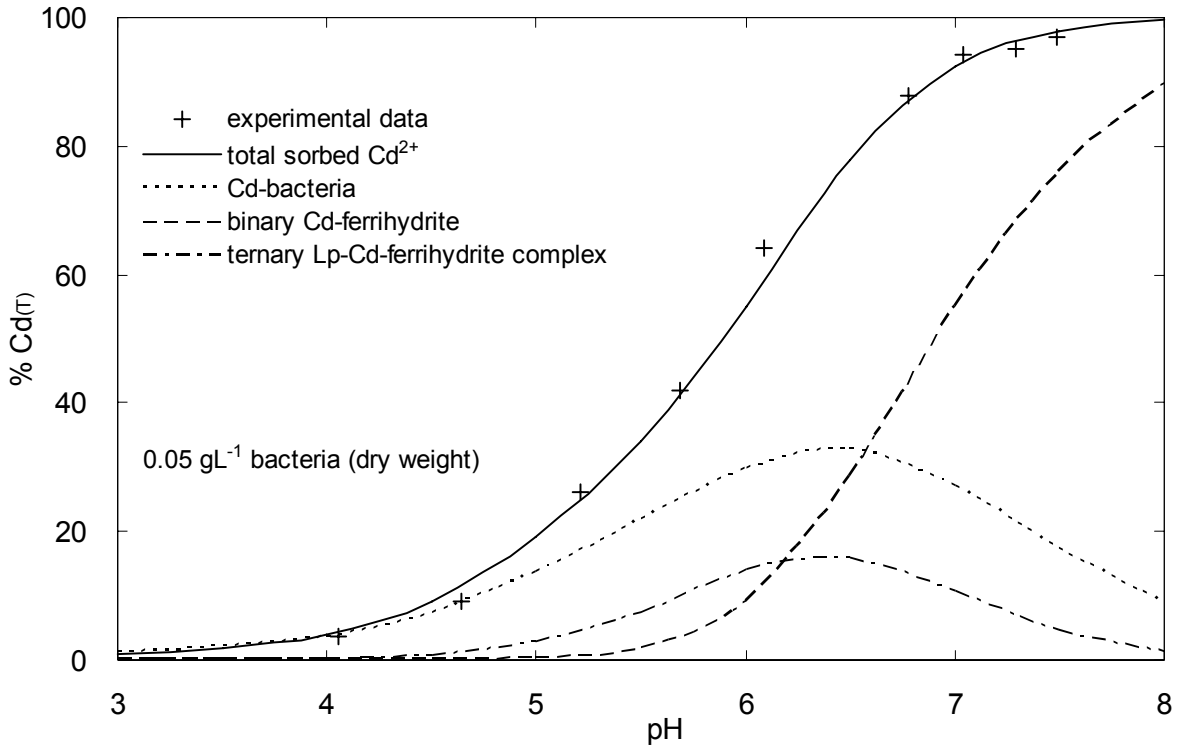

Figure 7.11 Cadmium speciation in quaternary systems (QS2): experimental data (symbols) and modelled results (lines). I = 0.01 M $NaNO_3$, $Cd_{(T)}$= 1.78 μM, ferrihydrite = 0.1 gL^{-1}, $H_2L_{p(T)}$ = 0.6 mM

It is also worth considering the effect of ferrihydrite on Cd^{2+} biosorption. Compared to Cd^{2+}-bacteria binary systems the presence of ferrihydrite decreased Cd^{2+} adsorption at pH less than ~ 6 but increased adsorption at pH over ~ 6 (Figures 7.6 and 7.9). The effects of ferrihydrite on Cd^{2+} sorption were due to two processes. On one hand ferrihydrite can mask bacterial surface sites through the ferrihydrite-bacteria interaction which would diminish Cd^{2+} adsorption. On the other hand ferrihydrite tends to increase Cd^{2+} sorption directly through binary surface complexes. The former effect is more significant at lower pH but less at higher pH (Figure 7.4). The latter effect is more significant at higher pH. Therefore Cd^{2+} adsorption onto ferrihydrite-bacteria composites are observed to be less than that in bacteria binary systems at lower pH. At higher pH the sorption onto ferrihydrite dominates and Cd^{2+} adsorption overall is increased.

Figures 7.6 and 7.9 show that the experimental data can be accurately reproduced by the modelling parameters developed. In addition Cd^{2+} speciation and distribution, as well as the interactions between various components in these complex quaternary systems, can be obtained from the model (Figures 7.8 and 7.11).

7.4. Cadmium sorption in live *Comamonas spp.*-ferrihydrite systems

In this final section Cd^{2+} adsorption is examined in systems with live *Comamonas spp.* where H_2L_p metabolism is occurring. For *Comamonas spp.* to metabolize H_2L_p certain nutrients are required and these were provided by solution Y (Chapter 5). In the investigation of H_2L_p metabolism experiments were performed to determine the minimum amount of nutrients required by *Comamonas spp.* to enable H_2L_p metabolism to occur. Before examining Cd^{2+} adsorption where H_2L_p is being metabolized another two factors are considered and described in this section; how the presence of the nutrients in solution Y will affect Cd^{2+} adsorption and whether Cd^{2+} adsorption on live *Comamonas spp.*-ferrihydrite and dead *Comamonas spp.*-ferrihydrite is different.

7.4.1 Effects of solution Y on Cd^{2+} adsorption in abiotic and biotic systems

Solution Y provides necessary nutrients for *Comamonas spp.* to metabolize H_2L_p and contains a variety of cations and anions which may influence metal or ligand adsorption onto iron oxide or bacteria surfaces. For example phosphate and sulfate can absorb onto the iron oxide surface, compete for surface sites with other ligands and also influence metal adsorption onto iron oxides by forming surface ternary complexes and aqueous complexes (Ali and Dzombak 1996c; Elzinga et al. 2001; Geelhoed et al. 1998; Li et al. 2006; Lin et al. 2004; Swedlund et al. 2003; Venema et al. 1997; Zhang and Peak 2007). Cations such as Mg^{2+} and Ca^{2+} can affect other metal ions adsorption (such as Cd^{2+}) onto iron oxide by competing for surface sites and they can also form complexes with ligands and therefore influence the target metal ion adsorption (Kuo 1986; Mustafaa et al. 2004; Weng et al. 2005). Competition between metal ions at bacterial surfaces has also been observed (Burnett et al. 2007).

Cadmium adsorption in eight different types of systems in the presence and absence of solution Y was investigated to examine the effects of solution Y on Cd^{2+} adsorption. The effects of solution Y on Cd^{2+} adsorption in all investigated systems are found to be negligible (Figure 7.12) due to the very low cation and anion concentrations (at μM level). Therefore,

cadmium species and distribution in biotic systems in the presence of solution Y can be described by using the same model parameters that were derived from the data in the absence of solution Y.

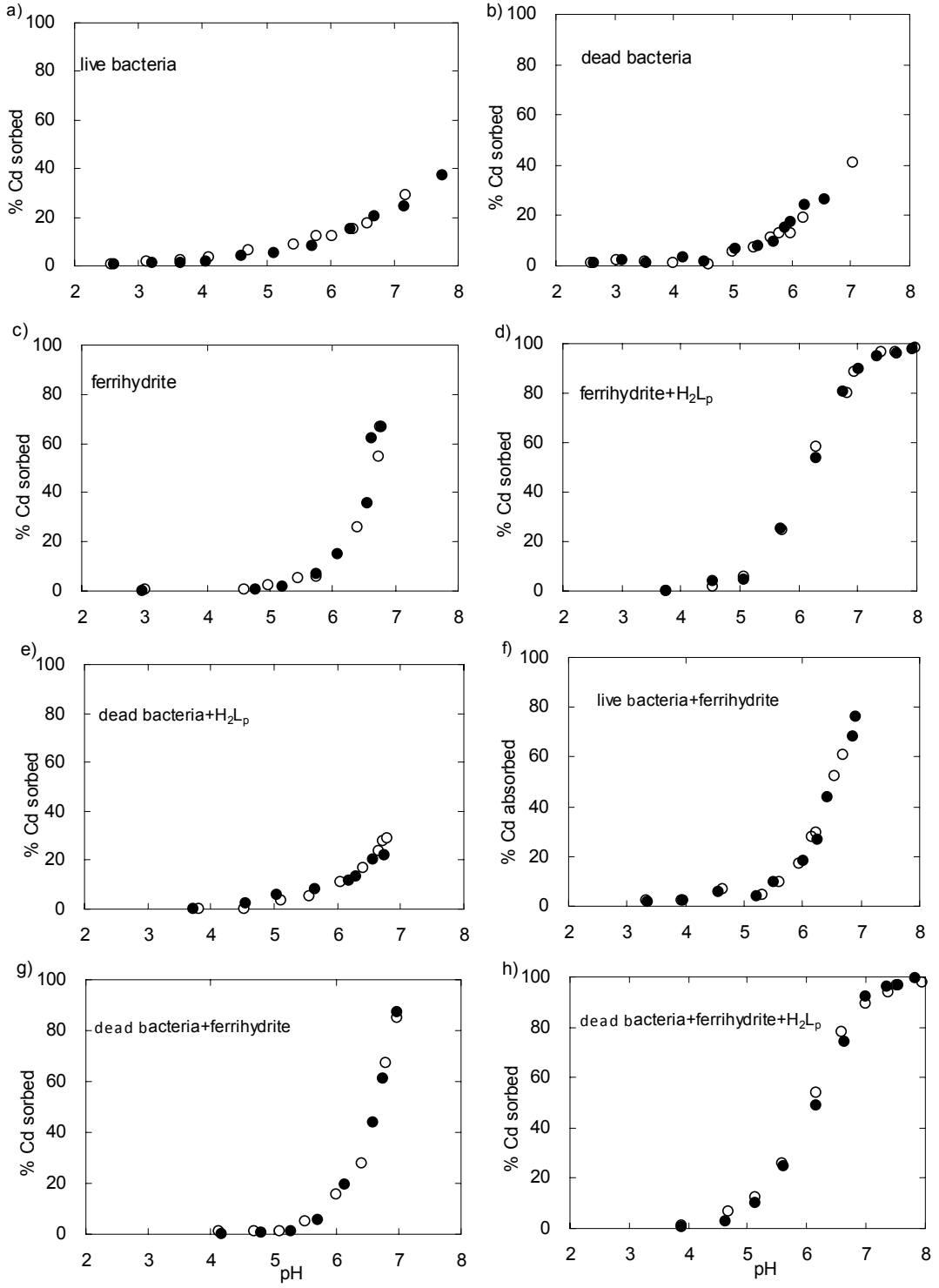

Figure 7.12 Cadmium adsorption in various systems in the presence and absence of solution Y. I = 0.01 M $NaNO_3$, $Cd_{(T)}$ = 1.78 μM, ferrihydrite = 0.1 gL^{-1}, $H_2L_{p(T)}$ = 0.6 mM, *Comamonas spp.*= 0.055 gL^{-1}. Open symbols are for data in the absence of solution Y, and solid symbols are for data in the presence of solution Y.

7.4.2 Comparison of Cd^{2+} adsorption onto live or dead *Comamonas spp.*

It has been reported that dead bacteria cells and live bacteria cells may absorb different amounts of metal ions. The metal sorptive capacity of dead cells may be greater, equivalent to or less than that of live cells depending on the bacteria species (Gabr et al. 2008; Kapoor and Viraraghavan 1995; Ledin 2000; Wang and Chen 2006). During the degradation of H_2L_p in the presence of *Comamonas spp.* and ferrihydrite the bacteria will be alive and Cd^{2+} adsorption onto a live bacteria-ferrihydrite system is therefore needed to be quantified. Cadmium adsorption onto live or dead *Comamonas spp*. in the absence or presence of 0.1 gL^{-1} ferrihydrite was examined over 72 h. The experimental data are given in Figures 7.13 and 7.14, with the modelling result for Cd^{2+} adsorption.

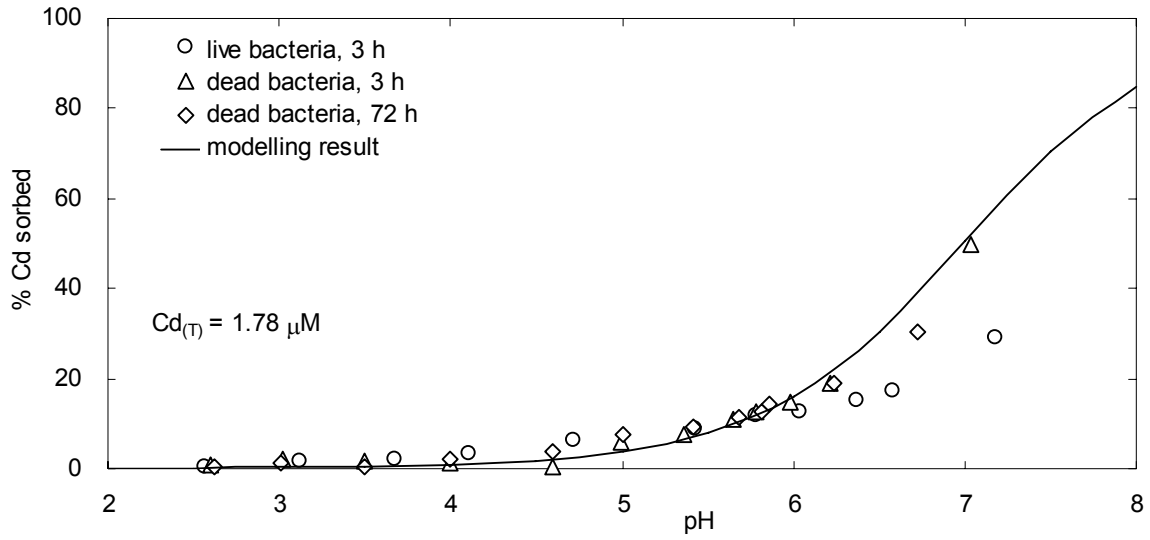

Figure 7.13 Cadmium sorption onto live and dead *Comamonas spp.* at different sorption time. I = 0.01 M $NaNO_3$, bacteria = 0.055 gL^{-1}

Figure 7.13 shows that 3 h is sufficient for Cd^{2+} adsorption onto dead *Comamonas spp.* to reach equilibrium because long equilibrium time 72 h did not increase Cd^{2+} sorption. The amount of Cd^{2+} adsorption onto live bacteria was observed to be almost equivalent to that of Cd^{2+} adsorption onto dead bacteria at pH < 6 but live bacteria absorbed less Cd^{2+} than dead bacteria at pH 6 ~ 7.2. However this difference in Cd^{2+} adsorption at higher pH between live and dead bacteria was not observed for systems containing ferrihydrite (Figure 7.14) because Cd^{2+} adsorption onto ferrihydrite dominates in these systems. More than 90 % *Comamonas spp.* were still alive after 72 h sorption time for samples with pH > 6 in all systems.

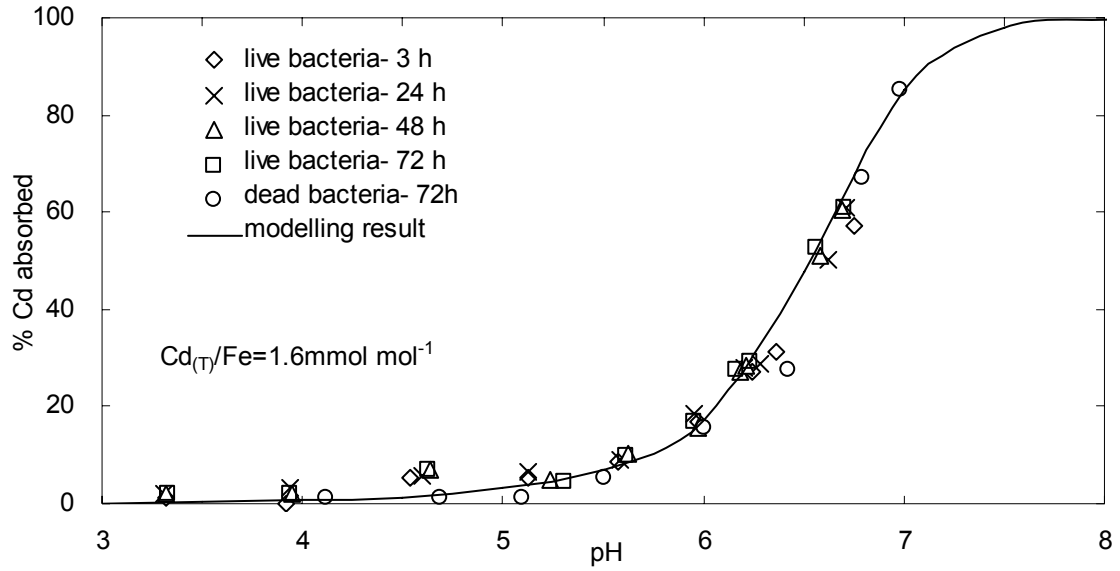

Figure 7.14 Cadmium sorption in *Comamonas spp.*-ferrihydrite system at different sorption time. I = 0.01 M $NaNO_3$, *Comamonas spp.* = 0.055 gL^{-1}, ferrihydrite = 0.1 gL^{-1}

Figure 7.14 shows that Cd^{2+} adsorption onto live *Comamonas spp.*-ferrihydrite appeared to reach sorption equilibrium within 3 h, without noticeable increase or decrease between 3 h and 72 h. Cadmium adsorption onto live *Comamonas spp.*-ferrihydrite showed nearly the same result as that of dead *Comamonas spp.*-ferrihydrite and therefore was well described by the modelling. Therefore the parameters derived in previous chapters can be applied to the investigation of Cd^{2+} adsorption in a system with live bacteria.

7.4.3 Cadmium sorption in live *Comamonas spp.*-ferrihydrite-H_2L_p systems

Previous investigation showed that H_2L_p can influence Cd^{2+} distribution in various systems. The objective of this section is to examine Cd^{2+} adsorption during H_2L_p degradation in systems comprised of Cd^{2+}, ferrihydrite, phthalic acid, *Comamonas spp.* and solution Y. Phthalic acid degradation, pH change, as well as Cd^{2+} adsorption was examined over 72 h. In order to avoid the accumulation of CO_2 and HCO_3^- the head space of the reaction vessels was flushed continuously with a 4:1 (V:V) mix of N_2 and O_2. Four experiments were conducted with initial pH values of 5.58, 6.04, 6.53 and 7.02 and these were termed Batch 1, 2, 3 and 4, respectively. The results are given in Figures 7.15, 7.16 and 7.17. With the exception of Batch 1, phthalic acid was completely degraded within 72 h. The starting pH of Batch 1 was less than 6 and in general faster H_2L_p degradation was observed at pH values closer to neutral.

During H_2L_p degradation the pH in each investigated system generally increased and the final pH values were 7.26, 9.24, 7.92 and 8.06 in Batch 1 to 4, respectively. A pH increase during H_2L_p biodegradation was also found by Fan et al (2004) using aerobic bacterial consortia enriched from a sewage sludge.

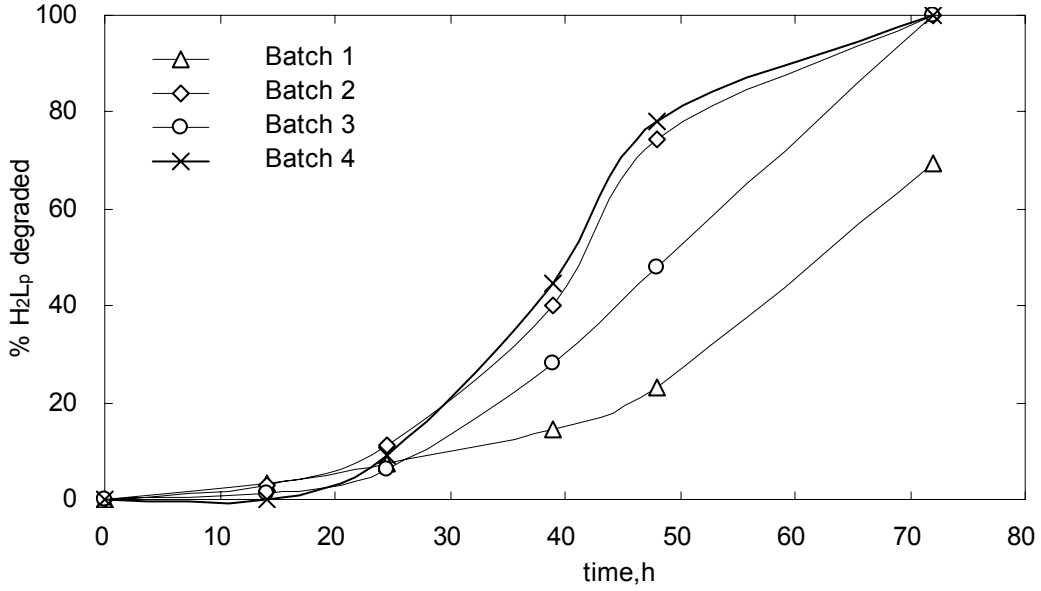

Figure 7.15 Phthalic acid degradation in Cd^{2+}-*Comamonas spp.*-ferrihydrite systems. I = 0.01 M $NaNO_3$, $H_2L_{p(T)}$ = 0.6mM, *Comamonas spp.* = 0.055 gL^{-1}, ferrihydrite = 0.1 gL^{-1}

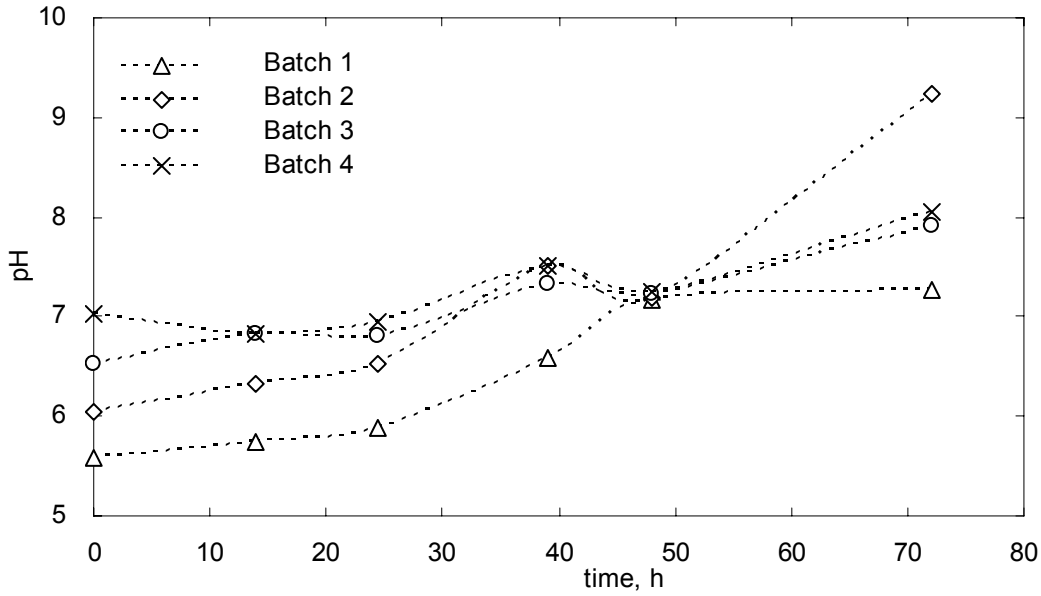

Figure 7.16 pH change during H_2L_p degradation in Cd^{2+}-*Comamonas spp.*-ferrihydrite systems. I = 0.01 M $NaNO_3$, *Comamonas spp.* = 0.01 gL^{-1} (dry weight), ferrihydrite = 0.1 gL^{-1}, $H_2L_{p(T)}$ = 0.6 mM at time = 0.

Cadmium adsorption during H_2L_p degradation is shown in Figure 7.17 with modelling results for 0.6 and 0 mM H_2L_p representing the two extremes of no H_2L_p degradation and complete H_2L_p degradation. With H_2L_p degradation cadmium adsorption is expected to shift from near the solid line for 0.6 mM H_2L_p towards the dash-dotted line for 0 mM H_2L_p. The observed Cd^{2+} adsorption during H_2L_p degradation was generally between these two lines, and in all batches the measured Cd^{2+} adsorption moved in the expected direction i.e. from the 0.6mM H_2L_p to the 0 mM H_2L_p model lines. One unfortunate consequence of the fact that the pH increased during H_2L_p metabolism was that in all experiments when H_2L_p was entirely metabolized the pH was so high that there was little difference in the modelled Cd^{2+} adsorption with and without H_2L_p.

While the general trend in Cd^{2+} sorption edge shift was predicted most data points were between 5 and 15 % lower than the predicted values. There are several possible reasons for this. Cadmium sorption may need longer equilibration time. The pH and Cd^{2+} adsorption were measured in a dynamic system during H_2L_p degradation. Under these conditions, the systems is not tending towards an equilibrium, rather the pH and H_2L_p concentrations are in a state of flux until all H_2L_p is metabolized. It is also possible that metal biosorption by *Comamonas spp.* during biodegradation might be different from that with starving or inactive cells. To our knowledge whether metal adsorption onto growing bacteria cells during biodegradation is different from that of starving or inactive cells is unknown. Another possible reason for Cd^{2+} sorption being lower than expected is that systems with biodegradation occurring are chemically more complex than those without bacterial metabolism. Under aerobic conditions various organic ligands are produced as intermediates during H_2L_p degradation (Eaton 2001). Phthalic acid metabolism generally goes via dihydroxyl phthalate, to protocatechuate, then to acetate or pyruvate. These organic ligands would (if present) influence Cd^{2+} speciation and distribution. However apart from H_2L_p there were no other organic ligands with carboxylic functional groups detected by either HPLC or GC-MS in this work during H_2L_p metabolism. A full assessment of the effects of H_2L_p metabolism on Cd^{2+} adsorption would require further study.

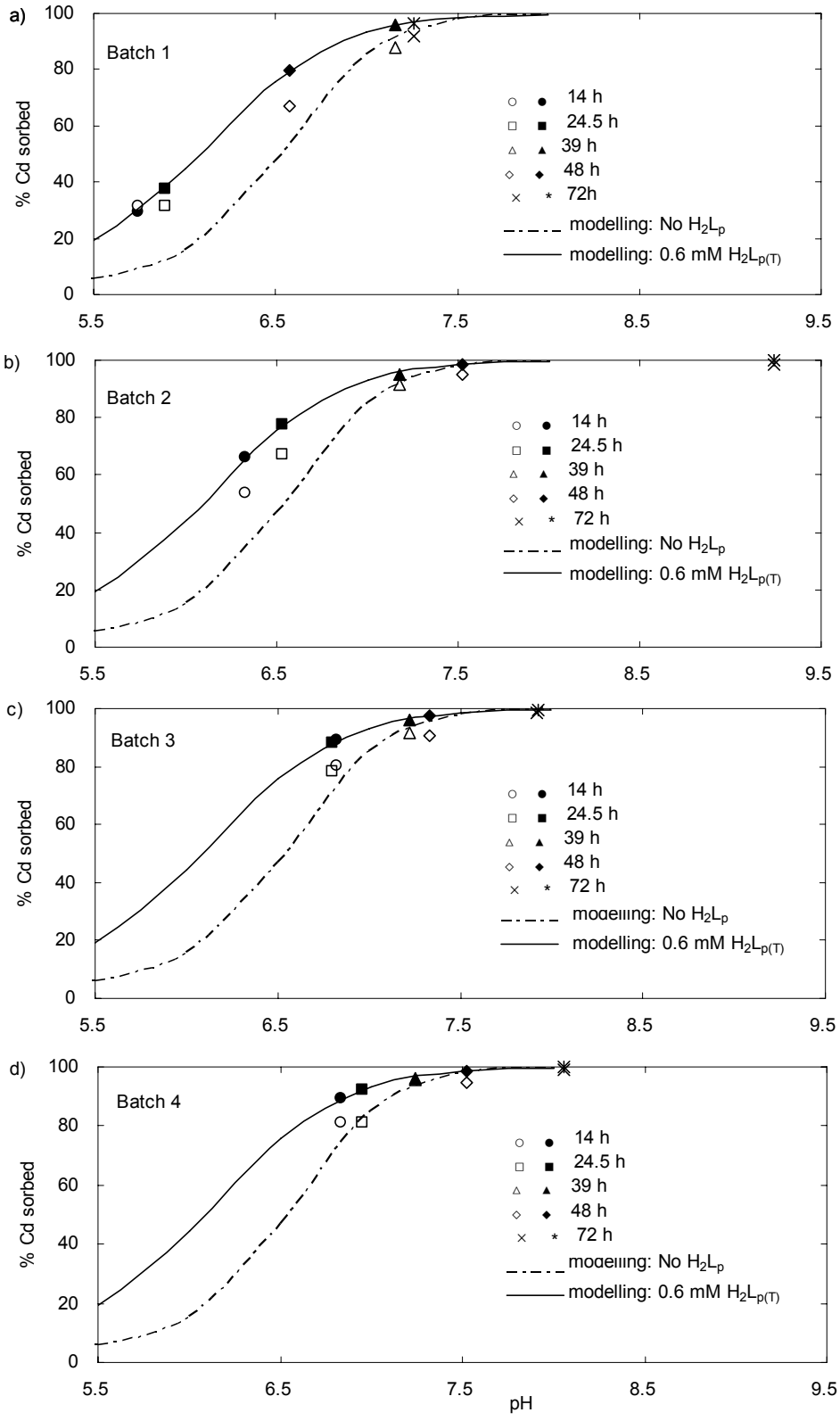

Figure 7.17 Cadmium sorption during H_2L_p degradation in *Comamonas spp.*-ferrihydrite system. a, b, c and d represent results for Batch 1 to 4, respectively. I = 0.01 M $NaNO_3$, *Comamonas spp.* = 0.055 gL^{-1}, $H_2L_{p(T)}$= 0.6 mM, ferrihydrite = 0.1 gL^{-1} at time = 0. Symbols ○, □, ▵, ◇ and × are experimental data corresponding to corresponded modelling result ●, ■, ▲, ◆ and *. Dash-dotted and solid line are modelling results for Cd^{2+} adsorption in the absence of presence of H_2L_p in dead *Comamonas spp.*-ferrihydrite systems, respectively.

The results shown in Figure7.17 indicate that metal distribution in a complex system containing biodegradable organic ligands, active bacteria and mineral oxides is difficult to describe precisely with geochemical modelling. However the general trends and approximate metal adsorption can be predicted by comparing similar systems containing inactive bacteria, with/without the presence of organic ligands. Biodegradation products should also be taken into account as they may be effective ligands that can form strong solution complexes with metal ions.

The pH is another important factor affecting metal speciation that should be considered. Most bacteria existing in natural aquatic environments and wastewater treatment plants prefer a circum-neutral pH where metal adsorption onto mineral particles-bacteria composite can generally reach a very high level unless there are strong organic ligands that might diminish metal adsorption by forming metal-ligand solution complexes.

7.5. Conclusions

Cadmium adsorption was examined in ternary and quaternary systems containing both ferrihydrite and bacteria. The effect of H_2L_p and H_2L_p metabolism was examined. Cadmium adsorption onto ferrihydrite-*Comamonas spp.* composites is less than additive but can be successfully described with surface complexation modelling by assuming two surface reactions describing the interactions between bacteria and ferrihydrite so that Cd^{2+} species and distribution in these systems can be modelled. Cadmium adsorption in *Comamonas spp.*-ferrihydrite systems did not show noticeable differences between dead or live *Comamonas spp.* though in the absence of ferrihydrite live *Comamonas spp.* were found to absorb slightly less Cd^{2+} than dead bacteria at pH > 6.

Cadmium adsorption in quaternary systems in the presence of H_2L_p was initially investigated using dead *Comamonas spp.* and therefore with no H_2L_p metabolism. The effect of H_2L_p on Cd^{2+} adsorption in these "static" quaternary systems could be modelled using the surface and solution parameters that had been derived from various binary and ternary systems described in earlier sections.

The effects of H_2L_p degradation on Cd^{2+} species and distribution were determined in a dynamic system containing live bacteria, cadmium, phthalic acid, ferrihydrite and trace nutrients. Results showed that the trends in Cd^{2+} adsorption in these dynamic systems could be predicted using the model parameters from systems containing inactive bacteria. It is

difficult to precisely quantify Cd^{2+} adsorption in the dynamic process due to the uncertainty of organic ligand biodegradation products, as well as the bacteria population. Neutral pH is not only the preferable pH for many bacteria, but also results in larger metal ion adsorption onto both bacteria and mineral oxides surface.

Chapter 8. Applications, Conclusions and Future Work

8.1. Applications

Over the last several decades the knowledge of metal partitioning in both aquatic and soil systems has been improved by studies on metal adsorption onto mineral oxides and bacteria and the effects of organic ligands on metal adsorption has been considered in some studies. However no detailed experimental investigation has been reported on a system containing a metal ion, organic ligand, iron oxide and bacteria. Therefore, models developed in binary or ternary systems may not accurately predict metal distribution in realistic aquatic environments. The application of surface complexation modelling to describe interactions in systems containing bacteria is only in its infancy (Fein 2000).

This thesis examined systems from simple to more realistic systems containing metal ion, iron oxide, organic ligand and bacteria. Metal distribution could be accurately described by modelling based on the understanding of the complex interactions occurring in these systems. The findings from this work contribute to the understanding of the prevailing controls on metal behaviour in different fields, particularly, surface chemistry, environmental microbiology and geochemistry. The ability of the model parameters to predict Cd^{2+} distribution in the quaternary system demonstrates that the model can provide insight into the processes that determine soluble and particulate metal species in complex biogeochemical environments. Iron oxides, bacteria, organic ligands and metal ions are ubiquitous in natural environments and many engineered systems. Either bacteria or iron oxide can dominate metal adsorption (depending on the conditions) and the effect of organic ligands depends not only on the ligand but also on which phase dominates metal adsorption. The study on metal transport in soil and sediment, the management of water treatment systems, especially those using iron oxides and bacteria-bearing activated sludge, can benefit from elucidating the interactions occurring between the components.

It is not feasible for one thesis to examine all types of metal ions, mineral particles, bacteria and organic ligands. Therefore a system with Cd^{2+}, ferrihydrite, *Comamonas spp.* and phthalic acid was used as a model for metal ions, minerals, bacteria and organic matter, respectively. Ferrihydrite is ubiquitous in the natural environment and has been used as a proxy component representing suspended particulate matter when modelling aquatic

environments (Bibby and Webster-Brown 2006). Ferrihydrite is widely used in water treatment plants. *Comamonas* species are common bacteria in soil and water systems including water treatment plants. *Comamonas* strains can degrade a number of aromatic compounds, including phthalic acid, phthalate esters, dye, phenolic and benzoates compounds (Cui et al. 2004; Goodall and Peretti 1998; Jadhav et al. 2008; Song et al. 2005; Wang et al. 2003; Wang et al. 2004; Wu et al. 2005; Zámocký et al. 2001). Metal adsorption onto many bacteria species can be reasonably well modelled using one set of averaged parameters for site densities and adsorption reaction constants (Borrok et al. 2004; Yee and Fein 2001). Moreover, the effect of small organic ligand on cation adsorption by iron oxides can be qualitatively similar to that of natural organic ligands such as humic acids (Ali and Dzombak 1996b; Ali and Dzombak 1996c). For these reasons the result from this work can contribute to the understanding of metal speciation and sorption behaviour in realistic environments.

8.1.1 Engineered systems

Using iron oxides or iron oxide coated sand to absorb dissolved trace metals is a water treatment technology, which has been reported to be efficient at removing dissolved metals in the treatment of stormwater runoff, drinking water, wastewater and groundwater (Dyer et al. 2004; Genç-Fuhrman et al. 2007; Martin and Kempton 2000; Møller et al. 2002; Thirunavukkarasu et al. 2003). This technology also has a high efficiency (> 90 %) for removing microorganisms such as *Escherichia coli*, *Vibrio cholerae* and poliovirus from tap water and untreated wastewater (Lukasik et al. 1999). In addition, iron oxide has been used to remove non-biodegradable organic matters from secondary effluent (Choo and Kang 2003). Metal biosorption and bioremediation, using safe biomaterial such as non-pathogenic bacteria is regarded as a fast and cost-effective biotechnology especially for the treatment of high volume complex wastewater with low concentrations (1~100 mgL^{-1}) of toxic metals (Chien et al. 2007; Valls and Lorenzo 2002; Wang and Chen 2006). However immobilization of biosorption material is a barrier to its commercial application in wastewater treatment.

While iron oxides have been used to remove trace metals, organic matter and harmful bacteria from polluted water, little is known about the complex interactions that can occur in this process. For example when the aim of using an iron oxide is to remove toxic metals, the simultaneous removal of organic matter and bacteria, and the effect of this on metal adsorption were not considered in depth (Dyer et al. 2004; Møller et al. 2002). Similarly when activated sludge bearing a large quantity of bacteria was used to degrade organic

pollutants in wastwater treatment plants, little attention was paid to metal adsorption though it can efficiently accumulate metal ions (Fristoe and Nelson 1983; Nelson et al. 1981). Another example is bacterial material used as a cost-effective way to remove toxic metals from wastewater, the difficulty in immobilizing the bacteria cells has slowed down its application. Recently a technology has attempted to remove organic arsenic from wastewater by using an iron oxide-coated *Aspergillus niger* biomass (IOCB) (Pokhrel and Viraraghavan 2008).

This study has therefore provided information for water treatment systems, in particular, those containing iron oxide and/or bacteria. For an engineered system mainly using bacteria to degrade organic compounds there are several aspects that could be considered in addition to organic compounds degradation, into which this thesis has provided insight:

1) Trace metal adsorption onto bacteria and the effect of organic ligands on this process
2) The effect of iron oxides on trace metal adsorption in these systems
3) Changes of pH during biodegradation and the effect on the sorption and degradation processes
4) Possible effects of biodegradation intermediates on trace metal distribution
5) Organic compound adsorption onto bacteria

For systems using iron oxides to remove pollutants this thesis has also provided insight into some of the complex process occurring. These include:

1) Effect of organic ligands on metal adsorption
2) The effect of bacteria-iron oxide interactions on trace metal adsorption
3) Interactions that occur where organic ligands and bacteria are present and their effect on trace metal adsorption by an iron oxide

8.1.2 Natural environments

The geochemistry, bioavailability and toxicity of trace metals in natural environments are governed by its speciation which is influenced by a large number of interactions that occur between soluble and particulate phases. As particulate phases iron oxides may be significant minerals in lakes, streams, soil and sediments, and can be present as mixtures of ferrihydrite and goethite or lepidocrocite (Cornell and Schwertmann 2003). Bacteria may form

microcolonies or biofilms with diverse bacterial populations and different bacterial species (Shaw et al. 2008). Aqueous inorganic and organic ligands may form various complexes with metal ions and may also compete for surface sites with the target metal ion. It is therefore extremely difficult to develop a universal model capable of accurately predicting metal speciation and distribution due to the wide variations present in natural environments (Ružić 1996). Modelling the speciation of metals in the presence of both bacteria and mineral oxides under realistic conditions is still in its early stages. Yee and Fein (2003) applied surface complexation modelling to predict Cd^{2+} sorption behaviour in a system containing both ferrihydrite and bacteria without having to determine the concentration of each individual type of bacteria present but there was no experimental data available and the interactions between ferrihydrite and bacteria were not considered in their work. Based on this experimental examination of increasingly complex systems, the understanding of cadmium speciation and distribution determined by the interactions between soluble organic ligand, mineral oxide and bacteria was improved.

Complex interactions between metal, organic matter and bacteria can occur in environments impacted by mine acidic drainage e.g. Tui Mine at Mount Te Ahora, New Zealand. Mine acidic drainage is the deterioration of groundwater and/or local waterways caused by the discharge of high concentrations metal ions. It normally exhibits pH values below 7. Mine acidic drainage is considered an environmental problem facing the mining industry (Filion et al. 1990). The findings of this study can be utilised to gain an understanding of the effectiveness of iron oxides precipitates which form from acid mine discharges and their ability to immobilise metals in the presence of natural organic matter and bacteria under a variety of pH conditions.

Another potential application of this work is to determine the bioavailability of metal ions in bio-solids. Bio-solids often contain elevated concentrations of metal ions and have high bacterial and organic matter content. Bio-solids have been applied to land as a fertiliser due to their high nutrient content. Understanding the bioavailability of the metals ions within the bio-solids is necessary to determine appropriate land application rates.

The findings of this thesis can contribute to the understanding the geochemistry of trace metal soil and sediment under varying pH conditions. For example cadmium enrichment related to phosphoric fertilizer use is of concern in pastoral soils, because Cd^{2+} accumulates in the food chain. Concentrations of Cd^{2+} in grains and grazing animals in New Zealand have been

occasionally found to exceed the maximum permissible concentration (MPC) set by New Zealand Food Authorities. As described before this work used ferrihydrite to represent mineral oxides which are important component of the soil, phthalic acid to present carboxylic organic acid ligands which can enter the environment as a result of both natural and anthropogenbic activities, *Comamonas spp.* to present bacteria which are not only common in the environment but are able to metabolize some organic ligands. Some conclusions from this work can be applied to the understanding or modelling the fate and transport of cadmium. For example organic ligand can either increase or inhibit the mobility of cadmium depending on the conditions including the properties of the ligand, the pH and bacterial degradation. Therefore it can be concluded that the usage of pesticides might influence metal distribution particularly those who can form complex with metal ions. Bacteria in soil can affect metal mobility directly or indirectly: they can accumulate metal ions, they can also metabolise organic ligands or produce new organic ligands through biodegrading organic compounds and therefore influence metal chemistry indirectly.

8.2. Conclusions and future work

This thesis investigated trace metal speciation and distribution in various systems. Copper, cadmium and H_2L_p adsorption by ferrihydrite was examined for binary and ternary systems. In binary systems all adsorption was well reproduced using the DLM and H_2L_p adsorption was analogous to that of inorganic diprotic acids in terms of the relationship between the adsorption constants and acidity constants. In ternary systems H_2L_p caused both the enhancement (due to ternary complex formation) and inhibition (due to solution complex formation) of Cu^{2+} and Cd^{2+} sorption depending on the conditions. The relationship between binary metal adsorption constants and the ternary complex adsorption constants from this and previous studies suggest several properties of ternary complexes. Ternary complex structures on ferrihydrite and goethite are proposed to be either the same or similar. Cations having large adsorption constants also have large equilibrium constants for ternary complex formation. Ligands forming stronger solution complexes with cations will also form stronger surface ternary complexes, and ligands forming stronger surface ternary complexes will not necessarily strongly enhance cation adsorption.

Conditions for studying systems containing bacteria in this work were developed under which H_2L_p can be efficiently degraded, and the effect of organic ligand degradation on Cd^{2+} adsorption onto ferrihydrite can be examined. A non-electrostatic four site model was used to

derive proton adsorption constants and bacterial site densities from titration data, based on which constants for cadmium adsorption onto *Comamonas spp.* were optimized. Cadmium adsorption onto *Comamonas spp.* over a wide sorbate/sorbent ratio and pH can be reasonably modelled. The acid-base and Cd^{2+} adsorption behaviour of *Comamonas spp.* in this work were both within the range of previous results, indicating that the surface properties of *Comamonas spp.* are similar to some bacterial strains. Phthalic acid adsorption onto *Comamonas spp.* was negligible over a pH range of 3 to 8, and became significant only at pH < 3 where H_2L_p was fully protonated. The presence of H_2L_p decreased Cd^{2+} adsorption onto *Comamonas spp.* and this decrease was well reproduced with the inclusion of H_2L_p solution species. The inhibited Cd^{2+} adsorption in the presence of H_2L_p was due to the competition for Cd^{2+} between the bacterial cell surface and the solution complex formed by H_2L_p and Cd^{2+}.

Consistent with previous studies, cadmium adsorption onto ferrihydrite-*Comamonas spp.* composite is not an additive result due to the interactions between ferrihydrite and bacteria. Leaving this interaction out, combining DLM and NFSM slightly overestimated Cd^{2+} adsorption. Cadmium adsorption behaviour in the presence of ferrihydrite and *Comamonas spp.* can be predicted by assuming two surface reactions describing the interaction between ferrihydrite and bacteria with all related surface and solution reactions, adsorption constants and surface site densities. The effect of H_2L_p on Cd^{2+} adsorption in these "static" quaternary systems could be modelled using the surface and solution parameters that had been derived from various binary and ternary systems.

Cadmium adsorption in quaternary systems in the presence of H_2L_p degradation was determined in a dynamic system containing live bacteria, cadmium, phthalic acid, ferrihydrite and trace nutrients. Results showed that the trends in Cd^{2+} adsorption in these dynamic systems could be predicted using the model parameters from systems containing inactive bacteria. It is difficult to precisely quantify Cd^{2+} adsorption in the dynamic process due to the uncertainty of organic ligand biodegradation products, the pH change, and the bacteria population. Even though the presence of organic ligand may increase metal adsorption onto iron oxides by forming ternary complex, the bacterial degradation of organic ligand may not necessarily cause metal release into solution. However, this does not deny that the adsorbed metal ion might be released into the solution because biodegradation intermediates may be strong organic ligands that could form aqueous complexes with metal ions.

By experimentally examining and modelling metal speciation and distribution in various systems with incrementally increasing complexity, this thesis was therefore able to provide a better understanding of metal fate and transport in complex and heterogenic realistic environments. By combining models that can describe metal adsorption onto inorganic mineral oxides and metal adsorption onto bacterial surface, this thesis has not only put a bridge to quantitatively describe metal adsorption behaviour in systems containing both mineral particulates and bacteria, but also expanded the application of the modelling to assess organic ligands effects on metal sorption behaviour in complex environments.

There is however plenty of scope for work to be done in the future to improve the understanding of metal speciation in natural aquatic environments. Using *in situ* spectroscopic techniques considerable progress has been made to probe sorption mechanisms at iron oxide and bacterial surfaces. This work proposed ternary complexes formed between Cd^{2+} and H_2L_p and ferrihydrite could be expected to have the same structure (or at least similar) as those formed on goethite. As no spectroscopic data are available for ferrihydrite-Cd-L_p ternary surface complexes, future work will be needed to gain a clearer picture of this ternary structure. *In situ* specstroscopic techniques would also be necessary to provide an insight into the understanding of the interactions in quaternary systems containing metal ions, ligands, iron oxides and bacteria. The spectroscopic data, if available and capable of being incorporated to modelling, might enhance the ability of geochemical models to describe and predict metal distribution. In our dynamic systems with H_2L_p degradation occurring, metal adsorption was not precisely described by the modelling due to several possible reasons. For example the lack of a full understanding of the pathway of H_2L_p biodegradation by *Comamonas spp.* and difficulty in quantifying bacterial populations. Other analytical methods such as HPLC-MS and HPLC-FTIR would help to examine biodegradation intermediates, and voltammetry analysis might be useful to explore metal solution complexes formed during organic ligand metabolism. Methodology to quantify bacterial population in dynamic systems, once developed, will be essential to improve the ability and accuracy of surface complex modelling to describe metal distribution in dynamic systems.

References

Aftring RP, Chalker BE, Taylor BF. 1981. Degradation of phthalic acids by denitrifying, mixed cultures of bacteria. Applied and Environmental Microbiology 41(5):1177-1183.

Aftring RP, Taylor BF. 1981. Aerobic and anaerobic catabolism of phthalic acid by a nitrate-respiring bacterium. Archives of Microbiology 130(2):101-104.

Ali MA, Dzombak DA. 1996a. Competitive sorption of simple organic acids and sulfate on goethite. Environmental Science & Technology 30(4):1061-1071.

Ali MA, Dzombak DA. 1996b. Effects of simple organic acid on sorption of Cu^{2+} and Ca^{2+} on goethite. Geochimica et cosmochimica acta 60(2):291-304.

Ali MA, Dzombak DA. 1996c. Interactions of copper, organic acids, and sulfate in goethite suspensions. Geochimica et Cosmochimica Acta 60(24):5045-5053.

Altschul SF, Madden TL, Schäffer AA, Zhang J, Zhang Z, Miller W, Lipman DJ. 1997. Gapped BLAST and PSI-BLAST: A new generation of protein database search programs. Nucleic Acids Research 25(7):3389-3402.

Angove MJ, Wells JD, Johnson BB. 1999. Adsorption of cadmium(II) onto goethite and kaolinite in the presence of benzene carboxylic acids. Colloids and Surfaces A: Physicochemical and Engineering Aspects 146:243-251.

Arai Y, Sparks DL. 2001. ATR-FTIR spectroscopic investigation on phosphate adsorption mechanisms at the ferrihydrite-water interface. Journal of Colloid and Interface Science 241(2):317-326.

Baca SG, Filippova IG, Gherco OA, Gdaniec M, Simonov YA, Gerbeleu NV, Franz P, Basler R, Decurtins S. 2005. Nickel(II)-, cobalt(II)-, copper(II)-, and zinc(II)-phthalate and 1-methylimidazole coordination compounds: Synthesis, crystal structures and magnetic properties. Inorganica Chimica Acta 357(12):3419-3429.

Baca SG, Malinovskii ST, Franz P, Ambrus C, Stoeckli-Evans H, Gerbeleu N, Decurtins S. 2004. Synthesis, structure and magnetic properties of cobalt(II) and copper(II) coordination polymers assembled by phthalate and 4-methylimidazole. Journal of Solid State Chemistry 177(8):2841-2849.

Beveridge TJ. 1978. The response of cell walls of Bacillus subtilis to metals and to electron-microscopic stains. Can J Microbiol 24(2):89-104.

Beveridge TJ. 2001. Use of the Gram stain in microbiology Biotechnic and Histochemistry 76(3):111-118.

Beveridge TJ, Koval SF. 1981. Binding of metals to cell envelopes of *Escherichia coli* K-12. Applied and environmental microbiology 42(1):325-335.

Bibby RL, Webster-Brown JG. 2006. Trace metal adsorption onto urban stream suspended particulate matter (Auckland region, New Zealand). Applied Geochemistry 21(7):1135-1151.

Boily J-F, Sjöberg S, Persson P. 2000. Benzenecarboxylate surface complexation at the goethite (α-FeOOH)/water interface: II. Linking IR spectroscopic observations to mechanistic surface complexation models for phthalate, trimellitate, and pyromellitate. Geochimica et Cosmochimica Acta 64(20):3453-3470.

Boily J-F, Sjöberg S, Persson P. 2005. Structures and stabilities of Cd(II) and Cd(II)-phthalate complexes at the goethite-water interface. Geochim. Cosmochim. Acta 69(13):3219-3235.

Borrok D, Aumend K, Fein JB. 2007. Significance of ternary bacteria–metal–natural organic matter complexes determined through experimentation and chemical equilibrium modeling Chemical Geology 238(1-2):44-62.

Borrok D, Fein JB. 2004. Distribution of protons and Cd between bacterial surfaces and dissolved humic substances determined through chemical equilibrium modeling. Geochimica et Cosmochimica Acta 68(14):3043-3052.

Borrok D, Fein JB, Kulpa CF. 2004. Proton and Cd adsorption onto natural bacterial consortia: Testing universal adsorption behavior. Geochimica et Cosmochimica Acta 68(15):3231–3238.

Borrok DM, Fein JB. 2005. The impact of ionic strength on the adsorption of protons, Pb, Cd, and Sr onto the surfaces of Gram negative bacteria: testing non-electrostatic, diffuse, and triple-layer models Journal of Colloid and Interface Science 286(1):110-126.

Boyanov MI, Kelly SD, Kemner KM, Bunker BA, Fein JB, Fowle DA. 2003. Adsorption of cadmium to *Bacillus subtilis* bacterial cell walls: a pH-dependent X-ray absorption fine structure spectroscopy study Geochimica et Cosmochimica Acta 67(18):3299-3311.

Buerge-Weirich D, Behra P, Sigg L. 2003. Adsorption of copper, nickel, and cadmium on goethite in the presence of organic ligands. Aquatic Geochemistry 9(2):65-85.

Buerge-Weirich D, Hari R, Xue H, Behra P, Sigg L. 2002. Adsorption of Cu, Cd, and Ni on goethite in the presence of natural groundwater ligands. Environmental Science & Technology 36(3):328-336.

Burnett P-GG, Daughney CJ, Peak D. 2006. Cd adsorption onto *Anoxybacillus flavithermus*: Surface complexation modeling and spectroscopic investigations. Geochimica et Cosmochimica Acta 70:5253–5269.

Burnett P-GG, Handley K, Peak D, Daughney CJ. 2007. Divalent metal adsorption by the thermophile *Anoxybacillus flavithermus* in single and multi-metal systems. Chemical Geology 244:493-506.

Bushnell LD, Hass HF. 1940. The utilization of cerain hydrocarbons by microorganisms. Journal of Bacteriology 41:653-673.

Carta D, Casula MF, Corrias A, Falqui A, Navarra G, Pinna G. 2009. Structural and magnetic characterization of synthetic ferrihydrite nanoparticles. Materials Chemistry and Physics 113:349-355.

Cello FD, Pepi M, Baldi F, Fani R. 1997. Molecular characterization of an n-alkane-degrading bacterial community and identification of a new species, Acinetobacter venetianus. Research in Microbiology 148(3):237-249.

Chien C-C, Hung C-W, Han C-T. 2007. Removal of cadmium ions during stationary growth phase by an extremely cadmium-resistant strain of Stenotrophomonas sp. Environmental toxicology and chemistry 26(4):664-668.

Choo K-H, Kang S-K. 2003. Removal of residual organic matter from secondary effluent by iron oxides adsorption. Desalination 154:139-146.

Cornell RM, Schwertmann U. 2003. The Iron Oxides: Structure, Properties, Reactions, Occurrences and Uses. New York Wiley-VCH.

Cui M, Chen F, Fu J, Sheng G, Sun G. 2004. Microbial metabolism of quinoline by *Comamonas sp.* World Journal of Microbiology & Biotechnology 20:539-543.

Daughney CJ, Fein JB. 1998a. The effect of ionic strength on the adsorption of H^+, Cd^{2+}, Pb^{2+}, and Cu^{2+} by *Bacillus subtilis* and *Bacillus licheniformis*: A surface complexation model. Journal of Colloid and Interface Science 198:53-77.

Daughney CJ, Fein JB. 1998b. Sorption of 2,4,6-Trichlorophenol by *Bacillus subtilis*. Environmental Science & Technology 32(6):749-752.

Daughney CJ, Fowle DA, Fortin D. 2000. The effect of growth phase on proton and metal adsorption by *Bacillus subtilis*. Geochimica et Cosmochimica Acta 65(7):1025-1035.

Davis JA, Leckie JO. 1978. Surface ionization and complexation at the oxide/water interface II. Surface properties of amorphous iron oxyhydroxide and adsorption of metal ions. Journal of Colloid and Interface Science 67(1):90-107.

Dyer JA, Sparks DL, Scrivner NC, Trivedi P, Sanders SJ. 2004. Treatment of zinc-contaminated water using a multistage ferrihydrite sorption system. Journal of Colloid and Interface Science 270(1):66-76.

Dzombak DA, Morel FMM. 1990. Surface complexation modeling: hydrous ferric oxide. New York: John Wiley & Sons.

Eaton RW. 2001. Plasmid-Encoded Phthalate Catabolic Pathway in *Arthrobacter keyseri* 12B†. Journal of Bacteriology 183(12):3689-3703.

Eaton RW, Nitterauer JD. 1994. Biotransformation of benzothiophene by isopropylbenzene-degrading bacteria. Journal of Bacteriology 176(13):3992-4002.

Elzinga EJ, Peak D, Sparks DL. 2001. Spectroscopic studies of Pb(II)-sulfate interactions at the goethite-water interface. Geochimica et Cosmochimica Acta 65(14):2219-2230.

Elzinga EJ, Sparks DL. 2007. Phosphate adsorption onto hematite: An in situ ATR-FTIR investigation of the effects of pH and loading level on the mode of phosphate surface complexation. Journal of Colloid and Interface Science 308(1):53-70.

Engelhardt G, Wallnöfer PR, Rast HG, Fiedler F. 1976. Metabolism of o phthalic acid by different gram negative and gram positive soil bacteria. Archives of Microbiology 109(1-2):109-114.

Evanko CR, Dzombak DA. 1999. Surface complexation modeling of organic acid sorption to goethite. Journal of Colloid and Interface Science 214(2):189-206.

Fan Y, Wang Y, Qian P-Y, Gu J-D. 2004. Optimization of phthalic acid batch biodegradation and the use of modified Richards model for modelling degradation. International Biodeterioration & Biodegradation 53(1):57-63.

Fein JB. 2000. Quantifying the effects of bacteria on adsorption reactions in water–rock systems. Chemical Geology 169:265-280.

Fein JB, Boily J-F, Güçlü K, Kaulbach E. 1999. Experimental study of humic acid adsorption onto bacteria and Al-oxide mineral surfaces. Chemical Geology 162(1):33-45.

Fein JB, Boily J-F, Yee N, Gorman-Lewis D, Turner BF. 2005. Potentiometric titrations of Bacillus subtilis cells to low pH and a comparison of modeling approaches. Geochimica et Cosmochimica Acta 69(5):1123-1132.

Fein JB, Daughney CJ, Yee N, Davis TA. 1997. A chemical equilibrium model for metal adsorption onto bacterial surfaces. Geochimica et cosmochimica acta 61(16):3319 - 3328

Fein JB, Delea D. 1999. Experimental study of the effect of EDTA on Cd adsorption by *Bacillus subtilis*: a test of the chemical equilibrium approach. Chemical Geology 161:375-383.

Ferris FG, Hallberg RO, Lyvén B, Pedersen K. 2000. Retention of strontium, cesium, lead and uranium by bacterial iron oxides from a subterranean environment. Applied Geochemistry 15(7):1035-1042.

Ferris FG, Konhauser KO, Lyvén B, Pedersen K. 1999. Accumulation of metals by bacteriogenic iron oxides in a subterranean environment. Geomicrobiology Journal 16(2):181-192.

Ferris FG, Tazaki K, Fyfe WS. 1989. Iron oxides in acid mine drainage environments and their association with bacteria. Chemical Geology 74(3-4):321-330.

Filion MP, Sirois LL, Ferguson K. 1990. Acid mine drainage research in Canada. CIM Bulletin 83(944):33-40.

Filius JD, Hiemstra T, Van Riemsdijk WH. 1997. Adsorption of small weak organic acids on goethite: Modeling of mechanisms. Journal of Colloid and Interface Science 195(2):368-380.

Fowle DA, Fein JB. 2000. Experimental measurements of the reversibility of metal–bacteria adsorption reactions. Chemical Geology 168:27-36.

Fristoe BR, Nelson PO. 1983. Equilibrium chemical modelling of heavy metals in activated sludge Water Research 17(7):771-778.

Gabr RM, Hassan SHA, Shoreit AAM. 2008. Biosorption of lead and nickel by living and non-living cells of *Pseudomonas aeruginosa* ASU 6a International Biodeterioration & Biodegradation 62:195-203.

Geelhoed JS, Hiemstra T, Van Riemsdijk WH. 1998. Competitive interaction between phosphate and citrate on goethite. Environmental Science & Technology 32(14):2119-2123.

Geen Av, Roberson AP, Leckie JO. 1994. Complexation of carbonate species at the goethite surface: Implications for adsorption of metal ions in natural waters. Geochimica et Cosmochimica Acta 58(9):2073-2086.

Genç-Fuhrman H, Mikkelsena PS, Ledin A. 2007. Simultaneous removal of As, Cd, Cr, Cu, Ni and Zn from stormwater: Experimental comparison of 11 different sorbents Water Research 41(3):591-602.

Ginn BR, Fein JB. 2008. The effect of species diversity on metal adsorption onto bacteria. Geochimica et Cosmochimica Acta 72:3939–3948.

Glasauer S, Langley S, Beveridge TJ. 2001. Sorption of Fe (Hydr)Oxides to the Surface of *Shewanella putrefaciens*: Cell-Bound Fine-Grained Minerals Are Not Always Formed De Novo. Applied and Environmental Microbiology 67(12):5544-5550.

Goodall JL, Peretti SW. 1998. Dynamic modeling of *meta*- and *para*-nitrobenzoate metabolism by a mixed co-immobilized culture of *Comamonas spp.* JS46 and JS47. Biotechnology and Bioengineering 59(4):507 -516

Gustafsson JP. 2006. Visual MINTEQ. Version 2.51. Stockholm, Sweden.

Hanks P. 2000. Collins English Dictionary. Harper Collins Publishers.

Hanna K. 2007. Sorption of two aromatic acids onto iron oxides: Experimental study and modeling. Journal of Colloid and Interface Science 309(2):419-428.

Hanzel D, Hanzel D, Bilinski H, Himdan TA, Miljak M, Vancina V. 1990. A study of trinuclear iron (III) *o*-phthalates. Hyperfine Interactions 53:339-344.

Harden VP, Harris JO. 1953. The isoelectric point of bacterial cells. Journal of Bacteriology 65(2):198-202.

Hennig C, Panak PJ, Reich T, Roßberg A, Raff J, Selenska-Pobell S, Matz W, Bucher JJ, Bernhard G, Nitsche H. 2001. EXAFS investigation of uranium(VI) complexes formed at *Bacillus cereus* and *Bacillus sphaericus* surfaces. Radiochim. Acts 89:625-631.

Herbelin A, Westall J. 1999. FITEQL: A computer program for determination of chemical equilibrium constants from experimental data Version 4.0. Oregon.

Hwang YS, Liu J, Lenhart JJ, Hadad CM. 2007. Surface complexes of phthalic acid at the hematite/water interface. Journal of Colloid and Interface Science 307(1):124-134.

Jadhav UU, Dawkar VV, Ghodake GS, Govindwar SP. 2008. Biodegradation of Direct Red 5B, a textile dye by newly isolated *Comamonas sp.* UVS. . Journal of Hazardous Materials 158:507-516.

Jianlong W, Xuan Z, Weizhong W. 2004. Biodegradation of phthalic acid esters(PAEs) in soil bioaugmented with acclimated activated sludge. Process Biochemistry 39(12):1837-1841.

Johnson KJ, Szymanowski JES, Borrok D, Huynh TQ, Fein JB. 2007. Proton and metal adsorption onto bacterial consortia: Stability constants for metal–bacterial surface complexes Chemical Geology 239:13–26.

Kapoor A, Viraraghavan T. 1995. Fungal biosorption — an alternative treatment option for heavy metal bearing wastewaters: a review Bioresource Technology 53:196-206.

Kelly SD, Boyanov MI, Bunker BA, Fein JB, Fowle DA, Yeeb N, Kemnera KM. 2001. XAFS determination of the bacterial cell wall functional groups responsible for complexation of Cd and U as a function of pH. Journal of synchrotron radiation 8(2):946-948.

Kennedy CB, Scott SD, Ferris FG. 2003. Characterizationof bacteriogenic iron oxide deposits from Axial Volcano, Juan de Fuca Ridge, northeast Pacific ocean. Geomicrobiology Journal 20(3):199-214.

Klavins M, Eglite L, Serzane J. 1999. Methods for analysis of aquatic humic substances. Critical Reviews in Analytical Chemistry 29(3):187-193.

Kleerebezem R, Hulshoff Pol LW, Lettinga G. 1999. Anaerobic biodegradability of phthalic acid isomers and related compounds. Biodegradation 10(1):63-73.

Kulczycki E, Fowle DA, Fortin D, Ferris FG. 2005. Sorption of cadmium and lead by bacteria-ferrihydrite composites. Geomicrobiology Journal 22(6):299-310.

Kuo S. 1986. Concurrent sorption of phosphate and zinc, cadmium, or calcium by a hydrous ferric oxide. Soil Science Society of America Journal 50(6):1412-1419.

Kuo S, McNeal BL. 1984. Effects of pH and phosphate on cadmium sorption by a hydrous ferric oxide. Soil Science Society of America Journal 48(5):1040-1044.

Lackovic K, Angove MJ, Wells JD, Johnson BB. 2004. Modeling the adsorption of Cd(II) onto goethite in the presence of citric acid. Journal of Colloid and Interface Science 269:37-45.

Ledin M. 2000. Accumulation of metals by microorganisms-processes and importance for soil systems. Earth-Science Reviews 51:1-31.

Ledin M, Pedersen K, Allard1 B. 1997. Effects of pH and ionic strength on the adsorption of Cs, Sr, Eu, Zn, Cd and Hg by *Pseudomonas putida*. Water, air, and soil pollution 93:367-381.

Li W, Zhang S, Jiang W, Shan X. 2006. Effect of phosphate on the adsorption of Cu and Cd on natural hematite. Chemosphere 63(8):1235-1241.

Lin SH, Kao HC, Cheng CH, Juang RS. 2004. An EXFAS study of the structures of copper and phosphate sorbed onto goethite. Colloids and Surfaces A: Physicochemical and Engineering Aspects 234(1-3):71-75.

Lloyd D, Hayes AJ. 1995. Vigour, vitality and viability of microorganisms. FEMS microbiology letters 133(1):1-7.

Lofferer-Krößbacher M, Klima J, Psenner R. 1998. Determination of bacterial cell dry mass by transmission electron microscopy and densitometric image analysis. Applied and Environmental Microbiology 64(2):688-694.

Lucas Vaz JL, Duc G, Petit-Ramel M, Faure R, Vittori O. 1996. Cd(II) complexes with phthalic acid: Solution study and crystal structure of cadmium(II) phthalate hydrate. Canadian Journal of Chemistry 74(3):359-364.

Lukasik J, Cheng Y-F, Lu F, Ramplin M, Farrah SR. 1999. Removal of microorganisms from water by columns containing sand coated with ferric and aluminum hydroxides. Water Research 33(3):769-777.

Manceau A, Charlet L. 1994. Mechanism of selenate adsorption on goethite and hydrous ferric oxide. Journal of colloid and interface science 168(1):87-93.

Martell AE, Hancock RD. 1996. Metal Complexes in Aqueous Solutions. New York: Plenum Press.

Martin TA, Kempton JH. 2000. In situ stabilization of metal-contaminated groundwater by hydrous ferric oxide: An experimental and modeling investigation. Environmental Science & Technology 34:3229-3234.

Martinez RE, Ferris FG. 2005. Review of the surface chemical heterogeneity of bacteriogenic iron oxides: Proton and cadmium sorption. American Journal of Science 305:854-871.

Martinez RE, Ferris FG, Pedersen K. 2004. Cadmium complexation by bacteriogenic iron oxides from a subterranean environment. Journal of Colloid and Interface Science 275(1):82-89.

Martinez RE, Smith DS, Ferris FG, Pedersen K. 2003. Surface Chemical Heterogeneity of Bacteriogenic Iron Oxides from a Subterranean Environment. Environmental Science and Technology 37(24):5671-5677.

Martinez RE, Smith DS, Kulczycki E, Ferris FG. 2002. Determination of intrinsic bacterial surface acidity constants using a Donnan shell model and a continuous p*K*a distribution method. Journal of Colloid and Interface Science 253:130-139.

Mavrocordatos D, Fortin D. 2002. Quantitative characterization of biotic iron oxides by analytical electron microscopy. Mineralogical Society of America 87(7):940-946.

Michel FM, Ehm L, Antao SM, Lee PL, Chupas PJ, Liu G, Strongin DR, Schoonen MAA, Phillips BL, Parise JB. 2007. The structure of ferrihydrite, a nanocrystalline material. Science 316(5832):1726-1729.

Mishra B, Boyanov MI, Bunker BA, Kelly SD, Kemner KM, Nerenberg R, Read-Daily BL, Fein JB. 2009. An X-ray absorption spectroscopy study of Cd binding onto bacterial consortia. Geochimica et Cosmochimica Acta doi: 10.1016/j.gca.2008.11.032.

Møller J, Ledin A, Mikkelsen PS. 2002. Removal of dissolved heavy metals from pre-settled stormwater runoff by iron-oxide coated sand (IOCS). Global Solutions for Urban Drainage:1-10.

Motomizu S, Wakimoto T, Tôei K. 1983. Spectrophotometric determination of phosphate in river waters with molybdate and malachite green. Analyst 108(1284):361-367.

Mullen MD, Wolf DC, Ferris FG, Beveridge TJ, Flemming CA, Bailey GW. 1989. Bacterial sorption of heavy metals. Applied and Environmental Microbiology 55(12):3143-3149.

Murphy PJ, Posner AM, Quirk JP. 1976. Characterization of partially neutralized ferric nitrate solutions. Journal of Colloid and Interface Science 56(2):270-283.

Mustafaa G, Singha B, Kookanab RS. 2004. Cadmium adsorption and desorption behaviour on goethite at low equilibrium concentrations: effects of pH and index cations Chemosphere 57(10):1325-1333.

Nakazawa T, Hayashi E. 1977. Phthalate metabolism in *pseudomonas testosteroni*: Accumulation of 4,5-dihydroxyphthalate by a mutant strain. Journal of Bacteriology 131(1):42-48.

Nelson PO, Chung AK, Hudson MC. 1981. Factors affecting the fate of heavy metals in the activated sludge process. Journal of the Water Pollution Control Federation 53(8):1323-1333.

Nilsson N, Persson P, Lovgren L, Sjoberg S. 1996. Competitive surface complexation of *o*-phthalate and phosphate on goethite (α-FeOOH) particles. Geochimica et Cosmochimica Acta 60(22):4385-4395.

Ostergren JD, Bargar JR, Gordon E. Brown J, Parks GA. 1999. Combined EXAFS and FTIR investigation of sulfate and carbonate effects on Pb(ll) sorption to goethite (α-FeOOH). Journal of Synchrotron Radiation 6:645-647.

Ostergren JD, Brown GEJ, Parks GA, Persson P. 2000a. Inorganic ligand effects on Pb(II) sorption to goethite (alpha-FeOOH) II Sulfate. J. Colloid Interface Sci. 225:483-493.

Ostergren JD, Gordon E. Brown J, Parks GA, Persson P. 2000b. Inorganic ligand effects on Pb(II) sorption to goethite (α-FeOOH): II. Sulfate. Journal of Colloid and Interface Science 225(2):483-493.

Parikh SJ, Chorover J. 2006. ATR-FTIR Spectroscopy Reveals Bond Formation During Bacterial Adhesion to Iron Oxide. Langmuir 22:8492-8500.

Peacock CL, Sherman DM. 2004. Copper(II) sorption onto goethite, hematite and lepidocrocite: A surface complexation model based on ab initio molecular geometries and EXAFS spectroscopy. Geochimica et Cosmochimica Acta 68(12):2623–2637.

Peak D, Ford RG, Sparks DL. 1999. An in situ ATR-FTIR investigation of sulfate bonding mechanisms on goethite. Journal of Colloid and Interface Science 218(1):289-299.

Persson P, Lövgren L. 1996. Potentiometric and spectroscopic studies of sulfate complexation at the goethite-water interface. Geochimica et Cosmochimica Acta 60(15):2789-2799.

Pichler T, Veizera J. 1999. Precipitation of Fe(III) oxyhydroxide deposits from shallow-water hydrothermal fluids in Tutum Bay, Ambitle Island, Papua New Guinea. Chemical Geology 162(1):15-31.

Pokhrel D, Viraraghavan T. 2008. Organic arsenic removal from an aqueous solution by iron oxide-coated fungal biomass: An analysis of factors influencing adsorption. Chemical Engineering Journal 140:165-172.

Pyman MAF, Posner AM. 1978. The surface areas of amorphous mixed oxides and their relation to potentiometric titration. Journal of Colloid and Interface Science 66(1):85-94.

Quan CS, Liu Q, Tian WJ, Kikuchi J, Fan SD. 2005. Biodegradation of an endocrine-disrupting chemical, di-2-ethylhexyl phthalate, by *Bacillus subtilis* No. 66. Applied Microbiology and Biotechnology 66(6):702-710.

Rancourt DG, Meunier J-F. 2008. Constraints on structural models of ferrihydrite as a nanocrystalline material. American Mineralogist 93:1412-1417.

Ribbons DW, Evans WC. 1960. Oxidative metabolism of phthalic acid by soil pseudomonads. Biochemical Journal 76:310-318.

Ružić I. 1996. Trace metal complexation at heterogeneous binding sites in aquatic systems. Marine Chemistry 53:1-15.

Rybicka EH, Calmano W, Breeger A. 1995. Heavy metals sorption/desorption on competing clay minerals; an experimental study. Applied Clay Science 9(5):369-381.

Salomons W, Förstner U. 1984. Metals in the Hydrocycle. Berlin Heidelberg, Germany: Springer-Verlag

Schwertman U, Cornell RM. 1991. Iron oxide in the laboratory: preparation and characterization. New York.

Seki H, Suzuki A, Mitsueda S-I. 1998. Biosorption of heavy metal Ions on *Rhodobacter sphaeroides* and *Alcaligenes eutrophus* H16. Journal of Colloid and Interface Science 197:185–190.

Shaw AK, Halpern AL, Beeson K, Tran B, Venter JC, Martiny JBH. 2008. It's all relative: ranking the diversity of aquatic bacterial communities. Environmental Microbiology 10(9):2200-2210.

Small TD, Warren LA, Roden EE, Ferris FG. 1999. Sorption of strontium by bacteria, Fe(III) oxide, and bacteria-Fe(III) oxide composites. Environmental Science & Technology 33:4465-4470.

Sokolov I, Smith DS, Henderson GS, Gorby YA, Ferris FG. 2001. Cell surface electrochemical heterogeneity of the Fe(III)-reducing bacteria *Shewanella* putrefaciens. Environmental Science & Technology 2001(35):341-347.

Song Y, Swedlund PJ, Singhal N. 2008. Copper(II) and Cadmium(II) Sorption onto Ferrihydrite in the Presence of Phthalic Acid: Some Properties of the Ternary Complex. Environmental Science & Technology 42(11):4008-4013.

Song Y, Swedlund PJ, Singhal N, Swift S. 2009. Cadmium (II) speciation in complex aquatic systems: A study with ferrihydrite, bacteria and an organic ligand. Environmental Science and Technology. Accepted in July 2009.

Song Z, Edwards SR, Burns RG. 2005. Biodegradation of naphthalene-2-sulfonic acid present in tannery wastewater by bacterial isolates *Arthrobacter* sp. 2AC and *Comamonas* sp. 4BC. Biodegradation 16(3):237 -252

Spadini L, Charlet L, Manceau A, Schindler PW, Ragnarsdottir KV. 2003. Hydrous ferric oxide: Evaluation of Cd-HFO surface complexation models combining CdK EXAFS data, potentiometric titration results, and surface site structures identified from mineralogical knowledge. Journal of Colloid and Interface Science 266(1):1-18.

Sposito G. 1984. The surface chemistry of soils. New York: Clarendon Press Oxford.

Sposito G. 1989. The Chemistry of Soils. New York: Oxford University Press.

Staples CA, Peterson DR, Parkerton TF, Adams WJ. 1997. The environmental fate of phthalate esters: A literature review Chemosphere 35(4):667-749.

Stumm W, James JM. 1996. Aquatic chemistry: chemical equilibria and rates in natural waters. New York Wiley.

Swedlund P. 2004. Modelling of Cu, Zn, Cd and Pb adsorption by iron oxyhydroxides in SO_4-rich systems simulating acid mine drainage [PhD thesis]. Auckland: University of Auckland.

Swedlund PJ, Webster JG. 1999. Adsorption and polymerisation of silicic acid on ferrihydrite, and its effect on arsenic adsorption. Water Research 33(16):3413-3422.

Swedlund PJ, Webster JG. 2001. Cu and Zn ternary surface complex formation with SO4 on ferrihydrite and schwertmannite. Applied Geochemistry 16(5):503-511.

Swedlund PJ, Webster JG, Miskelly GM. 2003. The effect of SO4 on the ferrihydrite adsorption of Co, Pb and Cd: ternary complexes and site heterogeneity. Applied Geochemistry 18(11):1671-1689.

Swedlund PJ, Webster JG, Miskelly GM. 2009. Goethite adsorption of Cu(II), Pb(II), Cd(II), and Zn(II) in the presence of sulfate: Properties of the ternary complex. Geochimica et Cosmochimica Acta 73:1548-1562.

Taylor BF, Ribbons DW. 1983. Bacterial decarboxylation of *o*-phthalic acids. Applied and Environmental Microbiology 46(6):1276-1281.

Tejedor-Tejedor MI, Yost EC, Anderson MA. 1992. Characterization of benzoic and phenolic complexes at the goethite/aqueous solution interface using cylindrical internal reflection Fourier transform infrared spectroscopy. II: Bonding structures. Langmuir 8(2):525-533.

Thirunavukkarasu OS, Viraraghavan T, Subramanian KS. 2003. Arsenic removal from drinking water iusing iron oxide coated sand. Water, Air, and Soil Pollution 142:95-111.

Tipping E. 1981. The adsorption of aquatic humic substances by iron oxides. Geochimica et Cosmochimica Acta 45(2):191-199.

Toner B, Manceau A, Metthew A M, Millet DB, Sposito G. 2005. Zinc sorption by a bacterial biofilm. Environmental Science & Technology 39:8288-8294.

Towe KM, Bradley WF. 1967. Mineralogical constitution of colloidal “hydrous ferric oxides”. Journal of Colloid and Interface Science 24(3):384-392.

Trivedi P, Dyer JA, Sparks DL. 2003. Lead sorption onto ferrihydrite. 1. A macroscopic and spectroscopic assessment Environmental Science & Technology 37(5):908-914.

Valls M, Lorenzo Vd. 2002. Exploiting the genetic and biochemical capacities of bacteria for the remediation of heavy metal pollution. FEMS Microbiology Reviews 26(4):327-338.

Van Nostrand JD, Sowder AG, Bertsch PM, Morris PJ. 2005. Effect of pH on the toxicity of nickel and other divalent metals to *Burkholderia cepacia* PR1301. Environmental toxicology and chemistry 24(11):2742-2750.

Vasconcelos M, Azenha MAO, Cabral JPS. 1997. Comparison of availability of copper(II) complexes with organic ligands to bacterial cells and to chitin. Environmental Toxicology and Chemistry 16(10):2029-2039.

Vazquez GJ, Dodge CJ, Francis AJ. 2008. Interaction of uranium(VI) with phthalic acid. Inorganic Chemistry 47:10739-10743.

Venema P, Hiemstra T, Riemsdijk WHv. 1996. Multisite adsorption of cadmium on goethite. Journal of Colloid and Interface Science 183(2):515-527.

Venema P, Hiemstra T, Van Riemsdijk WH. 1997. Interaction of cadmium with phosphate on goethite. Journal of Colloid and Interface Science 192(1):94-103.

Violante A, Huang PM, Gadd GM. 2008. Biophysico-chemical Processes of Heavy Metals and Metalloids in Soil Environments: A John Wiley & Sons, Inc., Publication.

Violante A, Ricciardella M, Pigna M. 2003. Adsorption of heavy metals on mixed Fe-Al oxides in the absence or presence of organic ligands. Water, Air, and Soil Pollution 145(1-4):289-306.

Walker SG, Flemming CA, Ferris FG, Beveridge TJ, Bailey GW. 1989. Physicochemical interaction of *Escherichia coli* cell envelopes and *Bacillus subtilis* cell walls with two clays and ability of the composite to immobilize heavy metals from solution. Applied and Environmental Microbiology 55(11):2976-2984.

Wang J, Chen C. 2006. Biosorption of heavy metals by *Saccharomyces cerevisiae*: A review. Biotechnology Advances 24:427-451.

Wang J, Liu P, Qian Y. 1996. Biodegradation of phthalic acid esters by acclimated activated sludge. Environment International 22(6):737-741.

Wang J, Liu P, Qian Y. 1997a. Biodegradation of phthalic acid esters by immobilized microbial cells. Environment International 23(6):775-782.

Wang J, Liu P, Shi H, Qian Y. 1997b. Biodegradation of phthalic acid ester in soil by indigenous and introduced microorganisms. Chemosphere 35(8):1747-1754.

Wang K, Xing B. 2004. Mutual effects of cadmium and phosphate on their adsorption and desorption by goethite. Environmental Pollution 127(1):13-20.

Wang Y, Fan Y, Gu J-D. 2003. Aerobic degradation of phthalic acid by *Comamonas acidovoran* Fy-1 and dimethyl phthalate ester by two reconstituted consortia from sewage sludge at high concentrations World Journal of Microbiology & Biotechnology 19(8):811-815.

Wang Y, Yamazoe A, Suzuki S, Liu C-T, Aono T, Oyaizu H. 2004. Isolation and characterization of dibenzofuran-Degrading *Comamonas sp.* strains isolated from white clover roots Current Microbiology 49(4):288-294.

Weng L, Temminghoff EJM, Lofts S, Tipping E, Riemsdijk WHV. 2002. Complexation with dissolved organic matter and solubility control of heavy metals in a sandy soil Environmental Science & Technology 36(2):4804 -4810.

Weng LP, K. KL, Tjisse H, L. MJC, H. VRW. 2005. Interactions of calcium and fulvic acid at the goethite-water interface. Geochimica et Cosmochimica Acta 69(2):325-339.

Wightman PG, Fein JB. 2001. Ternary interactions in a humic acid-Cd-bacteria system. Chemical Geology 180:55-65.

Wu J-F, Sun C-W, Jiang C-Y, Liu Z-P, Liu S-J. 2005. A novel 2-aminophenol 1,6-dioxygenase involved in the degradation of *p*-chloronitrobenzene by *Comamonas* strain CNB-1: purification, properties, genetic cloning and expression in *Escherichia coli*. Archives of Microbiology 193:1-8.

Xu RK, Xiao SC, Zhang H, Jiang J, Ji GL. 2007. Adsorption of phthalic acid and salicylic acid by two variable charge soils as influenced by sulphate and phosphate. European Journal of Soil Science 58:335-342.

Xu Y, Boonfueng T, Axe L, Maeng S, Tyson T. 2006. Surface complexation of Pb(II) on amorphous iron oxide and manganese oxide: Spectroscopic and time studies. Journal of Colloid and Interface Science 299(1):28-40.

Xue H, Sigg L. 1999. Comparison of the complexation of Cu and Cd by humic or fulvic acids and by ligands observed in lake waters. Aquatic Geochemistry 5(4):313-335.

Yee N, Fein J. 2001. Cd adsorption onto bacterial surfaces: A universal adsorption edge? Geochimica et Cosmochimica Acta 65(13):2037-2042.

Yee N, Fein JB. 2003. Quantifying metal adsorption onto bacteria mixtures: A test and application of the surface complexation model. Geomicrobiology Journal 20:43-60.

Young LB, Harvey HH. 1992. The relative importance of manganese and iron oxides and organic matter in the sorption of trace metals by surficial lake sediments. Geochimica et Cosmochimica Acta 56(3):1175-1186.

Zámocký M, Godočíková J, Koller F, Polek B. 2001. Potential application of catalase-peroxidase from Comamonas terrigena N3H in the biodegradation of phenolic compounds. Antonie van Leeuwenhoek 79:109-117.

Zhang GY, Peak D. 2007. Studies of Cd(II)–sulfate interactions at the goethite–water interface by ATR-FTIR spectroscopy. Geochimica et Cosmochimica Acta 71:2158-2169.

References

Appendix

Unless stated, tables in appendix are numbered according to the figures they refer to.

The concentration of bacterial cells is on a basis of wet weight, unless stated.

The ferrihydrite concentration is either expressed by molar concentration of Fe, or on a basis of a stoichiometry $Fe_2O_3 \cdot H_2O$ with a molecular weight of 89 $gmol^{-1}$ (Dzombak and Morel 1990).

Table A3. 1

Expt. Conditions $[Cu_{(T)}] = 16\ \mu M$; $[Fe] = 9.4\ mM$; $I = 0.01\ M\ NaNO_3$		*Expt. Conditions* $[Cu_{(T)}] = 23.6\ \mu M$; $[Fe] = 0.94\ mM$; $I = 0.01\ M\ NaNO_3$	
pH	% Cu sorbed	pH	% Cu sorbed
3.50	0.00	3.59	0.00
4.08	6.80	4.19	2.60
4.38	22.80	4.58	5.90
4.94	81.90	5.05	16.60
5.12	86.80	5.54	51.20
5.57	95.40	5.83	71.00
6.12	99.10	5.85	71.80
6.28	100.00	6.32	94.70
6.68	100.00	6.55	98.00
7.92	100.00	7.04	99.80

Table A3. 2

Expt. Conditions $[Cd_{(T)}] = 0.89\ \mu M$; $[Fe] = 10.24\ mM$; $I = 0.01\ M\ NaNO_3$		*Expt. Conditions* $[Cd_{(T)}] = 9.14\ \mu M$; $[Fe] = 1.02\ mM$; $I = 0.01\ M\ NaNO_3$	
pH	% Cd sorbed	pH	% Cd sorbed
4.09	0.00	4.15	0.20
4.58	3.03	4.80	0.49
5.05	3.45	5.17	0.52
5.51	10.34	5.62	3.06
6.14	49.49	5.99	5.91
6.51	83.10	6.65	18.58
6.79	93.69	6.74	23.36
7.27	98.86	7.23	66.28
7.95	99.56	7.71	84.43

Appendix

Table A3.5a

Expt. Conditions $[H_2L_{p(T)}]$ = 0.6 mM; [Fe] = 9.4 mM; I = 0.01 M $NaNO_3$		*Expt. Conditions* $[H_2L_{p(T)}]$ = 6.0 mM; [Fe] = 9.4 mM; I = 0.01 M $NaNO_3$		*Expt. Conditions* $[H_2L_{p(T)}]$ = 29.1 mM; [Fe] = 9.4 mM; I = 0.01 M $NaNO_3$	
pH	% H_2L_p sorbed	pH	% H_2L_p sorbed	pH	% H_2L_p sorbed
3.53	100.00	3.57	34.74	3.50	7.37
4.34	100.00	4.24	27.69	4.53	6.39
4.88	100.00	4.87	27.18	5.12	6.20
5.30	100.00	5.22	25.61	5.64	4.80
5.77	100.00	5.81	20.60	6.86	0.51
6.12	98.72	6.40	19.50	7.37	2.81
6.54	89.98	6.97	13.92	8.10	1.92
7.08	71.32	7.48	11.94	8.99	1.05
7.61	37.97	8.03	7.48		
8.67	5.13	8.95	1.37		

Table A3.5b

Expt. Conditions $[H_2L_{p(T)}]$ = 0.6 mM; [Fe] = 0.94 mM; I = 0.01 M $NaNO_3$		*Expt. Conditions* $[H_2L_{p(T)}]$ = 6.0 mM; [Fe] = 0.94 mM; I = 0.01 M $NaNO_3$		*Expt. Conditions* $[H_2L_{p(T)}]$ = 29.1 mM; [Fe] = 0.94 mM; I = 0.1 M $NaNO_3$	
pH	% H_2L_p sorbed	pH	% H_2L_p sorbed	pH	% H_2L_p sorbed
3.56	27.30	3.57	3.17	3.50	1.46
4.25	25.38	4.26	4.27	4.72	1.12
4.67	21.40	5.01	0.18	5.29	0.75
5.26	21.40	5.40	2.38	5.86	0.10
5.88	17.78	5.96	0.76	7.02	0.00
6.32	15.80	6.75	0.23	7.54	0.00
7.20	10.66	7.31	1.88	8.39	0.00
7.85	6.58	7.58	1.35		
8.68	4.98	8.30	0.00		

Table A4.1a

Expt. Conditions $[Cu_{(T)}] = 16\ \mu M$; $[H_2L_{p(T)}] = 0.6$ mM; $[Fe] = 9.4$ mM; $I = 0.01$ M $NaNO_3$		*Expt. Conditions* $[Cu_{(T)}] = 16\ \mu M$; $[H_2L_{p(T)}] = 6$ mM; $[Fe] = 9.4$ mM; $I = 0.01$ M $NaNO_3$		*Expt. Conditions* $[Cu_{(T)}] = 13.7\ \mu M$; $[H_2L_{p(T)}] = 28$ mM; $[Fe] = 7$ mM; $I = 0.1$ M $NaNO_3$	
pH	% Cu sorbed	pH	% Cu sorbed	pH	% Cu sorbed
3.66	0.00	3.58	15.30	3.64	0.70
4.48	44.95	4.26	48.10	4.18	11.60
5.02	91.75	4.82	77.40	4.69	39.50
5.40	95.44	5.18	89.50	5.13	69.80
6.02	99.14	5.74	95.60	5.68	89.20
6.66	100.00	6.40	98.00	6.12	98.90
7.18	100.00	6.90	99.30	6.64	100.00
7.72	100.00	7.46	100.00	7.40	100.00
8.17	100.00	7.93	100.00	7.94	100.00
8.79	100.00	8.94	100.00		

Table A4.1b

Expt. Conditions $[Cu_{(T)}] = 23.6\ \mu M$; $[H_2L_{p(T)}] = 0.6$ mM; $[Fe] = 0.94$ mM; $I = 0.01$ M $NaNO_3$		*Expt. Conditions* $[Cu_{(T)}] = 23.6\ \mu M$; $[H_2L_{p(T)}] = 6$ mM; $[Fe] = 0.94$ mM; $I = 0.01$ M $NaNO_3$		*Expt. Conditions* $[Cu_{(T)}] = 20.6\ \mu M$; $[H_2L_{p(T)}] = 28$ mM; $[Fe] = 0.7$ mM; $I = 0.1$ M $NaNO_3$	
pH	% Cu sorbed	pH	% Cu sorbed	pH	% Cu sorbed
3.61	0.00	3.63	0.90	4.55	6.80
4.12	2.60	3.87	1.80	5.11	11.50
4.62	20.70	4.43	13.30	5.57	17.33
5.05	31.40	4.98	20.70	6.01	30.83
5.64	65.20	5.59	36.40	6.50	57.02
6.27	93.20	6.25	71.80	6.89	84.04
7.37	98.20	7.18	98.20	9.00	100.00
7.57	99.00	7.56	99.80		
8.21	99.80	8.21	99.80		
8.58	99.80	8.84	99.80		

Table A4.7a

Expt. Conditions $[Cd_{(T)}] = 0.89\ \mu M$; $[H_2L_{p(T)}] = 0.6$ mM ; [Fe] = 10.24 mM ; I = 0.01 M $NaNO_3$		*Expt. Conditions* $[Cd_{(T)}] = 0.89\ \mu M$; $[H_2L_{p(T)}] = 6$ mM ; [Fe] = 9.69 mM ; I = 0.01 M $NaNO_3$		*Expt. Conditions* $[Cd_{(T)}] = 0.89\ \mu M$; $[H_2L_{p(T)}] = 30$ mM ; [Fe] = 10.13 mM ; I = 0.1 M $NaNO_3$	
pH	% Cd sorbed	pH	% Cd sorbed	pH	% Cd sorbed
4.29	0.00	4.28	9.09	4.14	6.06
4.81	3.03	4.73	21.21	4.61	15.15
5.41	13.79	5.22	48.02	5.12	27.59
5.99	69.78	5.74	72.55	5.58	48.02
6.41	94.34	6.33	93.33	6.12	78.58
6.81	98.27	6.88	98.00	6.71	92.81
7.26	99.29	7.36	99.41	7.24	93.42
7.52	99.53	7.65	100.00		
8.48	99.72	8.34	100.00		

Table A4.7b

Expt. Conditions $[Cd_{(T)}] = 9.14\ \mu M$; $[H_2L_{p(T)}] = 0.6$ mM ; [Fe] = 1.02 mM ; I = 0.01 M $NaNO_3$		*Expt. Conditions* $[Cd_{(T)}] = 9.14\ \mu M$; $[H_2L_{p(T)}] = 6$ mM ; [Fe] = 1.12 mM ; I = 0.01 M $NaNO_3$		*Expt. Conditions* $[Cd_{(T)}] = 9.14\ \mu M$; $[H_2L_{p(T)}] = 30$ mM ; [Fe] = 0.97 mM ; I = 0.1 M $NaNO_3$	
pH	% Cd sorbed	pH	% Cd sorbed	pH	% Cd sorbed
4.12	0.83	4.08	1.79	4.07	1.47
4.67	1.46	4.43	2.10	4.61	1.78
5.12	4.65	5.05	5.92	5.10	3.38
5.67	16.95	5.68	16.32	5.64	5.90
6.44	42.34	6.07	24.28	5.67	6.54
6.82	60.56	6.63	39.87	6.31	21.36
7.24	78.32	7.31	74.97	6.88	42.33
8.25	98.89	7.78	91.15	7.50	62.63
		8.53	98.52	8.38	93.75

Table A5.1a

Expt. Conditions

Bacillus subtilis growing in BHI broth

Time (h)	OD_{600}	Log (CFU)	BHI volume (mL)	Cell dry weight (mg)
0	0.03	8.52	50	13
1	0.07	8.62	100	25
2	0.12	8.76	200	48
3	0.35	9.09		
4	1.18	9.44		
5	1.37	9.91		
6	1.41	10.00		
7	1.42	10.03		

Table A5.2 – Batch 1

Expt. Conditions

$[H_2L_{p(T)}]$ = 6 mM; I = 0.01 M $NaNO_3$

Time (h)	pH	% degraded $H_2L_{p(T)}$
0.0	3.61	0.00
16.0	3.64	22.90
24.5	3.63	12.90
48.5	3.66	15.90
74.0	3.70	13.50
97.0	3.86	16.20
169.0	4.03	15.90
236.0	4.98	17.30

Table A5.2 – Batch 2

Expt. Conditions

$[H_2L_{p(T)}]$ = 6 mM; I = 0.01 M $NaNO_3$

Time (h)	pH	% degraded $H_2L_{p(T)}$
0.0	4.41	0.00
16.0	4.39	8.00
24.5	4.41	10.60
48.5	4.44	12.60
74.0	4.60	11.20
97.0	4.68	11.40
169.0	4.94	31.30
236.0	5.76	14.70

Table A5.2 – Batch 3

Expt. Conditions

$[H_2L_{p(T)}]$ = 6 mM ; I = 0.01 M $NaNO_3$

Time (h)	pH	% degraded $H_2L_{p(T)}$
0.0	5.18	0.00
16.0	5.12	8.10
24.5	5.15	7.70
48.5	5.27	12.00
74.0	5.39	8.30
97.0	5.48	9.90
169.0	5.54	17.60
236.0	6.28	20.90

Table A5.2 – Batch 4

Expt. Conditions

$[H_2L_{p(T)}]$ = 6 mM ; I = 0.01 M $NaNO_3$

Time (h)	pH	% degraded $H_2L_{p(T)}$
0.0	5.91	0.00
16.0	5.83	16.70
24.5	5.89	6.70
48.5	5.99	16.80
74.0	6.27	49.00
97.0	6.48	63.60
169.0	6.66	89.20
236.0	6.83	100.00

Table A5.2 – Batch 5

Expt. Conditions

$[H_2L_{p(T)}]$ = 6 mM ; I = 0.01 M $NaNO_3$

Time (h)	pH	% degraded $H_2L_{p(T)}$
0.0	6.39	0.00
16.0	6.24	9.80
24.5	6.28	8.70
48.5	6.32	54.20
74.0	6.51	70.70
97.0	6.62	88.60
169.0	6.71	100.00
236.0	7.08	100.00

Table A5.2 – Batch 6

Expt. Conditions

$[H_2L_{p(T)}]$ = 6 mM ; I = 0.01 M $NaNO_3$

Time (h)	pH	% degraded $H_2L_{p(T)}$
0.0	6.90	0.00
16.0	6.41	8.60
24.5	6.41	8.40
48.5	6.52	11.00
74.0	6.47	53.70
97.0	6.60	77.30
169.0	6.77	100.00
236.0	6.95	100.00

Table A5.2 – Batch 7

Expt. Conditions

$[H_2L_{p(T)}]$ = 6 mM ; I = 0.01 M $NaNO_3$

Time (h)	pH	% degraded $H_2L_{p(T)}$
0.0	7.61	0.00
16.0	6.51	10.90
24.5	6.45	7.20
48.5	6.53	13.20
74.0	6.46	30.60
97.0	6.51	58.80
169.0	6.70	85.50
236.0	6.88	100.00

Table A5.2 – Batch 8

Expt. Conditions

$[H_2L_{p(T)}]$ = 6 mM ; I = 0.01 M $NaNO_3$

Time (h)	pH	% degraded $H_2L_{p(T)}$
0.0	8.08	0.00
16.0	6.53	8.50
24.5	6.51	10.20
48.5	6.61	15.00
74.0	6.76	18.30
97.0	6.48	53.30
169.0	6.74	84.30
236.0	6.84	100.00

Table A5.3 – Batch 1

Expt. Conditions

$[H_2L_{p(T)}]$ = 6 mM ; $[Cd_{(T)}]$ = 16 µM ;

I = 0.01 M $NaNO_3$

Time (h)	pH	% degraded $H_2L_{p(T)}$
0.0	4.00	0.00
16.0	4.17	11.73
24.5	4.13	9.27
48.5	4.12	14.38
74.0	4.37	13.06
97.0	4.43	12.92
169.0	4.74	12.78
236.0	6.60	100.00

Table A5.3 – Batch 2

Expt. Conditions

$[H_2L_{p(T)}]$ = 6 mM ; $[Cd_{(T)}]$ = 16 µM ;

I = 0.01 M $NaNO_3$

Time (h)	pH	% degraded $H_2L_{p(T)}$
0.0	4.78	0.00
16.0	4.73	31.11
24.5	4.73	10.90
48.5	4.79	12.12
74.0	4.95	9.99
97.0	4.97	11.64
169.0	6.37	70.05
236.0	7.05	100.00

Table A5.3 – Batch 3

Expt. Conditions

$[H_2L_{p(T)}]$ = 6 mM ; $[Cd_{(T)}]$ = 16 µM ;

I = 0.01 M $NaNO_3$

Time (h)	pH	% degraded $H_2L_{p(T)}$
0.0	5.05	0.00
16.0	5.07	20.04
24.5	5.07	11.89
48.5	5.19	18.30
74.0	5.33	11.13
97.0	5.36	11.31
169.0	6.42	51.20
236.0	7.05	100.00

Table A5.3 – Batch 4

Expt. Conditions

$[H_2L_{p(T)}]$ = 6 mM ; $[Cd_{(T)}]$ = 16 µM ;

I = 0.01 M $NaNO_3$

Time (h)	pH	% degraded $H_2L_{p(T)}$
0.0	5.68	0.00
16.0	5.65	25.42
24.5	5.69	11.86
48.5	5.79	10.98
74.0	5.90	10.89
97.0	6.03	8.59
169.0	6.59	54.70
236.0	7.11	100.00

Table A5.3 – Batch 5

Expt. Conditions

$[H_2L_{p(T)}]$ = 6 mM ; $[Cd_{(T)}]$ = 16 µM ;

I = 0.01 M $NaNO_3$

Time (h)	pH	% degraded $H_2L_{p(T)}$
0.0	6.24	0.00
16.0	6.18	7.60
24.5	6.25	11.59
48.5	6.37	12.03
74.0	6.54	11.91
97.0	6.76	10.96
169.0	6.71	59.55
236.0	7.14	100.00

Table A5.3 – Batch 6

Expt. Conditions

$[H_2L_{p(T)}]$ = 6 mM ; $[Cd_{(T)}]$ = 16 µM ;

I = 0.01 M $NaNO_3$

Time (h)	pH	% degraded $H_2L_{p(T)}$
0.0	7.08	0.00
16.0	6.46	16.21
24.5	6.45	12.55
48.5	6.49	13.20
74.0	6.66	12.69
97.0	6.89	14.52
169.0	6.63	57.78
236.0	7.15	100.00

Table A5.3 – Batch 7

Expt. Conditions

$[H_2L_{p(T)}]$ = 6 mM; $[Cd_{(T)}]$ = 16 µM;

I = 0.01 M $NaNO_3$

Time (h)	pH	% degraded $H_2L_{p(T)}$
0.0	7.59	0.00
16.0	6.63	13.59
24.5	6.49	11.77
48.5	6.50	15.81
74.0	6.68	13.42
97.0	6.83	13.25
169.0	6.68	42.24
236.0	7.09	100.00

Table A5.3 – Batch 8

Expt. Conditions

$[H_2L_{p(T)}]$ = 6 mM; $[Cd_{(T)}]$ = 16 µM;

I = 0.01 M $NaNO_3$

Time (h)	pH	% degraded $H_2L_{p(T)}$
0.0	8.57	0.00
16.0	7.23	13.89
24.5	6.83	12.72
48.5	6.45	17.56
74.0	6.65	11.95
97.0	6.83	12.24
169.0	6.68	53.40
236.0	7.09	100.00

Table A 5.6

Expt. Conditions $[H_2L_{p(T)}]$ = 6 mM; *I = 0.01 M* $NaNO_3$			*Expt. Conditions* $[H_2L_{p(T)}]$ = 6 mM; *Ferrihydrite = 0.1gL*$^{-1}$; *I = 0.01 M* $NaNO_3$			*Expt. Conditions* $[H_2L_{p(T)}]$ = 6 mM; *BHB; Initial pH = 6.3*		*Expt. Conditions* $[H_2L_{p(T)}]$ = 6 mM; *Ferrihydrite = 0.1 gL*$^{-1}$; *BHB; Initial pH = 6.3*	
Time (h)	pH	% degraded $H_2L_{p(T)}$	Time (h)	pH	% degraded $H_2L_{p(T)}$	Time (h)	% degraded $H_2L_{p(T)}$	Time (h)	% degraded $H_2L_{p(T)}$
0.0	5.91	0.00	0.0	6.10	0.00	0	0.00	0	4.31
16.0	5.83	16.69	24.5	6.94	0.00	24	1.96	24	0.64
24.5	5.89	17.17	48.5	6.88	0.41	48	5.72	48	1.83
48.5	5.99	18.30	74.0	6.97	0.33	88	19.85	88	7.29
74.0	6.27	49.02	97.0	7.05	0.66	124	79.80	124	11.46
97.0	6.48	63.64	236.0	7.10	0.84	160	99.80	160	17.85
169.0	6.66	89.15				280	100.00	280	41.59

Table A 5.7

Expt. Conditions: $[H_2L_{p(T)}]$ = 6 mM; Neutral pH; BHB							
Time (h)	C1 OD_{600}	C2 OD_{600}	C3 OD_{600}	(C1+C2) OD_{600}	(C1+C3) OD_{600}	(C2+C3) OD_{600}	(C1+C2+C3) OD_{600}
0	0.004	0.009	0.009	0.016	0.013	0.017	0.021
19	0.683	0.006	0.006	0.654	0.591	0.014	0.637
32	0.702	0.011	0.010	0.700	0.697	0.017	0.686
56	0.675	0.021	0.015	0.661	0.651	0.025	0.684
78	0.631	0.019	0.015	0.639	0.622	0.020	0.656
104	0.622	0.018	0.016	0.625	0.594	0.025	0.639
145	0.570	0.021	0.016	0.560	0.549	0.024	0.586

Table A 5.8

Expt. Conditions : Comamonas spp. growing in TSBYE broth

Time (h)	OD_{600}	Log (CFU)		TSBYE Volume (mL)	Cell dry weight (mg)
0	0.05	8.63		20	5
1	0.09	8.77		50	11
2	0.16	8.79		100	24
3	0.27	8.90		200	50
4	0.51	9.09			
5	0.79	9.28			
6	0.98	9.50			
7	1.08	9.70			
8	1.13	9.86			
24	1.46				

Table A5.5

Expt. Conditions:$[H_2L_{p(T)}]$ *= 6 mM;*

$[Cd_{(T)}]$ *= 16 µM; T = 97 h; I = 0.01 M* $NaNO_3$

pH	% sorbed $H_2L_{p(T)}$
4.38	21.69
5.11	20.77
5.67	21.22
6.76	13.88
7.05	13.38
7.36	10.04
7.63	6.35
7.80	3.84

Table A 5.9 a

Expt. Conditions : $H_2L_{p(T)}]$ *= 0.6 mM; I = 0.01 M* $NaNO_3$*; Solution Y; neutral initial pH*

Time (h)	OD_{600}							
	0.2 mM $[PO_4^{-3}]$	*0.3 mM* $[PO_4^{-3}]$	*0.4 mM* $[PO_4^{-3}]$	*0.5 mM* $[PO_4^{-3}]$	*0.6 mM* $[PO_4^{-3}]$	*0.7 mM* $[PO_4^{-3}]$	*0.8 mM* $[PO_4^{-3}]$	*1.0 mM* $[PO_4^{-3}]$
0	0.23	0.23	0.23	0.23	0.22	0.22	0.23	0.22
24	0.44	0.43	0.43	0.43	0.44	0.45	0.43	0.45
72	0.55	0.54	0.57	0.55	0.54	0.52	0.55	0.57
96	0.55	0.54	0.54	0.54	0.53	0.51	0.53	0.51
120	0.49	0.48	0.49	0.48	0.48	0.47	0.48	0.49
180	0.46	0.46	0.47	0.46	0.46	0.47	0.46	0.47
252	0.42	0.41	0.42	0.43	0.43	0.43	0.43	0.44

Table A 5.9 b

Expt. Conditions: $[H_2L_{p(T)}]$ = 0.6 mM; $[Cd_{(T)}]$ = 8.9 μM; I = 0.01 M $NaNO_3$; Solution Y; neutral initial pH								
Time (h)	OD_{600}							
	0.2 mM $[PO_4^{-3}]$	*0.3 mM* $[PO_4^{-3}]$	*0.4 mM* $[PO_4^{-3}]$	*0.5 mM* $[PO_4^{-3}]$	*0.6 mM* $[PO_4^{-3}]$	*0.7 mM* $[PO_4^{-3}]$	*0.8 mM* $[PO_4^{-3}]$	*1.0 mM* $[PO_4^{-3}]$
0	0.24	0.23	0.23	0.23	0.24	0.23	0.23	0.22
24	0.44	0.42	0.42	0.43	0.42	0.41	0.42	0.42
72	0.59	0.60	0.57	0.57	0.57	0.56	0.56	0.56
96	0.53	0.53	0.53	0.54	0.53	0.51	0.52	0.52
120	0.48	0.48	0.48	0.48	0.48	0.47	0.47	0.46
180	0.43	0.42	0.46	0.44	0.45	0.43	0.43	0.44
252	0.41	0.39	0.43	0.42	0.42	0.40	0.38	0.41

Table A 5.9 c

Expt. Conditions: $[H_2L_{p(T)}]$ = 0.6 mM; $[Cu_{(T)}]$ = 23.6 μM; I = 0.01 M $NaNO_3$; Solution Y; neutral initial pH								
Time (h)	OD_{600}							
	0.2 mM $[PO_4^{-3}]$	*0.3 mM* $[PO_4^{-3}]$	*0.4 mM* $[PO_4^{-3}]$	*0.5 mM* $[PO_4^{-3}]$	*0.6 mM* $[PO_4^{-3}]$	*0.7 mM* $[PO_4^{-3}]$	*0.8 mM* $[PO_4^{-3}]$	*1.0 mM* $[PO_4^{-3}]$
0	0.23	0.23	0.23	0.24	0.23	0.24	0.23	0.24
24	0.23	0.23	0.23	0.23	0.23	0.23	0.23	0.23
72	0.32	0.33	0.34	0.34	0.27	0.31	0.33	0.29
96	0.33	0.33	0.32	0.33	0.28	0.31	0.34	0.34
120	0.33	0.32	0.33	0.34	0.28	0.31	0.33	0.33
180	0.33	0.31	0.37	0.41	0.30	0.31	0.34	0.34
252	0.33	0.28	0.38	0.43	0.29	0.29	0.32	0.30

Table A 5.10 The ratio of wet weight/dry weight of *Comamonas spp.* cells

wet weight, g	*dry weight, g*	*wet weight/dry weight*
2.284	0.421	5.43
2.309	0.427	5.40
2.337	0.430	5.44
2.297	0.423	5.43
2.471	0.457	5.42
Average		5.42

Table A 5.11a pH change with time in Test 1

Expt. Conditions

$H_2L_{p(T)}$ = 0.6 mM; I = 0.01 M $NaNO_3$; Solution Y; Comamonas spp. =0.055 gL^{-1}

Batch No.	*1*	*2*	*3*	*4*	*5*	*6*	*7*	*8*
0 h	4.1	4.5	5.0	5.5	6.1	6.5	7.2	7.5
60 h	4.4	4.7	5.1	6.0	6.3	6.4	6.5	6.5
96 h	4.5	4.9	5.4	6.4	6.4	6.7	6.7	6.7

Table A 5.11b H_2L_p degradation (%H_2L_p degraded) with time in Test 1

Expt. Conditions

$H_2L_{p(T)}$ = 0.6 mM; I = 0.01 M $NaNO_3$; Solution Y; Comamonas spp. =0.055 gL^{-1}

Batch No.	*1*	*2*	*3*	*4*	*5*	*6*	*7*	*8*
0 h	0.0	0.0	0.0	0.0	0.0	0.0	0.0	0.0
60 h	0.0	0.0	11.8	100.0	100.0	100.0	100.0	100.0
96 h	0.0	0.1	15.8	100.0	100.0	100.0	100.0	100.0

Table A 5.12a pH change with time in Test 2

Expt. Conditions

[$H_2L_{p(T)}$] = 0.6 mM; I = 0.01 M $NaNO_3$; Solution Y; Comamonas spp. =0.055 gL^{-1}; $Cd_{(T)}$ = 8.9 µM

Batch No..	*1*	*2*	*3*	*4*	*5*	*6*	*7*	*8*
0 h	4.1	4.5	5.0	5.6	6.1	6.7	7.2	7.5
60 h	4.5	4.9	5.2	6.1	6.3	6.4	6.4	6.6
96 h	4.5	5.1	5.5	6.3	6.4	6.5	6.5	6.7

Table A 5.12b H_2L_p degradation (%H_2L_p degraded) with time in Test 2

Expt. Conditions *solution Y, 0.01 M $NaNO_3$, 0.6 mM $H_2L_{p(T)}$, $Cd_{(T)}$ = 8.9 µM; Comamonas spp. =0.055 gL^{-1}*								
Batch No.	*1*	*2*	*3*	*4*	*5*	*6*	*7*	*8*
0 h	0.0	0.0	0.0	0.0	0.0	0.0	0.0	0.0
60 h	0.0	1.7	11.6	100.0	100.0	100.0	100.0	100.0
96 h	0.0	1.8	19.6	100.0	100.0	100.0	100.0	100.0

Table A 5.13a Batch description for Test 3-H_2L_p degradation in the presence of ferrihydrite*

Batch No.	*1-1*	*1-2*	*2-1*	*2-2*	*3-1*	*3-2*	*4-1*	*4-2*
8.9 µM $Cd_{(T)}$	-	-	+	+	-	-	+	+
0.6 mM H_2L_p	+	+	+	+	+	+	+	+
0.1 gL^{-1} (dry) Comamonas spp.	+	+	+	+	+	+	+	+
solution Y (with 1 µM NaH_2PO_4)	+	+	+	+	-	-	-	-
solution Y (with 60µM NaH_2PO_4)	-	-	-	-	+	+	+	+
0.1 gL^{-1} ferrihydrite	+	+	+	+	+	+	+	+

*- refers to “the component was not involved in this sample” and + refers to “ the component was involved in this sample”

Table A 5.13b pH change with time in Test 3

Batch No.	*1-1*	*1-2*	*2-1*	*2-2*	*3-1*	*3-2*	*4-1*	*4-2*
0 h	6.3	6.3	6.3	6.3	6.3	6.3	6.3	6.3
60 h	6.4	6.2	6.3	6.3	6.4	6.4	6.4	6.4
96 h	6.6	6.5	6.5	6.4	6.3	6.5	6.4	6.4

Table A 5.13c Phthalic acid degradation (%H_2L_p degraded) with time in Test 3

Batch No.	*1-1*	*1-2*	*2-1*	*2-2*	*3-1*	*3-2*	*4-1*	*4-2*
0 h	0.0	0.0	0.0	0.0	0.0	0.0	0.0	0.0
60 h	100.0	100.0	100.0	100.0	100.0	100.0	100.0	100.0
96 h	100.0	100.0	100.0	100.0	100.0	100.0	100.0	100.0

Table A 6.1

Sample 1: *Comamonas spp. = 56.3 gL^{-1}* *I= 0.01 M $NaNO_3$*		*Sample 2:* *Comamonas spp. = 56.3 gL^{-1}* *I= 0.01 M $NaNO_3$*		*Sample 3:* *Comamonas spp. = 56.3 gL^{-1}* *I= 0.01 M $NaNO_3$*	
-log[H^+]	TOTH, mM	-log[H^+]	TOTH, mM	-log[H^+]	TOTH, mM
2.571	15.908	2.536	15.908	2.571	16.161
2.606	15.568	2.567	15.568	2.600	15.821
2.654	15.229	2.601	15.229	2.631	15.482
2.696	14.892	2.637	14.892	2.664	15.145
2.962	13.271	2.912	12.967	2.930	13.091
3.229	12.109	3.174	11.685	3.178	11.748
3.458	11.358	3.398	10.877	3.398	10.850
3.710	10.700	3.637	10.194	3.645	10.058
4.008	10.081	3.919	9.550	3.903	9.378
4.332	9.560	4.233	8.994	4.244	8.707
4.575	9.135	4.510	8.543	4.554	8.260
4.858	8.523	4.800	7.919	4.781	7.887
5.105	8.057	5.013	7.516	5.076	7.379
5.457	7.292	5.370	6.758	5.473	6.713
5.925	6.480	5.820	5.955	5.891	6.008
6.510	5.765	6.387	5.228	6.374	5.304
6.923	5.425	6.772	4.883	6.825	4.811
7.335	5.125	7.166	4.577	7.224	4.479
7.993	4.762	7.762	4.227	7.686	4.168
8.467	4.466	8.275	3.933	8.228	3.859
8.852	4.135	8.817	3.515	8.662	3.551
9.092	3.842	9.022	3.226	8.952	3.254
9.458	3.253	9.362	2.599	9.302	2.719
9.812	2.581	9.693	1.883	9.647	2.075
10.127	1.857	10.015	1.109	9.971	1.362
10.421	1.048	10.310	0.286	10.292	0.582
10.684	0.159	10.583	-0.598	10.572	-0.236

Table A 6.2a

Expt. Conditions $[Cd_{(T)}] = 1.78\ \mu M$; *32.4 µmol* $Cd_{(T)}$*/ g bacteria cells* *I = 0.01 M* $NaNO_3$		*Expt. Conditions* $[Cd_{(T)}] = 1.78\ \mu M$; *3.24 µmol* $Cd_{(T)}$*/ g bacteria cells* *I = 0.01 M* $NaNO_3$		*Expt. Conditions* $[Cd_{(T)}] = 1.78\ \mu M$; *1.08 µmol* $Cd_{(T)}$*/ g bacteria cells* *I = 0.01 M* $NaNO_3$		*Expt. Conditions* $[Cd_{(T)}] = 1.78\ \mu M$; *0.65 µmol* $Cd_{(T)}$*/ g bacteria cells* *I = 0.01 M* $NaNO_3$	
pH	% Cd sorbed	pH	% Cd sorbed	pH	% Cd sorbed	pH	% Cd sorbed
2.60	1.03	2.53	0.88	2.55	4.10	2.60	4.84
3.02	2.12	3.07	1.75	3.21	8.21	3.14	8.06
3.50	1.59	3.71	3.51	3.99	20.00	3.81	19.67
4.00	1.06	4.22	7.02	5.47	72.22	4.56	46.67
4.60	0.53	5.11	31.03	5.76	83.75	5.43	81.25
4.99	5.82	5.72	48.28	5.86	86.25	5.87	91.25
5.36	7.41	5.89	55.17	5.98	87.50	5.93	92.50
5.65	11.11	5.95	58.62	6.01	88.75	5.96	92.50
5.78	12.70	6.04	60.34	6.10	90.00	6.06	93.75
5.98	14.70	6.23	65.52	6.22	90.00	6.10	96.25
6.21	19.10	6.29	68.33	6.23	91.25	6.17	96.25
7.03	49.60	6.34	70.00	6.31	92.50	6.31	97.50
		6.42	73.33	6.35	93.75	6.34	97.50
		6.50	75.00	6.51	93.75	6.35	97.50
		6.72	77.50	6.83	95.00	6.46	97.50
						6.63	97.50

Table A 6.5

Expt. Conditions *$[H_2L_{p(T)}]$ = 0.6 mM;* *Comamonas spp. = 0.55 gL^{-1}* *I= 0.01 M $NaNO_3$*	
pH	% $H_2L_{p(T)}$ adsorbed
2.03	6.36
2.6	4.32
3.06	2.28
3.57	0.72
4.04	0.70
4.67	0.46
5.21	0.43
5.83	0.00
6.14	0.00
6.56	0.00
6.89	0.46
7.09	0.41
7.14	0.12
7.5	0.44
7.94	0.00

Table A 6.6

Expt. Conditions $[Cd_{(T)}] = 1.78\ \mu M$; dead Comamonas spp.=0.055 gL^{-1} $I = 0.01\ M\ NaNO_3$		*Expt. Conditions* $[Cd_{(T)}] = 1.78\ \mu M$; $[H_2L_{p(T)}] = 0.6\ mM$; dead Comamonas spp. = 0.055 gL^{-1} $I = 0.01\ M\ NaNO_3$		*Expt. Conditions* $[Cd_{(T)}] = 1.78 \mu M$; dead Comamonas spp. = 0.275 gL^{-1} $I = 0.01\ M\ NaNO_3$		*Expt. Conditions* $[Cd_{(T)}] = 1.78\ \mu M$; $[H_2L_{p(T)}] = 0.6\ mM$; dead Comamonas spp. = 0.275 gL^{-1} $I = 0.01\ M\ NaNO_3$	
pH	%Cd sorbed	pH	%Cd sorbed	pH	%Cd sorbed	pH	%Cd sorbed
2.6	1.03	3.82	0.00	3.53	3.59	3.84	1.56
3.02	2.12	4.54	0.00	4.56	10.65	4.5	5.73
3.5	1.59	5.11	3.70	5.02	25.94	5.14	18.23
4.00	1.06	5.57	5.29	5.58	37.50	5.73	32.42
4.6	0.53	6.05	11.11	6.12	55.39	6.12	43.96
4.99	5.82	6.42	16.93	6.59	77.21	6.55	57.14
5.36	7.41	6.65	23.81	7.13	85.34	6.71	60.99
5.65	11.11	6.72	27.53			6.92	69.94
5.78	12.70	6.8	28.65				
5.98	14.70						
6.21	19.10						
7.03	49.60						

Table A7.1, 7.3

Expt. Conditions $[Cd_{(T)}] = 1.78\ \mu M$; *Ferrihydrite = 0.1* gL^{-1}; *dead Comamonas spp. = 2.75* gL^{-1}; *I= 0.01 M* $NaNO_3$		*Expt. Conditions* $[Cd_{(T)}] = 1.78\ \mu M$; *Ferrihydrite = 0.1* gL^{-1}; *dead Comamonas spp.=0.55* gL^{-1}; *I= 0.01 M* $NaNO_3$		*Expt. Conditions* $[Cd_{(T)}] = 1.78\ \mu M$; *Ferrihydrite = 0.1* gL^{-1}; *dead Comamonas spp. = 0.275* gL^{-1}; *I= 0.01 M* $NaNO_3$		*Expt. Conditions* $[Cd_{(T)}] = 1.78\ \mu M$; *Ferrihydrite = 0.1* gL^{-1}; *dead Comamonas spp. = 0.055* gL^{-1}; *I= 0.01 M* $NaNO_3$	
pH	% Cd sorbed	pH	%Cd sorbed	pH	% Cd sorbed	pH	%Cd sorbed
3.55	17.15	3.61	4.63	4.21	3.08	4.12	1.09
4.36	34.15	4.32	9.66	4.97	13.33	4.69	1.09
4.69	47.40	4.86	19.77	5.21	22.56	5.1	1.10
5.4	73.62	5.36	34.63	5.55	33.33	5.5	5.15
5.64	84.60	5.6	48.25	5.95	44.09	6	15.56
5.92	86.82	6.09	69.34	6.45	72.50	6.42	27.70
6.14	91.42	6.33	78.04	6.57	76.00	6.79	67.05
6.35	93.92	6.87	87.53	6.66	80.00	6.98	85.24
6.51	93.29	7.16	93.75	7.16	95.26		
6.76	97.71	7.58	96.97				

Table A7.6

Expt. Conditions $[Cd_{(T)}] = 1.78\ \mu M$; *Ferrihydrite* $= 0.1\ gL^{-1}$ *I= 0.01 M* $NaNO_3$		*Expt. Conditions* $[Cd_{(T)}] = 1.78\ \mu M$; *Ferrihydrite* $= 0.1\ gL^{-1}$; $[H_2L_{p(T)}] = 0.6$ *mM* *I= 0.01 M* $NaNO_3$		*Expt. Conditions* $[Cd_{(T)}] = 1.78\ \mu M$ *Ferrihydrite* $= 0.1\ gL^{-1}$; $[H_2L_{p(T)}] = 0.6$ *mM* *Comamonas spp.* $= 0.055\ gL^{-1}$ *I= 0.01 M* $NaNO_3$	
pH	% Cd sorbed	pH	% Cd sorbed	pH	% Cd sorbed
3.01	0.52	3.74	0.00	3.89	1.11
4.6	0.54	4.54	1.71	4.68	6.84
4.98	2.17	5.08	5.71	5.13	12.11
5.45	4.89	5.73	24.46	5.58	25.81
5.75	5.98	6.3	58.15	6.17	53.76
6.39	29.58	6.82	85.85	6.6	78.33
6.74	54.65	6.94	89.92	7	89.83
6.77	66.86	7.39	96.32	7.39	95.74
		7.64	96.84	7.51	96.67
		7.98	98.42	7.96	98.00
				11.52	100.00

Table A 7.9

Expt. Conditions $[Cd_{(T)}] = 1.78\ \mu M$; *Ferrihydrite* $= 0.1\ gL^{-1}$ *I= 0.01 M* $NaNO_3$		*Expt. Conditions* $[Cd_{(T)}] = 1.78\ \mu M$; *Ferrihydrite* $= 0.1\ gL^{-1}$; $[H_2L_{p(T)}] = 0.6$ *mM* *I= 0.01 M* $NaNO_3$		*Expt. Conditions* $[Cd_{(T)}] = 1.78\ \mu M$; *Ferrihydrite* $= 0.1\ gL^{-1}$; $[H_2L_{p(T)}] = 0.6$ *mM*; *Bacteria* $= 0.275\ gL^{-1}$ *I= 0.01 M* $NaNO_3$	
pH	% Cd sorbed	pH	% Cd sorbed	pH	% Cd sorbed
3.01	0.52	3.74	0.00	4.05	3.59
4.6	0.54	4.54	1.71	4.64	9.23
4.98	2.17	5.08	5.71	5.21	26.15
5.45	4.89	5.73	24.46	5.69	41.94
5.75	5.98	6.3	58.15	6.09	64.00
6.39	25.58	6.82	85.85	6.78	87.89
6.74	54.65	6.94	89.92	7.04	94.21
6.77	66.86	7.39	96.32	7.29	95.26
		7.64	96.84	7.49	96.84
		7.98	98.42		

Table A7.12a

Expt. Conditions *$[Cd_{(T)}]$ = 1.78 μM* *Alive Comamonas spp. = 0.055 gL^{-1};* *I= 0.01 M $NaNO_3$*		*Expt. Conditions* *$[Cd_{(T)}]$ = 1.78 μM* *Alive Comamonas spp. = 0.055 gL^{-1};* *I= 0.01 M $NaNO_3$* *Solution Y*	
pH	% Cd sorbed	pH	% Cd sorbed
2.57	0.54	2.61	0.53
3.12	1.63	3.21	1.09
3.67	2.17	3.67	1.09
4.11	3.26	4.05	1.63
4.72	6.52	4.62	3.80
5.43	8.70	5.12	5.43
5.78	11.96	5.73	8.15
6.04	12.50	6.32	15.33
6.37	15.09	6.7	20.22
6.58	17.39	7.16	24.57
7.18	28.97	7.76	37.28

Table A7.12b

Expt. Conditions *$[Cd_{(T)}]$ = 1.78 μM;* *Dead Comamonas spp. = 0.055 gL^{-1};* *I= 0.01 M $NaNO_3$*		*Expt. Conditions* *$[Cd_{(T)}]$ = 1.78 μM;* *Dead Comamonas spp. = 0.055 gL^{-1};* *I= 0.01 M $NaNO_3$; Solution Y*	
pH	% Cd sorbed	pH	% Cd sorbed
2.60	1.03	2.64	1.03
3.02	2.12	3.12	2.12
3.50	1.59	3.53	1.06
4.00	1.06	4.17	3.17
4.60	0.53	4.52	1.59
4.99	5.82	5.05	6.88
5.36	7.41	5.42	7.94
5.65	11.11	5.7	9.52
5.78	12.70	5.89	15.34
5.98	12.70	5.98	17.46
6.21	19.10	6.23	24.16
7.03	41.01	6.55	26.40

Table A7.12c

Expt. Conditions $[Cd_{(T)}] = 1.78\ \mu M$; *Ferrihydrite = 0.1* gL^{-1}; *I= 0.01 M* $NaNO_3$		*Expt. Conditions* $[Cd_{(T)}] = 1.78\ \mu M$; *Ferrihydrite = 0.1* gL^{-1}; *I= 0.01 M* $NaNO_3$; *Solution Y*	
pH	% Cd sorbed	pH	% Cd sorbed
3.01	0.52	2.96	0.00
4.60	0.54	4.77	0.54
4.98	2.17	5.21	1.63
5.45	4.89	5.74	7.07
5.75	5.98	6.08	15.22
6.39	25.58	6.56	35.47
6.74	54.65	6.62	62.21
6.77	66.86	6.79	66.86

Table A7.12d

Expt. Conditions $[Cd_{(T)}] = 1.78\ \mu M$; *Ferrihydrite = 0.1* gL^{-1}; $[H_2L_{p(T)}] = 0.6$ *mM*; *I= 0.01 M* $NaNO_3$		*Expt. Conditions* $[Cd_{(T)}] = 1.78\ \mu M$; *Ferrihydrite = 0.1* gL^{-1}; $[H_2L_{p(T)}] = 0.6$ *mM*; *I= 0.01 M* $NaNO_3$; *Solution Y*	
pH	% Cd sorbed	pH	% Cd sorbed
3.74	0.00	3.74	0.00
4.54	1.71	4.55	4.00
5.08	5.71	5.08	4.57
5.73	24.46	5.69	25.14
6.30	58.15	6.3	53.80
6.82	79.79	6.76	80.85
6.94	88.42	7.02	90.00
7.39	96.32	7.32	94.74
7.64	96.84	7.67	95.79
7.98	98.42	7.93	97.89

Table A7.12e

Expt. Conditions		*Expt. Conditions*	
$[Cd_{(T)}]$ = 1.78 μM;		*$[Cd_{(T)}]$ = 1.78 μM;*	
$[H_2L_{p(T)}]$ = 0.6 mM;		*$[H_2L_{p(T)}]$ = 0.6 mM;*	
Dead Comamonas spp. = 0.055 gL^{-1};		*Dead Comamonas spp. = 0.055 gL^{-1};*	
I= 0.01 M $NaNO_3$		*I= 0.01 M $NaNO_3$; Solution Y*	
pH	% Cd sorbed	pH	% Cd sorbed
3.82	0.00	3.72	0.00
4.54	0.00	4.55	2.08
5.11	3.70	5.05	5.73
5.57	5.29	5.65	7.81
6.05	11.11	6.19	11.46
6.42	16.93	6.3	13.54
6.65	23.81	6.56	20.31
6.72	27.53	6.74	21.98
6.80	28.65		

Table A7.12f

Expt. Conditions		*Expt. Conditions*	
$[Cd_{(T)}]$ = 1.78 μM;		*$[Cd_{(T)}]$ = 1.78 μM;*	
Ferrihydrite=0.1 gL^{-1};		*Ferrihydrite = 0.1 gL^{-1};*	
Alive Comamonas spp. = 0.055 gL^{-1};		*Alive Comamonas spp. = 0.055 gL^{-1};*	
I= 0.01 M $NaNO_3$		*I= 0.01 M $NaNO_3$; Solution Y*	
pH	% Cd sorbed	pH	% Cd sorbed
3.33	2.23	3.35	1.73
3.94	2.17	3.96	2.17
4.63	6.99	4.57	5.49
5.31	4.37	5.21	3.87
5.61	9.68	5.51	9.68
5.95	16.79	6.01	18.29
6.16	27.65	6.26	26.52
6.23	29.29	6.43	43.79
6.56	52.55	6.86	68.05
6.70	60.94	6.90	75.94

Table A7.12g

Expt. Conditions *$[Cd_{(T)}]$ = 1.78 μM;* *Ferrihydrite = 0.1 gL^{-1};* *Dead Comamonas spp. = 0.055 gL^{-1};* *I= 0.01 M $NaNO_3$*		*Expt. Conditions* *$[Cd_{(T)}]$ = 1.78 μM;* *Ferrihydrite = 0.1 gL^{-1};* *Dead Comamonas spp. = 0.055 gL^{-1};* *I= 0.01 M $NaNO_3$; solution Y*	
pH	% Cd sorbed	pH	% Cd sorbed
4.12	1.09	4.18	0.00
4.69	1.09	4.81	0.54
5.10	1.10	5.28	1.10
5.50	5.15	5.72	5.73
6.00	15.56	6.14	19.61
6.42	27.70	6.59	43.68
6.79	67.05	6.76	60.92
6.98	85.24	6.98	87.14

Table A7.12h

Expt. Conditions *$[Cd_{(T)}]$ = 1.78 μM;* *$[H_2L_{p(T)}]$ = 0.6 mM;* *Ferrihydrite = 0.1 gL^{-1};* *Dead Comamonas spp. = 0.055 gL^{-1};* *I= 0.01 M $NaNO_3$*		*Expt. Conditions* *$[Cd_{(T)}]$ = 1.78 μM;* *$[H_2L_{p(T)}]$ = 0.6 mM;* *Ferrihydrite = 0.1gL^{-1};* *Dead Comamonas spp. = 0.055 gL^{-1};* *I= 0.01 M $NaNO_3$; solution Y*	
pH	% Cd sorbed	pH	% Cd sorbed
3.89	1.11	3.89	0.53
4.68	6.84	4.64	2.63
5.13	12.11	5.13	10.00
5.58	25.81	5.60	24.74
6.17	53.76	6.16	48.92
6.60	78.33	6.63	73.89
7.00	89.33	7.00	92.00
7.39	94.00	7.36	96.00
7.51	96.67		
7.96	98.00		
11.52	100.00		

Table A 7.13

Expt. Conditions $[Cd_{(T)}] = 1.78\ \mu M$; *Alive bacteria* $= 0.055\ gL^{-1}$; $I = 0.01\ M\ NaNO_3$; $T = 3\ h$		*Expt. Conditions* $[Cd_{(T)}] = 1.78\ \mu M$; *Dead bateria* $= 0.055\ gL^{-1}$; $I = 0.01\ M\ NaNO_3$; $T = 3\ h$		*Expt. Conditions* $[Cd_{(T)}] = 1.78\ \mu M$; *Dead bacteria* $= 0.055\ gL^{-1}$; $I = 0.01\ M\ NaNO_3$; $T = 72\ h$	
pH	% Cd sorbed	pH	% Cd sorbed	pH	% Cd sorbed
2.57	0.54	2.62	0.53	2.60	1.03
3.12	1.63	3.01	1.09	3.02	2.12
3.67	2.17	3.5	0.54	3.50	1.59
4.11	3.26	4.00	2.17	4.00	1.06
4.72	6.52	4.6	3.80	4.60	0.53
5.43	8.70	5.01	7.61	4.99	5.82
5.78	11.96	5.42	9.24	5.36	7.41
6.04	12.50	5.68	11.41	5.65	11.11
6.37	15.09	5.82	12.50	5.78	12.70
6.58	17.39	5.86	14.37	5.98	12.70
7.18	28.97	6.24	18.97	6.21	19.10
		6.72	30.46	7.03	41.01

Table A 7.14

Expt. Conditions $[Cd_{(T)}] = 1.78\ \mu M$ *Ferrihydrite = 0.1 gL^{-1}* *Alive bacteria = 0.055 gL^{-1}* *I = 0.01 M $NaNO_3$;* *T = 3 h*		*Expt. Conditions* $[Cd_{(T)}] = 1.78\ \mu M$ *Ferrihydrite = 0.1 gL^{-1}* *Alive bacteria = 0.055 gL^{-1}* *I = 0.01 M $NaNO_3$;* *T = 24 h*		*Expt. Conditions* $[Cd_{(T)}] = 1.78\ \mu M$ *Ferrihydrite = 0.1 gL^{-1}* *Alive bacteria = 0.055 gL^{-1}* *I = 0.01 M $NaNO_3$;* *T = 48 h*		*Expt. Conditions* $[Cd_{(T)}] = 1.78\ \mu M$ *Ferrihydrite = 0.1 gL^{-1}* *Alive bacteria = 0.055 gL^{-1}* *I = 0.01 M $NaNO_3$;* *T = 72 h*		*Expt. Conditions* $[Cd_{(T)}] = 1.78\ \mu M$ *Ferrihydrite = 0.1 gL^{-1}* *Dead bacteria.= 0.055 gL^{-1}* *I = 0.01 M $NaNO_3$;* *T = 72 h*	
pH	% Cd sorbed	pH	% Cd sorbed	pH	% Cd sorbed	pH	% Cd sorbed	pH	% Cd sorbed
3.32	1.12	3.31	2.23	3.32	2.23	3.33	2.23	4.12	1.09
3.92	0.00	3.94	3.26	3.95	2.17	3.94	2.17	5.10	1.10
4.54	5.38	4.60	5.91	4.64	6.99	4.63	6.99	5.50	5.15
5.13	5.46	5.13	6.56	5.24	4.92	5.31	4.37	6.00	17.11
5.57	8.60	5.58	9.14	5.62	10.22	5.61	9.68	6.42	27.70
5.97	16.79	5.95	18.42	5.97	15.70	5.95	16.79	6.79	67.05
6.24	27.12	6.20	28.18	6.18	27.12	6.16	27.65	7.00	85.05
6.36	31.31	6.28	28.79	6.21	28.28	6.23	29.29		
6.75	57.14	6.62	50.00	6.58	51.02	6.56	52.55		
		6.71	60.94	6.69	60.42	6.70	60.94		

Tables A 7.15-7.16

Expt. Conditions

$[Cd_{(T)}]$ = 1.78 μM; Comamonas spp. = 0.055 gL^{-1}; Ferrihydrite = 0.1 gL^{-1}; $H_2L_{p(T)}$= 0.6 mM (at time = 0);I= 0.01 M $NaNO_3$

Time (h)	Batch 1		Batch 2		Batch 3		Batch 4	
	pH	% H_2L_p degraded	pH	% H_2L_p degraded	pH	% H_2L_p degraded	pH	% H_2L_p degraded
0	5.58	0.00	6.04	0.00	6.53	0	7.02	0.00
14.0	5.74	3.27	6.33	2.91	6.82	1.25	6.83	0.00
24.5	5.89	7.54	6.53	11.28	6.80	6.09	6.95	9.15
39.0	6.58	14.60	7.52	40.20	7.33	28.03	7.52	44.66
48.0	7.16	23.24	7.18	74.46	7.22	47.79	7.24	77.96
72.0	7.26	69.34	9.24	99.98	7.92	99.99	8.08	99.99

Table A 7.17

Expt. Conditions

$[Cd_{(T)}]$ = 1.78 μM; Comamonas spp. = 0.055 gL^{-1}; Ferrihydrite = 0.1 gL^{-1}; $H_2L_{p(T)}$= 0.6 mM (at time = 0);I= 0.01 M $NaNO_3$

Time (h)	Batch 1		Batch 2		Batch 3		Batch 4	
	pH	% Cd sorbed	pH	% Cd sorbed	pH	% Cd sorbed	pH	% Cd sorbed
0.0	5.58	0.00	6.04	0.00	6.53	0.00	7.02	0.00
14.0	5.74	31.30	6.33	53.95	6.82	80.54	6.83	80.98
24.5	5.89	31.39	6.53	67.10	6.80	78.40	6.95	81.27
39.0	6.58	66.86	7.52	95.14	7.33	90.79	7.52	94.81
48.0	7.16	87.86	7.18	91.35	7.22	91.66	7.24	95.41
72.0	7.26	92.10	9.24	98.65	7.92	97.16	8.08	98.83